TESIS DOCTORAL

ESTUDIOS BIOFÍSICOS DE PÉPTIDOS SINTÉTICOS DE LA PROTEÍNA DE ENVOLTURA E1 DEL GBV-C/HGV Y SU RELACIÓN CON EL VIH

Mª Jesús Sánchez Martín

Barcelona, 2011

Universidad de Barcelona
Facultad de Farmacia
Departamento de Fisicoquímica

CSIC-IQAC
Departamento de Química Biomédica
Unidad de Síntesis y Aplicaciones Biomédicas de Péptidos

CSIC iQAC

UNIVERSITAT DE BARCELONA

UNIVERSIDAD DE BARCELONA
FACULTAD DE FARMACIA
DEPARTAMENTO DE FISICOQUÍMICA

PROGRAMA DE DOCTORAT: "Investigación, desarrollo y control de medicamentos"

Estudios biofísicos de péptidos sintéticos de la proteína de envoltura E1 del GBV-C/HGV y su relación con el VIH

Memoria presentada por Mª Jesús Sánchez Martín para optar al grado de doctor por la Universidad de Barcelona

Directores:

Dra. Isabel Haro Villar

Dra. Mª Asunción Alsina Esteller

Doctoranda:

Mª Jesús Sánchez Martín

Barcelona, 2011

Una experiencia nunca es un fracaso, pues siempre viene a demostrar algo.

Thomas Alva Edison

A mi familia
Por estar siempre ahí
Y a los que no están
Porque éste también era
Su sueño…

Ésta quizá sea la parte menos importante en cuanto a ciencia se refiere, pero es la más que más importancia tiene, en mi opinión, en el terreno personal. Es una forma de intentar reflejar lo mucho que te ha ayudado la gente aunque muchas veces no seas capaz de demostrarles lo agradecida que les estás. Y aunque es difícil plasmarlo en un papel, voy a intentarlo:

En primer lugar, de la Unidad de Síntesis y Aplicaciones Biomédicas de Péptidos del IQAC-CSIC, quisiera agradecerle a mi directora, la Dra. Isabel Haro, la oportunidad que me dado de poder realizar la tesis doctoral, así como sus pautas y consejos científicos para llevar a cabo este trabajo. Además, agradecer a todo el departamento su buena acogida en el laboratorio, a Mª José, Elena, Jessi, Leticia, Ramona, Aimeé su disposición a ayudar, sus ánimos y los ratos de tertulias que hemos compartido.

Por otro lado, del departamento de Fisicoquímica en la facultad de farmacia, donde he pasado la mayor parte de mi doctorado, tengo que agradecerle a mi directora, la Dra. Mª Asunción Alsina, de nuevo la oportunidad que me brindó para poder realizar la tesis doctoral, sus consejos, tanto científicos como en el terreno personal, su constante preocupación por todo y por todos y la calidad humana que "derrocha"… he aprendido mucho.

Muchas gracias a la Dra. Pujol por introducirme en el mundo de las monocapas y guiarme a lo largo de todo este trabajo, agradecerle los consejos y los ratos compartidos, su dedicación y confianza plenas, gracias por estar siempre dispuesta a ayudar y porque nunca le ha faltado un detalle conmigo.

A la Dra. Mª Antònia Busquets por ser también mi guía a lo largo de este trabajo, tanto científica como personalmente. Gracias por guiarme a través del mundo de los liposomas, gracias por ser uno de los pilares que me han ayudado en muchas ocasiones a no tirar la toalla, por sus consejos y ayuda desinteresada…gracias.

Al Dr. Joan Estelrich, siempre dispuesto a ayudar, darle las gracias por los consejos, por los ratos compartidos, por el trato personal, amistad y ayuda en todos los campos…

Sonia… qué voy a decir… has sido mi compañera de viaje, hemos compartido alegrías, lágrimas, nervios… todo lo que hemos vivido en este tiempo… gracias por estar siempre ahí, el haberte conocido es una razón más por la que han merecido la pena estos cuatro años… gracias.

Darle las gracias a Òscar, por ser mi guía en el mundo del AFM, por su ayuda, sus consejos y la amistad que me ha brindado…gracias. Carme, siempre con una sonrisa, gracias por estar siempre dispuesta a ayudar y por los buenos ratos compartidos…

Alba, gracias por los ratos de laboratorio compartidos, las tertulias y tu disposición a ayudar… Eli, compañera en este final de etapa, gracias por tu ayuda y por todas esas risas compartidas.

Roser y Montse, dos pilares imprescindibles en el departamento, sin vosotras, muchas veces, no hubiera podido avanzar, gracias. Y cómo no agradecerle al resto de personas del departamento, todas ellas en algún momento a lo largo de estos cuatro años han resultado imprescindibles: Josefina, Montse, Marisa, Mª Antònia, Tere, Jordi, Marta, Javi… gracias. Vicky, gracias por tu apoyo constante, tu preocupación por mi futuro y por agotar todas las opciones por tal de ayudarme, gracias… Yolanda, gracias por ayudarme siempre que has podido y por los buenos ratos de risas que nos haces pasar… A todos, gracias.

Y estas últimas líneas se las voy a dedicar a las personas que siempre han estado ahí, en los buenos y en los malos momentos, esa es mi familia… Sin ellos y su apoyo constante en todas mis decisiones, no hubiera sido posible llegar hasta aquí. Espero que se sientan orgullosos de mí.

Quiero darte las gracias Albert por tu paciencia, por tu apoyo, por aguantar mis nervios y mis enfados, por hacerme reír y por secar mis lágrimas, gracias por haberte conocido… A mi nueva familia, Nuri, Isidro, Jose, Sonia, Ariadna y Judith… un abrazo, una sonrisa, un consejo, todo te empuja a seguir…gracias.

David, Neus, Eric y Pau, hermano, cuñada y sobrinos, gracias por formar parte de mi vida, por ayudarme tanto como lo habéis hecho, por compartir mis mejores y peores momentos, por todo ello gracias… Eric y Pau, no sabéis lo importante que ha sido para mí el que me hagáis reír o me deis un abrazo… espero que cumpláis vuestras ilusiones y vuestras metas como yo estoy cumpliendo ahora mismo las mías…

A mis padres… sois mi vida, mi apoyo, los pilares que me sostienen, los que habéis luchado tanto para que yo llegara hasta aquí, los que me habéis enseñado a trabajar y a luchar por las cosas, los que me habéis inculcado unos valores de los que me enorgullezco… sin vosotros este trabajo no hubiera sido posible y, por todo ello y mucho más, os estoy agradecida y os quiero.

Y gracias a tantos otros que se me quedan en el tintero de la memoria… no me lo tengáis en cuenta.

Abreviaturas, acrónimos y símbolos

ADN	Ácido desoxirribonucleico
AFM	Microscopio de fuerzas atómicas, del inglés Atomic Force Microscopy
ANTS	Ácido 8-aminonaftaleno-1,3,6-trisulfónico
ARN	Ácido ribonucleico
BAM	Microscopio del ángulo de Brewster, del inglés Brewster angle microscopy
CD	Dicroísmo circular, del inglés *circular dichroism*
DIEA	N,N-diisopropiletilamina
DIPCDI	N,N'-diisopropilcarbodiimida
DMF	N-N'-dimetilformamida
DMPC	Dimiristoilfosfatidilcolina
DMPG	Dimiristoilfosfatidilglicerol
DMSO	Dimetilsulfóxido
DPH	Difenilhexatrieno
DPPG	Dipalmitoilfosfatidilgliceron
DPX	Bromuro de N,N'-p-xilenobis(piridinio)
DSC	Calorimetría diferencial de barrido, del inglés *Differential Scanning Calorimetry*
EDT	1,2-etanoditiol
ELISA	Ensayo inmunoenzimático en fase sólida, del inglés *enzyme-linked immunosorbent assay*
EM	Espectrometría de masas
Fmoc	9-fluorometoxicarbonil
FRET	Transferencia de energía por resonancia, del inglés *fluorescence resonace energy transfer*
GBV-C/HGV	GB virus C / virus de la hepatitis G
gp	Glicoproteína
GUV	Vesículas unilamelares gigantes, del inglés *Giant Unilamellar Vesicles*
HATU	2-(7-aza-1H-benzotriazol-1-il)-1,1,3,3-tetrametiluronio hexafluorofosfato
Hepes	Ácido N-(2-hidroxietil)piperazina-N'-(2-etanosulfónico)
HOBt	1-Hidroxibenzotriazol

HPLC	Cromatografía líquida de alta resolución, del inglés *High Performance Liquid Chromatography*
INNTI	Inhibidores No Nucleósidos de la Transcriptasa Inversa
INTI	Inhibidores Nucleósidos/Nucleótidos de la Transcriptasa Inversa
ITC	Calorimetría isotérmica de titulación, del inglés *Isothermal Titration Calorimetry*
LUV	Vesículas unilamelares grandes, del inglés *Large Unilamellar Vesicles*
MLV	Vesículas multilamelares, del inglés *Multilamellar vesicles*
NBD-PE	N-(7-nitrobenz-2-oxa-1,3-diazol-4-il)–1,2-dihexadecanoil-sn-glicero-3-fosfoetanolamina
NS	No estructural
PC	Fosfatidilcolina
PF	Péptido de fusión
PG	Fosfatidilglicerol
POPG	Palmitoiloleoilfosfatidilglicerol
PS	Fosfatidilserina
Rho-PE	Rodamina B 1,2 –dihexaecanoil-sn-glicero-3-fosfoetanolamina
SEM	Microscopio Electrónico de Barrido, del inglés *Scanning Electron* Microscope
SIDA	Síndrome de la Inmunodeficiencia Adquirida
SPPS	Síntesis de péptidos en fase sólida, del inglés *solid-phase peptide synthesis*
SPR	Resonancia de plasmón de superficie, del inglés *Surface Plasmon Resonance*
SUV	Vesículas unilamelares pequeñas, del inglés *Small Unilamellar Vesicles*
TARGA	Tratamiento antirretroviral de gran actividad
tBut	Tert-butil
TFA	Ácido trifluoroacético
TFE	2,2,2-trifluoroetanol
TIS	Triisopropilsilano
T_m	temperatura de transición
TMA-DPH	trimetilamino-difenilhexatrieno
VIH	Virus de la Inmunodeficiencia Humana
θ	elipticidad molar
λ	longitud de onda

Anexo 1. Aminoácidos, código de tres letras, una letra y estructura

aminoácido	estructura	aminoácido	estructura
Alanina, Ala, A	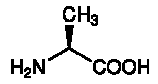	Isoleucina, Ile, I	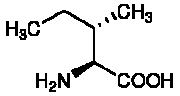
Ácido aspártico, Asp, D	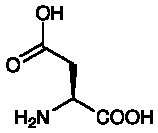	Leucina, Leu, L	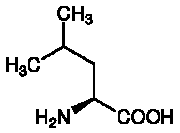
Ácido glutámico, Glu, E	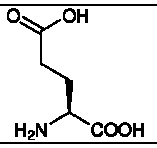	Lisina, Lys, K	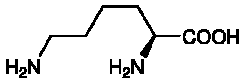
Arginina, Arg, R	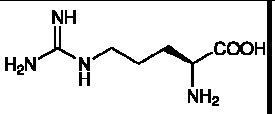	Metionina, Met, M	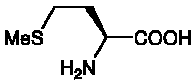
Asparagina, Asn, N	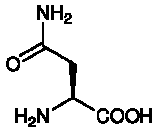	Prolina, Pro, P	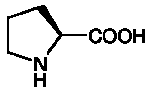
Cisteína, Cys, C	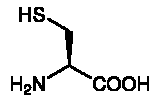	Serina, Ser, S	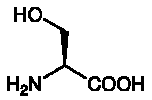
Fenilalanina, Phe, F	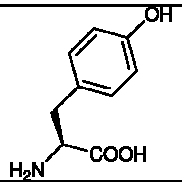	Treonina, Thr, T	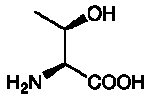
Glutamina, Gln, Q	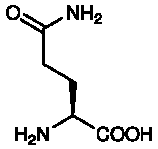	Tirosina, Tyr, Y	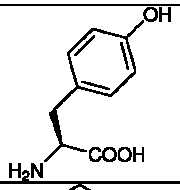
Glicina, Gly, G	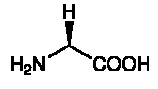	Triptófano, Trp, W	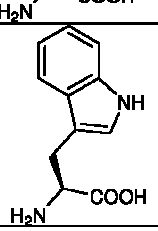
Histidina, His, H	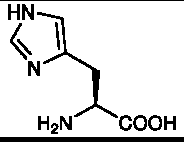	Valina, Val, V	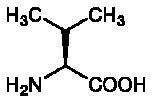

Índice

Página

1. Introducción

La hepatitis viral se conoce desde hace miles de años. Las antiguas civilizaciones de China y Babilonia describen la enfermedad como epidemias con ictericia. La existencia de una forma de transmisión parenteral ya aparece documentada en 1885, en pacientes con sífilis tratados con agujas sin esterilizar. En 1930 se establece la existencia clínica de hepatitis por transfusión de sangre y plasma, confirmándose luego en 1942 al estudiar posteriormente los sueros, en los cuales se encontró el virus B. Con estos estudios se define el concepto de la existencia de dos formas de hepatitis: La llamada infecciosa de corto periodo de incubación, trasmitida por vía fecal-oral y la hepatitis postransfusional, de largo periodo de incubación [1].

En 1947 MacCallum las denomina hepatitis A y hepatitis B, respectivamente, identificándose posteriormente los respectivos virus en las heces y en el suero de los infectados, donde también se hallaron los anticuerpos específicos.

En 1980 se descubre el virus delta en los portadores del virus B. Al persistir la hepatitis postransfusional a pesar de aislar a los donantes, B negativos, se establece la existencia de otros virus a los que se les llamó virus de la hepatitis noA noB. Durante más de 15 años se trató de identificar a este virus, hasta que se descubre el virus de la hepatitis C, que ocasiona el 90% de las hepatitis postransfusionales. La existencia de otro virus de transmisión fecal-oral, noA, se perfila a partir de 1956 cuando se describen epidemias de hepatitis en varias regiones del mundo, con cuadro clínico y epidemiológico semejante al de la hepatitis A sin serlo por no presentar los anticuerpos anti A. En 1980 se descubre al virus E en las heces, y en 1995 se identifica el virus G. En países desarrollados, aproximadamente del 4 al 5% de las hepatitis adquiridas no tienen etiología viral específica y se presupone la existencia de otros agentes productores. En la literatura médica se utilizan diversos nombres para señalar a estos virus, siendo uno de ellos hepatitis F. En resumen, hasta la fecha se conocen hasta 6 tipos de virus causantes de hepatitis viral: los virus A, B, C, D, E y G, cada uno con características diferentes [2].

1.1. Virus de la hepatitis G

La historia de la hepatitis G comienza en la década de los 60 cuando un cirujano de Chicago con iniciales GB contrajo una hepatitis aguda de origen desconocido [3], pero no fue hasta tres décadas más tarde que el virus de la hepatitis G fue descubierto simultáneamente por dos laboratorios distintos que lo denominaron GB virus C (GBV-C) [4] y hepatitis G virus (HGV) [5], respectivamente. Ambos laboratorios lo descubrieron procedente del plasma de un paciente con hepatitis. El grupo que lo denominó GBV-C lo aisló después de inocular el plasma de dicho paciente a tamarinos. En estos primates también se descubrieron otros virus, denominados GBV-A y GBV-B, que infectan únicamente a esta especie. El virus GBV-C/HGV ha sido identificado tanto en chimpancés como en humanos, aunque en cada especie las cepas son distintas [6].

Estudios realizados en diferentes laboratorios de investigación compararon los virus GBV-C y HGV y observaron que poseen más de un 95% de homología en la secuencia de aminoácidos, y aproximadamente un 85% de homología en la secuencia de nucleótidos, lo que permitió llegar a la conclusión de que se trata del mismo virus [7].

La organización del genoma del virus GBV-C/HGV es similar a la de GBV-A, GBV-B y al virus de la hepatitis C, con el cual presenta una homología del 25% en la cadena nucleotídica.

La infección con GBV-C/HGV en humanos es frecuente y puede identificarse mediante la detección de ARN en el suero [8]. El virus puede permanecer durante muchos años sin ninguna evidencia de síntomas clínicos o enfermedad, tanto en pacientes inmunodeprimidos como en la población sana [9].

La vía principal de transmisión de este virus es a través de la sangre o de sus derivados. La elevada exposición a productos relacionados con la sangre, ya sea en pacientes hemodializados [10], con trasplante de órganos [11] o en personas drogadictas [12] plantea un gran riesgo de adquirir el virus de la hepatitis G, siendo del 14-38% la presencia de GBV-C/ HGV o de un 50-70% la presencia de anticuerpos anti-E2 [13, 14]. Otras posibles vías de infección pueden ser mediante contacto sexual [15] o verticalmente de madre a hijo

[16]. La prevalencia del virus en personas que no han estado en contacto con patógenos que puedan transmitirse a través de la sangre es del 1-4% [17, 18].

El GBV-C/HGV (figura 1) es un virus perteneciente a la familia *Flaviviridae* de tipo ARN de cadena sencilla y polaridad positiva. Su genoma consta aproximadamente de 9400 nucleótidos que codifican para una única poliproteína de alrededor de 2900 aminoácidos. En el extremo amino de esta poliproteína se encuentran las proteínas de envoltura E1 y E2, mientras que las no estructurales NS2, NS3, NS4 y NS5 se encuentran en el extremo carboxilo de la poliproteína.

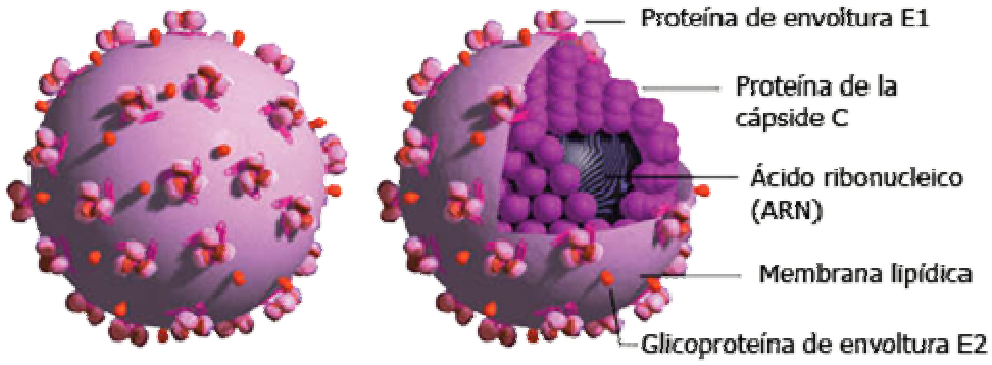

Figura 1. Modelo de la estructura del virus GBV-C/HGV. Fuente: www.prn.org

Las personas con una infección activa de GBV-C/HGV normalmente no presentan anticuerpos contra la proteína estructural E2 [19]. La presencia de estos anticuerpos es indicativa de la eliminación del virus en sangre, por lo tanto, se puede determinar mediante la técnica del ELISA (ensayo inmunoenzimático) una infección pasada [20]. En donantes de sangre se ha encontrado que entre un 10 y un 20 % de la población tiene anticuerpos anti-E2 [21]. Finalmente, tras un período de tiempo de unos 10 años se van eliminando los anticuerpos anti-E2 en sangre.

El virus en humanos parece ser asintomático, aunque algunos autores lo han relacionado con la hepatitis crónica e incluso con hepatitis fulminante [22, 23]. Se ha estudiado el posible efecto de una co-infección con el virus de la hepatitis

C, pero la presencia de GBV-C/HGV no produce ningún cambio respecto a pacientes únicamente infectados con hepatitis C [24].

1.2. Virus de la inmunodeficiencia humana y síndrome de la inmunodeficiencia adquirida

El SIDA, palabra procedente del acrónimo con que se hace referencia al síndrome de inmunodeficiencia adquirida, representa la expresión patológica final de la infección por VIH o virus de la inmunodeficiencia humana, cuya capacidad para atacar los linfocitos CD4 supone la destrucción del sistema inmunitario del paciente afectado, dejándolo expuesto a la agresión de numerosas infecciones oportunistas que conllevan la muerte del enfermo.

El SIDA constituye la primera pandemia de la segunda mitad del siglo XX, pero sus orígenes hay que buscarlos en África central, donde probablemente se produjo la primera infección de un ser humano. Un estudio retrospectivo, realizado con sueros almacenados en distintas partes del mundo, nos muestra que el primer caso de infección por VIH fue en Zaire en 1959. [25] Los primeros casos constatados en Estados Unidos corresponden ya al año 1968. Según parece, tras mantenerse localizado durante un tiempo en una pequeña zona de África central, el virus comenzó a propagarse por el resto del continente a principios de la década de los sesenta, pasó al Caribe, donde es endémico, y desde allí pudo llegar a Europa y América.

En 1981 se describieron los primeros casos de SIDA, y en 1983 se identificó al virus de la inmunodeficiencia humana como el agente etiológico de dicha enfermedad. En 1984, el virus adquirió su denominación definitiva: *human immunodeficiency virus* (HIV), que en castellano se expresa como virus de la inmunodeficiencia humana (VIH) [26]; hoy conocido como VIH-1. En 1986, se identificó un segundo agente viral, parecido al VIH-1 en casi el 50% de su genoma, que fue denominado VIH-2. [27, 28]

La inmensa mayoría de los casos de SIDA se deben a virus clasificados dentro del tipo VIH-1, mientras que la casi totalidad de los casos de SIDA atribuibles al

VIH-2 se han presentado en países de la región occidental africana como Senegal, Ghana, Nigeria, Guinea-Bissau, Zimbabue, Mali y Costa de Marfil.
Desde el inicio de la epidemia se estima que en todo el mundo se han producido más de 16 millones de muertes por sida. En la actualidad se calcula que viven unos 33 millones de personas infectadas por el VIH, más del 90% de ellas en países del Tercer Mundo. España, con más de 79.363 casos de SIDA declarados, es uno de los países europeos con mayor tasa de incidencia [29].

1.2.1. Composición y estructura de los viriones maduros del VIH

El VIH pertenece a la familia *Retroviridae*, la cual se caracteriza por usar un enzima, denominado transcriptasa inversa, para copiar su ARN en una doble cadena de ADN y poder replicarse. [30, 31] Dentro de la familia *Retroviridae*, el VIH está clasificado como un lentivirus. Los lentivirus son retrovirus exógenos no oncogénicos, generalmente causantes de infecciones crónicas del sistema inmune y del sistema nervioso central. Todos los lentivirus exhiben una morfología y morfogénesis común: los viriones presentan una forma esférica de aproximadamente 110 nm de diámetro y constan de una bicapa lipídica externa que recubre un *core* nucleoproteico que contiene material genético viral.

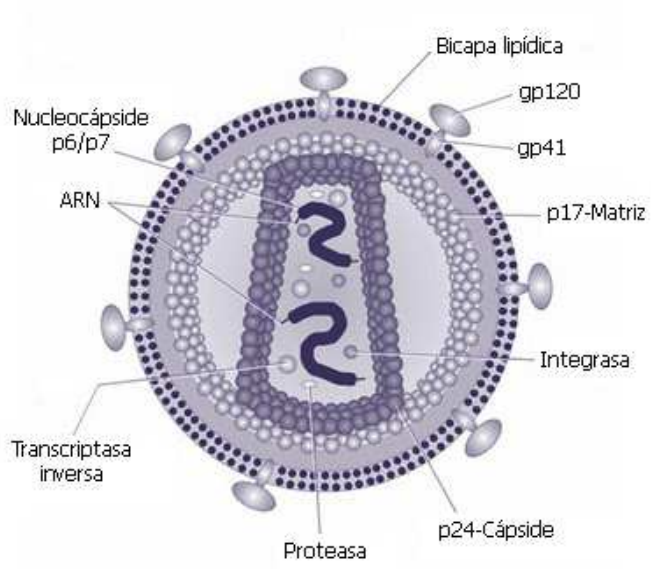

Figura 2. Esquema corte transversal del virus de la inmunodeficiencia humana.

El VIH (figura 2) es un retrovirus que, gracias a la interacción de las glicoproteínas gp120 y gp41 de su membrana con los receptores celulares CD4, penetra en las células del organismo, sobre todo en los linfocitos T CD4. En el interior de las células, la transcriptasa inversa del VIH transcribe el ARN viral a ADN, que se integra en el ADN celular. En dichas células se forman nuevos viriones, para cuya maduración son fundamentales enzimas como las proteasas. Finalmente, las células infectadas se destruyen como consecuencia de la acción patógena del VIH. Dado que los linfocitos T CD4 juegan un papel fundamental en el sistema inmunitario, su pérdida determina la aparición de las infecciones oportunistas y las neoplasias que caracterizan al SIDA [32].

1.2.2. Transmisión del VIH, progresión y tratamiento de la enfermedad

Las principales vías de transmisión del VIH son la sexual, la parenteral y la vertical.

- En la transmisión sexual, la sangre, el semen o el fluido vaginal de una persona VIH positiva entra en el torrente sanguíneo de una persona VIH negativa durante la relación sexual sin protección.
- En la transmisión sanguínea, el virus de una persona VIH positiva entra en el torrente sanguíneo a través de desgarros de la piel o mucosas, durante un accidente laboral, una transfusión o derivados, trasplantes de órganos (riesgo muy disminuido actualmente) o al compartir objetos punzantes.
- En la transmisión vertical el virus de una madre VIH positiva se transmite al bebé durante el embarazo, el parto o la lactancia. La tasa de transmisión materno-infantil ha llegado a suponer entre el 14 y el 35% de las nuevas infecciones. No obstante, a partir del año 1994 se han utilizado fármacos antirretrovirales como la Zidovudina® (AZT) como profilaxis de transmisión vertical, siendo la tasa actual de transmisión vertical en los países desarrollados inferior al 1%.

En la mayoría de los países desarrollados la principal vía de transmisión del VIH es la homosexual. Sin embargo, en España el mecanismo más importante es la adicción a las drogas parenterales. En los países del Tercer Mundo predomina la transmisión heterosexual. El diagnóstico de la infección por el VIH se realiza habitualmente mediante la detección de anticuerpos contra el virus: en primer lugar se emplea un test ELISA, y si es positivo se efectúa un test confirmatorio, generalmente el Western Blot. La infección por el VIH empieza a manifestarse con un síndrome mononucleósico, que coincide con la aparición de anticuerpos contra el virus, pocas semanas después del contagio, aunque en muchos pacientes este cuadro pasa totalmente inadvertido. Seguidamente, los sujetos infectados quedan completamente asintomáticos durante unos 10 años (aunque puede haber grandes variaciones), hasta que la progresiva depleción de linfocitos T CD4 y el deterioro inmunológico que se produce facilitan el desarrollo de las infecciones oportunistas, las neoplasias y otras enfermedades características del SIDA, que finalmente pueden conducir a la muerte.

La profilaxis de determinadas infecciones oportunistas y el adecuado diagnóstico y tratamiento de las enfermedades asociadas, permiten mejorar la calidad de vida y la supervivencia de los sujetos con infección por el VIH. Pero han sido los medicamentos antirretrovirales, activos contra el propio VIH, los que han hecho que mejore sustancialmente el pronóstico de la infección por el VIH en los últimos años.

Los fármacos antirretrovirales disponibles en la actualidad actúan en varias etapas del ciclo vital del VIH y pertenecen a cinco grupos principales:

Inhibidores Nucleósidos/Nucleótidos de Transcriptasa Inversa

El primer grupo de medicamentos antirretrovirales son los Inhibidores Nucleósidos/Nucleótidos de la Transcriptasa Inversa (INTI o INTR). Constituyeron el primer tipo de medicamento disponible para tratar la infección del VIH en 1987. Los INTI (también conocidos como nucleósidos análogos) interfieren con la acción de una proteína del VIH denominada transcriptasa inversa necesaria para que el virus haga nuevas copias de sí mismo. La mayoría de los regímenes contienen al menos dos de estos medicamentos.

Inhibidores No Nucleósidos de la Transcriptasa Inversa

El segundo grupo de medicamentos antirretrovirales son los Inhibidores No Nucleósidos de la Transcriptasa Inversa (INNTI o INNTR), que comenzaron a aprobarse en 1997. Al igual que los INTI, los INNTI (también conocidos como no nucleósidos) detienen la duplicación del VIH dentro de las células inhibiendo la transcriptasa inversa.

Inhibidores de la proteasa

El tercer tipo de antirretrovirales es el grupo de los inhibidores de la proteasa que es otra proteína involucrada en el proceso de duplicación del VIH. El primer inhibidor de la proteasa fue aprobado en 1995.

Inhibidores de la Fusión e Inhibidores de la Entrada

El cuarto grupo de antirretrovirales está compuesto por los inhibidores de la entrada, que incluyen a los inhibidores de la fusión. Los inhibidores de la entrada previenen el ingreso del VIH a las células inmunológicas humanas.

Un inhibidor de la fusión, comúnmente denominado T-20, fue autorizado tanto en los Estados Unidos como en Europa desde 2003, pero sólo para ser utilizado por personas que ya han probado otros tratamientos. El T-20 difiere de los otros antirretrovirales en que necesita ser inyectado (de lo contrario es digerido en el estómago).

En agosto de 2007, un nuevo tipo de inhibidor de la entrada conocido como Maraviroc® fue autorizado en los Estados Unidos. Este nuevo medicamento se conoce como un inhibidor de CCR5 ya que bloquea al correceptor CCR5 en las células inmunológicas humanas, previniendo que el VIH se adhiera a la superficie de las células.

Inhibidores de la integrasa

El grupo final de antirretrovirales consiste en solamente una droga, el Raltegravir®, que fue aprobado en los Estados Unidos en octubre de 2007. Raltegravir® inhibe una enzima denominada integrasa, que el VIH necesita para insertar su material genético en las células humanas.

Para que sean realmente eficaces, estos medicamentos deben emplearse en combinaciones, que se conocen con el nombre de tratamiento antirretroviral de gran actividad (TARGA). Hasta el día de hoy, los mejores resultados se publicaron en febrero de 2011 por un grupo de investigadores del Hospital Clínic de Barcelona que han desarrollado una vacuna basada en técnicas de terapia celular con células dendríticas de los propios pacientes [33].

1.2.3. Péptidos inhibidores del VIH-1

En los últimos años ha aumentado el uso de péptidos sintéticos como agentes terapéuticos del VIH. La principal ventaja de los péptidos sintéticos como agentes terapéuticos es su baja toxicidad y la versatilidad que presentan las secuencias peptídicas a ser modificadas, pudiendo mejorar así su distribución en el organismo y, por tanto, su eficacia.

En la actualidad, el único péptido inhibidor aprobado es el T20 o Enfurtivide®, pero existe un gran número de péptidos que se encuentran en fase preclínica, fase I y fase II de desarrollo. El T20 es un péptido sintético de 36 aminoácidos, derivado de un epítopo conservado de la región HR2 de la glicoproteína gp41 (región 127-162 del HR2 del gp41), que inhibe potentemente la entrada del VIH a la célula mediante su unión competitiva a la región HR1 de la gp41 [34-36] evitando que ésta se una a la región HR2 viral y, por tanto, no se forme la estructura en horquilla trimérica necesaria para la fusión. A pesar de derivar de una región conservada del virus, ya han aparecido mutantes resistentes.

Desde la aparición del T20, han surgido nuevos péptidos inhibidores de la glicoproteína gp41, el T-1249 o Tifuvirtide® y el T-649 [37, 38], análogos del T20, y el péptido C34, que incorpora más aminoácidos de la región N-terminal que el T20.

Todos ellos presentan una actividad antiviral más elevada que la del T20 pero su administración sigue siendo subcutánea y eso trae consigo diferentes reacciones adversas no deseadas que impiden su uso clínico.

Otro péptido derivado del T20 es el C46 pero también han aparecido mutantes resistentes a este inhibidor. [39]

Recientemente se ha demostrado que un péptido aislado de hemofiltrados humanos, denominado VIRIP [40], inhibe la fusión del VIH-1. El VIRIP es un péptido de 20 aminoácidos que inhibe la replicación del VIH a concentraciones inferiores a las del T20, lo que lo convierte en un agente terapéutico muy atractivo. El VIRIP se une al péptido de fusión del VIH-1 inhibiendo la inserción de este en la membrana celular. Además, se ha confirmado que no es tóxico a concentraciones elevadas y que modificaciones de un par de aminoácidos de la secuencia aumenta su actividad antiviral dos órdenes de magnitud.

1.3. GBV-C y VIH

Debido a sus vías de transmisión, GBV-C/HGV está presente en elevada proporción en personas infectadas con el VIH. Hasta un 39% de los individuos positivos para el VIH pueden presentar infección activa por GBV-C/HGV y otro 47% presenta anticuerpos anti-E2 [41].

La viremia del GBV-C/HGV en estos individuos está asociada a una disminución de la mortalidad, una progresión más lenta hacia el desarrollo del SIDA y a una mayor supervivencia de los enfermos una vez que el SIDA se ha desarrollado [42-44]. Por otro lado, la pérdida del GBV-C/HGV, especialmente sin desarrollar anticuerpos anti-E2, conduce a un acelerado avance de la infección por VIH [45, 46].

El primer estudio publicado que evalúa el efecto del GBV-C/HGV en el curso de la infección por VIH fue realizado sobre una cohorte japonesa de 41 pacientes de hemofilia VIH positivos. [47] En este estudio se detectó el GBV-C/HGV en 11 de los 41 pacientes estudiados, esto es un 26.8%. Los pacientes co-infectados tenían niveles de ARN de VIH inferiores y mostraron una progresión más lenta de la enfermedad, así como una mayor supervivencia.

Poco después Heringlake y col. publicaron un estudio donde los pacientes seropositivos co-infectados con GBV-C/HGV presentaban niveles más altos de células T CD4 que los pacientes seropositivos monoinfectados. [48, 49] En otros casos, se ha demostrado que los pacientes co-infectados con una replicación activa del GBV-C/HGV además tienen una mayor calidad de vida y presentan

una mejor respuesta inicial a la terapia antirretroviral. [50] Además, la carga viral en estos pacientes es más baja. [43, 44, 51] Por otro lado, se ha demostrado que la desaparición del GBV-C/HGV en individuos infectados por VIH estaba asociada a una progresión más rápida de la enfermedad. [52]

Esto sugiere que es importante conocer el estado de la infección por GBV-C/HGV en estos pacientes y si se han desarrollado o no anticuerpos contra GBV-C/HGV. Los estudios realizados hasta el momento apuntan a que existe un mecanismo múltiple por el que la infección del GBV-C/HGV mejora la progresión del VIH. Basado en un modelo de co-infección, GBV-C/HGV puede inhibir el VIH induciendo a las quimiocinas, por una regulación decreciente de los co-receptores del VIH, influyendo a las citoquinas o teniendo otros efectos indefinidos sobre los linfocitos huésped [44, 53]. Jung et al. [54] demostraron que células transfectadas con ARN de tipo infeccioso o con un mutante que expresaba el tercer N-terminal de la poliproteína (incluyendo las regiones de codificación E1 y E2) daban lugar a la inhibición de la replicación del VIH, al aumento de la liberación de quimiocinas, y a la disminución de la expresión de CCR5. Esto indica que las proteínas de envoltura pueden estar implicadas en la inhibición de la replicación del VIH.

El mecanismo por el cual se produce esta inhibición todavía no es del todo conocido, lo que sí parece estar claro es la reducción de la progresión de la enfermedad.

1.4. Interacción virus-célula

El primer paso para que se produzca una infección de un virus a una célula, consiste en la unión de las proteínas estructurales del virus con los receptores de membrana específicos de la célula, que pueden ser proteínas, lípidos o carbohidratos. Una vez producida esta unión, la entrada del virus a la célula puede realizarse mediante endocitosis o bien, por fusión de la envoltura viral con la membrana celular [55]. En este segundo mecanismo, la fusión se produce mediante unas glicoproteínas específicas del virus que, al unirse a la membrana celular, cambian su conformación y se convierten en fusogénicas. La región de la proteína que directamente interacciona con la membrana se ha

denominado "péptido de fusión", y es esta región la que desencadena el proceso de entrada en la célula [56]. Los péptidos de fusión de los diferentes virus, tienen características comunes [57]. Además de los denominados péptidos de fusión, existen otras regiones en las glicoproteínas que también intervienen en el proceso de fusión [58-60].

1.4.1. Glicoproteínas de fusión

Se han definido dos tipos de glicoproteínas de fusión:

-Clase I: las glicoproteínas de envoltura del virus se sintetizan como precursores inactivos, los cuales una vez escindidos por proteasas de la célula huésped son activos. La nueva región N-terminal que se forma contiene el péptido de fusión. Las proteínas de envoltura que contienen los péptidos de fusión amino terminales, generalmente presentan estructuras de tipo α-hélice. Se ha descrito que la forma activa de la proteína de fusión es un trímero [61], el cual se coloca perpendicularmente a la membrana celular. La proteína de fusión más estudiada dentro de este grupo es la hemaglutinina del virus de la gripe [62]. También encontramos virus de los géneros retrovirus como es el caso del VIH [63, 64], paramixovirus [65] y filovirus [66].

-Clase II: las proteínas de fusión de clase II, normalmente, no presentan una estructura de α-hélice, teniendo habitualmente una conformación de tipo lámina β [67]. Generalmente, estas proteínas presentan secuencias de fusión internas (péptidos de fusión internos, PFI) que se caracterizan por tener en el centro de la secuencia un residuo de prolina cuya función es importante para que se produzca la fusión [68]. Dentro de este grupo, encontramos varios géneros como el rhabdovirus [69], el flavivirus [70] y el alfavirus [71]. El virus de la hepatitis G pertenece al género flavivirus, pero tiene una estructura similar al virus de la hepatitis C del género hepacivirus, ya que existe una gran homología entre sus proteínas estructurales (E1 y E2) [72].

Los mecanismos de fusión de los dos tipos de proteínas (I y II) son similares a pesar de las diferencias conformacionales que existen entre ellas, ya que en

ambas proteínas la forma activa es un trímero dispuesto perpendicularmente a la membrana lipídica [57].

Los péptidos de fusión suelen estar formados por una secuencia de unos 20 residuos. Los aminoácidos de pequeño tamaño como la alanina y la glicina se encuentran en elevada proporción, lo que confiere a los péptidos de fusión una elevada plasticidad, facilitando de este modo la interacción con las membranas biológicas [73]. Además, contienen una proporción elevada de aminoácidos hidrofóbicos [74]. Los péptidos de fusión se unen a la membrana celular y deshidratan la bicapa externa, consiguiendo reducir la barrera energética al formar un intermediario lipídico más curvado que, finalmente, deriva en la fusión de las dos membranas. Debido a la gran importancia de los péptidos de fusión en la penetración celular, se han realizado muchos estudios con péptidos sintéticos, que corresponden al segmento de fusión del virus, con membranas celulares [75] o bien, con modelos de membrana como son los liposomas [76].

1.5. Membranas biológicas

El modelo de mosaico fluido que describe las membranas lipídicas fue introducido en 1972 por Singer y Nicholson. En este modelo se muestra la bicapa lipídica como un ambiente dinámico y de aspecto líquido que permite el paso de moléculas a través de su estructura.

La membrana está compuesta básicamente de lípidos (fosfolípidos y colesterol) y proteínas. Los lípidos y las proteínas pueden estar conjugados con otros grupos como los carbohidratos. Los fosfolípidos son los lípidos más abundantes en las membranas celulares. Son componentes esenciales dada su capacidad para formar bicapas espontáneamente cuando son dispersados en agua. Este comportamiento se debe a su estructura anfifílica, ya que su molécula consiste en una cabeza polar con un grupo fosfato y una región no polar hidrocarbonada (figura 3). Los fosfolípidos están constituidos por un grupo glicerol que actúa de puente uniendo dos cadenas hidrocarbonadas hidrofóbicas a un grupo hidrófilo conectado por un enlace éster fosfato, que forma la "cabeza polar". Según la clasificación de lípidos adoptada por Small (1986), los fosfolípidos pertenecen al

grupo de anfifílicos de clase II, es decir, son insolubles pero capaces de organizarse en agua para formar fases de cristal líquido.

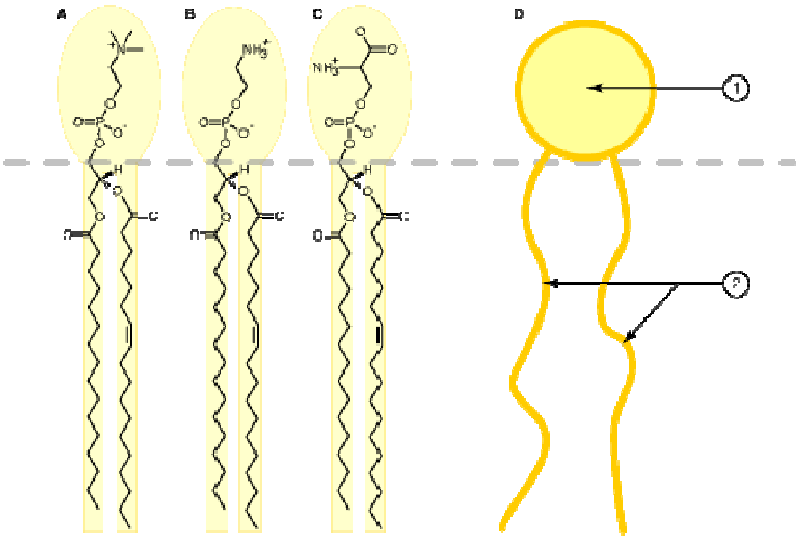

Figura 3. Estructura de algunos de fosfolípidos; A: Fosfatidilcolina, B: fosfatidiletanolamina y C: Fosfatidilserina. D: Representación esquemática de un fosfolípido; 1: Cabeza hidrófila, 2: Colas hidrófobas.

El fosfolípido más utilizado en los estudios de interacciones de membranas es la fosfatidilcolina (phosphatidylcholine, PC), que tiene carácter zwitteriónico y se encuentra presente en las membranas biológicas en elevada proporción. Otros fosfolípidos ampliamente estudiados con carga negativa son el fosfatidilglicerol (phosphatidylglicerol, PG) y la fosfatidilserina (phosphatidylserine, PS), que también se encuentran presentes en la cara interna de las membranas celulares, estando la PS presente en mayor porcentaje [77].

Existen diferentes fosfolípidos según la longitud de la cadena hidrocarbonada. Los fosfolípidos utilizados en este trabajo son de origen sintético. Se ha empleado dimiristoilfosfatidilcolina (DMPC C:14, C:14), zwitteriónico, y dimiristoilfosfatidilglicerol (DMPG C:14, C:14), 1-palmitoil-2-oleoilfosfatidilglicerol (POPG C:16, C:18) y dipalmitoilfosfatidilglicerol (DPPG C:16, C:16), cargados negativamente.

Para determinados estudios se han utilizado fosfolípidos modificados: con bromo, 1,2-di-(9,10-dibromo)-estearoil-sn-glicero-3-fosfocolina y con sondas

fluorescentes como NBD-PE (nitrobenzoxadiazolfosfatidiletanolamina) y Rho-PE (rodamina-fosfatidiletanolamina).

1.5.1. Comportamiento de fase lipídico

Los cambios en las condiciones del medio, especialmente los relacionados con la composición de la mezcla (liotropismo) y la temperatura (termotropismo), dan lugar a una gran variedad de fases en dispersiones de fosfolípidos. Estos cambios afectan tanto a las interacciones entre partículas como a las fuerzas intermoleculares de los agregados, lo que produce cambios de forma y tamaño. La estructura más favorable es la bicapa lipídica, aunque también se forman micelas y fases hexagonales invertidas.

En las membranas biológicas se pueden encontrar diversas fases, pero la fase de cristal líquido fluido ($L\alpha$) es biológicamente la más relevante [78]. A bajas temperaturas, las bicapas lipídicas se presentan en fase gel (L_β). La transición de esta fase (moléculas estrechamente ordenadas) a la fase fluida ($L\alpha$) (mayor libertad de movimiento de las moléculas) tiene lugar a la temperatura de transición (T_m) [79]. Dicha temperatura depende de las características de los constituyentes de la membrana (grado de insaturación, longitud de las cadenas hidrocarbonadas, grupo polar, etc.). Cuando la temperatura excede la T_m, se produce un cierto desorden de las cadenas hidrocarbonadas en el interior de la bicapa y una mayor libertad de movimiento de las moléculas, afectando tanto a la fluidez y la microviscosidad de las bicapas fosfolipídicas, como a la miscibilidad de las diferentes especies lipídicas.

Un adecuado conocimiento de las transiciones de fase y de la fluidez de las membranas de fosfolípidos es importante para la elaboración de agregados fosfolipídicos, ya que determinan las propiedades como la permeabilidad de la membrana, la capacidad de agregación y fusión de las partículas, o la capacidad para incorporar otro tipo de moléculas (tensioactivos, fármacos, péptidos, proteínas, anticuerpos…). Dichas propiedades afectarán en gran medida la estabilidad de los agregados y su comportamiento en los sistemas biológicos.

1.6. Modelos de membrana

1.6.1. Agregados fosfolipídicos

El estado de agregación de los fosfolípidos en dispersión acuosa depende básicamente de la longitud de la cadena de los ácidos grasos que junto con el volumen de la cabeza polar determinan la geometría de las moléculas. Los fosfolípidos con cadenas hidrocarbonadas de 4 átomos de carbono o menos, presentan un estado agregación monomérico; los fosfolípidos con cadenas de 6 a 8 átomos de carbono, y por encima de una concentración determinada, tienden a agregarse de forma micelar; y los fosfolípidos de cadenas más largas presentan un estado de agregación laminar. El estado laminar resulta de la estructuración de los fosfolípidos formando bicapas, de modo que los restos hidrófobos se orientan poniéndose en contacto entre sí y protegidos de las moléculas de agua, mientras que las partes hidrófilas están en contacto con el agua [80].

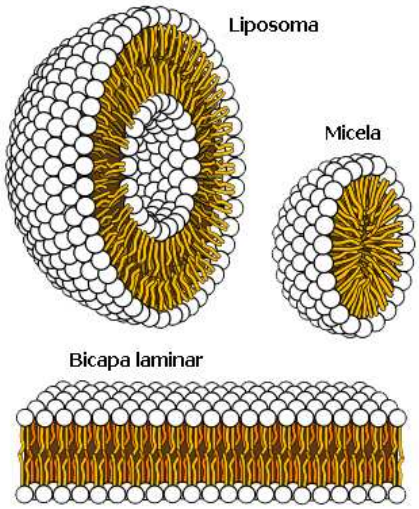

Figura 4. Diferentes estados de agregación de los fosfolípidos en dispersión acuosa.

La formación de esta estructura de bicapa (modelo simple de membrana) que excluye el agua del núcleo hidrofóbico se produce para alcanzar un nivel de energía libre más bajo y por consiguiente una mayor estabilidad para el agregado. La máxima estabilidad se consigue cuando las bicapas se pliegan

para formar vesículas cerradas o liposomas. La figura 4 muestra distintos estados de agregación de los fosfolípidos.

1.6.1.1. Liposomas

Los liposomas son vesículas compuestas principalmente por fosfolípidos ordenados en bicapas. Estas vesículas contienen una fase acuosa interna y están suspendidas en una fase acuosa externa. Se utilizan básicamente como modelos de membrana y también para transportar principios activos. Dependiendo del número de bicapas y del tamaño del liposoma se pueden clasificar de la siguiente manera [77]:

-Liposomas multilamelares (multilamellar vesicles, MLVs): están formados por varias bicapas concéntricas (entre 7 y 10) y su tamaño es muy diverso (de 100 a 1000 nm). La obtención es muy rápida y nos permite estudiar las interacciones entre los fosfolípidos y los péptidos en estudio. En este trabajo se han utilizado en los ensayos de dicroísmo circular y de calorimetría diferencial de barrido (DSC).

- *Liposomas unilamelares gigantes* (giant unilamellar vesicles, GUVs): su tamaño es mayor de 1 μm y son de gran utilidad porque pueden ser observados mediante el microscopio óptico.

- *Liposomas unilamelares grandes* (large unilamellar vesicles, LUVs): su tamaño oscila entre 100 y 500 nm. Estos liposomas se caracterizan por tener una tensión superficial muy similar a la de las membranas celulares (30-32 mN/m). Los liposomas unilamelares son los modelos de membrana más estudiados para intentar comprender las propiedades físicas, químicas y mecanísticas de las membranas biológicas. En esta tesis se han empleado en los estudios de fluorescencia, en ensayos de unión de péptidos a los liposomas y en resonancia de plasmón de superficie.

- *Liposomas unilamelares pequeños* (small unilamellar vesicles, SUVs): tal como su nombre indica son liposomas de tamaño pequeño, entre 15-50 nm. Estos liposomas tienen una mayor curvatura que los LUVs, lo que les confiere una

menor estabilidad. En este trabajo han sido utilizados en técnicas espectrofluorimétricas.

1.6.2. Capas lipídicas monomoleculares

Las capas lipídicas monomoleculares constituyen un modelo de membrana sencillo, muy utilizado para el estudio del comportamiento de los lípidos entre sí o con otras moléculas biológicamente activas. En particular, los experimentos de penetración en monocapas permiten determinar las interacciones existentes entre monocapas lipídicas y péptidos y/o proteínas, proporcionando información que puede ser extrapolable a las interacciones que acontecerían entre estos péptidos o proteínas con bicapas lipídicas, como los liposomas y las membranas celulares.[81]

Las experiencias realizadas en la interfase aire-agua nos informan sobre la flexibilidad y el carácter tensioactivo de las moléculas objeto del estudio. Este modelo de membrana presenta una ventaja destacable sobre los otros existentes, que radica en la posibilidad de controlar de forma sencilla la ordenación de las moléculas, cambiando el área molecular y la presión superficial de la monocapa. Los datos obtenidos a partir de la variación de estas medidas dan una información básica acerca de las interacciones lípido-lípido, lípido-subfase o lípido-molécula activa. [82]

1.6.2.1. Monocapas de adsorción

Los compuestos anfipáticos tienden a situarse en la interfase aire-agua cuando se depositan en una subfase acuosa, formándose una monocapa de adsorción. Esto da lugar a un aumento en la presión superficial o una disminución en la tensión superficial que proporciona la medida de la actividad superficial de la sustancia. Las moléculas que se encuentran en la interfase están en equilibrio dinámico con las moléculas que se encuentran disueltas en la subfase. Según Langmuir [83], las moléculas adsorbidas en la interfase aire-agua se comportan, de alguna manera, como las moléculas de los gases perfectos y adquieren un cierto grado de orientación.

1.6.2.2. Monocapas de extensión

Al extender sobre una solución soporte una sustancia insoluble en él y no volátil (bien depositándola en forma pura o en solución diluida con un disolvente volátil fácilmente eliminable), se forma una película superficial con un espesor equivalente a una molécula, llamada monocapa de extensión.

Para que se extienda bien una monocapa la sustancia tiene que ser anfifílica. Así, los grupos polares se dirigirán hacia la parte acuosa y los grupos apolares se situarán hacia el aire e impedirán que las moléculas difundan hacia la subfase. Al extender un fosfolípido la cabeza polar se dirige hacia la fase acuosa y las cadenas hidrocarbonadas hacia el aire.

La disposición de estas películas monomoleculares es similar a la de las membranas fosfolipídicas, por lo que se utilizan como modelos de membrana.

Una monocapa puede presentar varios estados asemejándose a los tres estados de la materia: sólido, líquido y gas. Al comprimir una monocapa se van mostrando los diferentes estados de ordenación: primero el estado gaseoso, donde las moléculas se encuentran separadas aunque existan interacciones entre ellas. Al comprimir más la monocapa aumentan las fuerzas de Van der Waals y las moléculas se encuentran en estado de líquido expandido (fase fluida bastante compresible) seguido del estado de líquido condensado o también conocido como sólido expandido donde las interacciones atractivas entre las cadenas alquílicas comienzan a ser importantes, induciendo un apilamiento compacto entre ellas y teniendo una compresibilidad bastante baja. Finalmente se llega al estado sólido, donde las moléculas tienen una mayor ordenación molecular y ya no pueden moverse libremente [83]. Para una temperatura constante, si representamos el cambio de la presión superficial (mN/m) respecto al área molecular (nm^2/molécula), obtendremos la isoterma de compresión π-A. En la Figura 5 se representa una isoterma de compresión mostrando los diferentes estados de ordenación posibles.

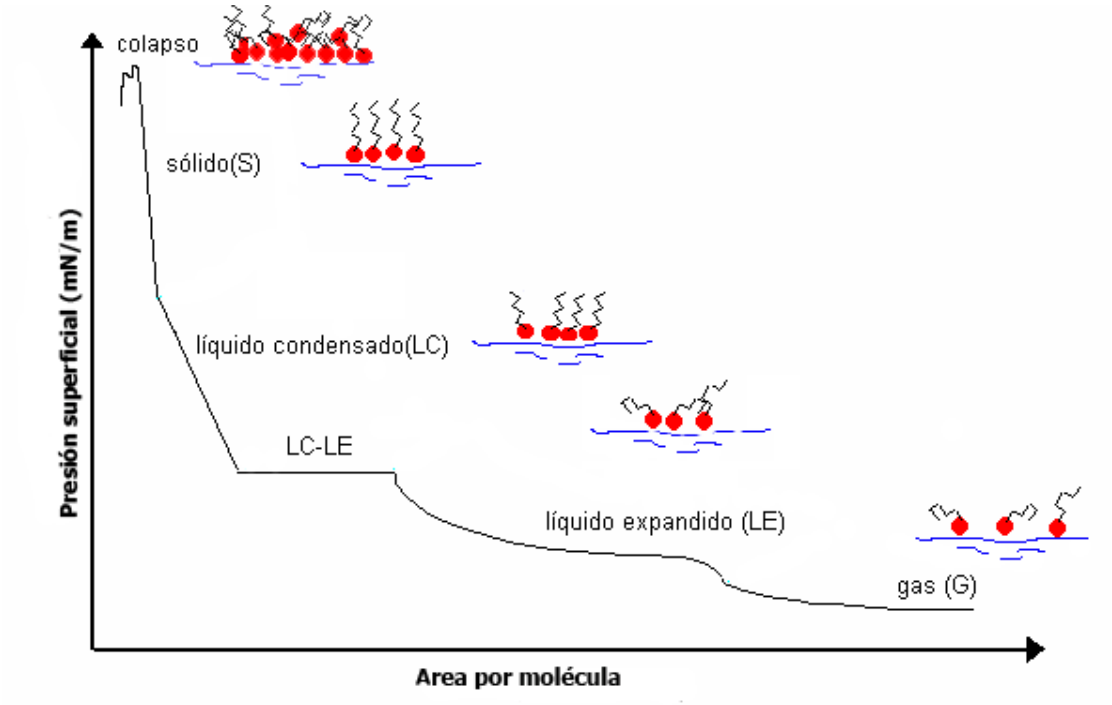

Figura 5. Isoterma de compresión donde se muestran todos los estados que se pueden presentar: estado gaseoso (G), estado de líquido expandido (LE), estado de líquido condensado (LC) y estado sólido (S).

A medida que el área por molécula se reduce, aparece en la isoterma una meseta (*plateau*), región de presión superficial constante, que corresponde a la transición de gas a líquido, en la que coexisten las dos fases. De la misma forma, encontramos otra transición de fase del estado líquido expandido a líquido condensado que suele manifestarse a temperaturas altas y cuando la molécula posee cadenas hidrocarbonadas cortas, desapareciendo a bajas temperaturas y al aumentar la longitud de la cadena.[84]

La estabilidad de una capa monomolecular viene condicionada por la presión de colapso [85] y por la disolución de las moléculas que la constituyen.

Cuando comprimimos una monocapa mediante una barrera móvil, llega un momento en que se produce una expulsión considerable de las moléculas de la misma. Se define la presión de colapso como la mayor presión a la que se puede comprimir una monocapa sin que se produzca una expulsión manifiesta de las moléculas que la componen. El colapso de la monocapa se produce cuando se alcanzan valores de área por molécula muy pequeños, menores al

área física real mínima que ocupa la molécula. En este punto es donde comienza a producirse la formación de multicapas.

Esta clasificación es general y no todas las isotermas de compresión muestran todas las fases indicadas ya que la forma de la isoterma, las fases que se observan y la estabilidad de la monocapa dependen mucho del sistema estudiado y de las condiciones experimentales bajo las cuales se realiza la isoterma, esto es, temperatura, pH de la subfase acuosa, existencia de iones, velocidad de la barrera durante la compresión, etc. [86-89]

1.7. Introducción a las técnicas utilizadas

1.7.1. Síntesis de péptidos en fase sólida

En la presente tesis doctoral se estudian varias secuencias peptídicas pertenecientes a la proteína estructural E1 del virus de la hepatitis G con el fin de seleccionar aquellos péptidos con potencial capacidad de inhibición de la replicación del VIH-1.

Se realiza la síntesis múltiple en paralelo de secuencias peptídicas lineales que cubren la totalidad de la estructura primaria de la proteína E1 del virus GBV-C/HGV (figura 6).

E1(D90600_japan)

ILAPATHACRANGQYFLTNCCAPEDIGFCLEGGCLVALGCTICTD
QCWPLYQAGLAVRPGKSAAQLVGELGSLYGPLSVSAYVAGILGL
GEVYSGVLTVGVALTRRVYPVPNLTCAVACELKWESEFWRWTE
QLASNYWILEYLWKVPFDFWRGVISLTPLLVCVAALLLLEQRIV
MVFLLVTMAGMSQG

Figura 6. Estructura primaria más conservada de la proteína E1 del GBV-C/HGV extraída de la base de d atos del Genbank.

La idea de la síntesis de péptidos en fase sólida (SPPS, del inglés *solid-phase peptide synthesis*) fue descrita por primera vez por Merrifield en 1963 [90] y

hoy en día es la manera más habitual y sencilla de obtener péptidos. Este método se basa en la unión del aminoácido carboxiterminal (C-terminal) a un soporte insoluble y la posterior elongación secuencial, aminoácido tras aminoácido, de la cadena peptídica. El crecimiento de la cadena peptídica tiene lugar siempre por el extremo carboxilo mediante la adición sucesiva de los aminoácidos que tienen tanto el extremo α-amino como las cadenas laterales de los aminoácidos convenientemente protegidos. En este trabajo se ha utilizado la estrategia Fmoc/tBu que emplea el grupo 9-fluorometoxicarbonil (Fmoc) como protector temporal del grupo α-amino y grupos del tipo tert-butil (tBu) para proteger las cadenas laterales de los aminoácidos trifuncionales. Una de las ventajas de la SPPS es la posibilidad de eliminar excesos de reactivos y productos secundarios mediante la filtración y el lavado del polímero que contiene el péptido en crecimiento. Con la adición de excesos de reactivos se pueden obtener rendimientos prácticamente cuantitativos.

Cada adición de aminoácido presenta el mismo ciclo:

- desprotección del grupo Fmoc mediante la adición de una mezcla de dimetilformamida (DMF) que contiene un 20% de piperidina.
- realización de un test de ninhidrina o test de Kaiser [91] para comprobar la presencia de grupos amino libres.
- adición del aminoácido protegido con el grupo Fmoc junto con los reactivos de acoplamiento, 2-(7-aza-1H-benzotriazol-1-il)-1,1,3,3-tetrametiluronio hexafluorofosfato/N,N'-diisopropiletilamina (HATU/DIEA) o diisopropilcarbodiimida/1-hidroxibenzotriazol (DIPCDI/HOBt), en exceso de tres equivalentes.
- lavado y test de ninhidrina para comprobar la incorporación del aminoácido.

Finalizada la síntesis se procede al secado de la resina y al desanclaje del péptido de ésta mediante un tratamiento ácido: ácido trifluoroacético (TFA) en presencia de capturadores tales como agua, etanoditiol (EDT) y triisopropilsilano (TIS). En la Figura 7 se puede observar el esquema de síntesis empleado con la estrategia de protección Fmoc/tBu.

Una vez sintetizados los péptidos, los crudos peptídicos se purifican mediante cromatografía líquida de alta resolución (HPLC). Finalmente, son analizados mediante espectrometría de masas y HPLC a escala analítica.

La síntesis múltiple en paralelo de los péptidos se lleva a cabo utilizando un sintetizador semiautomático (Multisyntech GmbH). Este equipo dispone de un bloque de reacción compuesto de 24 reactores de 5 ml y una válvula de 8 vías que permite la dispensación de hasta 7 disolventes diferentes mediante una jeringa conectada a una bomba. Gracias a una placa dosificadora, los reactivos y los disolventes se distribuyen simultáneamente en los reactores. El equipo dispone de agitación permitiendo la mezcla homogénea de los reactivos así como de una bomba de vacío para la eliminación del exceso de disolventes y reactivos.

Al finalizar la síntesis los péptidos se purifican por cromatografía líquida de alta resolución a escala semipreparativa y se caracterizan por cromatografía líquida de alta resolución a escala analítica y espectrometría de masas para confirmar la presencia del péptido deseado.

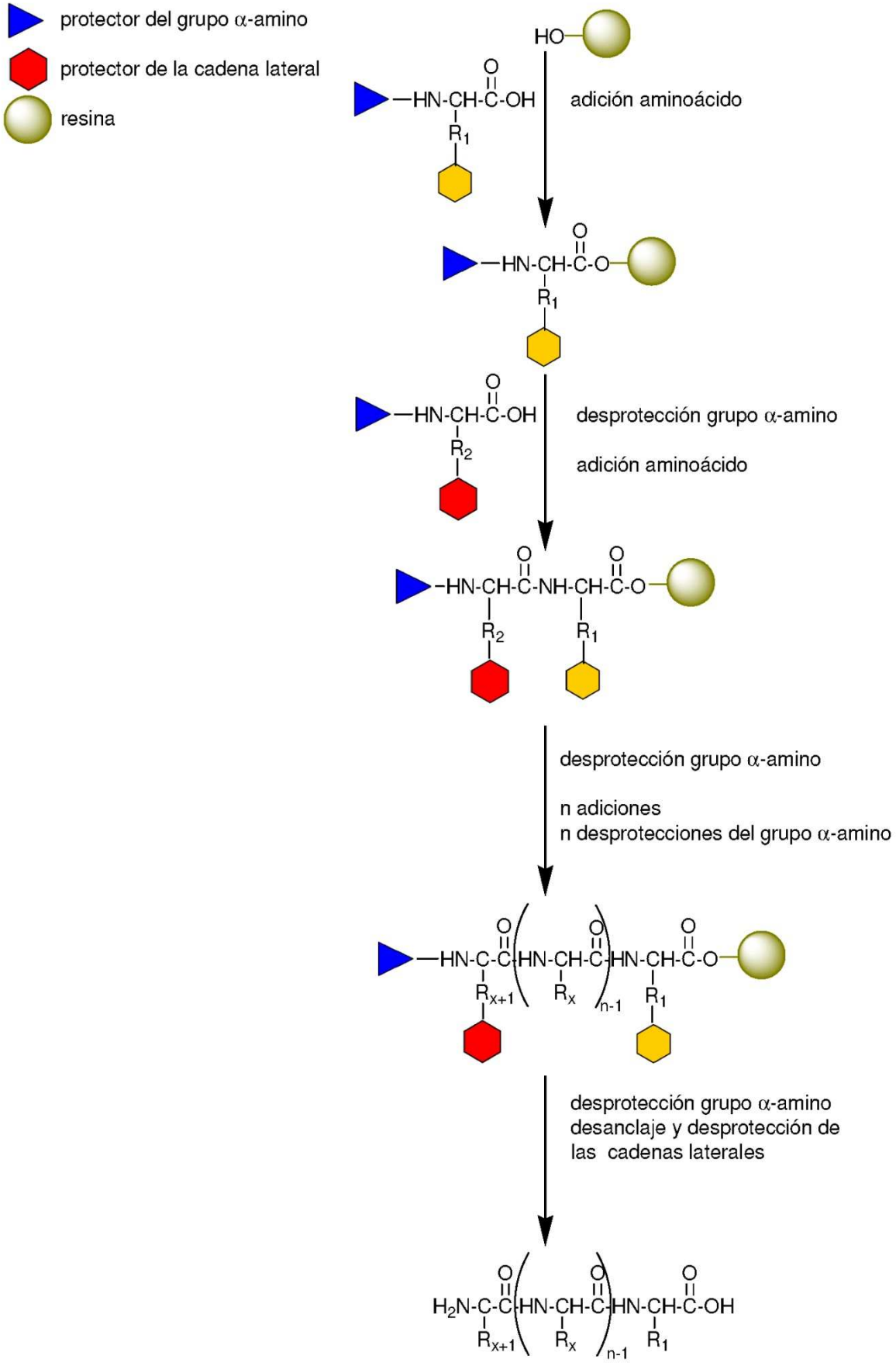

Figura 7. Esquema general de la síntesis en fase sólida

1.7.2. Espectroscopia de fluorescencia

La espectroscopia de fluorescencia es una técnica que permite a caracterizar una molécula con propiedades fluorescentes y conocer las interacciones de ésta con los disolventes del medio, con otras moléculas o con modelos de membrana. Los péptidos son moléculas que pueden contener grupos cromóforos en su estructura, como el anillo aromático del triptófano, de la fenilalanina o de la tirosina. En la presente tesis doctoral, aprovechando la fluorescencia intrínseca de un péptido cuya secuencia contiene triptófano, se analizan los cambios producidos en el entorno de este grupo cromóforo cuando interacciona con modelos de membrana como los liposomas. Asimismo, se mide la capacidad de los péptidos de permeabilizar las vesículas que contienen fluoróforos en su interior, la capacidad de fusionar membranas, o bien la situación de los péptidos en la membrana fosfolipídica.

1.7.2.1. Fluorescencia intrínseca

La fluorescencia intrínseca de los péptidos cambia según el entorno del grupo cromóforo, en nuestro caso el triptófano. El péptido en solución acuosa tiene un espectro definido por la longitud de onda en el máximo del espectro de emisión (λ) y por la intensidad de fluorescencia. [92] El estudio de los péptidos en presencia de liposomas, nos aporta información acerca del cambio en el entorno del triptófano en cada péptido, de forma que si el péptido interacciona con las vesículas fosfolipídicas, el triptófano se encuentra en un entorno más apolar. Este cambio se traduce en un desplazamiento del máximo de emisión a longitudes de onda menores.[93]

1.7.2.2. Liberación de contenidos vesiculares

La capacidad de los péptidos de desestabilizar las membranas fosfolipídicas se puede observar mediante el ensayo de liberación de marcadores fluorescentes. Cuando en el interior de los liposomas se encapsula una sonda fluorescente, Ácido 8-aminonaftaleno-1,3,6-trisulfónico (ANTS), y un apantallador de ésta, Bromuro de N,N'-*p*-xilenobis(piridinio) (DPX), no se produce emisión de fluorescencia. Si el péptido es capaz de desestabilizar la membrana y liberar las

sondas, el efecto de la dilución produce que el apantallador no sea efectivo y, por tanto, incrementa la intensidad de emisión de fluorescencia del ANTS (figura 8). [94]

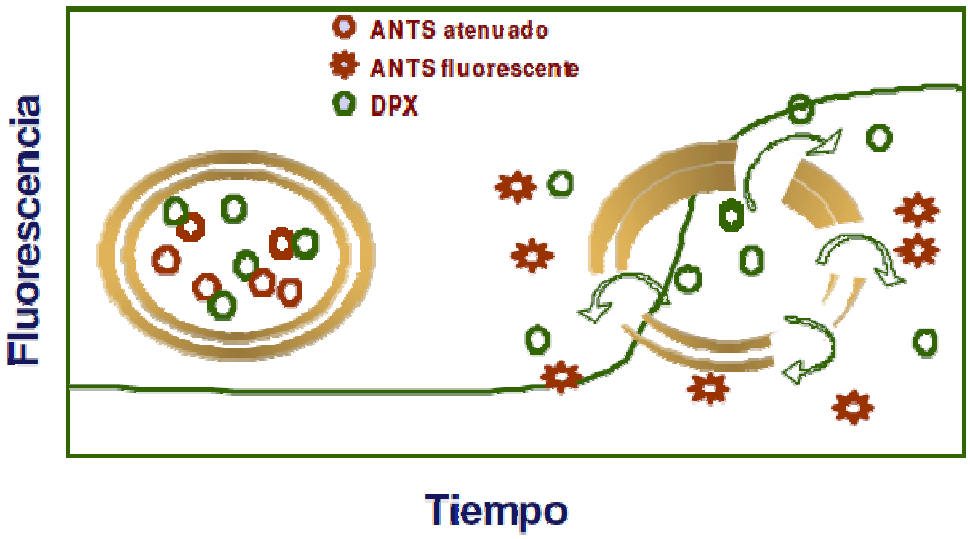

Figura 8. Esquema del ensayo de liberación de contenidos vesiculares

1.7.2.3. Fusión de membranas

La capacidad de un péptido para fusionar membranas se puede medir realizando el ensayo de transferencia de energía por resonancia (*fluorescence resonace energy transfer*, FRET). [95]

En este ensayo se utilizan dos sondas fluorescentes: un donador (NBD-PE) y un aceptor de energía (rodamina, Rho-PE), que forman parte de la composición de la bicapa lipídica (Figura 9). La sonda donadora es excitada y la energía producida de la emisión de fluorescencia sirve para excitar a la sonda aceptora. La eficacia de la transferencia de energía es mayor cuando las sondas se encuentran cercanas y es menor al aumentar la distancia. En el ensayo que se realiza se trabaja con dos poblaciones distintas de liposomas; unos liposomas sin marcar y otros marcados con las sondas fluorescentes. Si el péptido es capaz de fusionar las membranas de las distintas poblaciones, la transferencia de energía es menor y, por lo tanto, se observa un aumento en la emisión de fluorescencia de la sonda donadora.

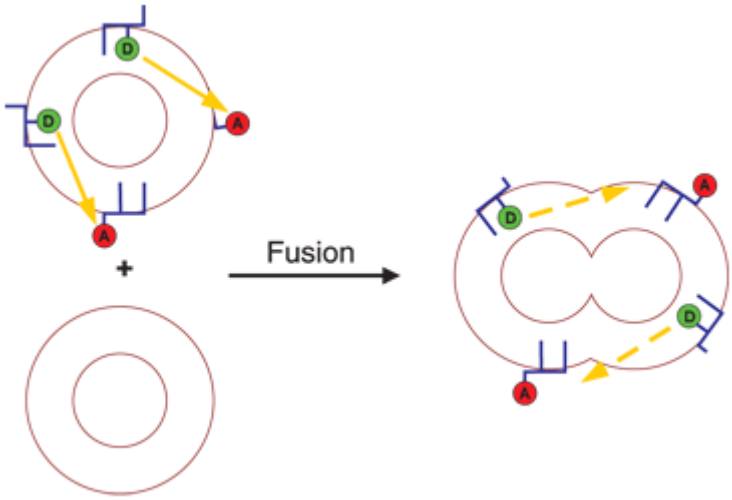

Figura 9. Esquema del ensayo de fusión de membranas basado en la transferencia de energía por resonancia de fluorescencia (FRET)

1.7.2.4. Ensayo de agregación

En este ensayo se estudia la capacidad de los péptidos de agregar liposomas. El efecto de agregación se manifiesta como un aumento en la dispersión de la luz si los dos monocromadores del fluorímetro están a la misma longitud de onda.[96]

1.7.2.5. Anisotropía de fluorescencia

La anisotropía o polarización de fluorescencia refleja la movilidad de las moléculas fluorescentes dentro de la membrana [97] y puede relacionarse con la fluidez del medio.

Al excitar un fluoróforo con luz polarizada, si el fluoróforo permanece inmóvil en el estado excitado, la emisión de fluorescencia estará también altamente polarizada; si por el contrario, el fluoróforo excitado se encuentra en movimiento, la fluorescencia resultante estará menos polarizada. Los fluoróforos empleados en este trabajo para el marcaje de los liposomas han sido el difenilhexatrieno (DPH) y el trimetilamino-difenilhexatrieno (TMA-DPH). El DPH, debido a su carácter hidrofóbico se sitúa específicamente en la zona apolar de los liposomas. [98] Los cambios en la polarización del DPH reflejan cambios en la movilidad de las cadenas hidrocarbonadas de los ácidos grasos [99], permitiendo observar el comportamiento del cambio de fase, de gel a

cristal líquido, y por lo tanto determinar la temperatura de transición. Cuando la bicapa se encuentra en estado gel hay menor movilidad de las bicapas y el DPH tiene menor libertad de movimiento durante el estado excitado, por tanto la polarización que emite es alta. A medida que la temperatura aumenta y se pasa al estado cristal líquido, la movilidad de las bicapas así como la oscilación del DPH también se incrementa, en consecuencia la polarización disminuye. Esta disminución es brusca alrededor de la temperatura de transición. [100] El TMA-DPH es un derivado del DPH con un grupo polar que orienta el fluoróforo paralelo a las cadenas alquílicas de los fosfolípidos, colocándose en la interfase agua/lípido.[101]

1.7.3. Estudios conformacionales

El estudio de la conformación de los péptidos es importante para conocer mejor las características intrínsecas de éstos. Los péptidos de secuencia aminoacídica corta, normalmente no presentan una conformación definida. Sin embargo, si éstos son capaces de unirse a los modelos de membrana en estudio pueden adoptar una conformación más ordenada, probablemente similar a la que se encuentra en la proteína nativa. En los péptidos de fusión se ha descrito que, la conformación adoptada por éstos durante la unión a la membrana celular es muy importante para su actividad fusogénica.

La estructura secundaria, está relacionada con el ordenamiento espacial de los aminoácidos próximos entre sí en la secuencia lineal. Cuando las relaciones estéricas son de naturaleza regular originan una estructura periódica. La hélice α, el giro β y la lámina β son elementos de estructura secundaria. Por el contrario, cuando una proteína o un péptido no tienen una estructura definida se dice que presentan una estructura desordenada o al azar.

1.7.3.1. Dicroísmo circular (CD)

La técnica de dicroísmo circular es una técnica espectroscópica no destructiva destinada al análisis conformacional de moléculas ópticamente activas. Éstas no disponen de un plano de simetría o centro de inversión, no siendo superponibles con su imagen especular. El CD es una de las técnicas más sensibles para la determinación de la conformación de las biomoléculas y la

monitorización de cambios estructurales de éstas. A pesar de que se trata de un método empírico, permite interpretar directamente los cambios en la estructura secundaria de un péptido o de una proteína.

En una proteína o péptido nos podemos encontrar con estructuras desordenadas o "random coil", *α*-hélice, lámina β o giro β (Figura 10).

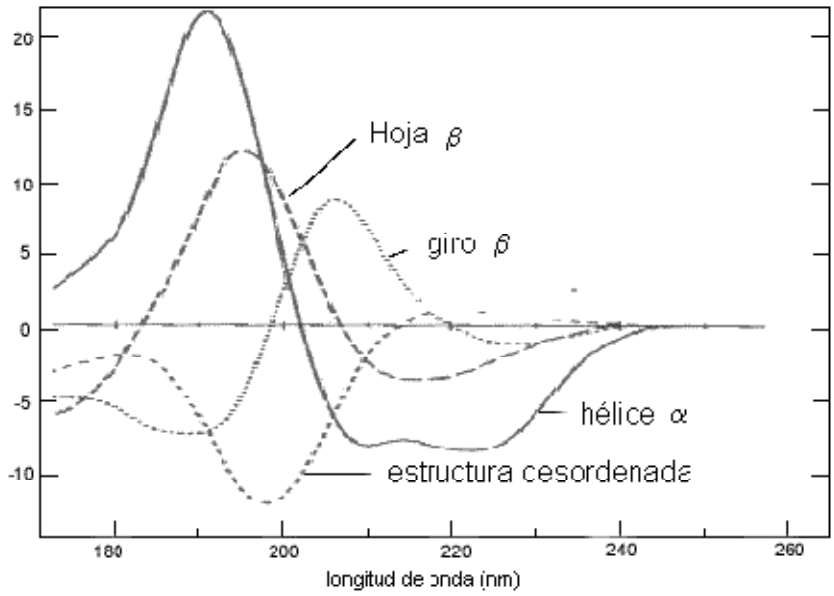

Figura 10. Espectros de dicroísmo circular de las estructuras que se encuentran en proteínas y péptidos.

1.7.4. Calorimetría diferencial de barrido (DSC)

Las bicapas lipídicas compuestas por fosfolípidos manifiestan una transición calorimétrica principal desde una fase en estado de *gel*, a bajas temperaturas, en la cual las cadenas lipídicas se encuentran rígidas y ordenadas, a una fase en estado fluido o de *cristal-líquido* a elevada temperatura, donde las cadenas tienen un mayor movimiento y el espesor de la bicapa es menor. La transición de fase es un proceso endotérmico que puede ser detectado mediante técnicas físicas al variar la temperatura. El estudio de estas transiciones de fase proporciona un método valioso para caracterizar las propiedades del estado fluido, el cual es el más relevante en las membranas biológicas.

La calorimetría diferencial de barrido (differential scanning calorimetry, DSC) es una herramienta fundamental para investigar la transición de fase de los fosfolípidos en modelos de membrana. El comportamiento termotrópico de los

fosfolípidos se ha estudiado ampliamente, y éste determina propiedades tales como la permeabilidad, la fusión, la agregación e, incluso, la unión a proteínas, que afectan a la estabilidad de los liposomas y a su comportamiento en sistemas biológicos. [102-104]

La temperatura de transición (T_m) para un fosfolípido puro tiene un valor característico que aumenta al incrementar la longitud de la cadena hidrocarbonada, dado que las interacciones hidrofóbicas que se producen son mayores. Si la bicapa está formada por fosfolípidos insaturados la temperatura de transición es menor, ya que los enlaces de tipo cis evitan un gran empaquetamiento siendo las interacciones de tipo Van der Waals menores. En las membranas biológicas esta transición de fase es mucho más amplia ya que es más compleja por estar formada por muchos componentes.

En el presente trabajo se estudian modelos de membrana constituidos por fosfolípidos y el efecto producido por los péptidos al interaccionar con éstos.

1.7.5. Microscopía de ángulo de Brewster (BAM)

El estudio de la morfología de las monocapas puede realizarse mediante el microscopio del ángulo de Brewster (*Brewster angle microscopy*, BAM). Se trata de una técnica óptica no invasiva muy utilizada para observar los cambios de fases de las monocapas o la influencia de distintas subfases, entre otras aplicaciones. El principio del ángulo de Brewster se basa en lo siguiente: al incidir un haz de luz no polarizada sobre una superficie transparente cuyo índice de refracción es mayor al del aire, parte de la luz se refracta y parte se refleja con luz parcialmente polarizada.

Si la luz incidente es p-polarizada, con un ángulo de incidencia correspondiente al ángulo de Brewster (θ = 53° para el agua), no hay luz reflejada. Sin embargo, cuando se deposita una monocapa en la interfase, se produce un cambio en el índice de refracción del medio así como del ángulo de Brewster, aumentando la reflectancia (Figura 11). Este aumento en la reflectancia hace que la monocapa pueda visualizarse como una imagen clara, sobre un fondo oscuro que pertenece al agua. [105]

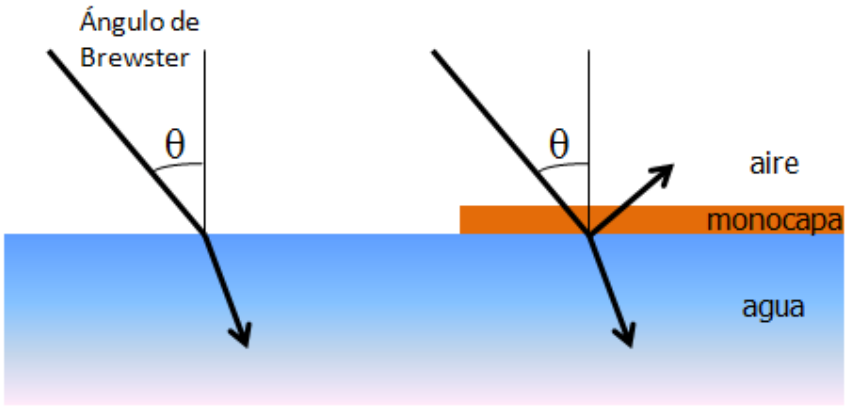

Figura 11. Esquema del cambio en la reflectividad al incidir luz p-polarizada con un ángulo igual al de Brewster en presencia de una monocapa en la interfase aire-agua.

Las monocapas pueden visualizarse *in situ*, y por lo tanto, esta técnica permite determinar mejor las interacciones y la morfología de las moléculas en estudio. La intensidad de cada punto de la imagen del microscopio depende del espesor y de las propiedades ópticas de la monocapa.

En este trabajo se han utilizado dos microscopios: MiniBAM (NFT. Göttigen, Alemania) y MicroBAM3 (NIMA Technology).

1.7.6. Calorimetría isotérmica de titulación (ITC)

La calorimetría isotérmica de titulación (*Isothermal Titration Calorimetry,* ITC) es una técnica analítica ampliamente utilizada en investigación que permite determinar cuantitativamente de manera directa la entalpía de unión de un molécula o de un complejo molecular, en general sencillo, sin necesidad de modelos o hipótesis adicionales, mediante la medida del calor liberado o absorbido a presión constante durante una reacción determinada.[106] Si el efecto térmico neto de la interacción es suficientemente grande, la estequiometria, la entalpía de formación y la constante de unión de estos complejos pueden determinarse, por lo que se puede calcular la energía de Gibbs (ΔG) de formación del complejo así como la entropía (ΔS) del proceso.

1.7.7. Microscopía confocal

La microscopía láser confocal es una técnica de observación microscópica que está logrando excelentes resultados en diversas ramas de la ciencia (medicina, biología, materiales, geología, etc.). Su éxito se debe a las indudables ventajas que ofrece frente a la microscopía óptica tradicional (imágenes de mayor nitidez y contraste, mayor resolución vertical y horizontal, etc.) y, sobre todo, a la posibilidad de obtener "secciones ópticas" de la muestra, lo que permite su estudio tridimensional.

Aunque el principio de la microscopía confocal fue patentado hace varios años [107] y los primeros microscopios basados en esta técnica que demostraron su validez fueron descritos en 1968 [108], su gran aceptación y espectacular desarrollo no ha tenido lugar hasta hace unos pocos años con el desarrollo del láser y de los ordenadores personales.

La mayor parte de las muestras observadas con microscopía óptica son traslúcidas o, en el caso de ser opacas, su superficie de reflexión no se encuentra perfectamente pulida. En ambos casos la luz interacciona con la muestra a varias profundidades por lo que la imagen que llega al observador presenta áreas borrosas debidas a la luz procedente de zonas fuera del plano de enfoque, lo que produce una degradación en el contraste y resolución de la imagen. El principio de la microscopía confocal se basa en eliminar la luz reflejada o fluorescente procedente de los planos fuera de foco. Para ello se ilumina una pequeña zona de la muestra y se toma el haz luminoso que proviene del plano focal, eliminándose los haces procedentes de los planos inferiores y superiores. [109]

La microscopía confocal es muy útil para el estudio de muchos problemas en biología, permitiendo un nuevo conocimiento de la estructura celular y sus procesos. Entre otras aplicaciones la microscopía confocal se utiliza en: estudios de estructura celular y citoesqueleto, medida de actividad intracelular (pH e iones), producción de reconstrucciones tridimensionales, etc. En este trabajo se ha utilizado para visualizar el efecto de los péptidos sobre modelos de membrana, en este caso, liposomas unilamelares gigantes.

1.7.8. Resonancia de plasmón de superficie

La introducción a principios de los años 90 de una nueva tecnología de biosensores basada en el fenómeno de resonancia de plasmón de superficie (SPR, del inglés *surface plasmon resonance*) ha permitido la visualización en tiempo real del proceso de interacción entre biomoléculas. [110-112]

Uno de los instrumentos biosensores más empleados es el modelo BIAcore™ desarrollado por BIACORE AB (Uppsala, Suecia). Se define como biosensor un instrumento que combina, por un lado, un mecanismo biológico y, por el otro, un transductor que genera una señal reconocible en respuesta al proceso biológico. [113] El BIAcore™ utiliza un biosensor basado en la resonancia del plasmón de superficie y el sistema es capaz de monitorizar de forma precisa y en tiempo real la interacción entre una especie unida a la superficie del sensor (ligando) y otra que circula en disolución (analito). [114]

En los últimos años la técnica de SPR se ha utilizado para el estudio de una gran variedad de interacciones, entre las que destacan las interacciones antígeno-anticuerpo y las interacciones de biomoléculas con modelos de membrana, prueba de ello es el gran número de publicaciones aparecidas en los últimos años. [115-118]

El sistema de detección de un instrumento de SPR está compuesto por un sistema óptico y por el chip sensor, en el cual tiene lugar el fenómeno de resonancia del plasmón de superficie y que está formado por un sustrato de vidrio en el que se deposita una lámina de oro de 50 nm de grosor sobre la cual se encuentra una matriz hidrófoba de 100 nm con un 2-3% de dextrano. Esta matriz constituye un medio compatible con las interacciones biomoleculares y permite la inmovilización de gran número de ligandos con bajos niveles de unión específica. El chip sensor forma parte de una unidad de microfluido por la cual circulan las disoluciones que interaccionarán con el ligando unido al chip. El fenómeno de resonancia de plasmón de superficie se produce cuando un haz de luz ilumina la interfase entre dos medios (en este caso vidrio y disolución acuosa) con distinto índice de refracción, entre los que se ha insertado una capa fina de metal (oro). La onda evanescente creada por la reflexión total interna interacciona con los electrones oscilantes o plasmones del metal,

causando una disminución en la intensidad de la luz reflejada. El ángulo de resonancia al que se da este fenómeno es sensible al índice de refracción de la solución próxima al metal. Como la longitud de onda de la luz incidente y el índice de refracción del vidrio y el oro se mantienen constantes, el ángulo de resonancia variará solamente con los cambios en el índice de refracción de la fase acuosa, y estos cambios son debidos a variaciones en la masa al interaccionar las biomoléculas en este medio (figura 12).

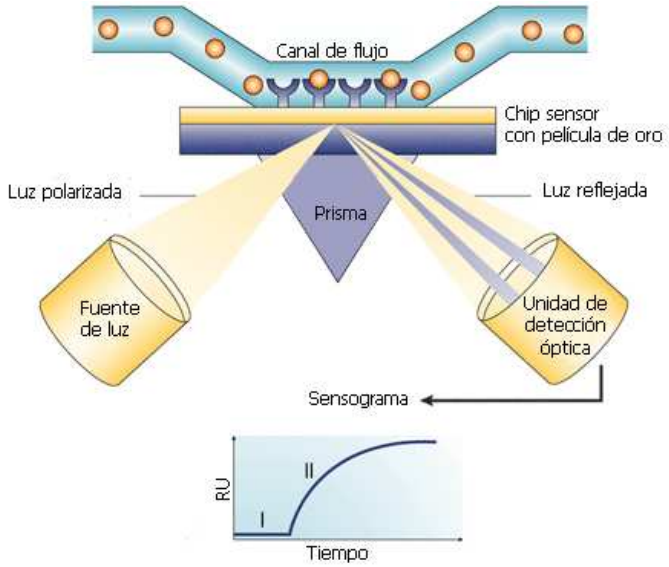

Figura 12. Esquema del modo de detección de un instrumento de resonancia de plasmón de superficie.

Entre las aplicaciones de la técnica de SPR destacan el estudio de identificación de epítopos, la determinación de patrones de interacción en la búsqueda de nuevas moléculas farmacológicamente activas, la determinación de constantes cinéticas de interacción entre biomoléculas [111, 119], los estudios conformacionales [120, 121] y de interacción con modelos de membrana. [122, 123]

1.7.9. Microscopio electrónico de barrido

El Microscopio Electrónico de Barrido (*Scanning Electron* Microscope, SEM) fue concebido en la década de 1930, y las primeras micrografías fueron obtenidas en los años cincuenta. Pero no fue hasta 1965 cuando el primer SEM comercial,

el Stereoscan, fue puesto en el mercado por la Universidad de Cambridge, en Inglaterra. Desde esa época hasta hoy, gracias a la continua investigación y desarrollo, la Óptica Electrónica permite observar cualquier tipo de espécimen con gran detalle y calidad de imagen, constituyéndose así el SEM en una herramienta de gran utilidad en el estudio de los materiales.

El SEM es un instrumento que emplea el bombardeo de un haz de electrones acelerados hasta una longitud de onda cien mil veces menor a la de la luz blanca (~500 nm), y condensados por lentes electromagnéticas. Así, debido a la generación de señales originadas por el impacto de electrones con la muestra, se obtiene una imagen.

Las principales características del SEM es su gran profundidad de campo, la cual permite que se enfoque a la vez una gran parte de la muestra. También produce imágenes de alta resolución. La preparación de las muestras es relativamente fácil pues la mayoría de SEMs sólo requieren que estas sean conductoras.

1.7.10. Microscopio de fuerzas atómicas

El microscopio de fuerzas atómicas (*Atomic Force Microscope*, AFM) se ha convertido en uno de los microscopios más utilizados de manera rutinaria para la obtención de imágenes con resolución atómica. [124]

La sonda del AFM detecta la topografía de la superficie por diferencias en la fuerza atómica (atracción y repulsión). Esta técnica se fundamenta en la medida de las fuerzas de interacción entre una punta muy afilada dispuesta en el extremo de una palanca flexible y la superficie de la muestra, mediante realización de una serie de rastreos horizontales. La muestra se deposita en un soporte sólido, que debe tener una elevada afinidad por la muestra.

El estudio por AFM de las películas de Langmuir-Blodgett (películas formadas en la interfase aire-agua y transferidas a un sustrato sólido a una presión superficial determinada) ha suscitado gran interés a causa de sus posibles aplicaciones tecnológicas. [125] En particular, el hecho de ser utilizadas como modelos de membrana y mediante el empleo del AFM ha permitido estudiar la morfología de las películas con una resolución en el rango de nanómetros,

además de poder observar el orden superficial de las películas y el límite de los dominios existentes [126], así como la separación de fases en sistemas multicomponentes. [127]

El modo de operación conocido como Modo Tapping (*Tapping mode*)[128] se ha utilizado ampliamente para la observación de muestras frágiles, blandas o que se verían dañadas de manera irreversible con otros modos de operación del AFM. En este modo de operación la punta tiene un contacto intermitente con la superficie de la muestra en cada ciclo, de manera que las fuerzas laterales que pueden dañar la muestra son mucho menores que en el modo de contacto. Por esto, el modo *tapping* es el más utilizado actualmente en la microscopía de fuerza atómica de muestras biológicas. [129]

1.7.11. Ensayos de hemólisis

El efecto de una sustancia hemolítica en contacto con glóbulos rojos produce un aumento en la absorbancia debido a la liberación de la hemoglobina. [130-132] Dado que se ha descrito que los péptidos fusogénicos tienen la capacidad de producir hemólisis [76], mediante este ensayo se puede medir la capacidad hemolítica de las secuencias sintetizadas.

1.7.12. Ensayos de citotoxicidad

El valor predictivo de las pruebas de citotoxicidad *in vitro* se basa en la idea de que productos químicos tóxicos afectan a funciones básicas de las células que son comunes a todas ellas, y la toxicidad se mide mediante la evaluación del daño celular. El desarrollo de ensayos de citotoxicidad *in vitro* ha sido impulsado por la necesidad de evaluar rápidamente la toxicidad de un gran número de compuestos, para limitar la experimentación con animales siempre que sea posible, y para poder llevar a cabo pruebas con pequeñas cantidades de compuesto. [133-135]

La evidente utilidad de los test de citotoxicidad ha llevado a muchas compañías farmacéuticas a examinar grandes bibliotecas de compuestos con el fin de eliminar compuestos potencialmente tóxicos en los inicios de los procesos de *drug discovery.*

Los ensayos de citotoxicidad se realizaron mediante el reactivo WST-1 (sales de tetrazolium / formazán) que permite analizar de una forma directa la viabilidad celular. Se trata de un ensayo colorimétrico, de cuantificación espectrofotométrica que se basa en la degradación de las sales de tetrazolium WST-1 a sales de formazán, mediante la acción de las deshidrogenadas mitocondriales, que se producen de forma natural cuando las células son viables. Esta técnica es sensible, rápida y sencilla cuando la comparamos con otras técnicas de medida de la proliferación celular.

2. Objetivos

La hipótesis de partida de este trabajo es la posible utilización de péptidos sintéticos el GBV-C/HGV en el diseño de inhibidores de la entrada del VIH en la célula huésped. Se pretende así contribuir a un mejor conocimiento del efecto del GBV-C/HGV en la progresión de la enfermedad causada por el VIH y de la interacción entre estos dos virus.

El objetivo principal de esta tesis doctoral consiste en diseñar y sintetizar péptidos derivados de la proteína E1 del GBV-C/HGV con la finalidad de estudiar la implicación de esta proteína en la inhibición de la infección por el VIH.

Los objetivos concretos son los siguientes:

1. Sintetizar, purificar y caracterizar dominios peptídicos de la proteína E1 del GBV-C/HGV.
2. Seleccionar péptidos del GBV-C/HGV capaces de inhibir la entrada del VIH-1 mediante:
   2.1. algoritmos teóricos de predicción.
   2.2. métodos biofísicos.
3. Estudiar la capacidad de los péptidos sintetizados de inhibir la actividad del péptido de fusión (PF) del VIH-1 en presencia de modelos de membrana como monocapas de extensión y liposomas. Utilizando con estos últimos técnicas como: DSC (Calorimetría diferencial de barrido), fluorescencia (espectroscopia de fluorescencia o microscopía confocal) o resonancia de plasmón de superficie.
4. Caracterizar la interacción entre el péptido de fusión del VIH-1 y aquellos péptidos del GBV-C/HGV previamente seleccionados como potenciales inhibidores mediante técnicas calorimétricas (ITC, Calorimetría Isotérmica de Titulación), estudios conformacionales (dicroísmo circular), o microscopia de fuerza atómica (AFM).

Los objetivos propuestos en la presente tesis se han logrado mediante las investigaciones publicadas en los artículos de la sección 3 (Resultados). En los artículos 1 y 2 se seleccionó un epítopo de la proteína E1 del GBV-C/HGV mediante algoritmos teóricos de predicción y se estudió su capacidad de interaccionar con modelos de membrana, tanto con liposomas como con monocapas de extensión. A continuación se sintetizaron el resto de secuencias pertenecientes a la proteína E1 y se seleccionaron aquellos posibles péptidos capaces de inhibir la actividad del péptido de fusión del VIH-1 mediante métodos biofísicos (artículo 3) y se estudió la capacidad de inhibición de dichos péptidos utilizando liposomas como modelos de membrana, así como el tipo de interacción entre estos péptidos y el péptido de fusión del VIH-1 y su capacidad hemolítica y citotóxica (artículos 3 y 4). Finalmente se estudió su capacidad de inhibición utilizando monocapas de extensión como modelos de membrana (artículos 5 y 6).

A continuación se exponen dichos artículos íntegros con un breve resumen en castellano.

3. Resultados

Los resultados de la presente tesis están reflejados en los siguientes artículos científicos, los cuales se presentan a continuación acompañados con un breve resumen en castellano.

Artículo 1. M.J. Sánchez-Martín, I. Haro, M.A. Alsina, M.A. Busquets and M. Pujol, A Langmuir Monolayer Study of the Interaction of E1(145-162) Hepatitis G Virus Peptide with Phospholipid Membranes, *The Journal of Physical Chemistry B*, 114 (2010) 448-456.

Artículo 2. M.J. Sánchez-Martín, J. Amigo, M. Pujol, I. Haro, M.A. Alsina and M.A. Busquets, Fluorescence study of the dynamic interaction between E1(145–162) sequence of hepatitis GB virus C and liposomes, *Analytical and bioanalytical chemistry*, 394 (2009) 1003-1010.

Artículo 3. M.J. Sánchez-Martín, K. Hristova, M. Pujol, M.J. Gómara, I. Haro, M. Asunción Alsina, M. Antònia Busquets, Analysis of HIV-1 fusion peptide inhibition by synthetic peptides from E1 protein of GB virus C, *Journal of Colloid and Interface Science* 360 (2011) 124-131.

Artículo 4. M.J. Sánchez-Martín, P. Urbán, M. Pujol, I. Haro, M.A. Alsina and M.A. Busquets, Biophysical investigations of GBV-C E1 peptides as potential inhibitors of HIV-FP, *ChemPhysChem* – en revisión.

Artículo 5. M.J Sánchez-Martín, M.A. Busquets, V. Girona, I. Haro, M.A. Alsina and M. Pujol, Effect of E1(64-81) hepatitis G peptide on the *in vitro* interaction of HIV-1 Fusion Peptide with membrane models, *Biochimica et biophysica acta*, In Press, Accepted Manuscript.

Artículo 6. M.J Sánchez-Martín, M.A. Busquets, I. Haro, M.A. Alsina and M. Pujol, Physicochemical characterization of GBV-C E1 peptides as potential inhibitors of HIV-1 Fusion Peptide: Interaction with model membranes, *Colloids and surfaces B* – en revisión.

3.1. Artículo 1. A Langmuir Monolayer Study of the Interaction of E1(145-162) Hepatitis G Virus Peptide with Phospholipid Membranes

Se seleccionó un epítopo correspondiente a la proteína estructural E1 del virus GBV-C/HGV situado en la región 145-162 a partir de los perfiles de hidrofilicidad y accesibilidad de las proteínas de acuerdo con Janin, Hoop & Woods y Fraga consideradas buenas escalas para predecir sitios antigénicos en proteínas. La secuencia E1(145-162) mostró unos perfiles adecuados como posible sitio antigénico. Para profundizar en la interacción de este péptido con la membrana lipídica, en este trabajo, se muestra un estudio detallado sobre las propiedades superficiales del péptido, su miscibilidad y el comportamiento de monocapas mixtas de E1(145-162) y tres fosfolípidos: dimiristoilfosfatidilglicerol (DMPG), dimiristoilfosfatidilcolina (DMPC) y palmitoil-oleil-fosfatidilglicerol (POPG). Estos estudios se llevaron a cabo usando la balanza de Langmuir mediante estudios de adsorción superficial, isotermas de compresión (π-*A*) y cinéticas de penetración. El microscopio de ángulo de Brewster (BAM) se utilizó para estudiar las propiedades morfológicas del péptido puro y de las monocapas mixtas. El péptido muestra actividad superficial dependiente de la concentración cuando se inyecta bajo un solución tamponada (HEPES/NaCl, pH 7.4). Esta tendencia a acumularse en la interfase aire/agua confirma su potencial capacidad de interaccionar con membranas; la mayor penetración del péptido en fosfolípidos se obtiene cuando las monocapas se encuentran en estado líquido expandido y los lípidos están cargados negativamente, probablemente debida a la interacción de esta carga con la carga global positiva del péptido. Los valores de área por molécula obtenidos sugieren que la principal estructura del péptido E1(145-162) es hélice-α en la interfase aire/agua, lo cual corrobora las predicciones mediante cálculos computacionales. Los estudios de miscibilidad indican que las mezclas están termodinámicamente favorecidas a bajas fracciones molares del péptido.

A Langmuir Monolayer Study of the Interaction of E1(145−162) Hepatitis G Virus Peptide with Phospholipid Membranes

Maria Jesús Sánchez-Martín,*,† Isabel Haro,‡ M. Asunción Alsina,† M. Antonia Busquets,† and Montserrat Pujol†

Physical Chemistry Department and Institute of Nanoscience and Nanotechnology, University of Barcelona, Av. Joan XXIII s/n, 08028 Barcelona, Spain, and Unit of Synthesis and Biomedical Application of Peptides, Department of Biomedical Chemistry, IQAC-CSIC, Jordi Girona 18, 08034 Barcelona, Spain

Received: July 21, 2009; Revised Manuscript Received: October 16, 2009

E1(145−162), a peptide corresponding to the structural protein E1 of the GB virus C, has been shown earlier to bind at pH 7.4 to vesicles containing 1,2-dimyiristoyl-*sn*-glycero-3-phospho-rac-(1-glycerol)] (DMPG) and 1,2-dimyiristoyl-*sn*-glycero-3-phosphocholine (DMPC) phospholipids. To deepen the understanding of the interaction of E1(145−162) with the lipid membrane, in this paper, we report a detailed study of the surface properties of peptide, miscibility properties, and behavior of mixed monomolecular films of it and three phospholipids DMPG, DMPC, and 1-palmitoyl-2-oleoyl-*sn*-glycero-3-phosphocholine (POPG). These studies were performed using the Langmuir balance by means of surface adsorption studies, surface pressure−mean molecular area compression isotherms, and penetration kinetics. The Brewster angle microscopy (BAM) was used to study the morphological properties of pure peptide and the mixed monolayers. The results show us that the peptide showed surface activity concentration dependent when injected beneath a buffered solution (HEPES/NaCl, pH 7.4). This tendency to accumulate into the air/water interface confirms its potential capacity to interact with membranes; the higher penetration of peptide into phospholipids is attained when the monolayers are in the liquid expanded state and the lipids are charged negatively maybe due to its negative electric charge that interacts with the positive global charge of the peptide sequence. The area per molecule values obtained suggested that the main arrangement structure for E1(145−162) peptide is the α-helical at the air−water interface that agreed with computational prediction calculations. Miscibility studies indicated that mixtures become thermodynamically favored at low peptide molar fraction.

1. Introduction

Hepatitis G virus (HGV/GBV-C) has been investigated in the context of Human Immunodeficiency Virus (HIV) infection, since recent studies have suggested that HGV/GBV-C infection in HIV-positive people is associated with prolonged survival[1] and the patients often die from liver failure instead of AIDS. Moreover, people coinfected with HIV and GBV-C/HGV have delayed progression of HIV disease,[2] indicating a beneficial influence of GBV-C on HIV infection, but the definitive mechanism of how GBV-C/HGV could inhibit the progression to AIDS is at present unknown.[3]

HGV/GBV-C virus was initially thought to be another hepatitis virus, but which has more recently been shown incapable of replicating in hepatocytes or of causing acute or chronic hepatic diseases, exerts beneficial effects on HIV infection.[4] These properties make GB virus C attractive for immunology studies. Given that GBV-HGV is an enveloped RNA virus similar to HIV and Hepatitis B virus, we hypothesize that, like those viruses, capside assembly is crucial for viral infection.[5] Thus, the study of peptides from capside proteins may help us to understand the mechanism of viral infection which takes place. We are currently examining the capacity of GBV-C/HGV synthetic peptides to interact and induce fusion in model membranes. The ability of E1(145−162) synthetic peptide from the exposed E1 structural protein of GBV-C/HGV to induce perturbations in a bilayer model was investigated in a previous work.[6] In this paper, we investigate the surface properties of E1(145−162) and computational prediction calculations are made in order to predict the structure of the peptide and to get an idea of its antigenicity. Moreover, the physicochemical characterization of the peptide sequence is done by studying its interaction with model membranes; lipopeptide interactions with lipid monolayers of the zwitterionic 1,2-dimyiristoyl-*sn*-glycero-3-phosphocholine (DMPC) and the negative 1,2-dimyiristoyl-*sn*-glycero-3-[phospho-rac-(1-glycerol)] (DMPG) and 1-palmitoyl-2-oleoyl-*sn*-glycero-3-phosphocholine (POPG) are studied. As can be seen, phospholipids have either choline (PC) or phosphatidylglycerol (PG) polar heads and have hydrocarbon chains that differ in length and saturation degree; these differences allowed the study of the lipid structure influence on E1(145−162) membrane interaction. In addition, Langmuir monolayers were examined by Brewster angle microscopy (BAM).

The information obtained with monolayer studies is useful to better understand the spontaneous mechanism by which hepatitis G peptides interact with membrane lipids. Thus, the structure of peptides and lipids, the penetration, and the thermodynamic parameters of the peptide−lipid binary systems are of great importance to know if E1(145−162) is a good candidate to assay in the following studies to design immunopeptides for antiviral therapies.

* Corresponding author. E-mail: mjesus_sanchez@hotmail.com. Phone: +34 93 402 45 58. Fax: +34 93 403 59 87.
† University of Barcelona.
‡ IQAC-CSIC.

10.1021/jp906900k
Published on Web 12/11/2009

2. Experimental Section

2.1. Materials. Amino acids and Rink amide resin (Tentagel R RAM, 0.19 mequiv/g) were obtained from Novabiochem (Nottingham, U.K.). Dimethylformamide (DMF) was purchased from Scharlau (Barcelona, Spain). Dichloromethane (DCM) and piperidine were purchased from Fluka (Neu-Ulm, Germany). Washing solvents such as acetic acid, diethyl ether, and trifluoroacetic acid (TFA) were obtained from Merck (Poole, Dorset, U.K.). *N*-Hydroxybenzotriazole (HOBt) and *N*,*N*′-diisopropylcarbodiimide (DIPCDI) coupling reagents were obtained from Fluka and Novabiochem, respectively. Other coupling reagents such as *O*-(7-azabenzotriazole-1-yl)-*N*,*N*,*N*′,*N*′-tetramethyluronium hexafluorophosphate (HATU) and *N*,*N*′-diisopropylethylenamine (DEIA) were obtained from GenScript Corporation and Fluka, respectively. Scavengers such as ethanedithiol (EDT) or triisopropylsilane (TIS) were from Sigma-Aldrich. 1,2-Dimyiristoyl-*sn*-glycero-3-phosphocholine (DMPC), 1,2-dimyiristoyl-*sn*-glycero-3-[phospho-*rac*-(1-glycerol)] (DMPG), and 1-palmitoyl-2-oleoyl-*sn*-glycero-3-phosphocholine (POPG) were purchased from Avanti Polar Lipids. Their purity was higher than 99%, and they were used without further purification.

Chloroform and methanol were purchased from Merck. Water was double distilled and deionized (Milli-Q system, Millipore) (18.2 MΩ cm, pH 5.8). The buffer in all experiments was 5 mM HEPES (from Sigma-Aldrich) and 20 mM NaCl (from Merck), pH 7.4.

E1(145−162) was synthesized by solid phase methodology and purified by reverse phase chromatography as described in previous work.[6] The primary amino acid sequence is WKVPFD-FWRGVISLTPLL.

2.2. Methods. Experimental measurements were recorded with a NIMA Langmuir film balance equipped with a Wilhelmy platinum plate (Nima Technology, Coventry) and a Teflon trough that was rinsed with ethanol and distilled water before use. All experiments were performed at room temperature.

2.2.1. Surface Activity of the Peptide. The surface activity of peptide was first studied to determine the equilibrium spreading pressure. Using a cylindrical PTFE trough (19.6 cm^2, 27.2 cm^3), increasing volumes of a 0.460 mM peptide solution in acetonitrile/H_2O were injected below the HEPES subphase (pH 7.4) through a lateral hole and the adsorption of the peptide at the air/water interface was therefore monitored by following the increase in surface pressure as a function of time under continuous stirring of the subphase.

2.2.2. Insertion of Peptide into Monolayers. The kinetics of insertion of E1(145−162) into monolayers of DMPC, DMPG, and POPG were measured using the same trough as for the surface activity. For these experiments, a 0.5 mg/mL lipid stock solution was prepared and added dropwise on the subphase until the desired lipid pressure was achieved. After 10−20 min, the equilibrium of the lipid monolayer was reached. Then, a 0.070 mM E1(145−162) solution was injected into the subphase through the side hole of the trough. The subphase was magnetically stirred during the measurements, and surface pressure changes were monitored as a function of time until it remained constant.

2.2.3. Surface Pressure−Mean Molecular Area Compression Isotherms. Compression isotherms were carried out on a Nima (U.K.) Langmuir Teflon trough (surface area 595 cm^2, volume 297.5 cm^3). By mixing appropriate volumes of chloroform stock solutions of phospholipids (0.7 mM) and of the peptide (0.7 mM), the lipid−peptide spreading solutions were obtained. Monolayers were formed by applying small drops of the spreading solutions on the HEPES subphase (pH 7.4) with a microsyringe (Hamilton Co., Reno, NV). After 15 min, monolayers of the desired composition were continuously compressed with an area reduction rate of 20 cm^2 min^{-1}. The films were compressed to their collapse pressure when possible. Each run was repeated three times, and the reproducibility was ±1 $Å^2$ $molecule^{-1}$.

2.2.4. Brewster Angle Microscopy. Brewster angle microscopy images were obtained on a MiniBam instrument (NFT, Göttigen, Germany) mounted on a Nima Langmuir balance trough. The instrument was equipped with a 30 mW laser emitting p-polarized light at 660 nm, which incises the air−water interface at 53.1° (Brewster angle). The shutter speed used was 1/50 s. All of the images were taken at room temperature.

2.2.5. Computational Calculations. Using the software disposable at http://www.expasy.ch/tools/, computerized prediction of antigenicity has been made after analyzing the hydrophilicity and accessibility profiles of the proteins according to Janin,[7] Hopp and Woods,[8] and Fraga.[9] Computational prediction calculations of the peptide 3D structure are made using the Phyre Prediction server.[10]

3. Results and Discussion

3.1. Peptide Antigenicity Analysis. The hydrophilicity and accessibility profiles of the proteins according to Janin,[7] Hopp and Woods,[8] and Fraga[9] have been considered as good predictors for defining antigenic sites within proteins.

The sequence E1(145−162) showed theoretically suitable antigenicity and accessibility profiles. Figure 1 shows the hydrophilicity, accessibility, and recognition factor plots of E1 protein, indicating with a dotted line where the sequence (145−162) is located.

3.2. Computational Prediction of Structure. The PDB code of the template structure is 1LN6. Figure 2a shows the 3D model of the peptide in tube representation and surface representation. The tube representation is colored by the secondary structure consensus represented in Figure 2b. According to multiple predictions, the WKVP motif has another structure other than the FDFWRGVISLTPLL part of the peptide. The second is likely to have a helical structure. In Figure 2b, predictions of the secondary structure are shown. Different methods where used (DSC, HNNC, MLRC, PHD, Predator) in order to obtain a consensus of the prediction (Sec.Cons.).[11] The consensus describes the majority of the peptide as a helix, but some methods predict the peptide as a coil. These results match with the 3D predicted structure that is a mixture between a coil and a helix. Despite these results, one has to bear in mind that in silico prediction methods were trained on available 3D protein structures. It was hardly possible to find a homologue for this small peptide in the PDB. Thus, the predictions made here have to be handled with care and might only be used as indicators; thus, the peptide might fold in a helical/coiled structure.

3.3. Peptide Surface Studies. ***3.3.1. Adsorption Kinetics.*** Figure 3a shows the kinetic adsorption process for the incorporation of E1(145−162) into the air/water interface at different peptide concentration in the subphase. A small gradual adsorption of peptide was observed at low peptide concentration. The higher the peptide concentration in the subphase, the faster the incorporation process and the higher the surface pressure attained. Figure 3b shows the adsorption isotherm profile for E1(145−162); the equilibrium pressure was achieved around 0.5 μM of the peptide in the subphase. The shape of the surface

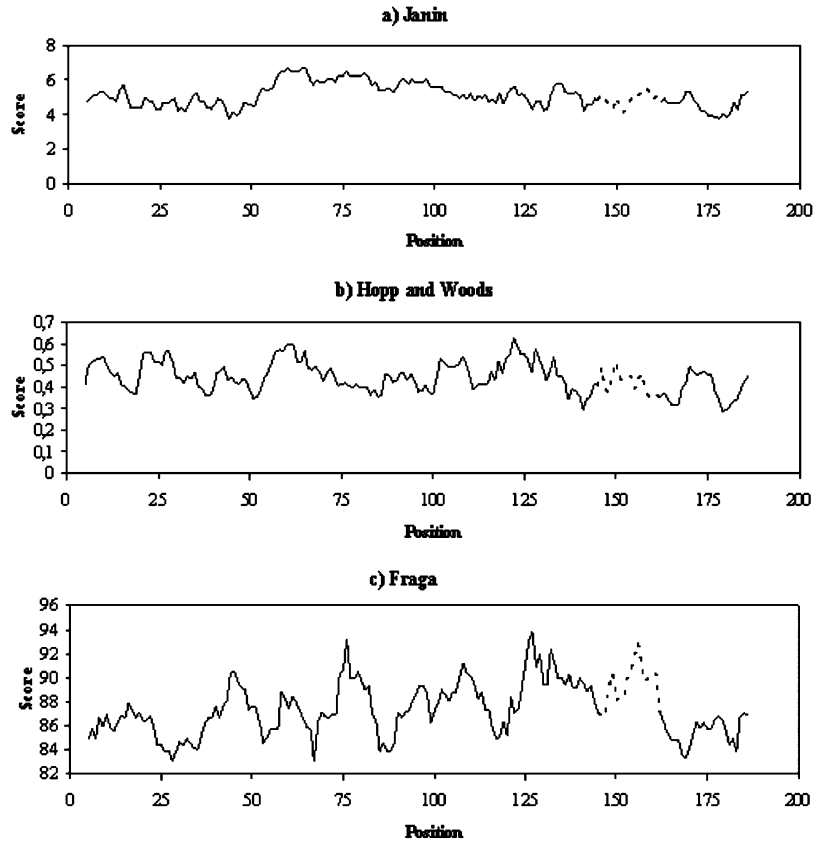

Figure 1. Profiles for the E1 protein of the hepatitis G virus by three different scales: (a) corresponds to the accessibility scale by Janin; (b) corresponds to the hydrophilicity scale by Hopp and Woods; (c) corresponds to the recognition factors analysis of Fraga. The dotted segment corresponds to the region of residues 145−162.

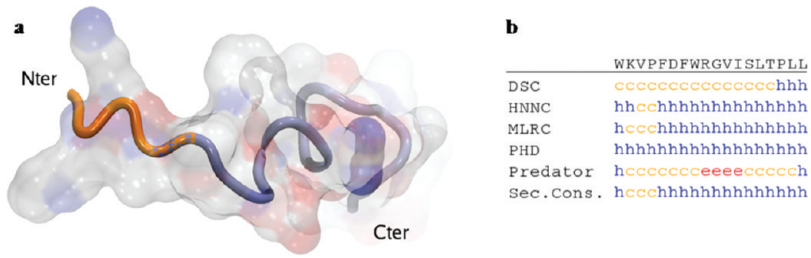

Figure 2. (a) 3D predicted model of E1(145−162). (b) Secondary structure prediction of E1(145−162).

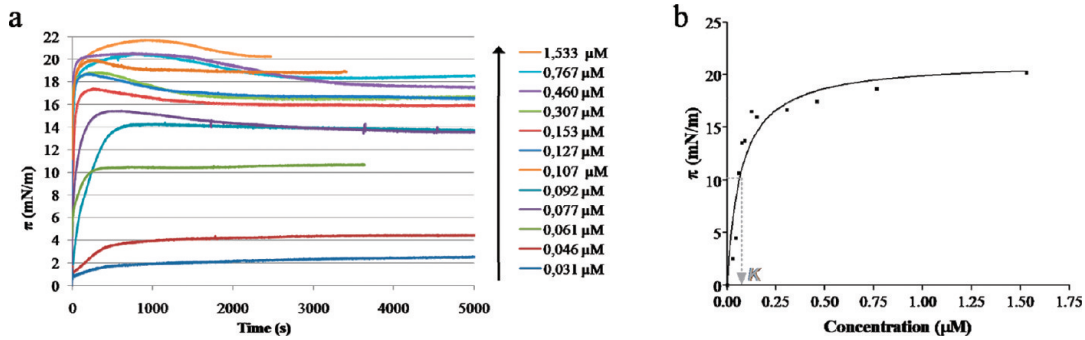

Figure 3. (a) Kinetic adsorption process for the incorporation of E1(145−162) into the air/water interface at different peptide concentrations. (b) Surface activity curve of E1(145−162).

activity curve approached a rectangular hyperbola, and it was fitted to eq 1 via nonlinear least-squares regression analysis.

$$\pi = \frac{C\pi_{max}}{K + C} \quad (1)$$

where C is the concentration, π_{max} is the maximum pressure that could be achieved, and K is a characteristic constant equal to the peptide concentration that achieves $^1/_2\pi_{max}$. Fitting the data, the values obtained were 21.27 mN/m for π_{max} and 0.070 μM for K ($R^2 = 0.893$). This K value was chosen to further penetration studies, as it corresponds to the suitable concentration of the peptide that should be used in the bulk subphase for experiments of penetration kinetics, lower than the equilibrium spreading pressure of the peptide.[12]

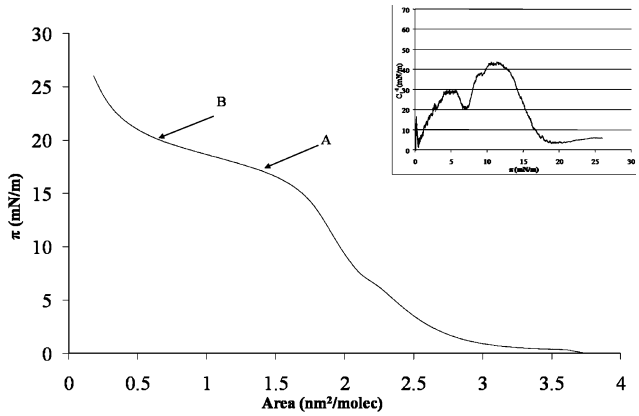

Figure 4. Surface pressure−mean molecular area isotherm of E1(145−162) peptide spread on a HEPES subphase. Inset: Compressibility modulus plot (C_s^{-1}) versus surface pressure.

By applying the Gibbs adsorption equation in its simpler form (eq 2), it is possible to calculate the peptide surface excess concentration (Γ)

$$\Gamma = \frac{\Delta\pi}{RT\,\Delta \ln C} \tag{2}$$

where R is the gas constant (8.31 J K^{-1} mol^{-1}), T is the temperature (298 K), $\Delta\pi$ is the pressure increase achieved 30 min after injection, and C is the peptide concentration.

The surface excess concentration has a value of 3.8×10^{-6} mol m^{-2}. It allows us to calculate the surface molecular area by means of eq 3, where N is Avogadro's constant.

$$A = \frac{1}{\Gamma N} \tag{3}$$

The area per molecule obtained was 0.437 nm^2 $molecule^{-1}$, which was very similar to that obtained at the surface molecular packing obtained at the same surface pressure as achieved by the adsorption process.

3.3.2. Surface Pressure−Mean Molecular Area Compression Isotherm of Peptide. Figure 4 shows the shape of the E1(145−162) monolayer when spread at the air−water interface on the HEPES subphase. The shape of the $\pi-A$ curve is very similar to the peptides with lower molecular weight.[13,14] It exhibits three regions with different slopes. Upon compression, the monolayer undergoes a transition at point A (see Figure 4) which is seen as a pseudoplateau and spans from molecular areas of 1.5 to 0.5 nm^2 $molecule^{-1}$. The inset shows the plot of the compressibility modulus versus surface pressure where the beginning and the end of the transition region can be seen clearly. Beyond this transition region, at low molecular areas, the surface pressure rises due to the increase of molecular packing but without altering the elasticity of the monolayer. Finally, the monolayer reaches a more condensed state but without a clear collapse point, not visible in the shape of the surface pressure−mean molecular area isotherms.

However, BAM images clearly revealed the disruption of the monolayer around 26 mN/m (Figure 5F), which was accepted as the collapse pressure. Before the transition region, at surface pressures below 5 mN/m, the pictures are homogeneous (see Figure 5A). Once arriving to the plateau surface pressure, circular white holes start to appear (Figure 5B−D), thus demonstrating that the film is less homogeneous. When the transition region is exceeded, these circular spots increase in number and size as the compression proceeds (Figure 5E). These spots may be considered evidence of the nucleation of 3D structures. Finally, the nuclei arrange themselves in lines (Figure 5F), leading to a kind of monolayer collapse. In previous work on the E2(347−363) hepatitis G peptide sequence that exhibits similar length but different hydrophilic/hydrophobic ratio, these 3D structures have been attributed to molecular aggregates.[15]

The molecular area limit (A_0) value, 1.25 nm^2 $molecule^{-1}$, calculated as the intersection of the steep part of the isotherm with the area axis when lateral compression takes place,[16] is in the same order to those obtained for peptides of similar amino acidic chain length and similar hydrophobic profiles based on their primary sequence.[17,18] According to the results obtained by computational prediction of structure, this value, together with the collapse pressure, is also compatible with an α-helical conformation. The mean area occupied by each amino acid residue (∼7 Å) proves that the peptide adopts a vertical orientation at the air−water interface.[17]

The surface compressibility modulus (C_s^{-1}) of the monolayer was calculated from surface pressure and area per molecule data applying eq 4.

$$C_s^{-1} = -A\left[\frac{\partial\pi}{\partial A}\right] \tag{4}$$

where A is the area per molecule at the indicated surface pressure and π is the corresponding surface pressure.

The surface compressibility modulus can be used to characterize the phase state of the monolayer[19] (for liquid expanded films, elasticity ranges from 12.5 to 50 mN/m, while, for the liquid condensed phase, it ranges from 100 to 250 mN/m).[20] In the inset of Figure 4, it can be seen that the main arrangement of a monolayer is an expanded state with a value of the compressibility modulus below 50 mN/m. As indicated before, upon compression, a plateau of high compressibility appeared between points A and B. This fact has been explained in different ways. It is possible that it was the result of the formation of a bilayer[21] or that was the result of the molecular segments lifted from the water surface,[22] or a change in orientation of the molecules upon compression.[23] In our case, the last explanation could be accepted, taking into account that the area value (2.5 nm^2/molecule) when extrapolating to surface pressure zero the steep region before beginning the transition, corresponding to a liquid expanded state, is compatible with a side by side horizontal orientation of the helices; the limiting area at the end of the transition (1.25 nm^2 $molecule^{-1}$), when the monolayer become incompressible, agrees with an orientation of E1(145−162) perpendicular to the interface, according to Maget-Dana[16] who reviewed the behavior of antimicrobial peptides and their main structure at the interface. E1(145−162) presents common features with some of these peptides. A small molecular weight, positive net charge, the polar/nonpolar ratio of the amphiphilic molecule between 0.5 and 1.2, and absence of disulfide bonds are characteristics that allow the peptide to adopt the α-helical conformation at the interface. On the other hand, as indicated before, BAM images reveal, along the transition region, 3D structures and its number increase with compression (Figure 5). This fact, indicative of the peptide's aggregation at moderate compression pressures corresponding to the liquid condensed phase, may also be compatible with an α-helical structure.

3.4. Peptide−Lipid Interactions. The characterization of membrane interactions with peptides or proteins is important for a better understanding of their mode of action. In order to determine some peptide−lipid binding properties, a monolayer approach where the peptides were inserted into the lipid monolayer is used.

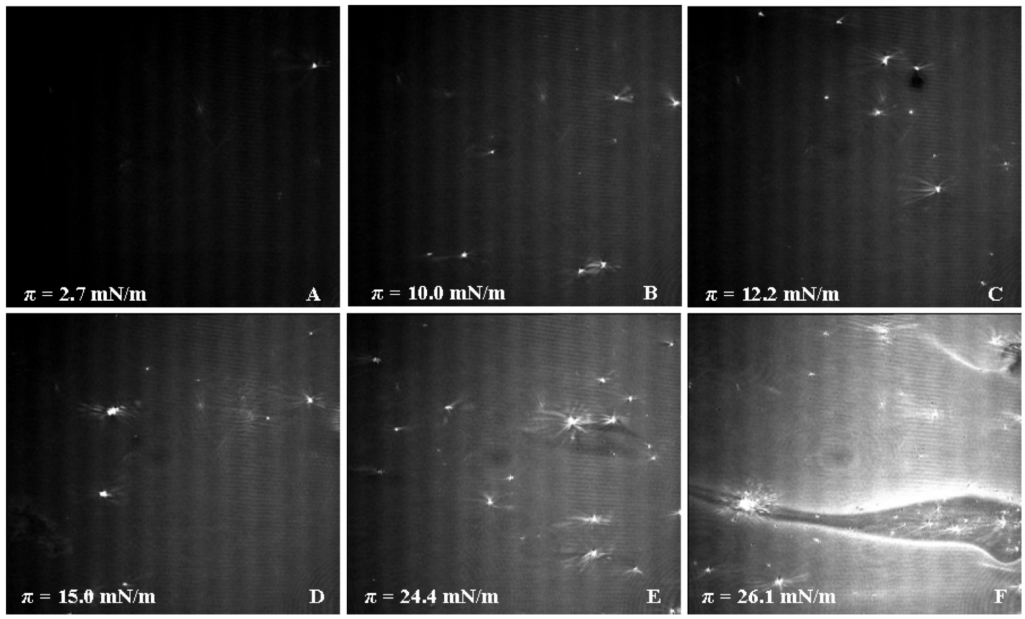

Figure 5. BAM images corresponding to E1(145−162) peptide monolayers spread on HEPES at different surface pressures.

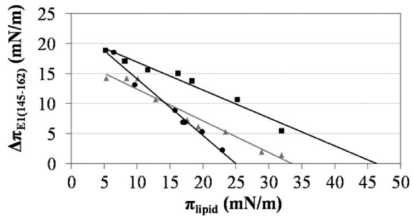

Figure 6. Surface pressure increase ($\Delta\pi$) caused by E1(145−162) in monolayers of different phospholipids in front of the lipid initial pressure (π_i). Black squares correspond to DMPG, gray triangles to DMPC, and black circles to POPG.

3.4.1. Penetration Kinetics. The ability of E1(145−162) peptide to penetrate into phospholipid monolayers was studied using a 0.070 μM peptide concentration in the HEPES buffered subphase, that corresponds to the *K* calculated from eq 1. Surface pressure increases ($\Delta\pi$) caused by E1(145−162) in monolayers of different phospholipids in front of the lipid initial pressure (π_i) are shown in Figure 6. For the three lipids, a general trend was observed: the greater the π_i, the lower the incorporation of peptide into the monolayer because of the greater packing of lipids at higher initial pressures.

The monolayer exclusion pressure,[24] that is, the surface pressure above which the peptide does not penetrate into the monolayer, was obtained by extrapolating the plot at $\Delta\pi = 0$ mN/m (Figure 6). It can be seen that the peptide interacts with the three lipids tested (DMPC, DMPG, and POPG). However, a more obvious interaction was observed when the monolayer was composed of DMPG. In this case, the exclusion pressure was 46.27 mN/m, clearly higher than those obtained when the monolayer was of DMPC (33.43 mN/m) or POPG (24.97 mN/m). These values show that the peptide could penetrate better into monolayers where the lipid is in an expanded state, as is the case of DMPG and DMPC for all of the pressures assayed and of POPG at pressures below 10 mN/m. POPG and DMPG differ in the hydrocarbonated chains and in the insaturations present on them. For POPG, which is in a liquid condensed state above 10 mN m^{-1}, the exclusion pressure is lower than that obtained for DMPG that is in an expanded state, corroborating that it is more difficult to penetrate into monolayers in liquid condensed state (see the below miscibility study). Below 5 mN m^{-1}, POPG is in liquid expanded state like DMPG, and as can be seen in Figure 6, for initial pressures below 10 mN m^{-1}, the peptide presents the same behavior. As happens with other positive charged peptides, E1(145−162) probably could penetrate into the biological membrane, characterized by a pressure between 25 and 35 mN/m.[25–27]

It is possible to compare also the influence on the insertion process of the polar head charge and the state of monolayers. DMPG forms anionic monolayers, while monolayers of DMPC are zwitterionic. The insertion of the peptide in the anionic monolayers is higher than that in the zwitterionic ones probably due to the positive charge of the peptide that interacts better with a negative monolayer. For the three lipids, below 10 mN/m of initial pressure, the incorporation of the peptide into the lipid monolayer was higher than in the surface activity process when 0.070 μM is injected. According to Brockman,[28] who has been working with peptides of similar properties, this fact means the process that takes place is the result of true peptide−lipid interaction and it is not just a mere adsorption.

3.4.2. Lipid−Peptide Miscibility. To know the effect of the E1(145−162) peptide on the state of phospholipid monolayers and better understand the lipid−peptide interaction that takes place, mixed monolayers of the peptide and the three phospholipids were obtained and the compression modulus for all systems was calculated according to eq 4. Figure 7 shows the shape of $\pi-A$ isotherms, and in the insets, the variation of compressibility modulus in the front of the surface pressure is shown.

For the three phospholipids, the presence of peptide produces an expansion of the monolayer at any molar fractions assayed. For pure DMPG monolayer (Figure 7b), the $\pi-A$ isotherm shows a phase transition from liquid expanded to liquid condensed state around 20 mN m^{-1} pressure, which is significantly modified when E1(145−162) peptide is further incorporated into the monolayers. The expansion observed for mixed monolayers indicates that the distance between the lipid hydrophobic chains increases due to the presence of peptide molecules in the film.

The pseudoplateau observed in the pure peptide monolayer slowly decreases with increasing lipid molar fraction in the mixture monolayer until $X_{lipid} = 0.8$ when it disappears

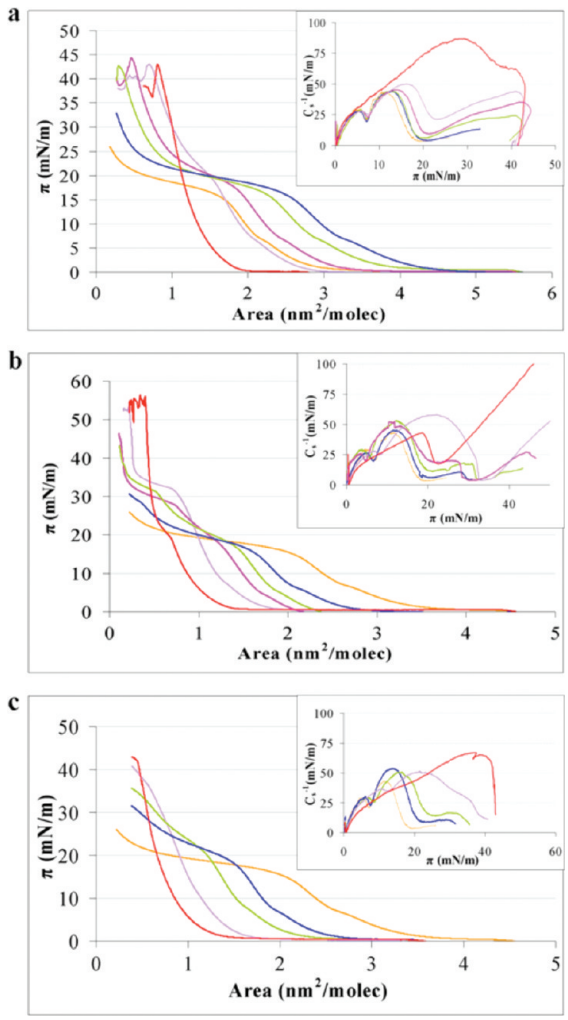

Figure 7. Surface pressure−mean molecular area (π−A) compression isotherms for E1(145−162) and the lipids: (a) DMPC, (b) DMPG, and (c) POPG spread on a HEPES subphase (pH 7.4) at different $X_{E1(145-162)}$: orange line for $X_{E1(145-162)} = 1$, purple line for $X_{E1(145-162)} = 0.2$, pink line for $X_{E1(145-162)} = 0.4$, green line for $X_{E1(145-162)} = 0.6$, blue line for $X_{E1(145-162)} = 0.8$, and red line for the lipid isotherm. Inset: Plots of compression modulus (C_s^{-1}) as a function of the surface pressure.

completely in the three cases studied. The compressibility modulus (C_s^{-1}) for all cases is shown in the insets of Figure 7. Between 10 and 20 mN m^{-1} approximately, the shape corresponding to this transition region can be seen. Similarly to the pure peptide, the monolayer is highly compressible at this region so the C_s^{-1} decreases together with the area molecule^{-1} values. When the lipid monolayer is in the liquid expanded state, the addition of peptide produces a slight increase in C_s^{-1} values in the case of DMPG and POPG but not for DMPC which did not modify the C_s^{-1} shape with the peptide addition. This fact suggests that the electric charge plays an additional role in the lipid−peptide interaction when the monolayer is in the liquid expanded state and correlates with the results obtained in penetration kinetics which demonstrated the higher penetration of peptide in DMPG and POPG instead of DMPC. At the liquid condensed state, C_s^{-1} decreases with $X_{E1(145-162)}$; such a decrease is specially marked for the monolayers of $X_{E1(145-162)} = 0.2$. Further additions of the peptide do not affect the value of C_{smax}^{-1}. Figure 8 shows the maximum C_s^{-1} values in function of peptide concentration where it can be seen, as indicated above, that the incorporation of E1(145−162) to phospholipid monolayers in the liquid condensed state causes their change to a liquid expanded state.

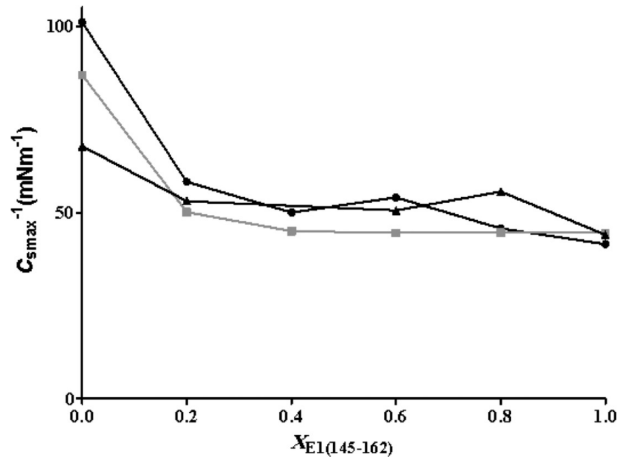

Figure 8. Maximum compressibility modulus values as a function of peptide concentration for the mixtures with the three phospholipids: black circles and black line for DMPG, gray squares and gray line for DMPC, and black triangles and black line for POPG. The lines represent the quadratic nonlinear fitting of the data.

The analysis of the collapse pressures can be helpful to examine the 2D behavior of the film components; the variation of π_c with the molar ratio of the components indicates two-dimensional miscibility. In the case of DMPC, the collapse pressure of pure lipid (42.7 mN·m^{-1}) barely changes upon varying the DMPC/E1(145−162) molar ratio until $X_{E1(145-162)} = 0.8$ which presents a lower value (∼34 mN/m). For mixtures of E1(145−162) with DMPG and POPG, collapse pressure varies with the monolayer composition that may be indicative of the miscibility within the range of molar fractions assayed. On the other hand, as it was observed for the pure peptide surface pressure−mean molecular area isotherm, for all mixed monolayers of DMPC and DMPG and for POPG above a molar fraction of 0.2, a transition region is observed upon compression. The extension of this region varies when the E1(145−162) proportion decreases until $X_{E1(145-162)} = 0.2$ in which the plateau disappeared.

The application of the additivity rule is very useful to evaluate the extent of intermolecular interactions in monolayers comprising two components. The additivity rule predicts that, in the case of an ideal mixture, the mean molecular area (A_{12}) at a given surface pressure will be equal to the weighted average (eq 5).

$$A_{12} = X_1A_1 + X_2A_2 \quad (5)$$

where A_1 and A_2 are the molecular areas of the single components at the same surface pressure and X_1 and X_2 are the mole fractions of components 1 and 2 in the mixed film. The comparison of the experimental mean molecular area with the expected values from the additivity rule application provides us with an important clue on the extent of miscibility and interactions in the binary monolayer. The linear dependence in the area−composition plots (Figure 9) indicates an ideal mixing or complete immiscibility of its components.[29]

Analysis of the plots reveals several situations depending on the lipid−peptide combination. DMPC−peptide mixed monolayers present small positive deviations of ideality, at any $X_{E1(145-162)}$ molar fraction assayed and at different pressures (5, 10, 20, and 25 mN/m). In the cases of DMPG and POPG, a similar pattern was observed. In both cases, the mixtures present positive deviations at pressures of 20 and 25 mN/m; meanwhile, at lower pressures (5 and 10 mN/m), they show an ideal

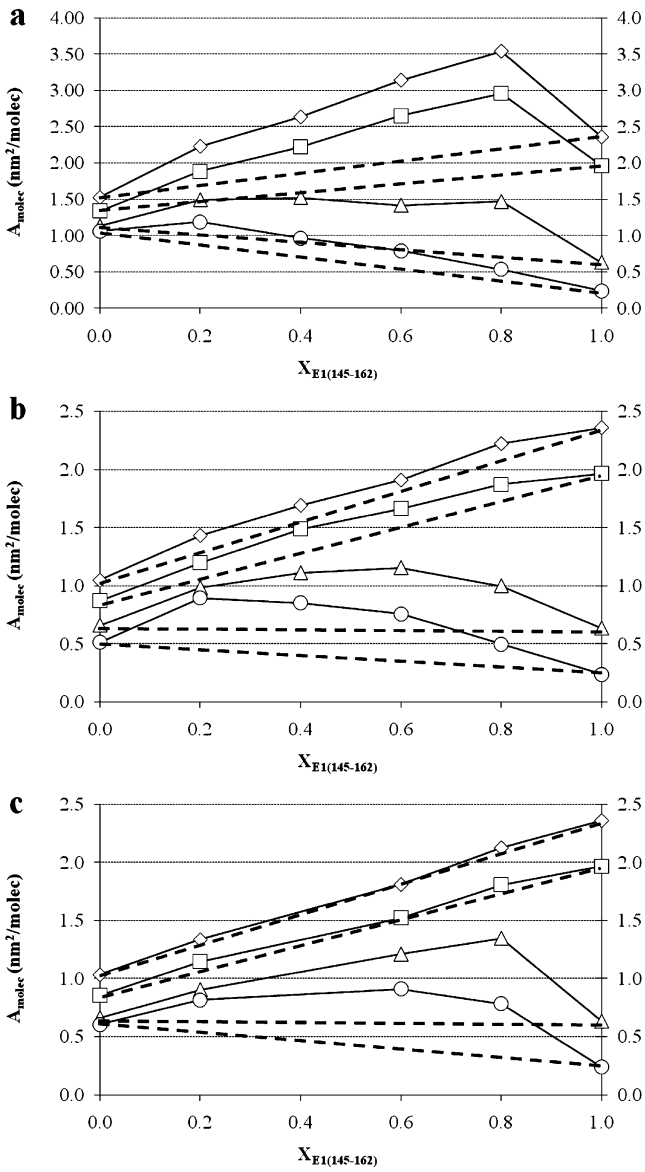

Figure 9. Plots of *A* for E1(145−162) as a function of the lipid molar fractions at different surface pressures for pure and mixed monolayers: (a) DMPC; (b) DMPG; (c) POPG. Surface pressures: (◇) 5 mN m^{-1}, (□) 10 mN m^{-1}, (△) 20 mN m^{-1}, (○) 25 mN m^{-1}.

behavior. This seems to be a consequence of the electric charge of DMPG and POPG contribution to the lipid−peptide interaction.

As indicated above, in all cases, the presence of peptide modifies the compressibility of the monolayer to a liquid expanded state. This expansion in the case of α-helical peptides and lipids in the liquid expanded state has been reported.[20] It is possible that the expansion reflects the formation of the molecular aggregates of peptide at the air/water interface, as has been described in the literature for similar peptides[15] or a change in the orientation of the peptide with respect to the air−water interface from a parallel to a more vertical position in the presence of lipid to satisfy the hydrophobic peptide−lipid interactions. However, it is also compatible with the formation of peptide−lipid complexes through hydrophobic interactions, as seen in a previous work,[6] in which we demonstrated that a new species appears when mixing liposomes (∼30 mN/m pressure membrane) of the same lipidic composition of the monolayers of this study and at $X_{E1(145-162)}$ of 0.2. It is probable that the peptide molar fraction plays a role in the explanation of the expansion observed in the different cases studied.

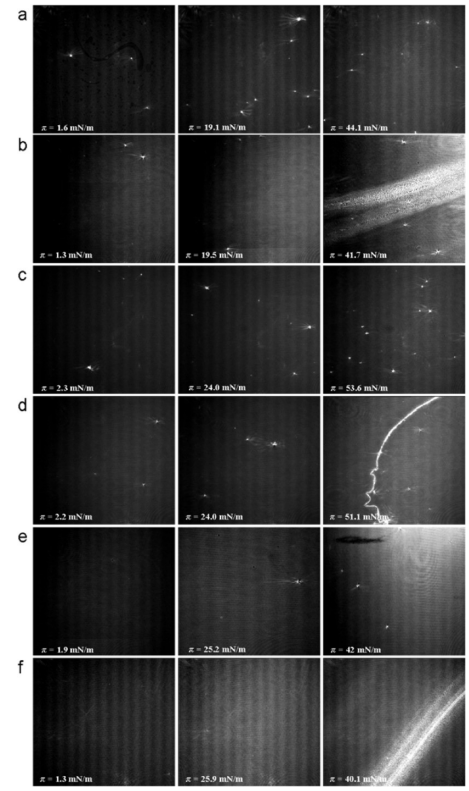

Figure 10. MiniBam images of lipid monolayers at three different pressures and their mixtures with E1(145−162) at a molar fraction of $X_{E1(145-162)} = 0.2$: (a) DMPC; (b) DMPC with E1(145−162); (c) DMPG; (d) DMPG with E1(145−162); (e) POPG; (f) POPG with E1(145−162).

As indicated above, in all cases, the presence of peptide modifies the compressibility of the monolayer to a liquid expanded state. This expansion in the case of α-helical peptides and lipids in the liquid expanded state has been reported.[20] It is possible that the expansion reflects the formation of peptide−lipid complexes through hydrophobic interactions or a change in the orientation of the peptide with respect to the air−water interface from a parallel to a more vertical position in the presence of lipid to satisfy the hydrophobic peptide−lipid interactions.

The BAM images shown in Figure 10 were obtained from monolayers of pure lipids (Figure 10a,c,e) and mixed monolayers of the three lipids and peptide at $X_{E1(145-162)} = 0.2$ (Figure 10b,d,f). As we have indicated above, the lipid/peptide (08:0.2) system is especially interesting because of its distinct behavior. Pictures reveal that the 3D structures observed when the peptide monolayer was compressed disappear in the presence of lipid, and until pressures near 25 mN/m, the monolayer is homogeneous in all cases, demonstrating the lipid−peptide miscibility. Upon compression in mixed monolayers at high pressures, when the collapse is reached, pictures show a clear phase separation. It seems that a peptide−lipid complex arranges itself and separates from the lipid matrix.

To get insight into the interactions established with E1(145−162) and the three phospholipids of this study, a thermodynamic point of view has been considered. The excess Gibbs energy of mixing (ΔG_M^{EX}) is a useful parameter to investigate on the lipid−peptide interactions. The examination of ΔG_M^{EX} values provides us further information on the energy of the miscibility process and the specific interactions of two components. The positive values indicate that the process of mixing is not thermodynamically favored so the mutual interactions between the two components are weaker than interactions between the pure component

TABLE 1: ΔG_M^{EX} (in J mol^{-1}) for Different Lipid−E1(145−162) Mixtures at Various Pressures

X_{lipid}	x (mN m^{-1})	DMPC	DMPG	POPG
0.2	5	−150	−283	−97
	10	−175	−766	−229
	20	−7463	−9820	−6670
	25	−7993	−13451	−3687
0.4	5	404	−656	−34
	10	852	−1108	−86
	20	−963	−6218	−5852
	25	2697	−6819	−5419
0.6	5	990	−739	−144
	10	1954	−837	537
	20	8005	−2282	−1385
	25	13456	−365	−142
0.8	5	671	−608	−208
	10	2172	−90	−328
	20	13193	4475	−2229
	25	23606	8456	−2766

molecules themselves. When $|\Delta G_M^{EX}| < RT$, the differences from ideality are considered not statistically significant and the mixture can be considered ideal.[30] A deep and step minimum in ΔG_M^{EX} indicates the formation of a complex between the two components.[16]

ΔG_M^{EX} has been calculated by eq 6,[31] where A_{12} is the mean area per molecule in the mixed film, A_1 and A_2 are the areas per molecule in the pure films, X_1 and X_2 are the molar fractions, and π is the surface pressure (mN m^{-1}).

$$\Delta G_M^{EX} = \int_{\pi\to 0}^{\pi} A_{12}\, d\pi - X_1 \int_{\pi\to 0}^{\pi} A_1\, d\pi - X_2 \int_{\pi\to 0}^{\pi} A_2\, d\pi \quad (6)$$

Table 1 shows the ΔG_M^{EX} values calculated for the lipid−peptide mixtures assayed at different surface pressures. In general, at low surface pressures, the mixtures have $|\Delta G_M^{EX}| < RT$ so they can be considered ideal. From the dependence of ΔG_M^{EX} on peptide concentration at a fixed film pressure, we could see that the values of ΔG_M^{EX} change from negative to positive with increasing $X_{E1(145-162)}$ for DMPC and DMPG with a minimum value obtained at $X_{E1(145-162)} \leq 0.2$ for both lipids. In the case of the POPG monolayer, ΔG_M^{EX} presents a different pattern with negative small values so the interactions are not significant except for $0.2 \leq X_{E1(145-162)} \leq 0.4$ values at surface pressures of 20 and 25 mN/m. These results allow us to corroborate the lipid−peptide miscibility at $X_{E1(145-162)} = 0.2$ at pressures between 20 and 25 mN/m when the monolayers present a transition zone compatible with the formation of a lipid/peptide complex which separates when the collapse is achieved.

4. Conclusions

We have studied the behavior of Langmuir monolayers of a synthetic peptide named E1(145−162), from the GB virus C/Hepatitis G virus, in the presence of DMPC, DMPG, and POPG. These results have proven that the peptide forms a stable monolayer and interacts with these model membranes, showing a higher interaction with negatively charged phospholipid, may be due to the positive charge of the peptide and the electrostatic interactions.

Moreover, the surface properties of E1(145−162) synthetic peptide are consistent with an α-helical structure adopted at the air−buffer saline interface with a main orientation perpendicular to the interface at high lateral packing compatible with biomembranes. As observed for other α-helical peptides, E1(145−162) produces the expansion of the surface pressure−mean molecular area compression isotherm of lipid showing a transition zone around 20 mN/m compatible with the peptide/lipid complex at $X_{E1(145-162)} = 0.2$, with these results being coherent with those obtained in a previous work,[6] where a new species appears when mixing liposomes of DMPC and DMPG with the peptide around the same molar fraction and that could be attributed to the binding and subsequent partial penetration of the peptide into the hydrophobic core of the bilayer. However, the hypothesis of peptide aggregation cannot be discarded considering the positive deviations from additivity observed mainly both at high mole fraction and surface pressure.

The interaction of E1(145−162) with phospholipid membrane models described allows us to propose it for ulterior studies to know the relationships between its orientation, structural properties, and physical properties of membranes in order to elucidate the role in the mechanism that regulates the entry of the Hepatitis G virus into the host cell and to consider its potential behavior as HIV-1 inhibitor.

Acknowledgment. This work is supported by project CTQ2006-15396-C02-02/01-BQU from Secretaría de Estado de Investigación, Ministerio de Ciencia e Innovación, Dirección General de Programas y transferencia de conocimiento, Subdirección General de Proyectos de Investigación (Spain). M.J.S.-M. is a recipient of a FPI program predoctoral grant. The authors are members of the consolidated research group by the Generalitat de Catalunya: *Peptides and Proteins: physicochemical studies* (2005SGR00278). The authors are grateful to Peter Schmidtke, Ph.D. Student at the Molecular Modeling and Bioinformatics Group of the department of Physical Chemistry (Faculty of Pharmacy, University of Barcelona), for his inestimable help on the computational prediction of the peptide structure.

References and Notes

(1) Casas, J.; Espina, M.; Haro, M.; Royo, F.; Alsina, M. A.; Haro, I.; Mestres, C. *Langmuir* **2006**, *22*, 246.
(2) Tillmann, H. L.; Manns, M. P. *Antiviral Res.* **2001**, *52*, 83.
(3) Perez, S.; Minones, J., Jr.; Espina, M.; Alsina, M. A.; Haro, I.; Mestres, C. *J. Phys. Chem. B* **2005**, *109*, 19970.
(4) Xiang, J.; Wunschmann, S.; Diekema, D. J.; Klinzman, D.; Patrick, K. D.; George, S. L.; Stapleton, J. T. *N. Engl. J. Med.* **2001**, *345*, 707.
(5) Moraes, M. L.; Bonardi, C.; Mendonca, C. R.; Campana, P. T.; Lottersberger, J.; Tonarelli, G.; Oliveira, O. N., Jr.; Beltramini, L. M. *Colloids Surf., B* **2005**, *41*, 15.
(6) Sanchez-Martin, M. J.; Amigo, J. M.; Pujol, M.; Haro, I.; Alsina, M. A.; Busquets, M. A. *Anal. Bioanal. Chem.* **2009**, *394*, 1003.
(7) Janin, J. *Nature* **1979**, *277*, 491.
(8) Hopp, T. P.; Woods, K. R. *Proc. Natl. Acad. Sci. U.S.A.* **1981**, *78*, 3824.
(9) Fraga, S. *Can. J. Chem.* **1982**, *60*, 2606.
(10) http://www.sbg.bio.ic.ac.uk/~phyre/index.cgi.
(11) http://npsa-pbil.ibcp.fr/cgi-bin/npsa_automat.pl?page=/NPSA/npsa_seccons.html.
(12) Rafalski, M.; Lear, J. D.; DeGrado, W. F. *Biochemistry* **1990**, *29*, 7917.
(13) Vila Romeu, N.; Minones Trillo, J.; Conde, O.; Casas, M.; Iribarnegaray, E. *Langmuir* **1997**, *13*, 71.
(14) Larios, C.; Minones, J., Jr.; Haro, I.; Alsina, M. A.; Busquets, M. A.; Trillo, J. M. *J. Phys. Chem. B* **2006**, *110*, 23292.
(15) Pérez-López, S.; Nieto-Suárez, M.; Mestres, C.; Alsina, M. A.; Haro, I.; Vila-Romeu, N. *Biophys. Chem.* **2009**, *141*, 153.
(16) Maget-Dana, R. *Biochim. Biophys. Acta* **1999**, *1462*, 109.
(17) Ambroggio, E. E.; Separovic, F.; Bowie, J.; Fidelio, G. D. *Biochim. Biophys. Acta* **2004**, *1664*, 31.
(18) Deshayes, S.; Plenat, T.; Aldrian-Herrada, G.; Divita, G.; Le Grimellec, C.; Heitz, F. *Biochemistry* **2004**, *43*, 7698.
(19) Alsina, M. A.; Ortiz, A.; Polo, D.; Comelles, F.; Reig, F. *J. Colloid Interface Sci.* **2006**, *294*, 385.
(20) Davies, J. T.; Rideal, E. K. *Interfacial Phenomena*; Academic Press: New York, 1961.
(21) Takeda, F.; Matsumoto, M.; Takenaka, T.; Fujiyoshi, Y.; Uyeda, N. *J. Colloid Interface Sci.* **1983**, *91*, 267.

(22) Kaku, M.; Hsiung, H.; Sogah, D. Y.; Levy, M.; Rodriguez-Parada, J. M. *Langmuir* **1992**, *8*, 1239.
(23) Hac-Wydro, K.; Kapusta, J.; Jagoda, A.; Wydro, P.; Dynarowicz-Latka, P. *Chem. Phys. Lipids* **2007**, *150*, 125.
(24) Bougis, P.; Rochat, H.; Pieroni, G.; Verger, R. *Biochemistry* **1981**, *20*, 4915.
(25) Nagle, J. F. *J. Membr. Biol.* **1976**, *27*, 233.
(26) Blume, A. *Biochim. Biophys. Acta* **1979**, *557*, 32.
(27) Demel, R. A.; Geurts van Kessel, W. S.; Zwaal, R. F.; Roelofsen, B.; van Deenen, L. L. *Biochim. Biophys. Acta* **1975**, *406*, 97.
(28) Brockman, H. *Curr. Opin. Struct. Biol.* **1999**, *9*, 438.
(29) Chattoraj, D. K.; Birdi, K. S. *Absorption and the Gibbs Surface Excess*; Plenum Press: New York, 1984; pp 219−222.
(30) Gaines, G. L. *Insoluble Monolayers at Liquid-Gas Interfaces*; Wiley-Interscience: New York, 1966; p 286.
(31) Pagano, R. E.; Gershfeld, N. L. *J. Colloid Interface Sci.* **1972**, *41*, 311.

JP906900K

3.2. Artículo 2. Fluorescence study of the dynamic interaction between E1(145-162) sequence of hepatitis GB virus C and liposomes

La caracterización físico-química de la secuencia peptídica E1(145-162) correspondiente a la proteína estructural E1 el virus de la hepatitis G se ha hecho estudiando su interacción con modelos de membrana. Vesículas unilamelares pequeñas (SUVs, *Small Unilamellar Vesicles*) de dimiristoilfosfatidilglicerol (DMPG) o dimiristoilfosfatidilcolina (DMPC) se han escogido como modelos de membrana. La incorporación y localización del péptido en la bicapa fosfolipídica se investigó mediante medidas de anisotropía de fluorescencia utilizando SUVs marcados con difenilhexatrieno (DPH) o trimetilamonio-DPH (TMA-DPH). La adición del péptido E1(145-162) mostró cambios significativos en los valores de anisotropía de la sonda localizada en la interfase lípido/agua. Estos resultados indican que el péptido E1(145-162) interacciona preferiblemente con la superficie del lípido sin penetrar dentro de la bicapa. Una serie de experimentos de fluorescencia basados en la fluorescencia intrínseca del péptido por la presencia de triptófano fueron planteados; en ellos se realizó una titulación del péptido con SUVs de DMPC y DMPG a dos temperaturas (25 y 37ºC) con el fin de evaluar si los cambios en la fluorescencia del triptófano podían ofrecer una evidencia directa de la interacción del péptido con las membranas. La adición de las vesículas de DMPC y DMPG desplazó el máximo de absorción hacia longitudes de onda más bajas y redujeron la intensidad de fluorescencia. Ambos efectos sugieren una interacción y una penetración parcial del péptido en la bicapa sin insertarse completamente. Las series de espectros de fluorescencia obtenidos se modelaron mediante el algoritmo MCR-ALS (Multivariate Curve Resolution-Alternating least squares). Los resultados muestran como la disminución de la concentración del péptido está directamente relacionada con la aparición de una nueva especie, que se corresponde con la unión lípido-péptido.

Anal Bioanal Chem (2009) 394:1003–1010
DOI 10.1007/s00216-008-2593-8

ORIGINAL PAPER

Fluorescence study of the dynamic interaction between E1 (145–162) sequence of hepatitis GB virus C and liposomes

Maria Jesús Sánchez-Martín · José Manuel Amigo · Montserrat Pujol · Isabel Haro · M. Asunción Alsina · M. Antonia Busquets

Received: 31 October 2008 / Revised: 16 December 2008 / Accepted: 19 December 2008 / Published online: 20 January 2009

Abstract The physicochemical characterization of the peptide sequence E1(145–162) corresponding to the structural protein E1 of the hepatitis G virus was done by studying its interaction with model membranes. Small unilamellar vesicles (SUVs) of dimyristoylphosphatidylglycerol or dimyristoylphosphatidylcholine were chosen as mimetic membranes. Peptide incorporation and location in the phospholipid bilayer was investigated by fluorescence anisotropy with SUVs labeled with diphenylhexatriene (DPH) or trimethylammonium–DPH. The addition of the peptide E1 (145–162) showed significant changes in the anisotropy values of the probe located at the air/water interface. These results indicate that the peptide E1(145–162) preferably interacts with the lipid surface without penetrating inside the bilayer. A series of fluorescence experiments based on tryptophan peptide fluorescence were modeled by means of multivariate curve resolution-alternating least squares (MCR-ALS) algorithm to further study the peptide interaction with bilayers at different temperatures. The preliminary results obtained with MCR-ALS showed how the peptide concentration decay is directly linked to the appearance of a new specie, which corresponds to the lipid-peptide binding. These results provide useful information for the design of synthetic immunopeptides that can be incorporated into a liposomal system with potential to promote a direct delivery of the membrane-incorporated immunogen to the immunocompetent cells, thus increasing the immuno response from the host.

Keywords Hepatitis GB virus C · HGV/GBV-C · MCR-ALS · Tryptophan fluorescence · Liposomes · Synthetic peptides · Anisotropy

Electronic supplementary material The online version of this article (doi:10.1007/s00216-008-2593-8) contains supplementary material, which is available to authorized users.

M. J. Sánchez-Martín (✉) · M. Pujol · M. A. Alsina · M. A. Busquets
Physical Chemistry Department, Faculty of Pharmacy, University of Barcelona, Associated Unit to the CSIC: Peptides and Proteins: Physicochemical Studies, IN2UB Av. Joan XXIII s/n, 08028 Barcelona, Spain
e-mail: mjesus_sanchez@hotmail.com

J. M. Amigo
Department of Food Science Quality & Technology, University of Copenhagen, Rolighedsvej 30, 1958 Frederiksberg-C, Denmark

I. Haro
Unit of Synthesis and Biomedical Application of Peptides, Department of Biomedical Chemistry, IQAC-CSIC, Jordi Girona 18, 08034 Barcelona, Spain

Introduction

Hepatitis G virus (HGV) and GB virus C (GBV-C) are two isolates of the same virus independently and simultaneously discovered by Simons [1] and Linnen [2] in 1996. The natural history of hepatitis G virus (HGV/GBV-C) infection is, at present, not fully understood, and its potential to cause hepatitis in humans is questionable [3]. Epidemiological studies indicate that it does not cause acute or chronic hepatitis.

Recently, HGV/GBV-C has been investigated in the context of human immunodeficiency virus (HIV) infection. Hepatitis virus infections are very frequent in patients suffering from HIV due to similar transmission routes. The impact of co-infection with hepatitis B (HBV) or C (HCV) virus on the outcome of AIDS patients is associated with an impaired survival, and these patients often die from liver failure instead of AIDS [4]. On the contrary, previous

studies have suggested that people co-infected with HIV and HGV/GBV-C have delayed progression of HIV disease indicating a beneficial influence of GBV-C on HIV infection [5].

HGV/GBV-C virus is the most closely related human virus to the HCV, both belonging to the small enveloped viruses of the *flaviviridae* family. The envelope proteins (E) of flaviviruses have been described as class II fusion proteins [6], characterized by putative fusion sequences known as fusion peptides. The ability of vesicle fusion and cell lysis by these fragments seems to correlate with the strong interaction of these peptides with membranes. The fusion peptides of several viruses have been studied using biophysical techniques in order to better understand the entry mechanism of the virus into the host cell.

Bearing on mind the potential use of synthetic peptides as antiviral therapies and in an attempt to better understand the molecular interaction of envelop E1 protein of HGV/GBV-C with lipid bilayers, an epitope of GBV-C located at the (145–162) region of this structural protein has been selected by means of theoretical algorithms prediction.

In the present work, the physicochemical characterization of E1(145–162) peptide was done by studying its interaction with model membranes. Its ability to induce perturbations in model membranes has been analyzed by fluorescence anisotropy and by monitoring the behavior of the peptide in presence of different concentrations of lipid at different temperatures. A series of experiments, based on tryptophan fluorescence emission spectra, were developed by measuring the emission spectrum depending on lipid concentration. The fluorescence evolution of the peptide was measured in presence of small unilamellar vesicles (SUVs) composed of dimyristoylphosphatidylcholine (DMPC), zwitterionic, or dimyristoylphosphatidylglycerol (DMPG), anionic, at 25 and 37 °C.

To extract information about the behavior of the interaction between E1(145–162) and lipids, the fluorescence patterns collected were modeled by means of multivariate curve resolution-alternating least squares algorithm (MCR-ALS) [7]. MCR-ALS is a very useful algorithm that has widely demonstrated its usefulness in the modeling of evolving reactions [8, 9]. The aim of MCR-ALS is to describe the evolution of the obtained fluorescence profiles through their pure components contributions individually, without assuming any previous kinetic model.

The aim of this work is to obtain information about the molecular interaction between the peptide and a model of lipid membrane in order to know if it may serve as an internal fusion peptide. Fluorescence measurements and its mathematical treatment provided insights into E1(142–165)–membrane interaction.

Some outlines of multivariate curve resolution-alternating least squares in evolving fluorescence reactions

Main features of MCR-ALS

When the emission spectral profiles are collected at certain excitation wavelength varying the lipid concentration, the information obtained can be arranged into a bidimensional matrix **D** ($M\times N$), wherein spectra are sorted in rows as a function of time (m rows). The n columns refer to the n different emission wavelengths monitored (Fig. 1).

MCR-ALS iteratively decomposes **D** into two submatrices, **C** ($M\times F$) and $\mathbf{S}^{\mathbf{T}}$ ($N\times F$), which contain the concentration and spectral profiles, respectively [10]. F is the number of absorbing chemical components. **E** ($M\times N$) is the matrix of residuals (Eq. 1; Fig. 1).

$$\mathbf{D} = \mathbf{C}\mathbf{S}^{\mathbf{T}} + \mathbf{E} \quad (1)$$

In essence, by using the MCR-ALS algorithm, the evolution of the relative concentration (**C**) of each compound in the reaction (F) and their pure spectra ($\mathbf{S}^{\mathbf{T}}$) is obtained.

Elucidating the number of components

Before starting the MCR-ALS decomposition, the value of F, i.e., the number of luminescence components, has to be determined, taking into consideration that the idea of luminescence component has to be understood as an entity that makes the signal vary (in our case, the fluorescence spectra collected with time) significantly from the noise of

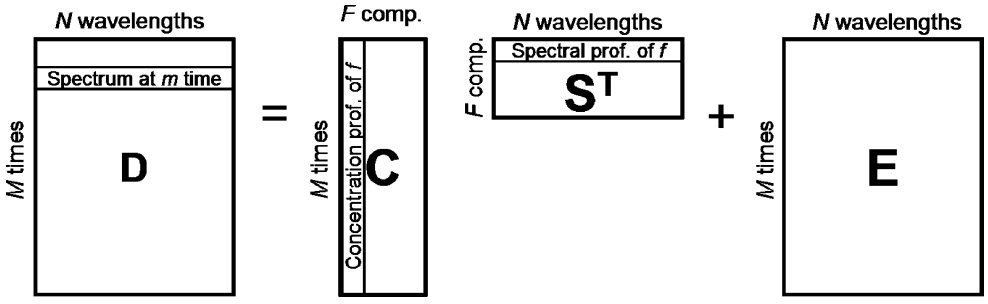

Fig. 1 MCR-ALS decomposition of **D** ($M\times N$) into the concentration **C** ($M\times F$) and spectral $\mathbf{S}^{\mathbf{T}}$ ($F\times N$) profiles. **E** ($M\times N$) is the residual matrix. *Comp.* components, *prof.* profiles

the data. If the signal-to-noise ratio is high enough, the components will only refer to the number of analytes that evolve in the reaction. Several methods have been described to guess the number of evolving components [11], but one of the most useful is evolving factor analysis (EFA) [7, 12]. This algorithm is a PCA-based method that, apart from a number of components, also offers an intuitive idea of the zone in where each component is relevant.

Obtaining initial estimations to start the iterations

MCR-ALS requires good initial estimations of the spectral or the concentration profiles for each component to start the iterations to converge to a good solution avoiding local minima. There are a lot of methodologies to obtain initial estimates in an easy way, like the previously mentioned EFA algorithm for the concentration profiles [13] or SIMPLISMA for the spectral profiles [14]. One straightforward way to obtain initial estimates of the spectral profiles is to choose some of the spectra from the **D** data matrix.

Imposing constraints to the iterations

The resolution of the product $\mathbf{CS^T}$ is not so evident since this product has no unique solution. This ambiguity associated with the resolved profiles, which can affect the quality of the derived information, can be highly minimized by means of the addition of several soft-modeling constraints [15, 16]. Among the number of constraints that can be imposed, the most useful in fluorescence are mainly non-negativity, which imposes the concentration or spectral profiles of the components that are supposed to be always positive; unimodality, which can be assumed that the shape of the profiles only have one minimum; and closure, which is used when the mass balance in the reaction remains constant.

Achieving the best solution

ALS is an iterative algorithm, so a stopping criterion has to be imposed to stop the iterations. The most common is the percentage of lack of fit (%LOF) that indicates the difference between the input data D and the data reproduced from the CS^T product for each iteration (Eq. 2) [10]. The optimization stops when the relative difference in lack of fit (%LOF) values between consecutive iterations is below than a threshold value (usually 0.1% [11]).

$$\%\mathrm{LOF} = 100 \times \sqrt{\frac{\sum_{i}^{I}\sum_{j}^{J} e_{mn}^2}{\sum_{i}^{I}\sum_{j}^{J} d_{mn}^2}} \qquad (2)$$

In this equation, e is each mnth element of the residual matrix **E**, and d is each mnth element of the **D** matrix.

Materials and methods

Reagents

Amino acids and Rink amide resin (Tentagel R RAM, 0.19 meq/g) were obtained from Novabiochem (Nottingham, UK). Dimethylformamide was purchased from Scharlau (Barcelona, Spain). Dichloromethane and piperidine were purchased from Fluka (Neu-Ulm, Germany). Washing solvents such as acetic acid, diethyl ether, and trifluoroacetic acid (TFA) were obtained from Merck (Poole, Dorset, UK). *N*-Hydroxybenzotriazole (HOBt) and *N*,*N*′-diisopropylcarbodiimide coupling reagents were obtained from Fluka and Novabiochem, respectively. Other coupling reagents as *O*-(7-azabenzotriazole-1-yl)-*N*, *N*,*N*′*N*′-tetramethyluronium hexafluorophosphate (HATU), and *N*, *N*′-diisopropylethylenamine (DEIA) were obtained from GenScript Corporation and Fluka, respectively. Scavengers such as ethanedithiol (EDT) or triisopropylsilane (TIS) were from Sigma-Aldrich. DMPG and DMPC were from Avanti Polar Lipids and were used without further purification. Chloroform and methanol were purchased from Merck. Water was double-distilled and deionized (MilliQ system, Millipore; 18.2 MΩ cm, pH 5.8). Buffer in all experiments was HEPES 5 mM, 20 mM NaCl, pH 7.4.

Peptide synthesis

The synthesis of the peptide E1(145–162), whose primary amino acid sequence is Trp-Lys-Val-Pro-Phe-Asp-Phe-Trp-Arg-Gly-Val-Ile-Ser-Leu-Thr-Pro-Leu-Leu, was carried out manually on a Tentagel R RAM resin (0.19 meq/g) by a solid phase methodology following an Fmoc/*tert*-butyl (tBu) strategy by means of a DIPCD/HOBt activation [17]. For difficult couplings, HATU and DEIA agents were used. Side protection was effected by the following: 2,2,5,7,8-pentamethyl-chroman-6-sulfonyl for Arg; tBu for Tyr, Ser, Thr, and Asp; and *t*-butyloxycarbonyl for Lys and Trp.

Threefold molar excess of Fmoc-amino acids was used throughout the synthesis. The stepwise addition of each residue was assessed by the Kaiser's (ninhydrin) test [18], and repeated couplings were carried out when a positive ninhydrin test was obtained.

The synthesized peptide was deprotected from the side-chain groups and cleaved from the resin with a treatment of TFA containing appropriate proportions of scavengers [19] such as H_2O, TIS, and EDT/94.5% TFA/2.5% H_2O/2.5% EDT/1% TIS.

The peptide was characterized by analytical HPLC Perkin Elmer with a LC-235 Diode Array Detector and a Binary LC Pump 250; the column used was a KROMASIL 100 C18 5 μm of 25×0.46 cm. The analysis was carried out using a linear gradient of 95% H_2O (0.05% TFA)/5% acetonitrile (0.05% TFA) to 5% H_2O (0.05% TFA)/95% acetonitrile (0.05% TFA). The characterization by electrospray mass spectrometry was carried out by UPLC-MS (AQUITY Ultra Performance LC™ from Waters using a BEH C18 column of 1.7 μm, 2.1×100 mm).

Preparation of lipid vesicles

DMPG or DMPC were dissolved in a chloroform/methanol (2:1, *v*/*v*) mixture, and the solutions were evaporated to dryness in vacuum with a rotary evaporator. The dried lipid film was subjected to high vacuum overnight to remove trace amounts of solvent. Then, the lipid films were hydrated with Hepes buffer (5 mmol/L, pH 7.4) obtaining multilamellar vesicles (MLVs). MLVs were further transformed to SUVs by bath sonication [20].

Fluorescence anisotropy of membrane lipids

The dynamics of lipids in liposome membranes in the presence of the peptide was determined by measuring the degree of depolarization of the fluorescence emitted from the probes diphenylhexatriene (DPH) and trimethylamino–diphenylhexatriene (TMA–DPH). DPH or TMA–DPH in THF was added to SUVs to achieve a final probe/lipid molar ratio of 1:700. Liposomes were incubated at 60 °C (i.e., above Tm) for at least 1 h before use to allow the probe to be incorporated. The peptide was mixed with SUVs having a peptide/lipid molar ratio of 1:790, and samples were allowed to equilibrate for 15 min before the measurements. Fluorescence polarization was measured in an AB-2 spectrofluorimeter SLM-Aminco under stirring (1 cm path-length quartz cuvettes) equipped with a Peltier device connected to a temperature controller. The widths of excitation and emission slits were 4 nm. The excitation and emission wavelengths were 365 and 425 nm, respectively. Samples were submitted at least to three heating and cooling cycles from 15 to 35 °C and vice versa, with steps of 1 °C. An equilibration time of 5 min was allowed after each temperature change. Fluorescence anisotropy (*r*) was calculated automatically by the software provided with the instrument, according to Eq. 3.

$$r = \frac{I_{Vv} - GI_{Vh}}{I_{Vv} + 2GI_{Vh}} \tag{3}$$

where $G=I_{Hv}/I_{Hh}$, the *g*-factor used to correct the anisotropy values for the unequal transmission of differently polarized light, and I_{Vv}, I_{Hh}, I_{Hv}, and I_{Vh}, are the various fluorescence intensities with the excitation and emission polarization filters, respectively, in vertical (v) and horizontal (h) orientations.

Fluorescence studies of intrinsic tryptophan in E1(142–165)

The fluorescence of the Trp residue was recorded as a function of the lipid/peptide molar ratio and corrected for the contribution of light scattering in the presence of vesicles. Emission fluorescence spectra were collected by keeping constant the initial concentration of the peptide (3.1 μM in HEPES 5 mM, pH 7.4) and incrementing the concentration of DMPG or DMPC. For this purpose, aliquots of 70 μM of DMPG or DMPC SUVs were added. After each addition, the emission spectrum was recorded in a range of 300 to 450 nm. The excitation and emission bandwidths were set at 4 nm each and the excitation wavelength was 280 nm. The interaction was tested at two temperatures (25 and 37 °C). Cuvette temperature was maintained with a peltier system piloted by a computer program (Microbeam S.A., Barcelona, Spain), and the temperature was registered with a thermocouple inserted into the cuvette. The suspensions were continuously stirred and left to equilibrate for 5 min before recording the spectrum. Peptide–phospholipid interactions were assessed by monitoring changes in the fluorescence spectra. Blue shifts were calculated as the differences in wavelength of the maxima in the emission spectra of the peptide, recorded with and without liposomes. Standard deviation for the blue shift was less than 0.5 nm.

EFA and MCR-ALS application

Recorded spectra were converted into ASCII files for further analysis by means of EFA and MCR-ALS software supported with MatLab v. 2008a (MathWorks, MA, USA). MCR-ALS software developed by Tauler et al. was used (http://www.ub.es/gesq/mcr.htm).

Identical constraints were imposed to all the experiments. Since the intensity in fluorescence is expected to have positive values, non-negativity constraint was imposed to both spectral and concentration profiles. The unimodality constraint was imposed to the concentration profiles. A %LOF value of 0.1% was imposed. The number of absorbing components was elucidated by using Evolving Factor Analysis implemented in PLS-Toolbox v. 4.0 (Eigenverctor Research, WA, USA) working under MatLab v. 2008a. The initial estimation of spectral profiles was obtained by selecting as many spectra as luminescence components for each experiment.

Results and discussion

The peptide E1(145–162) was successfully synthesized and characterized by HPLC and mass spectrometry (see Figure 1_ESM). The molecular weight of the peptide is 2,173.62, and the mass spectrum show the majoritary peaks of *m*/*z* ratio for *z*=+2 and *z*=+3, both protonated.

Effect of E1(145–162) sequence on membrane lipid order

Changes in fluorescence anisotropy of two fluorescent probes (TMA–DPH and DPH), incorporated in DMPC or DMPG SUVs, were measured in order to investigate peptide incorporation and location in different regions of the phospholipid bilayer. TMA–DPH is a hydrophobic molecule, which is anchored at the water/lipid interface due to its charged trimethylammonium group; on the other hand, DPH is anchored into the lipid membrane core and gives information on the fluidity of the non-polar regions of lipid structures. Since fluorescence anisotropy is highly dependent upon the viscosity of the solution in which the fluorophore is dissolved, it can be used to obtain information on the microviscosity of lipid membranes of the fluorophore partitions. *r* values are high at temperatures below the main transition temperature of the lipids, from gel to liquid crystalline state, due to the highly restricted rotation for the probe. Increasing the temperature resulted in a decrease of anisotropy as a consequence of the rotational depolarization concomitant with the decrease in the microviscosity of the membrane. On the other hand, differences in *r* are likely to reflect difference in the extent of binding of the peptide to the lipids.

Values of *r* upon peptide addition to SUVs depend on both lipid and probe (Fig. 2). In the case of DMPG/TMA–DPH (Fig. 2b), *r* in presence of peptide is higher than in absence, showing that the probe is in a more rigid environment. The heating and cooling cycle does not show a significant hysteresis (figure not shown). On the contrary, for SUVs of DMPC labeled with TMA–DPH (Fig. 2d), peptide addition results in a dramatically decrease in *r*, indicating that the probe is surrounded by a bilayer in a fluid state. Considering that the probes chosen for the present assay show intense fluorescence when they are bound to the lipid but do not exhibit fluorescence in aqueous solution, the low values of *r* are indicative of bilayer rupture.

On another hand, analyzing the peptide effect on a deeper part of the bilayer, DMPG SUVs labeled with DPH (Fig. 2a) show dispersed *r* values, probably as a consequence of vesicle aggregation. In addition, the cooling profile shows a remarkable hysteresis in the liquid crystal-

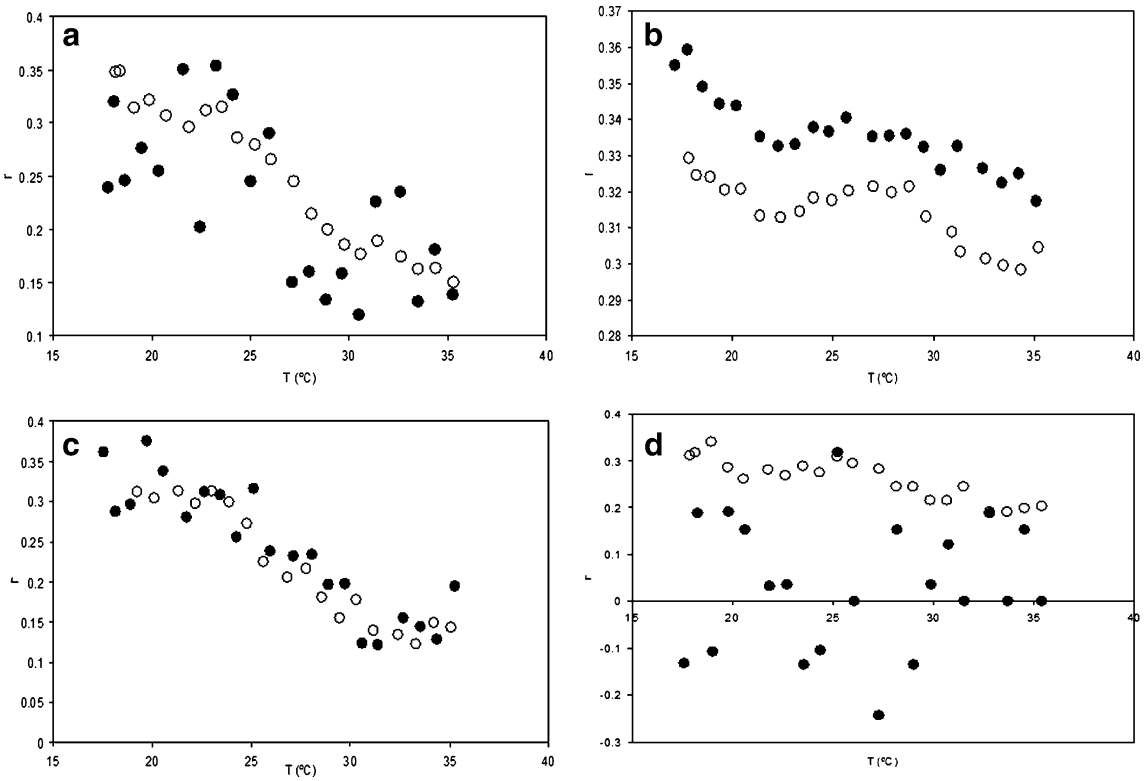

Fig. 2 Temperature transition profiles of DPH or TMA–DPH labeled SUVs in the presence (*filled dots*) and absence (*empty dots*) of peptide. **a** DMPG/DPH, **b** DMPG/TMA–DPH, **c** DMPC/DPH, and **d** DMPC/TMA–DPH. Each individual point is the mean ± *S* of three different experiments

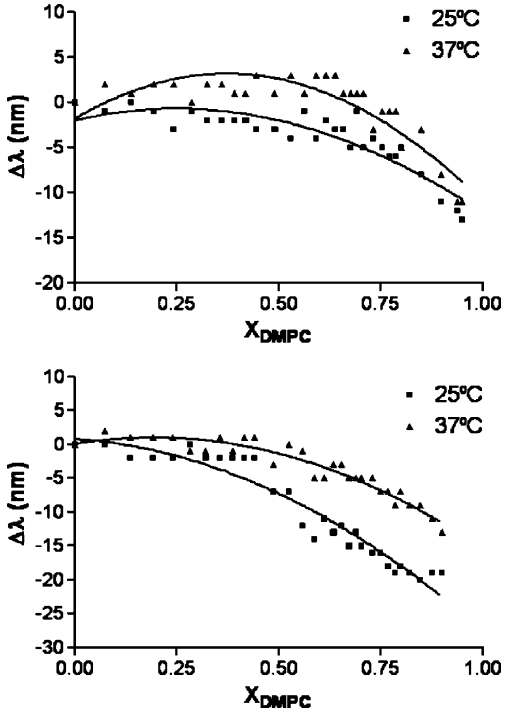

Fig. 3 Blue shift in Trp emission maximum in the presence of liposomes composed of DMPC or DMPG at 25 or 37 °C at different molar ratios (*X*)

to-gel transition, indicating that the probe is free in solution and therefore it is an irreversible process (figure not shown). In the case of DPH embedded into DMPC SUVs (Fig. 2c), the presence of peptide does not show a remarkable effect on the bilayer order. However, the dispersion of the values suggests vesicle aggregation.

Intrinsic emission fluorescence

The characteristics of Trp fluorescence are sensitive to changes caused by alterations in peptide conformation and membrane association. Changes in the microenvironment of the Trp of the E1(145–162) peptide upon binding to zwitterionic DMPC or to negatively charged DMPG lipid bilayers were monitored by measuring its Trp fluorescence.

Modifications in Trp fluorescence intensity are commonly observed when peripheral proteins interact with membranes. Often, the emission intensity increases, and the λ_{max} undergoes a blue shift when a Trp-containing protein moves from an aqueous solution to a membrane-bound state [21]. Our goal was to evaluate whether changes in Trp fluorescence could provide direct evidence of peptide interaction with membranes.

The maximal emission wavelength (λ_{max}) of E1(145–162) was 353 nm in buffer, thus indicating that the Trp is exposed to the medium [22]. Addition of DMPC or DMPG vesicles to E1(145–162) shifted the λ_{max} to shorter wavelengths and decreased the fluorescence intensity (Fig. 3). Both effects suggest that the Trp residue is located in a less polar environment, showing interaction and partial penetration of the peptides into the hydrophobic tail of the bilayer without being completely buried. On the other hand, as described for other peptides, this effect could result from an extended lipid conformation of the contact sites together with the intercalation of the Trp residue into the bilayers [23].

EFA and MCR-ALS results

As an example, the fluorescence pattern collected for DMPC at both temperatures is depicted in Fig. 4.

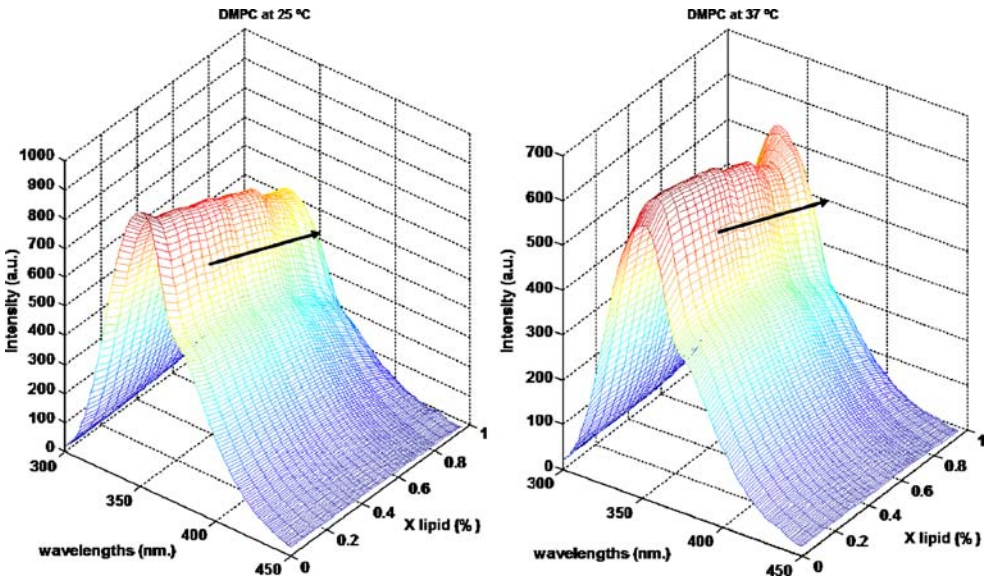

Fig. 4 Fluorescence pattern collected for DMPC by varying the molar ratio with lipid at two temperatures

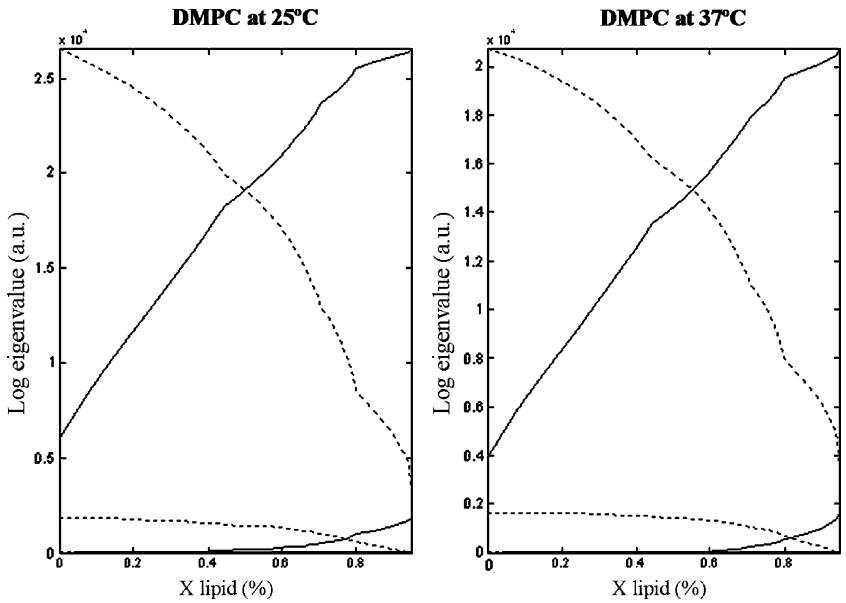

Fig. 5 Evolving factor analysis for DMPC at two temperatures. *Solid lines* indicate the forward EFA analysis, whereas *dotted lines* indicate the backward EFA analysis

At first sight, it could be thought that three components would appear in the media (peptide, lipid and the interaction between them). Nevertheless, previous analysis of the number of components by using evolving factor analysis denoted that there were two main components with luminescence in the wavelength working range (Fig. 5). This is because the lipid did not present luminescence by itself during the reaction. Therefore, the two absorbing components were the peptide and the interaction between peptide and lipid. This observation is very important for the further development of MCR-ALS models. The fact that there are only two components obliged not to impose closure constraint since the mass balance depends on the three components, but the change in the spectra is only due to two of those components.

Results obtained with MCR-ALS are depicted in Fig. 6. All the models obtained explained more than the 99.00% of the explained variance in the data. Moreover, the residuals did not reveal any systematic variation, and their values remained randomly distributed throughout the molar fraction. These observations supported the validity of the obtained MCR-ALS models.

The first remarkable observation was that the obtained spectral profiles were very similar within and between

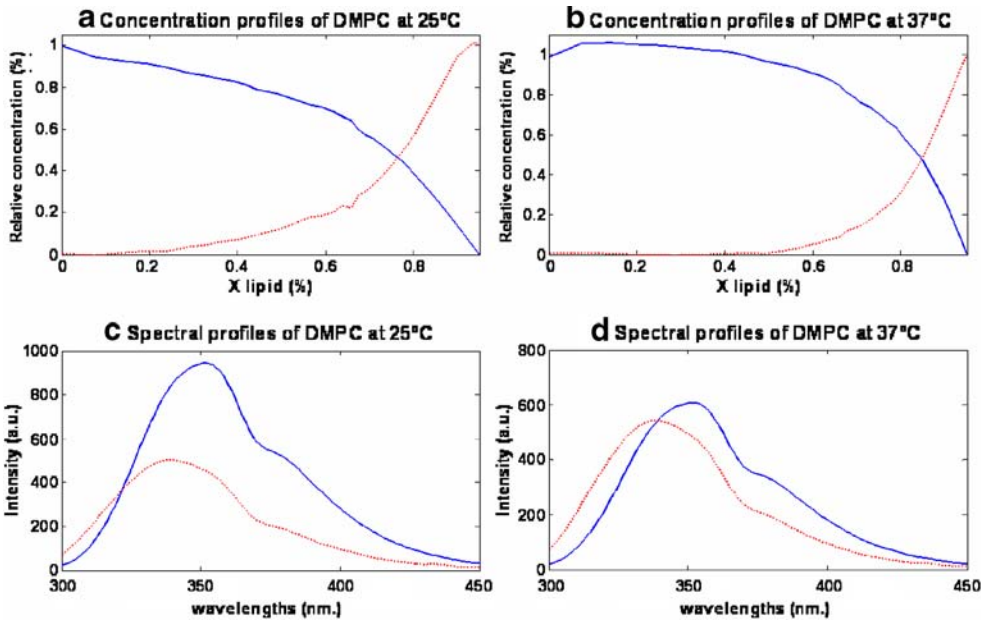

Fig. 6 MCR-ALS results. *Blue solid line* peptide E1(145–162). *Red dotted line* the interaction between E1(145–162) and lipid. **a** and **b** Concentration profiles obtained for DMPC at 25 and 37 °C, respectively. **c** and **d** Spectral profiles obtained for DMPC at 25 and 37 °C, respectively

temperatures (Only results for DMPC at both temperatures are shown in Fig. 6). This indicates that temperature influences in the behavior (concentration profiles) and not in the spectra of both peptide and lipid.

A new specie appears at a specific molar fraction depending on the temperature. This specie could be attributed to the binding and subsequent partial penetration of the peptide into the hydrophobic core of the bilayer, where the Trp residue senses a less polar environment, giving a minor fluorescence and shifting the maximum wavelength to the blue.

Conclusions

The use of synthetic peptides offers an effective approach for designing chemically well-defined molecules of specific activity. The experimental data obtained in this work reinforce the hypothesis that the E1(142–165) peptide could be an internal fusion peptide of HGV/GBV-C [24, 25]. This fact is supported by means of anisotropy measurements. Moreover, the known preference of Trp for the interfacial regions of membranes [26] was assessed by Trp fluorescence assays that show the shifting of the λ_{max} of the Trp residue to shorter wavelengths in presence of bilayers.

These results indicate that membrane penetration as well as cooperative interactions accompanies the bilayer association of the peptide derivative.

The usefulness of EFA and MCR-ALS to extract underlying information about the behavior of the peptides exposed to the lipidic bilayer tested has also been demonstrated, offering the possibility of further studies mainly focused on modeling and fitting the temperature effect to establish empirical functions to define the system.

Acknowledgments This work is supported by project CTQ2006-15396-C02-02/01-BQU from Secretaría de Estado de Investigación, Ministerio de Ciencia e Innovación, Dirección General de Programas y transferencia de conocimiento, Subdirección General de Proyectos de Investigación (Spain). M.J. Sánchez-Martín is a recipient of a FPI program pre-doctoral grant. José Manuel Amigo wants to thank the Danish Research Council for Technology and Production Sciences for his post-doctoral fellowship. The authors are members of the consolidated research group by the Generalitat de Catalunya: *Peptides and Proteins: physicochemical studies* (2005SGR00278).

References

1. Simons JN, Pilot-Matias TJ, Leary TP, Dawson GJ, Desai SM, Schlauder GG, Muerhoff AS, Erker JC, Buijk SL, Chalmers ML et al (1995) Proc Natl Acad Sci U S A 92:3401
2. Linnen J, Wages J Jr, Zhang-Keck ZY, Fry KE, Krawczynski KZ, Alter H, Koonin E, Gallagher M, Alter M, Hadziyannis S, Karayiannis P, Fung K, Nakatsuji Y, Shih JW, Young L, Piatak M Jr, Hoover C, Fernandez J, Chen S, Zou JC, Morris T, Hyams KC, Ismay S, Lifson JD, Hess G, Foung SK, Thomas H, Bradley D, Margolis H, Kim JP (1996) Science 271:505 New York, N.Y
3. Halasz R, Weiland O, Sallberg M (2001) Scand J Infect Dis 33:572
4. Tillmann HL, Manns MP (2001) Antivir Res 52:83
5. Xiang JH, Wunschmann S, Diekema DJ, Klinzman D, Patrick KD, George SL, Stapleton JT (2001) N Engl J Med 345:707
6. Voisset C, Dubuisson J (2004) Biol Cell 96:413
7. de Juan A, Tauler R (2006) CRC Crit Rev Anal Chem 36:163
8. Garrido M, Rius FX, Larrechi MS (2008) Analytical and Bioanalytical Chemistry 390:2059
9. Yongnian N, Shaojing S, Serge K (2008) Ana Chim Acta 6 2 8:49
10. Rodriguez-Rodriguez C, Amigo JM, Coello J, Maspoch S (2007) J Chem Educ 84:1190
11. Jaumot J, Gargallo R, de Juan A, Tauler R (2005) Chemometr Intell Lab Syst 76:101
12. Maeder M (1987) Anal Chem 59:527
13. Whitson AC, Maeder M (2001) J Chemom 15:475
14. Gargallo R, Tauler R, CuestaSanchez F, Massart DL (1996) TrAC-Trends Anal Chem 15:279
15. Amigo JM, de Juan A, Coello J, Maspoch S (2006) Anal Chim Acta 567:245
16. Amigo JM, de Juan A, Coello J, Maspoch S (2006) Anal Chim Acta 567:236
17. Chan WC, White PD (2000) Fmoc solid phase peptide synthesis. Oxford University Press, New Cork
18. Kaiser E, Colescot RL, Bossinge CD, Cook PI (1970) Anal Biochem 34:595
19. Rojo N, Gomara MJ, Alsina MA, Haro I (2003) J Pept Res 61:318
20. Butko P, Huang F, PusztaiCarey M, Surewicz WK (1996) Biochemistry 35:11355
21. Ladokhin AS, Jayasinghe S, White SH (2000) Anal Biochem 285:235
22. Wimley WC, White SH (2000) Biochemistry 39:4432
23. Zhao H, Sood R, Jutila A, Bose S, Fimland G, Nissen-Meyer J, Kinnunen PKJ (2006) Biochim Biophys Acta, Biomembr 1758:1461
24. de Souza DL, Frisch B, Duportail G, Schuber F (2002) Biochim Biophys Acta 1558:222
25. Munoz M, Rojo N, Haro I, Girona V, Mestres C, Busquets MA (2003) Talanta 60:483
26. Yau WM, Wimley WC, Gawrisch K, White SH (1998) Biochemistry 37:14713

3.3. Artículo 3. Analysis of HIV-1 fusion peptide inhibition by synthetic peptides from E1 protein of GB virus C

El objetivo de este estudio es identificar péptidos que puedan inhibir la actividad de la secuencia peptídica que representa el extremo N-terminal de la proteína gp41 del VIH, correspondiente al péptido de fusión del virus (PF del VIH-1). Se sintetizaron y estudiaron 58 péptidos solapados en 15 residuos correspondientes a la proteína E1 del virus de la hepatitis G (GBV-C). Cinco de los péptidos sintetizados: NCCAPEDIGFCLEGGCLV (P7), APEDIGFCLEGGCLVALG (P8), FCLEGGCLVALGCTICTD (P10), QAGLAVRPGKSAAQLVGE (P18) y AQLVGELGSLYGPLSVSA (P22), son capaces de inhibir la liberación de contenidos vesiculares causada por el PF VIH-1. Toda una serie de experimentos se llevaron a cabo para intentar determinar cómo estos péptidos de la proteína E1 interaccionan con el PF del VIH-1. Se han analizado las interacciones tanto en presencia como en ausencia de modelos de membrana. La calorimetría isotérmica de titulación (ITC) reveló que la unión de P7, P18 y P22 al PF VIH-1 es fuertemente endotérmica. La energía de Gibbs del proceso indica una unión espontanea entre los péptidos de la proteína E1 y el PF VIH-1. Por otro lado, el ensayo de microscopía confocal utilizando liposomas unilamelares gigantes (GUVs) como modelos de membrana mostró que la ruptura de la bicapa lipídica causada por el PF VIH-1 se inhibía por la presencia de cualquiera de los cinco péptidos seleccionados. Los resultados destacan que estos péptidos sintéticos de la proteína E1 pueden estar involucrados en la prevención de la entrada del VIH-1 pero su interacción con PF del VIH-1 es diferente según el caso. Los experimentos de diálisis muestran que los péptidos interaccionan en disolución, lo cual se corrobora para P7, P8 y P22 en los estudios de ITC; sin embargo, no podemos confirmarlo para los otros dos péptidos. Los diferentes comportamientos muestran que esta interacción no es tan simple y que los péptidos no interaccionan sólo en disolución o sólo en la membrana, sino mediante un mecanismo más complejo.

Journal of Colloid and Interface Science 360 (2011) 124–131

Contents lists available at ScienceDirect

Journal of Colloid and Interface Science

www.elsevier.com/locate/jcis

Analysis of HIV-1 fusion peptide inhibition by synthetic peptides from E1 protein of GB virus C

Maria Jesús Sánchez-Martín [a,*], Kalina Hristova [b], Montserrat Pujol [a], Maria J. Gómara [c], Isabel Haro [c], M. Asunción Alsina [a], M. Antònia Busquets [a]

[a] Physical Chemistry Department, Faculty of Pharmacy, University of Barcelona, Associated Unit to the CSIC: Peptides and Proteins: Physicochemical Studies, IN2UB. Av. Joan XXIII s/n, 08028 Barcelona, Spain
[b] Department of Materials Science and Engineering, Johns Hopkins University, Baltimore, MD 21218, USA
[c] Unit of Synthesis and Biomedical Application of Peptides, Department of Biomedical Chemistry, IQAC-CSIC, Jordi Girona 18, 08034 Barcelona, Spain

ARTICLE INFO

Article history:
Received 28 February 2011
Accepted 12 April 2011
Available online 24 April 2011

Keywords:
HIV-1 FP inhibition
Hepatitis G virus
Peptide synthesis
Bilayers as model membranes
Giant unilamellar vesicles
Confocal microscopy

ABSTRACT

The aim of this study was to identify proteins that could inhibit the activity of the peptide sequence representing the N-terminal of the surface protein gp41 of HIV, corresponding to the fusion peptide of the virus (HIV-1 FP). To do this we synthesized and studied 58 peptides corresponding to the envelope protein E1 of the hepatitis G virus (GBV-C).

Five of the E1 synthetic peptides: NCCAPEDIGFCLEGGCLV (P7), APEDIGFCLEGGCLVALG (P8), FCLEGGCL VALGCTICTD (P10), QAGLAVRPGKSAAQLVGE (P18) and AQLVGELGSLYGPLSVSA (P22) were capable of inhibiting the leakage of vesicular contents caused by HIV-1 FP. A series of experiments were carried out to determine how these E1 peptides interact with HIV-1 FP. Our studies analyzed the interactions with and without the presence of lipid membranes. Isothermal titration calorimetry revealed that the binding of P7, P18 and P22 peptides to HIV-1 FP is strongly endothermic, and that binding is entropy-driven. Gibbs energy for the process indicates a spontaneous binding between E1 peptides and HIV-1 FP. Moreover, confocal microscopy of Giant Unilamellar Vesicles revealed that the disruption of the lipid bilayer by HIV-1 FP alone was inhibited by the presence of any of the five selected peptides.

Our results highlight that these E1 synthetic peptides could be involved in preventing the entry of HIV-1 by binding to the HIV-1 FP. Therefore, the continued study into the interaction between GBV-C peptides and HIV-1 FP could lead to the development of new therapeutic agents for the treatment of AIDS.

1. Introduction

In recent years, synthetic peptides have attracted a great deal of attention in the multidisciplinary and emerging field of nanobiomedicine [1–3] due to the chemical diversity which can be tolerated within these nanostructures, their ease of synthesis, their high purity and their low production costs. The multiple applications of these compounds include their use in research, diagnosis and the treatment of viral infections such as AIDS and hepatitis [4–7].

Significant progress has been made in the treatment of human immunodeficiency virus (HIV) infection, but we are still far from the end of the battle against this disease. Current therapy consists of complex treatments of nucleoside analogs, non-nucleoside reverse transcriptase inhibitors, and viral protease inhibitors aimed at specific steps of the HIV replication cycle. These drugs target with high specificity, but caution should be exercised because rapid virus turnover in HIV infection can result in the emergence of resistant mutations and subsequent treatment failure [8,9]. However, the natural history of hepatitis G virus (GBV-C) infection is, at present, not fully understood and its potential to cause hepatitis in humans is questionable [10].

The GB virus C (GBV-C) was recently investigated in the context of HIV infection, because hepatitis virus infections are very frequent in patients suffering from HIV as they have similar transmission routes. Infection with the hepatitis B (HBV) or C (HCV) virus on AIDS patients has been associated with an impaired survival, and these patients often die from liver failure instead of AIDS [11]. In contrast, previous studies have suggested that people co-infected with HIV and GBV-C exhibit delayed progression of HIV, indicating a beneficial influence of GBV-C on patients with HIV infection [12]. Based on a co-infection model, GBV-C may inhibit HIV by inducing chemokines, down-regulating HIV co-receptor(s), influencing cytokine profiles, and having other as yet undefined effects on the host lymphocytes [12,13]. However, the mechanism

* Corresponding author. Fax: +34 93 403 59 87.
E-mail address: mjsanchez@ub.edu (M.J. Sánchez-Martín).

0021-9797/$ - see front matter © 2011 Elsevier Inc. All rights reserved.
doi:10.1016/j.jcis.2011.04.053

responsible for the beneficial effect that the GBV-C virus exerts on the course of infection caused by HIV has yet to be fully defined.

Jung et al. [14] demonstrated that cells transfected with either infectious RNA or a deletion mutant that expressed the N-terminal third of the polyprotein (including the E1 and E2 coding regions) resulted in inhibition of HIV replication, increased the release of chemokines, and decreased the surface expression of CCR5 compared to cells transfected with antisense GBV-C RNA. This indicates that the envelope proteins may be involved in the inhibition of HIV replication.

Recently, we described certain E2 GBV-C domains that interfere with the HIV-1 FP-vesicle interaction, decrease the cellular membrane fusion, and interfere with the HIV-1 infectivity in a dose-dependent manner [15].

Taking into account the attractive properties of synthetic peptides and the possible relation between the envelope GBV-C proteins and the inhibition of HIV replication, we studied the capacity of GBV-C E1 peptide sequences to inhibit the interaction and destabilization process of membranes induced by the fusion peptide (FP) of HIV-1. To achieve this, 58 E1 peptides from GBV-C were synthesized and characterized.

Recent studies have reported the importance of leakage experiments or isothermal titration calorimetry studies [16–19] in understanding the membrane interacting properties of synthetic peptides. Thus, several biophysical techniques were used to cover different aspects of GBV-C peptide/HIV-1 FP interaction in the presence and absence of lipid vesicles. As a first indication of the ability of GBV-C sequences to inhibit pore formation caused by HIV-1 FP we chose the leakage of the vesicular content assay [16,17,20]. From the results of this initial test, five sequences were selected for further studies. Then, the binding of these selected peptide sequences to large unilamellar vesicles was studied by comparing two separation methods: centrifugation and equilibrium dialysis. The same experiment was used to study the E1 peptides inhibition capacity towards HIV-1 FP binding. The thermodynamics of peptide-peptide interaction in solution was also analyzed by isothermal titration calorimetry. Finally, the inhibition effect was observed using a confocal microscopy.

As far as the lipid composition is concerned, whenever possible we chose negatively charged phospholipids because it was found that HIV-1 FP binds stronger to negative phospholipids than to lipid devoid of charge. The exception was the preparation of giant unilamellar vesicles where a zwitterionic lipid was used but labeled with a negative probe, therefore giving a global negative charge.

Our results indicate the capacity of certain peptide sequences of the GBV-C E1 protein to inhibit the fusion process of liposomes induced by the FP of the HIV-1 glycoprotein gp41.

2. Experimental

2.1. Materials

Amino acids and Rink amide resin (Tentagel R RAM, 0.19 meq/g) were obtained from *Novabiochem* (Nottingham, UK). Dimethylformamide (DMF) was purchased from *Scharlau* (Barcelona, Spain). Dichloromethane (DCM) and piperidine were purchased from *Fluka* (Neu-Ulm, Germany). Acetic acid, diethyl ether, and trifluoroacetic acid (TFA) were obtained from *Merck* (Poole, Dorset, UK). *N*-hydroxybenzotriazole (HOBt) and *N*,*N*′-diisopropylcarbodiimide (DIPCDI) coupling reagents were obtained from *Fluka* and *Novabiochem*, respectively. Other coupling reagents such as O-(7-azabenzotriazole-1-yl)-N, *N*,*N*′*N*′-tetramethyluronium hexafluorophos phate (HATU) and *N*,*N*′-diisopropylethylenamine (DEIA) were obtained from *GenScript Corporation* and *Fluka*, respectively. Scavengers such as ethanedithiol (EDT) and triisopropylsilane (TIS) were obtained from Sigma–Aldrich.

1,2-dimyristoyl-sn-glycero-3-phosphocholine (DMPC), 1-palmitoyl-2-oleoyl-sn-glycero-3-phosphocholine (POPG), and 1,2-di-(9,10-dibromo) stearoyl-sn-glycero-3-phosphocholine (Br-PC) and Rho-PE [(1,2-dioleoyl-*sn*-glycero-3-phosphoethanolamine-N-(lissamine rhodamine B sulfonyl) (ammonium salt) (18:1 lissamine rhodamine PE)] were purchased from Avanti Polar Lipids. The purity of these lipids was above 99% and they were used without further purification.

Chloroform and methanol were purchased from Merck. Water was double distilled and deionized (MilliQ system, Millipore) (18.2 MΩ cm, pH 5.8). The buffer used in all experiments was HEPES (from Sigma–Aldrich) 5 mM and NaCl (from Merck) 20 mM, pH 7.4.

2.2. Peptides synthesis

A scan of the GBV-C E1 protein (Genbank D90600, Japan) was carried out by the semiautomatic multiple syntheses of 18-mer peptides overlapped by fifteen residues. The resulting 58 linear peptides were synthesized on a Multisyntech synthesizer using a Tentagel R RAM resin (0.19 meq/g). This resin enables carboxamide peptides to be obtained at the C-terminal end, by a solid phase methodology following an Fmoc/tBu strategy by means of HATU and DEIA activation. Side protection was effected by the following: 2,2,5,7,8-pentamethyl-chroman-6-sulfonyl (Pmc) for Arg, tert-Butyl (tBu) for Tyr, Ser, Thr and Asp and t-butyloxycarbonyl (Boc) for Lys and Trp. Threefold molar excess of Fmoc-amino acids was used throughout the synthesis. In the manual synthesis, the stepwise addition of each residue was assessed by the Kaiser's (ninhydrin) test [21] and repeated couplings were carried out when a positive ninhydrin test was obtained.

The synthesized peptides were deprotected from the side-chain groups and cleaved from the resin with a treatment of trifluoroacetic acid (TFA) containing appropriate proportions of scavengers [22] such as H_2O, triisopropylsilane (TIS), and ethanedithiol (EDT): 94% TFA: 2.5% H_2O: 2.5% EDT: 1% TIS.

Peptides were characterized using an analytical HPLC Perkin Elmer with an LC-235 Diode Array Detector and a Binary LC Pump 250; the column used was a KROMASIL 100 C18 5 μm of 25 × 0.46 cm. The analysis was carried out using a linear gradient of 95% H_2O (0.05% TFA)/5% acetonitrile (0.05% TFA) to 5% H_2O (0.05% TFA)/95% acetonitrile (0.05% TFA). The characterization by electrospray mass spectrometry was carried out using UPLC-MS (AQUITY Ultra Performance LC™ from Waters, using a BEH C18 column of 1.7 μm, 2.1 × 100 mm). The peptides were purified to as much as 90% by analytical HPLC at 215 nm (for further details see Supporting information, Table 1).

Peptides synthesized manually (P7, P8, P10, P18 and P22) were purified by semi-preparative HPLC in a Kromasil-C8 column and characterized by ES–MS, achieving a final purity of over 95%.

The fusion peptide of the HIV-1 glycoprotein gp41, HIV-1 FP/AVGIGALFLGFLGAAGSTMGAAS, was also synthesized by manual SPPS but using a 100% polyethylene glycol-based ChemMatrix resin that proved to be a more effective support for the solid-phase synthesis of hydrophobic and highly structured peptides. The final purity of the peptides achieved using HPLC was higher than 95%.

2.3. Preparation of lipid vesicles

2.3.1. Large unilamellar vesicles

Phospholipids were dissolved in a chloroform:methanol (2:1, v/v) mixture and the solutions were evaporated to dryness in a vacuum with a rotary evaporator. The dried lipid film was subjected to a high vacuum overnight to remove trace amounts of solvent. Then, the lipid films were hydrated with Hepes buffer (5 mmol/L,

pH 7.4) containing NaCl 20 mM to obtain multilamellar vesicles (MLVs). MLVs were further transformed to large unilamellar vesicles (LUVs) by extrusion under moderate pressure through a polycarbonate filter of 0.1 μm pore size [23]. The lipid concentration of the stock solutions was 1.5 mM.

2.3.2. Giant unilamellar vesicles

Giant liposomes were made using the gentle hydration method [24–26] of DMPC films doped with glucose [27] but with slight differences in the preparation method.

Two solutions of (i) DMPC 10 mM in chloroform and (ii) glucose 20 mM in methanol were prepared. Solutions containing 50 μL of DMPC and 250 μL of glucose were then mixed with 0.6% of Rho-PE, which acted as a labeling probe to allow us to view the vesicles during the confocal microscopy experiments. The mixture was evaporated in the rotary evaporator to form the film and dried under a nitrogen stream for 1 h. The dry lipid film was hydrated with 2 mL of distilled water and the liposomes left to grow at 40 °C for 24 h. The cloud of vesicles formed was then collected.

2.4. Leakage of vesicular contents: ANTS/DPX assay

For the ANTS (8-aminonaphtalene-1,3,6-trisulfonic acid)-DPX (*N*,*N*′-p-xylene-bis(pyridinium bromide) leakage assay [28,29], approximately 20 mg of POPG was dissolved in a mixture of chloroform and methanol (2:1), which was subsequently removed under a stream of nitrogen. Approximately 2 mL of buffer was added to the dry lipid. The buffer contained 12.5 mM ANTS and 45 mM DPX from Molecular Probes (Eugene, OR) and 20 mM NaCl and 5 mM Hepes. The osmolarity of the ANTS/DPX solution was adjusted so that it was equal to that of the buffer in a cryoscopic osmometer (Fiske One-ten). The suspension was frozen and thawed 10 times to ensure maximum entrapment prior to extrusion [30]. A stock solution of LUV of approximately 0.1 μm in diameter was formed by extrusion pressure through Nucleopore polycarbonate membranes. The vesicles were separated from unencapsulated material on Sephadex G-75 (Pharmacia, Uppsala, Sweden), and equilibrated with 100 mM NaCl/5 mM Hepes buffer (pH 7.4). The final concentration of the lipid was 0.1 mM.

Fluorescence was measured in an Aminco Bowman AB2 (Microbeam, SA) spectrofluorimeter before and after detergent was added. Before being added to the suspension of LUVs, each GBV-C peptide sequence corresponding to the E1 protein was incubated for 30 min with the HIV-1 FP in dimethylsulfoxide (DMSO). Following this, the fluorescence was measured again. The amount of DMSO, with respect to the total volume of the assay, was always less than 5%. No significant differences in fluorescence were observed when adding the equivalent volume of DMSO in the absence of a peptide. The dequenching of co-encapsulated ANTS and DPX fluorescence resulting from dilution was measured to assess the leakage of aqueous contents from vesicles. Leakage was monitored by measuring the increase in the ANTS/DPX fluorescence intensity at 520 nm, with an excitation of 355 nm and slits of 8 nm. HIV-1 FP/E1 peptide ratios ranged from 1/1 to 1/20. The percentage of leakage was calculated according to the equation below:

$$\%\text{leakage} = \frac{(F - F_0)}{(F_{100} - F_0)} \times 100 \quad (1)$$

where F_0 is the initial fluorescence of LUVs, F is the fluorescence intensity after adding the peptide, and F_{100} is the fluorescence intensity after the addition of 10 μL of a 10% (v/v) Triton-100 solution (complete lysis of LUVs).

2.5. Peptide binding to lipid vesicles

HPLC has been previously used for the determination of peptide concentrations in the presence of LUV [31]. The column used was a VYDAC 218TP54 C18 of 5 μm, 25 × 0.46 cm. The analysis was carried out using a linear gradient of 95% H_2O (0.05% TFA)/5% acetonitrile (0.05% TFA) to 5% H_2O (0.05% TFA)/95% acetonitrile (0.05% TFA) for 30 min and absorbance was monitored at 215 nm. Two separation methods were used to determine the amount of peptide bound to lipid vesicles.

2.5.1. Centrifugation method

The protocol developed by White et al. [32] was followed in this study. Briefly, an aliquot of a mixture of peptide and liposomes is centrifuged to separate peptides bound to the vesicles from those that are unbound. Subsequently, the sediment holds the fraction containing the peptide bound to the lipid vesicles, while the free unbound peptide remains in the supernatant.

In order to facilitate vesicles sedimentation, we used LUVs made with Br-PC, of which 20% was POPG. The brominated lipid is used because it enables the liposomes in a centrifugal field to be sedimented, and the negatively-charged lipid is required to facilitate the highest interaction possible between the HIV-1 FP and the liposomes.

Stock solutions of 1 mg ml^{-1} of E1 peptides were used. Appropriate volumes of these peptides were selected to obtain a final concentration of 0.2 mM in the final mixture with the brominated liposomes. E1 peptides were incubated with the HIV-1 FP in DMSO for a period of 30 min at a molar ratio HIV-1 FP:E1 peptide of 1:20. The E1 peptides alone and the mixtures of both peptides were then incubated with the brominated liposomes (0.565 mM) for a period of 30 min; an aliquot of the lipid-peptide solution was withdrawn for the HPLC analysis of total peptide and the samples were then sedimented using a Microfuge® 18 Centrifuge of Beckman Coulter™. The sedimentation was done progressively by spinning at 4500, 9000 and then 16,000*g* for 30 min each time so that the liposomes were sedimented gently at first and then spun into a tight pellet. Following this, the peptide concentration of the supernatant was analyzed by HPLC as described before.

2.5.2. Equilibrium dialysis

The basic principle of equilibrium dialysis is that two half cells, one containing a small volume of lipid solution and the other containing buffer, are separated by a membrane that is permeable to peptides but impermeable to lipid vesicles. We used the RED (rapid equilibrium dialysis) Device Inserts from Thermo Scientific and a Teflon® high-grade Reusable Base Plate. The sampling of total and free peptide is done directly in an equilibrium dialysis, and there is an explicit assumption that the free peptide has the same concentration on both sides of the dialysis membrane [33].

To determine the incubation time necessary to achieve the equilibrium, 200 μL of a solution of peptide 0.5 mg ml^{-1} in DMSO were added to the sample chamber and 350 μL of buffer were added to the buffer sample. The device was then incubated at room temperature at approximately 100 rpm on an orbital shaker. An aliquot of each chamber was analyzed by HPLC after 4, 24 and 48 h.

To run the binding experiments, the E1 peptides were incubated with HIV-1 FP, in a molar ratio of 1:20, and then with liposomes as in the centrifugation assay, before adding them to the sample chamber. After 48 h, the samples were analyzed by HPLC.

2.6. Isothermal titration calorimetry

Isothermal titration calorimetric (ITC) experiments were recorded on a VP-ITC micro-calorimeter (MicroCal, LLC, Northampton, MA). All the peptides were dissolved in DMSO. Briefly, a

solution of 1 mg ml^{-1} of E1 peptides was injected into the chamber containing 25 μM HIV-1 FP. The calorimeter was first equilibrated at 20 °C, and the baseline was monitored during equilibration. The time between injections was 10 min, and the stirring speed was 300 rpm. The heats of dilution were determined in control experiments by injecting E1 peptides into DMSO. They were then subtracted from the heats produced in the corresponding peptide–peptide binding experiments. Control experiments were also performed by titrating DMSO into HIV-1 FP. The total observed heat effects were corrected for these small contributions. All titration data were subsequently analyzed using the Origin 7 software (MicroCal, LLC).

2.7. Confocal microscopy

Confocal microscopy studies were run to visualize how HIV-1 FP affected liposomes and to assess whether the E1 peptides were capable of inhibiting the activity of HIV-1 FP. Experiments were performed in an Olympus Fluoview (FV500) with an Olympus IX70 microscopy associated.

Firstly, the HIV-1 FP was incubated during 30 min with E1 synthetic peptides at different molar ratios, which were 1:1, 1:10 and 1:20. As the results for 1:10 and 1:20 were similar, the lower molar ratio (1:10) was selected to run all the experiments, moreover, this molar ratio also gave good results in the leakage of vesicular contents assay. Following this, 50 μL of liposomes were added to this mixture (1:10), 50 μL were added to HIV-1 FP alone and 50 μL of liposomes were used as a control. Subsequently, the mixtures were subjected to fixation with 3.2% of p-formaldehyde [34] to avoid the aggregation of the liposomes.

3. Results and discussion

3.1. Leakage of vesicular contents: ANTS/DPX assay

After synthesizing 58 overlapped peptides of the envelope protein E1 of GBV-C, the initial proposed work was the study of their capacity to inhibit the interaction and destabilization processes of membranes, induced by HIV-1 FP. This was carried out using the vesicular content leakage assay, as previously described for the E2 GBV-C sequences [15].

The biophysical assay on the vesicle contents release [16,17,20] was used to select the appropriate E1 GBV-C peptide sequences. Firstly, HIV-1 was tested for its ability to induce leakage from large unilamellar phospholipid vesicles (LUVs) of a defined composition. POPG LUVs were used as it was previously reported that HIV-1 binds to negative phospholipids more strongly than to lipids with no net charge [35].

For the assay, a stock solution of 1 mg ml^{-1} of HIV-1 FP in DMSO was used and E1 peptides were dissolved to a concentration of 0.2 mg ml^{-1}. The volume of HIV-1 FP solution providing approximately half of the total vesicle contents release was selected and each GBV-C peptide sequence corresponding to the E1 protein was incubated for 30 min with this concentration of HIV-1 FP. The molar ratio was 1:20 and each experiment was repeated three times.

We found that 53 peptides destabilized the membranes in the same way as the fusion peptide. Only five of the peptides were capable of inhibiting the vesicle contents leakage caused by HIV-1 FP (Fig. 1a) at a molar ratio of 1:20 (HIV-1 FP:E1 peptide). These peptides were named P7, P8, P10, P18 and P22, which correspond to regions the E1(19-36), E1(22-39), E1(28-45), E1(52-69) and E1(64-81), respectively.

Several ratios of the HIV-1 fusion peptide and these 5 peptides (1:1, 1:2, 1:5, 1:10 and 1:20) were tested in the leakage assay. As shown in Fig. 1b, when the proportions of the E1 peptides were low, inhibition did not occur. Taking into account that the amount of HIV-1 FP used provides approximately half of the total vesicle contents release (horizontal red line), we observed that for P8 and P22 we needed a minimum molar ratio of 1:10 to decrease the percentage leakage to under 50%. For P7, P10 and P18 a molar ratio of 1:5 was enough to decrease the % leakage. Below these molar ratios, the leakage obtained was equal to the sum of the leakage caused by the HIV-1 FP and by the E1 peptides.

Results found in this experiment indicate a dual behavior of the peptides. In general, at low E1 peptide concentrations, leakage caused by the HIV-1 FP is not inhibited but rather it increases as a consequence of a synergism between the HIV-1 FP and E1 sequences. Above a certain molar ratio, depending on the peptide, leakage is not completely but highly inhibited. These five peptides were selected for the subsequent studies to corroborate their capacity of inhibition of the vesicle contents leakage caused by HIV-1 FP.

3.2. Peptide binding to lipid vesicles

3.2.1. Centrifugation method

For this assay a brominated phosphocholine (Br-PC) was required to ensure the separation of the liposome-peptide(s) complex. The first question proposed was whether HIV-1 FP would interact with liposomes composed of zwitterionic phospholipids such as Br-PC, because HIV-1 FP binds more effectively to negatively charged phospholipids. Therefore, we needed to know the minimal amount of POPG in Br-PC liposomes that yielded the maximal percentage of leakage in the presence of HIV-1 FP. Thus, the

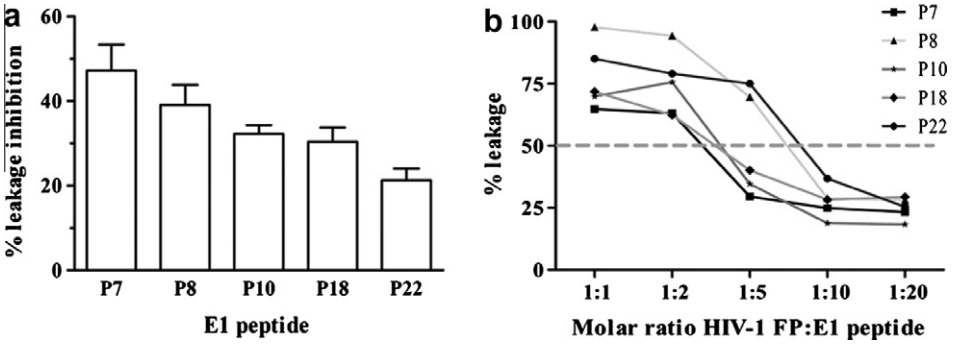

Fig. 1. (a) Inhibitory effect of E1 GBV-C peptides on HIV-1 FP induced leakage. The molar ratio of the HIV-1FP:E1 peptide is 1:20. (b) HIV-1 fusion peptide leakage in the presence of P7,P8,P10,P18 and P22 at different molar ratios. E1 peptides were incubated with the HIV-1 FP amount that causes 50% of leakage (dotted line). Molar ratio POPG/HIV-1 FP: 5/1. All experiments were repeated three times.

first step was to repeat the leakage assay for the HIV-1 FP using liposomes with different molar ratios of POPG and Br-PC.

The amount of HIV-1 FP that provided approximately half of the total vesicle contents release of pure POPG vesicles was tested and was used for all the phospholipid mixtures. The results are shown in Fig. 2.

We found that the leakage of solutes from Br-PC vesicles was low (approximately 15%), but increased more than 4-fold in the presence of POPG. The leakage was similar for all POPG concentrations, ranging from 20% to 100%. While this appears surprising since charge interactions are believed to play a major role in the peptide-lipid interactions that we have studied. However, the close proximity of the POPG headgroups at high POPG concentrations can shift the p*K*a of these headgroups, such that the fraction of charged POPG lipids does not vary much above 20% POPG. Thus, the mixture POPG:Br-PC 20:80 was selected for the binding experiments, as it contains 20% POPG to ensure strong binding, as well as 80% Br-PC, to ensure the sedimentation of the liposomes upon centrifugation. Liposomes were incubated with the peptides alone and with mixtures of HIV-1 FP and E1 peptides.

The initial amount of peptide was analyzed by HPLC before centrifugation. This value corresponded to the total concentration of peptide added that can bind to LUVs. Free peptide or unbound peptide concentration was measured under the same analytical conditions from the supernatant after centrifugation. Each determination was done in triplicate.

The results are shown in Table 1. For P7 and P18 when incubated with HIV-1 FP, the percentage of E1 peptides bound increased, while the percentage of bound HIV-1 FP decreased, showing the inhibition of the interaction of HIV-1 FP with liposomes. For P10 and P22 the percentage of bound E1 peptides decreased, as did the binding of HIV-1 FP to liposomes. The only peptide that seemed to have no interaction with HIV-1 FP was

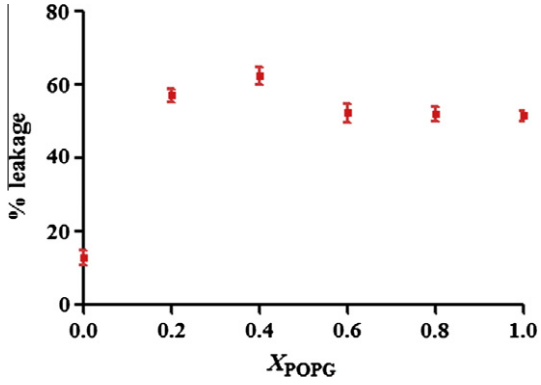

Fig. 2. Percentage of leakage of vesicular contents (ANTS/DPX loaded LUVS) caused by HIV-1 FP to liposomes with different molar ratios of POPG:Br-PC, expressed as molar fraction of POPG. Each point is the average of at least three determinations.

Table 1
Percentage of bound E1 peptides in the presence and absence of HIV-1 FP bound to POPG:Br-PC liposomes.

	% Bound El peptide	% Bound HIV-1 FP
HIV-1 FP		76.3 ± 0.2
P7	−0.4 ± 0.1	
P7 + HIV-1 FP	21.2 ± 0.0	8.0 ± 0.1
P8	22.8 ± 0.5	
P8 + HIV-1 FP	19.9 ± 0.5	76.1 ± 0.4
P10	23.0 ± 0.6	
P10 + HIV-1 FP	4.3 ± 0.4	38. ± 0.4
P18	1.7 ± 0.1	
P18 + HIV-1 FP	12.7 ± 0.2	3.2 ± 0.2

Table 2
Mole fraction partition coefficients of E1 synthetic peptides and HIV-1 FP separately and when mixed.

	Kx (El peptides)	Kx (HIV-1 FP)
P7	No binding	
P7 + HIV-1 FP	6.43×10^5	2.04×10^5
P8	8.67×10^5	
P8 + HIV-1 FP	5.75×10^5	7.50×10^6
P10	8.65×10^5	
P10 + HIV-1 FP	6.45×10^4	9.34×10^5
P18	6.04×10^4	
P18 + HIV-1 FP	2.12×10^5	4.89×10^4
P22	9.19×10^5	
P22 + HIV-1 FP	No binding	2.94×10^5
HIV-1 FP	4.68×10^6	4.68×10^6

P8; as the activity of HIV-1 FP remained equal, it seems that P8 and HIV-1 FP act independently, in the same way as in the leakage assay when a molar ratio of below 1:10 was used. Negative values appeared when there was no binding (due to experimental errors).

The data obtained in this study allowed us to calculate the mole fraction partition coefficient of the peptides following Equation 2:

$$K_x = \frac{([P]_{total} - [P]_{free})/[L]}{[P]_{free}/[W]} \quad (2)$$

where $[P]_{total}$ and $[P]_{free}$ are the aqueous peptide concentrations measured before and after the centrifugation, respectively, and $[L]$ and $[W]$ are the molar concentrations of lipid and water [32].

The results are shown in Table 2. We observed that the partition coefficients of HIV-1 FP decreased when mixed with peptides that inhibit its activity.

3.2.2. Equilibrium dialysis

We measured the time required to reach the equilibrium as explained above and found it to be 48 h for all samples. We then carried out two series of experiments: firstly, we added the liposomes to the sample cell that was the one that will contain the peptides and secondly we added the liposomes to the buffer cell. In both cases, after 48 h, the E1 peptides were equilibrated between the sample cell and the buffer cell, indicating that there is no interaction with the liposomes, independently of whether they are alone or mixed with the fusion peptide.

In all cases, however, the amount of HIV-1 FP remaining with the peptides was higher than in the buffer cell. The results obtained are shown in Table 3. The values correspond to the average of three determinations. We found that when the liposomes were in the same cell as HIV-1 FP alone, it was not equilibrated, which could mean that there is an interaction between HIV-1 FP and the liposomes, forming a complex that could not pass through the membrane. Thus, when HIV-1 FP was mixed with the E1 peptides we could not deduce whether there was an interaction between them or whether it was simply bound to the liposomes. Although for P18, the amount of HIV-1 FP remaining in the sample cell was higher. When the liposomes were added to the buffer cell, HIV-1 FP was equilibrated between both cells, except when in the presence of the E1 peptides. This could be evidence of an interaction between E1 peptides and HIV-1 FP in solution.

3.3. Isothermal titration calorimetry

To asses this interaction further, thermodynamic parameters associated with the binding of E1 peptides to HIV-1 FP were determined by isothermal titration calorimetry (ITC). A binding curve was then obtained from a plot of the heats from each injection against the ratio of ligand and binding partner in the cell. Therefore, the results from an ITC can provide an insight into the

Table 3
Percentage of HIV-1 FP incubated with E1 peptides in a molar ratio of 1:20 present after 48 h of equilibrium dialysis. Experiments were carried out by adding the liposomes to the same cell of HIV-1 FP (sample cell) and then adding them separately.

	Liposomes in sample cell		Liposomes in buffer cell	
	% HIV-1 FP sample cell	%HIV-1 FP buffer cell	% HIV-1 FP sample cell	% HIV-1 FP buffer cell
P7	83.7 ± 0.4	16.3 ± 0.1	62.5 ± 0.6	34.8 ± 0.3
P8	87.9 ± 0.4	12.1 ± 0.4	74.7 ± 0.4	25.3 ± 0.1
P10	73.4 ± 0.3	26.6 ± 0.2	67.1 ± 0.4	32.9 ± 0.4
P18	92.5 ± 0.1	7.5 ± 0.2	81.2 ± 0.5	18.8 ± 0.4
P22	85.2 ± 0.0	14.8 ± 0.4	78.6 ± 0.3	21.4 ± 0.2
HIV-1 FP	82.5 ± 0.1	17.5 ± 0.3	50.6 ± 0.4	49.4 ± 0.3

Table 4
Physicochemical parameters corresponding to the reaction between HIV-1 FP and E1 synthetic peptides.

	ΔH/kcal/mol	$-T\Delta S$/kcal/mol	N	K_a/M^{-1}	Kd/μM
P7	3.21 ± 0.34	−10.46	0.47 ± 0.04	$2.03 \pm 0.46 \times 10^5$	4.93
P18	9.32 ± 0.81	−15.646	0.73 ± 0.05	$4.33 \pm 0.30 \times 10^4$	23.1
P22	9.60 ± 0.40	−16.09	0.88 ± 0.03	$6.12 \pm 0.31 \times 10^4$	16.3

N = Stoichiometry; K_a = association constant; K_d = dissociation constant.

dominant forces associated with binding [19,36]. Due to the insolubility of the HIV-1 FP, a microcalorimetry titration experiment was performed using DMSO as a solvent. For P8 and P10 the system did not reach saturation, while for P7, P18 and P22 the heat signal diminished until only heats of dilution were observed. The corresponding binding curves are shown in Fig. 3. The binding of P7, P18 and P22 to HIV-1 FP was endothermic, indicated by positive peaks. The hyperbolic titration curve demonstrates that the binding site of HIV-1 FP was saturated with the corresponding peptide (Fig. 3 top). The cumulative reaction enthalpy as a function of the peptide molar ratio is shown in Fig. 3 (bottom). The solid line corresponds to the best theoretical fit to the experimental data. The binding enthalpy (ΔH) of the GBV-C peptides to the HIV-1 FP and the entropy change (ΔS) are shown in Table 4.

This information provides insight into the dominant forces driving the association between E1 peptides and HIV-1 FP. The binding of these peptides is strongly endothermic (ΔH positive) and binding is entropy-driven. The negative Gibbs energy (ΔG), defined as $\Delta G = \Delta H - T\,\Delta S$, indicates that the binding of these two peptides is spontaneous. The binding stoichiometry (N) of E1 peptides to HIV-1 FP is approximately 1:1 for P18 and P22 and 2:1 for P7.

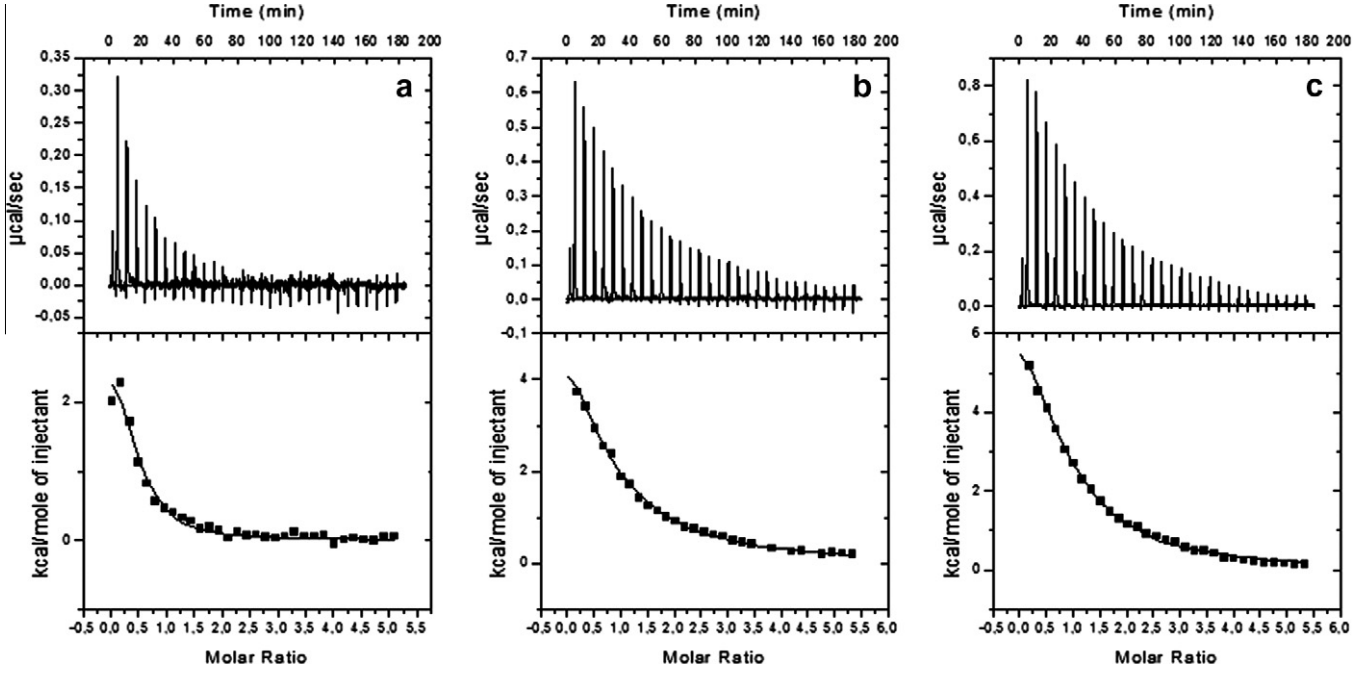

Fig. 3. Isothermal titration calorimetry results for the E1 synthetic peptides/HIV-1 FP interaction. Each figure corresponds to a different E1 peptide: a = P7, b = P18 and c = P22.

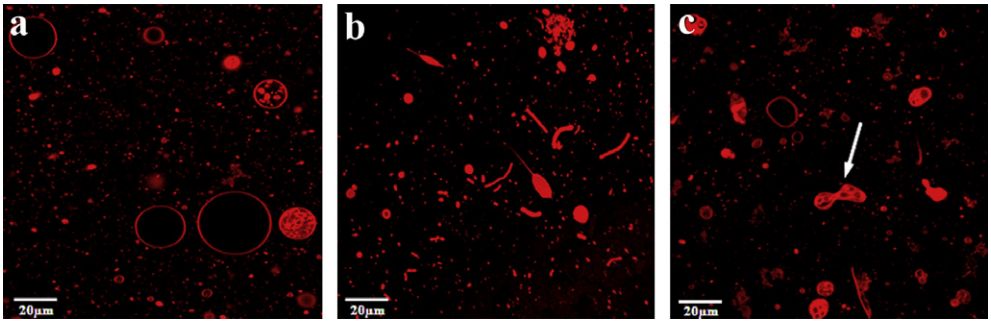

Fig. 4. Confocal microscopy images of (a) DMPC GUVs, (b) DMPC GUVs mixed with HIV-1 FP, showing broken liposomes and (c)DMPC GUVs mixed with HIV-1 FP, showing the fusion between two vesicles.

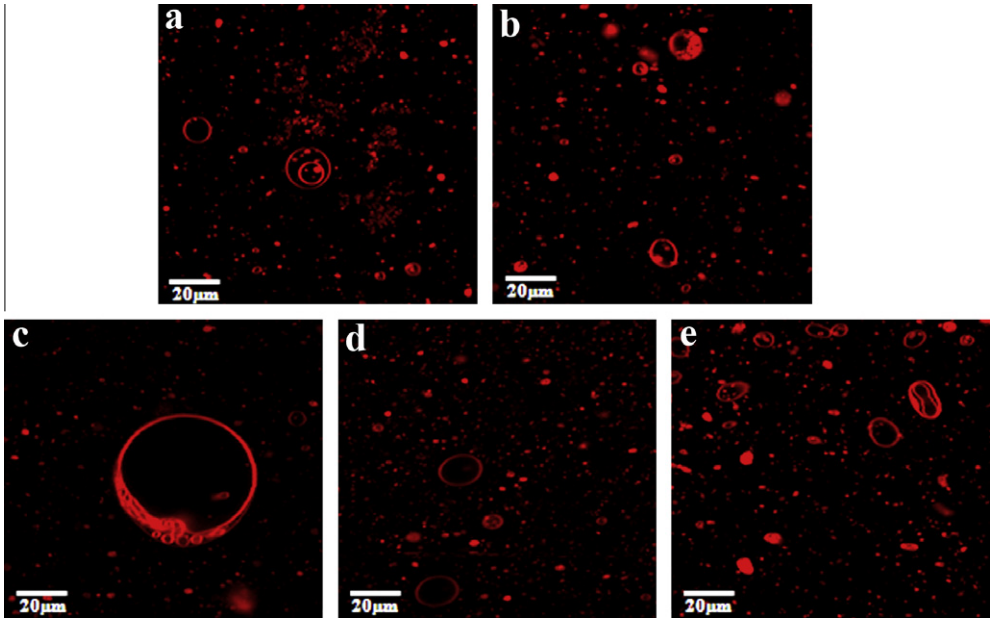

Fig. 5. Confocal microscopy images of DMPC GUVs mixed with HIV-1 FP, which was incubated with E1 synthetic peptides: P7 (a), P8 (b), P10 (c), P18 (d), and P22 (e).

3.4. Confocal microscopy

Giant vesicles are often used in biological research not only because their properties are similar to those of cell membranes [27], but also because of the size of the membrane model systems, which enables visualization by optical microscopy and micromanipulation of individual vesicles [37].

Rodriguez et al. [37] proved that the charge has an important influence on the vesicle formation, showing that the yield of clean unilamellar vesicles decreases when the amount of charged lipid is above 10%. Since Rhodamine-PE is negatively charged, DMPC was chosen as a neutral phospholipid for preparing giant vesicles; PC, however, is a chief component of the cell membrane. We obtained vesicles from 10 to 50 μm. Firstly, HIV-1 FP was added to the vesicles. We then observed the appearance of elongated structures, corresponding to broken liposomes (Fig 4b). In addition, we saw that HIV-1 FP favored membrane fusion, shown in Fig. 4c.

HIV-1 FP was incubated with E1 synthetic peptides before adding them to the liposomes solution. The images in Fig. 5 show that GUVs are intact and therefore stable in the presence of the peptides mixture.

Confocal microscopy revealed what happens to the membranes when mixed with HIV-1 FP, providing additional evidence of the inhibiting activity of these five peptides, which correspond to the structural protein E1 of GBV-C.

4. Conclusions

We found five GBV-C related peptides with the ability to inhibit the interaction of the HIV-1 fusion peptide with model membranes.

When E1 peptides were mixed with HIV-1 FP, we observed different behaviors. On the one hand, some E1 peptides such as P7 and P18 increased their binding with liposomes in the presence of HIV-1 FP. We also found that less HIV-1 FP was bound to liposomes than when it was not mixed with peptides. In contrast, P10 and P22 decreased their binding to liposomes also reducing the percentage of HIV-1 FP bound to liposomes; P8 did not inhibit HIV-1 FP binding to liposomes, but the leakage assay revealed an inhibition of the pore formation caused by HIV-1 FP. Moreover, the dialysis experiments revealed that the percentage of HIV-1 FP remaining with E1 peptides was higher than the percentage remaining with the liposomes. Confocal microscopy revealed similar inhibition activity for all of E1 peptides.

Each peptide has a different behavior in the presence of HIV-1 FP. Equilibrium dialysis experiments indicate that the peptides interact in solution, which was corroborated by ITC experiments for P7, P18 and P22. However, we could not confirm the same for the other peptides. Additional assays for P8 and P10 should be carried out to understand how they interact with HIV-1 FP.

The different results obtained could indicate that HIV-1 FP and these peptides interact in different ways. The different methods that we used provide different glimpses of their behavior. There is evidence that the interactions are complex. It appears that the peptides are not interacting on the membrane only or in solution. Thus, the exact mechanism behind the interaction needs to be investigated further.

Thus, these peptides could be involved in the prevention of HIV-1 entry by binding to the HIV-1 FP. In order to test the use of this peptide as an antiviral therapeutic agent, other assays are currently being performed.

Acknowledgments

This study was supported by project CTQ2006-15396-C02-02/01-BQU from the *Secretaría de Estado de Investigación, Ministerio de Ciencia e Innovación, Dirección General de Programas y transferencia de conocimiento, Subdirección General de Proyectos de Investigación* (Spain), and supported in part by NIH grant GM 068619. M.J. Sánchez-Martín is a recipient of an FPI program pre-doctoral grant. The authors are members of the consolidated research group by the Generalitat de Catalunya: *Peptides and Proteins: physicochemical studies* (2005SGR00278). The authors thank Dr. Marta Taulés Marín, of the Confocal Microscopy and Cellular Micromanipulation Unit, and Dr. Rafel Prohens López of the Fine Chemistry Unit, from the Barcelona Science Park, for heir invaluable assistance.

Appendix A. Supplementary material

Supplementary data associated with this article can be found, in the online version, at doi:10.1016/j.jcis.2011.04.053.

References

[1] M.D. Resh, Biochim. Biophys Acta Mol. Cell Res. 1451 (1) (1999) 1–16.
[2] S. Michael, N. Edgar, K. Norman, B. Benjamin, K. Jürgen, W. Alfred, W. Herbert 5 (1999) 1239–1252.
[3] S. Thennarasu, D.-K. Lee, A. Tan, U. PrasadKari, A. Ramamoorthy, Biochim. Biophys. Acta Biomembr. 1711 (1) (2005) 49–58.
[4] R. Arnon, R.J. Horwitz, Curr. Opin. Immunol. 4 (4) (1992) 449–453.
[5] O.M. Vol'pinaIvanov, A. Surovoi, V.T. Ivanov, Biomed. Sci. 1 (1) (1990) 23–32.
[6] Y. Itoh, E. Takai, H. Ohnuma, K. Kitajima, F. Tsuda, A. Machida, S. Mishiro, T. Nakamura, Y. Miyakawa, M. Mayumi, Proc. Natl Acad. Sci. USA 83 (23) (1986) 9174–9178.
[7] H.G. Franquelim, L.s.M.S. Loura, N.C. Santos, M.A.R.B. Castanho, J. Am. Chem. Soc. 130 (19) (2008) 6215–6223.
[8] J. Cohen, Science 277 (5322) (1997) 32–33.
[9] N.A. Roberts, J.C. Craig, J. Sheldon, AIDS 12 (5) (1998) 453–460.
[10] R. Halasz, O. Weiland, M. Sallberg, Scand. J. Infect. Dis. 33 (8) (2001) 572–580.
[11] H.L. Tillmann, M.P. Manns, Antiviral Res. 52 (2) (2001) 83–90.
[12] J. Xiang, S. Wunschmann, D.J. Diekema, D. Klinzman, K.D. Patrick, S.L. George, J.T. Stapleton, N. Engl. J. Med. 345 (10) (2001) 707–714.
[13] J. Xiang, S.L. George, S. Wunschmann, Q. Chang, D. Klinzman, J.T. Stapleton, Lancet 363 (9426) (2004) 2040–2046.
[14] S. Jung, O. Knauer, N. Donhauser, M. Eichenmüller, M. Helm, B. Fleckenstein, H. Reil 19 (2005) 1267–1272.
[15] E. Herrera, S. Tenckhoff, M.J. Gomara, R. Galatola, M.J. Bleda, C. Gil, G. Ercilla, J.M. Gatell, H.L. Tillmann, I. Haro, J. Med. Chem. 53 (16) (2010) 6054–6063.
[16] J.R. Brender, K. Hartman, K.R. Reid, R.T. Kennedy, A. Ramamoorthy, Biochemistry 47 (48) (2008) 12680–12688.
[17] J.R. Brender, K. Hartman, L.M. Gottler, M.E. Cavitt, D.W. Youngstrom, A. Ramamoorthy, Biophys. J. 97 (9) (2009) 2474–2483.
[18] A. Ramamoorthy, D.K. Lee, T. Narasimhaswamy, R.P. Nanga, Biochim. Biophys. Acta 1798 (2) (2010) 223–227.
[19] R.F. Epand, W.L. Maloy, A. Ramamoorthy, R.M. Epand, Biochemistry 49 (19) (2010) 4076–4084.
[20] H. Ellens, J. Bentz, F.C. Szoka, Biochemistry 23 (7) (1984) 1532–1538.
[21] E. Kaiser, R.L. Colescot, B.D. Bossinge, P.I. Cook, Anal. Biochem. 34 (2) (1970) 595–598.
[22] N. Rojo, M.J. Gomara, M.A. Alsina, I. Haro, J. Pept. Res. 61 (6) (2003) 318–330.
[23] M.J. Hope, M.B. Bally, L.D. Mayer, A.S. Janoff, P.R. Cullis, Chem. Phys. Lipids 40 (2-4) (1986) 89–107.
[24] J.P. Reeves, R.M. Dowben, J. Cell Physiol. 73 (1) (1969) 49–60.
[25] A. Darszon, C.A. Vandenberg, M. Schonfeld, M.H. Ellisman, N.C. Spitzer, M. Montal, Proc. Natl. Acad. Sci. USA 77 (1) (1980) 239–243.
[26] D. Needham, T.J. McIntosh, E. Evans, Biochemistry 27 (13) (1988) 4668–4673.
[27] K. Tsumoto, H. Matsuo, M. Tomita, T. Yoshimura, Colloids Surf. B 68 (1) (2009) 98–105.
[28] H. Ellens, J. Bentz, F.C. Szoka, Biochemistry 24 (13) (1985) 3099–3106.
[29] M. Smolarsky, D. Teitelbaum, M. Sela, C. Gitler, J. Immunol. Methods 15 (3) (1977) 255–265.
[30] U. Pick, Arch. Biochem. Biophys. 212 (1) (1981) 186–194.
[31] W.C. Wimley, S.H. White, Biochemistry 32 (25) (1993) 6307–6312.
[32] S.H. White, W.C. Wimley, A.S. Ladokhin, K. Hristova, Methods Enzymol. 295 (1998) 62–87.
[33] S.H. White, W.C. Wimley, A.S. Ladokhin, K. Hristova, Energ. Biol. Macromol., Pt B 295 (1998) 62–87.
[34] R. A. Gatti, A. Ostborn, A. Fagraeus, vol. 113 (1974) pp. 1361–1368.
[35] M. Wu, S.-Q. Nie, Y. Qiu, K.-C. Lin, S.-X. Wang, S.-F. Sui, Peptides Biol. Chem. (2002) 104–107.
[36] S. Thennarasu, R. Huang, D.K. Lee, P. Yang, L. Maloy, Z. Chen, A. Ramamoorthy, Biochemistry 49 (50) (2010) 10595–10605.
[37] N. Rodriguez, F. Pincet, S. Cribier, Colloids Surf. B 42 (2) (2005) 125–130.

3.4. Artículo 4. Biophysical investigations of GBV-C E1 peptides as potential inhibitors of HIV-FP

Cinco secuencias peptídicas correspondientes a la proteína E1 del GBV-C: NCCAPEDIGFCLEGGCLV (P7), APEDIGFCLEGGCLVALG (P8), FCLEGGCLVALGCTICTD (P10), QAGLAVRPGKSAAQLVGE (P18) y AQLVGELGSLYGPLSVSA (P22), se estudiaron ya que eran capaces de interferir en la interacción del péptido de fusión del VIH-1 (PF del VIH-1) con vesículas. En este trabajo, se estudiaron las interacciones de estos péptidos de la proteína E1 con el PF del VIH-1, así como con modelos de membrana, con el fin de corroborar su capacidad de inhibición y de entender si la interacción con el péptido de fusión tiene lugar en disolución o a nivel de membrana. Se llevaron a cabo estudios de agregación y fusión de membranas, de resonancia de plasmón de superficie y análisis conformacionales mediante dicroísmo circular. Además, se realizaron ensayos de toxicidad *in vitro* que incluyeron estudios de citotoxicidad en fibroblastos 3T3 y ensayos de hemólisis en sangre con el fin de evaluar si estos péptidos podrían ser utilizados en futuras terapias anti-VIH-1.

Los resultados mostraron que el P10 no es capaz de inhibir la fusión de membranas causada por el PF del VIH-1 y además provoca la agregación de liposomas y la fusión de membranas, por lo que se decidió descartarlo para futuros ensayos. El P18 y el P22 no inhiben la fusión de membranas pero sí la capacidad del PF del VIH-1 de formar poros en las bicapas, por la tanto no han sido descartados todavía. P7 y P8 se seleccionaron como los mejores candidatos para futuros estudios ya que son capaces de inhibir tanto la fusión de membranas como la interacción del PF del VIH-1 con las bicapas, siendo así candidatos potenciales para ser usados en futuras investigaciones anti-VIH-1.

Biophysical investigations of GBV-C E1 peptides as potential inhibitors of HIV-1 FP

María Jesús Sánchez-Martín[a*], *Patricia Urbán*[b,c,d], *Montserrat Pujol*[a], *Isabel Haro*[e], *M. Asunción Alsina*[a], *M. Antònia Busquets*[a].

[a]Physical Chemistry Department, Faculty of Pharmacy, University of Barcelona, Associated Unit to the CSIC: Peptides and proteins: Physicochemical studies. IN2UB. Av. Joan XXIII s/n, 08028 Barcelona, Spain.

[b]Nanobioengineering Group, Institute for Bioengineering of Catalonia, Baldiri i Reixac 10-12, Barcelona E08028, Spain

[c]Biomolecular Interactions Team, Nanoscience and Nanotechnology Institute (IN 2UB), University of Barcelona, Martí i Franquès 1, Barcelona E08028, Spain

[d]Barcelona Centre for International Health Research (CRESIB, Hospital Clínic-Universitat de Barcelona), Rosselló 132, Barcelona E08036, Spain

[e]Unit of Synthesis and Biomedical Application of Peptides. Department of Biomedical Chemistry, IQAC-CSIC, Jordi Girona 18, 08034, Barcelona, Spain

***Corresponding author:** e-mail: mjsanchez@ub.edu . Phone: +34 93 402 45 56; fax: +34 93 403 59 87

ABSTRACT

Five peptide sequences corresponding to the E1 protein of GBV-C: NCCAPEDIGFCLEGGCLV (P7), APEDIGFCLEGGCLVALG (P8), FCLEGGCLVALGCTICTD (P10), QAGLAVRPGKSAAQLVGE (P18) and AQLVGELGSLYGPLSVSA (P22) were synthesized as they were capable of interfering with the HIV-1 fusion peptide (HIV-1 FP)-vesicle interaction. In this work, the analysis of the interaction of these peptides with the HIV-1 FP was done, as well as with membrane models, in order to corroborate their inhibition ability and to understand if the interaction with the fusion peptide takes place in solution or at membrane level. Several studies were carried out as aggregation and membrane fusion, surface Plasmon resonance and the conformational analysis by circular dichroism. Moreover, *in vitro* toxicity assays, including citotoxicity studies in 3T3 fibroblasts and hemolysis assays in human red blood cells, were performed in order to evaluate if these peptides could be potentially used in the future as an anti-HIV-1 therapy.

Results showed that P10 is not capable to inhibiting the membrane fusion caused by HIV-1 and it aggregates liposomes and fuse membranes, thus we decided to discard it for futures studies. P18 and P22 do not inhibit membrane fusion but they inhibit the ability of HIV-1 FP to form pores into bilayers, thus, we have not discarded them yet. P7 and P8 were selected as the best candidates for future studies as they were capable of inhibiting the membrane fusion and the interaction of HIV-1 FP with bilayers. Therefore, these peptides could be potentially used in future anti-HIV-1 research.

Keywords: Liposomes, synthetic peptides, hepatitis G virus, VIH-1, fusion peptide, model membranes

1. INTRODUCTION

Hepatitis G virus (HGV), also known as GB virus C, is a member of the *Flaviviridae* family and is therefore distantly related to hepatitis C virus (HCV).[1] Researchers looking for a HGV-related disease have suggested that persons infected with both HIV and HGV progress to AIDS more slowly than those infected only with HIV.[2-4] Based on a co-infection model, GBV-C may influence HIV disease inhibiting HIV by inducing chemokines, down-regulating HIV co-receptor(s), influencing cytokine profiles, and other as yet undefined effects on the host lymphocytes.[5, 6] However, the mechanism responsible for the beneficial effect that the GBV-C virus has on the course of infection caused by HIV has not still completely been defined.

Jung et al.[7] demonstrated that cells transfected with either infectious RNA or a deletion mutant that expressed the N-terminal third of the polyprotein (including the E1 and E2 coding regions) resulted in inhibition of HIV replication, increased release of chemokines, and decreased surface expression of CCR5 compared to cells transfected with antisense GBV-C RNA, indicating that the envelope proteins may be involved in the inhibition of HIV replication.

The use of synthetic peptides offers an effective approach for designing chemically well-defined molecules of specific activity. Recently, we described certain E2 GBV-C domains that interfere with the HIV-1 fusion peptide (FP)-vesicle interaction, decrease the cellular membrane fusion, and interfere with the HIV-1 infectivity in a dose-dependent manner.[8]

The interaction of certain GBV-C peptide sequences of the E1 envelope protein, obtained by solid-phase peptide synthesis (SPPS), with the HIV-1 fusion peptide has been proven through the use of several biophysical techniques such as isothermal titration calorimetry, confocal microscopy, binding assays and fluorescence studies, among others. Results have shown that five peptide sequences corresponding to the envelope protein E1 of GBV-C were capable of interfering with the HIV-1 FP-vesicle interaction.[9] Consequently, the aim of this work was to analyze in depth the interaction of these peptides with the HIV-1 FP, as well as with membrane models, in order to corroborate their inhibition ability and to understand if the interaction with the fusion peptide takes place in solution or at membrane level. Thus, several studies were carried out as aggregation and membrane fusion, surface Plasmon resonance and the conformational analysis by circular dichroism. Moreover, *in vitro* toxicity assays,

including citotoxicity studies in 3T3 fibroblasts and hemolysis assays in human red blood cells, were performed in order to evaluate if these peptides could be potentially used in the future as an anti-HIV-1 therapy.

2. RESULTS AND DISCUSSION

E1 GBV-C peptides and HIV-1 FP were synthesized in order to study the interaction between them and with model membranes. The aim of the assays carried out in this work is to demonstrate the capacity of the E1 peptides for inhibiting the effect that the HIV-1 FP has on model membranes. Moreover, this work attempts to explain the type of interaction that occurs, since the mechanism by which inhibition occurs is unknown.

2.1. Aggregation measurements

In order to know if E1 peptides interact with model membranes, liposome aggregation measurements were carried out by measuring the changes in light scattering of POPG (0.1mM) LUVs upon peptide addition

Moreover, aggregation was confirmed by dynamic light scattering at 90º with a Zetasizer Nano as an increase in both turbidity and average particle size (Figure 1). Bigger particles with wider size distribution than for the liposomes alone (fig. 1a) appeared after peptide addition to the cuvette containing LUVs (fig. 1b). The polidispersion also increased and the error in the measure is high as the accuracy of the instrument when measuring big particles is low.

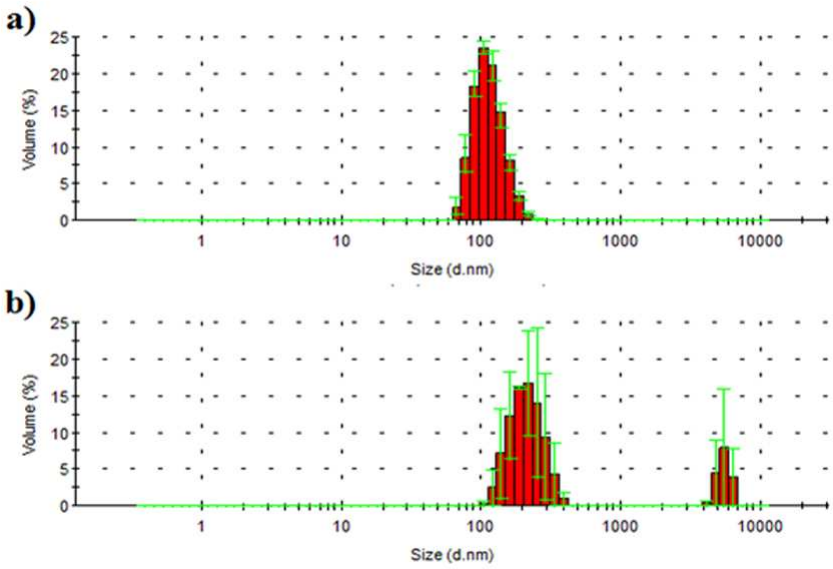

Figure 1. Distribution of hydrodynamic diameters expressed as z-diameters at 298 K of a) POPG LUVs and b) POPG LUVs after the addition of P10.

Results show that only P10 is capable to induce liposome aggregation. By this fact, P10 shows its affinity for acidic phospholipids, since the liposomes used were prepared by hydration of POPG. At least two main processes must occur for liposome aggregation; first, peptide molecules have to establish intimate associations with the membrane of the liposomes, and second, liposome-associated peptides have to interact with other liposome-associated peptides. [21] Moreover, the rate of liposome aggregation induced by P10 is concentration dependent.

The propensity of P10 to bind lipid bilayers may also be facilitated by its hydrophobicity and aggregation tendency. To confirm this hypothesis, we used the Aggrescan software [10] to screen the E1 sequences for the presence of hydrophobic patches that can favor aggregation. One such sequence is found at the P10 N-terminus (residues 7–16), and it is not present in the other sequences. An exposed hydrophobic patch may promote both protein–protein and also protein–lipid bilayer interactions. The fact that P10 has lipid aggregation ability, whereas the other sequences do not, also supports the presence of a potential 'aggregation-promoting' domain at the P10 N-terminus.[22] Table 1 shows the results obtained from Aggrescan software. In the present work, we have selected the following parameters: the number of hot spots in a sequence (NnHS) that are the regions of proteins with the highest aggregation propensity, the Total Hot Spot Area per residue (THSAr) and the global protein aggregation propensity (Na4vSS). We choose this particular set of values because, in Aggrescan, all of them are normalized relative to the number of amino acids in the sequence, allowing the direct comparison of peptides with different sizes.

Table 1. Number of hot spots in a sequence (NnHS), total area of these aggregation-prone regions (THSAr) and global protein aggregation propensity (Na4vSS) provided by Aggrescan software for P7, P8, P10, P18, P22 and HIV-1 FP sequences.

Sequence Name	P7	P8	P10	P18	P22	HIV-1 FP
Number of Hot Spots (nHS):	0	1	1	0	1	1
THSA per residue (THSAr):	0	0.19	0.31	0	0.11	0.38
Normalized a4v Sequence Sum for 100 residues (Na4vSS):	3.9	12.2	30.3	-10.2	21.3	29.5

Data show that P10 has similar values to HIV-1 FP, which also promotes vesicle aggregation and membrane destabilization.[23] P7 and P18 do not present a hot spot region and the other peptides, P8 and P22, present a region of very low aggregation propensity.

2.2. Fusion measurements.

Membrane fusion plays an essential role in cellular activities such as exocytosis, endocytosis, and vesicle transport of various cellular organelles. It is also an essential step of infection by enveloped viruses. Because the fusion of biological membranes is so important, studies on the mechanism of membrane fusion have been performed. Lipid mixing assays were carried out to see if E1 peptides promoted liposomes fusion. Moreover, E1 peptides were incubated with HIV-1 FP (HIV-1FP:E1 peptide 1:10) before adding them to the liposomes solution in order to check if E1 peptides were capable of inhibiting the ability of HIV-1 FP for fusing membranes.

E1 peptides alone do not seem to cause membrane fusion, except for P10 that presents a low percentage of fusion. This fact is coherent with the results obtained from the aggregation assays as fusion of phospholipid membranes is thought to involve three steps, vesicle aggregation, membrane destabilization, and merging of membranes [24-26], and P10 was the only one that showed the ability to aggregate liposomes. On the other hand, the selected concentration of HIV-1 FP produced a 9.3% of fusion that seems to be reduced when it was incubated with P7 and P8. Results show that P7 and P8 inhibit the membrane fusion caused by HIV-1 FP in 21.7 and 29.7%, respectively (table 2). Thus, they interfere with the HIV-1 fusion peptide vesicle interaction producing a notable decrease in the membrane fusion.

Table 2. Percentage of membrane fusion caused by E1 peptides and HIV-1 FP alone and after incubating them together. Percentage of inhibition of the fusion by E1 peptides.

	% Fusion		
	Peptide	**E1 Petide + HIV-1 FP**	**% Inhibition**
HIV-1 FP	9.3	–	–
P7	-0.1	7.3	21.7
P8	-0.1	6.5	29.7
P10	1.3	9.8	-5.4
P18	0.2	19.2	-106.7
P22	0.4	11.2	-21.3

P10, P18 and P22 instead of reducing the percentage of fusion caused by the fusion peptide, they made it higher. Thus, these peptides do not inhibit the membrane fusion.

2.3. Surface Plasmon Resonance studies

In order to know if the inhibition took place at the membrane level, surface plasmon resonance studies were carried out. Firstly, POPG liposomes were deposited on the L1 chip surface. SEM and AFM images of the L1 chip were recorded to test the stable immobilization of the lipid vesicles (figure 2).

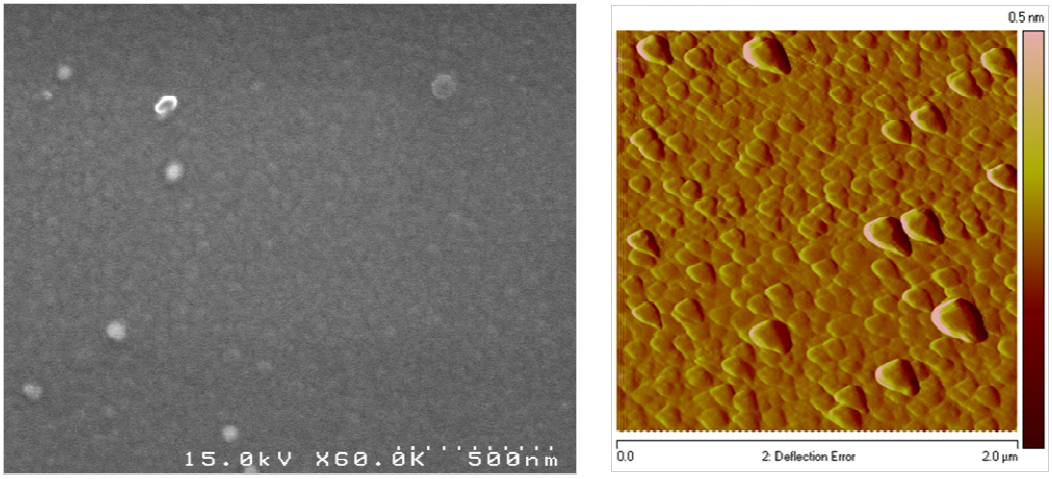

Figure 2. SEM (left) and AFM (right) images of POPG liposomes deposited on a L1 chip.

After attachment, the lipid bilayer structure is retained, facilitating the study of interactions in membrane-like environments.

Afterwards, the interaction of the peptides with liposomes was evaluated. Firstly, E1 peptides and HIV-1 FP separately were injected into de chip. Then, E1 peptides were incubated with HIV-1 FP at a molar ratio 10:1 and the mixtures were injected into the chip; on the other hand, HIV-1 FP, at the same concentration that in the mixtures, was also injected. Results are shown in figure 3.

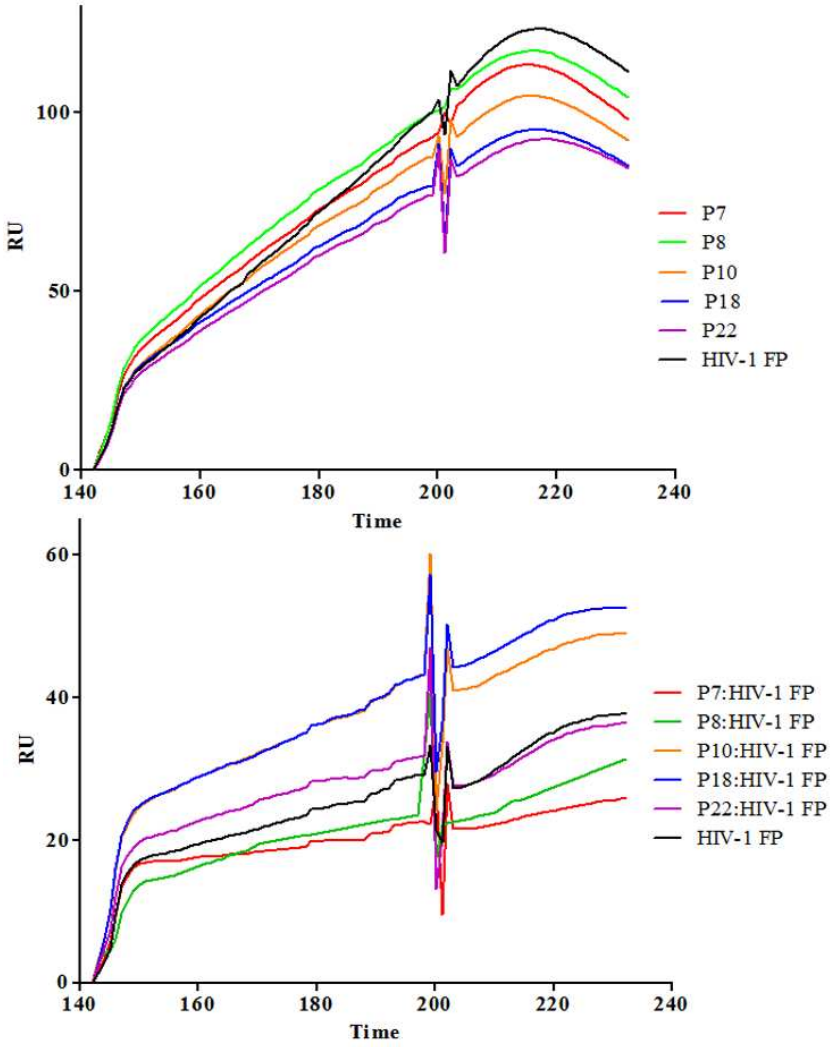

Figure 3. Sensograms for the direct binding of E1 synthetic peptides, HIV-1 FP (top) and their mixtures at a molar ratio 10:1 (bottom) to immobilized POPG liposomes on a L1 Chip.

HIV-1 FP and E1 peptides interact separately with the membranes, as the analytes bind the liposomes, an increase in RU (Response Units) is observed (figure 3 top), being HIV-1 FP that gave the highest binding. After the association time, the dissociation step

is observed as a decrease in SPR signal. Afterwards, the mixtures of HIV-1 FP and E1 peptides were injected (figure 3 bottom) and similar profiles were obtained but we can observe that the response is lower than when the peptides were alone. Moreover, P7 and P8 mixed with HIV-1 FP gave a lower response than HIV-1 FP alone, showing again a partial inhibition of the interaction of HIV-1 FP with the membranes. P10, P18 and P22 mixed with HIV-1 FP gave more RU than the fusion peptide alone, maybe due to the sum of both interactions. On the other hand, during the dissociation step of P7 and P8 mixed with HIV-1 FP, we could not observe a decrease in SPR signal, showing a strong bond between the peptides and the membrane.

2.4. Circular dichroism

In order to gain insights into the differences between peptides and the reason why their behavior is different, a conformational study was carried out. Circular dichroism experiments and the corresponding quantitative analysis of the experimental data using a deconvolution computer program were done. In general, short synthetic peptides do not have a preferential conformation in solution, but can sometimes adopt moderately stabilized secondary structures.[27] Initial CD experiments were carried out in water. In this medium the peptide spectra showed a negative band near 195 nm that is typical of random coil conformation. However, when the CD experiments were carried out in presence of an halogenated alcohol as TFE, that has been repeatedly demonstrated to be helicogenic, secondary structures were induced. The characteristic negative bands located at 205 and 222 nm and the positive band around 195 nm appeared showing the spectra like those of an α-helix structure. CD spectra of P10 showed a negative band with a peak between 215 and 220 nm which could be attributed to a β-structure contribution probably due to peptide aggregation (figure 4).

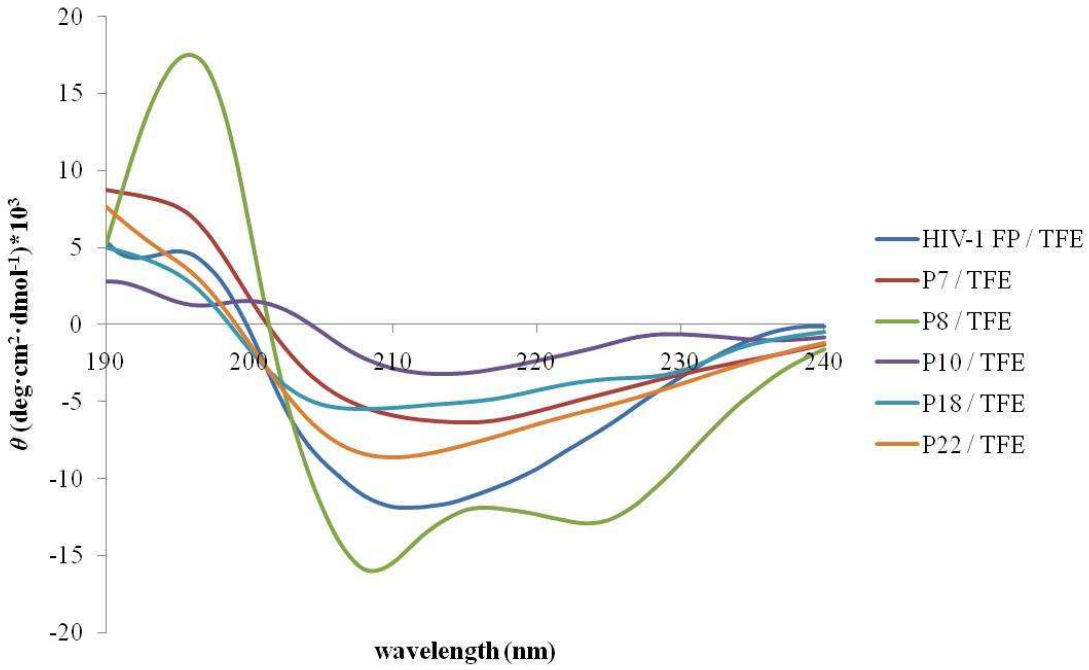

Figure 4. CD spectra of E1 synthetic peptides and HIV-1 FP in TFE recorded at 298 K and at a peptide concentration of 0.037mg/ml

A quantitative analysis of the CD experimental results was performed using Contin as it is a good program for the analysis of the conformation of polypeptides or short protein fragments.[17] Table 3 shows the estimation, from the CD spectra, of the content of α-helical conformation of the peptides according to molar ellipticity at 222 nm (calculated from equation 3) and to Contin's deconvolution program.

Table 3. Estimation, from the CD spectra, of the content of α-helical conformation of the HIV-1 FP and E1 peptides according to molar ellipticity at 222 nm and to Contin.

	% α -helix in TFE	
	$[\theta]_{222}$	Contin
HIV-1 FP / TFE	23.6	36.9
P7 / TFE	15.3	18.1
P8 / TFE	37.9	52.5
P10 / TFE	5.9	3.9
P18 / TFE	11.5	18.4
P22 / TFE	17.9	25.6

The low percentage of α-helix and the band attributed to a β-structure of P10 have been corroborated using Chou and Fasman secondary structure prediction server obtaining a secondary structure for P10 of 11.1% α-helix and 88.9% sheet. On the other hand, these results are consistent with the results obtained in the aggregation and membrane fusion experiments, as the ability to form higher order oligomers may be correlated with the induction of vesicle aggregation and fusion.[23]

2.5. WST Cytotoxicity and hemolysis assays

In order to study the effect of these peptides in contact with cell membranes, toxicity experiments in 3T3 mouse fibroblasts and hemolysis assays with human red blood cells (RBCs) were performed.

Results obtained in WST-1 citotoxicity assays (table 4) indicate that after 48h-incubation of peptides with 3T3 fibroblasts, cells show viability greater than 90% for all the peptides and concentrations tested. The percentage of cell viability was calculated using PBS diluted in culture media as a control.

Table 4. Percentage of cell viability of 3T3 fibroblasts incubated with P7, P8, P10, P18, P22 and HIV-1 FP peptides.

Concentration µg/mL / Peptide	250	125	62.5	31.25	15.63	7.81	3.90	1.95	0.98	0.49
P7	94,9 ± 2,8	96,6 ± 2,3	92,8 ± 2,3	93,1 ± 1,7	92,2 ± 1,6	91,9 ± 1,2	90,2 ± 2,3	95,0 ± 1,3	91,4 ± 3,8	91,7 ± 1,8
P8	94,5 ± 3,6	93,6 ± 4,5	91,1 ± 0,6	92,0 ± 1,4	92,6 ± 0,9	95,9 ± 1,5	93,3 ± 3,0	95,2 ± 2,8	94,5 ± 3,4	94,1 ± 4 ,4
P10	96,1 ± 3,4	94,4 ± 1,6	94,2 ± 3,4	93,8 ± 3,5	94,0 ± 2,7	95,3 ± 4,4	93,6 ± 2,1	94,4 ± 4,1	94,4 ± 1,6	97,0 ± 4,4
P18	94,9 ± 0,4	92,4 ± 1,1	92,4 ± 2,0	92,2 ± 1,2	92,1 ± 1,3	93,1 ± 2,0	93,2 ± 1,6	94,8 ± 1,2	95,0 ± 4,5	97,6 ± 3,6
P22	100,8 ± 3,8	100,8 ± 2,7	101,4 ± 4,3	100,2 ± 3,8	100,4 ± 1,2	101,9 ± 1,1	99,9 ± 3,1	99,0 ± 0,1	100,0 ± 0,9	100,8 ± 0,5
HIV-1 FP	94,7 ± 4,3	100,3 ± 0,5	100,2 ± 2,2	101,1 ± 2,7	101,3 ± 1,1	100,6 ± 2,4	98,7 ± 2,8	101,8 ± 2,4	101,5 ± 0,9	100,2 ± 1,1

In order to have more information about the behavior of these peptides once in contact with cell membranes, hemolysis assays were performed. After 90 minutes incubation of peptides with human RBCs, the absorbance of the supernatant was measured in order to determine if hemoglobin was present due to RBCs lysis. The percentage of hemolysis was calculated using 1% Triton X-100 final concentration as 100% hemolysis. As shown in table 5 none of the peptides tested exhibited hemolytic activity.

Table 5. Percentage of hemolysis induced by P7, P8, P10, P18, P22 and HIV-1 FP peptides.

Peptide \ Concentration (μg/mL)	250	125	62.5	31.25	15.6	7.8	3.9	1.95	0.98	0.49
P7	0,5 ± 0,1	0,6 ± 0,2	0,6 ± 0,4	0,8 ± 1,1	0,7 ± 0,3	1,1 ± 0,5	0,9 ± 0,3	0,3 ± 0,2	0,7 ± 0,4	1 ± 0,2
P8	0,7 ± 0,6	1,2 ± 0,3	1,4 ± 0,7	2,3 ± 0,5	1,7 ± 0,3	2 ± 0,5	2,1 ± 0,4	1,9 ± 0,5	1,8 ± 0,5	1,9 ± 0,5
P10	0,0 ± 0,1	0,0 ± 0,2	0,2 ± 0,1	0,0 ± 0,1	0,2 ± 0,2	0,5 ± 0,6	0,2 ± 0,1	0,4 ± 0,4	0,1 ± 0,2	0,8 ± 0,4
P18	0,4 ± 0,3	0,5 ± 0,3	0,5 ± 0,3	0,6 ± 0,6	0,9 ± 0,4	1 ± 0,5	1,2 ± 0,1	1,3 ± 0,1	1,4 ± 0,2	1,4 ± 0,2
P22	1,7 ± 0,4	1,7 ± 1,1	1,4 ± 0,4	1,7 ± 0,4	2,6 ± 0,7	1,9 ± 0,3	1,1 ± 0,6	1,6 ± 0,6	1,7 ± 0,5	1,6 ± 0,3
HIV-1 FP	2,1 ± 0,2	1,5 ± 0,2	1,2 ± 0,1	0,8 ± 0,1	0,9 ± 0,2	1,8 ± 0,9	1,1 ± 0,2	1,2 ± 0,2	1,1 ± 0,2	1,3 ± 0,5

3. EXPERIMENTAL

3.1. Materials

Amino acids and Rink amide resin (Tentagel R RAM, 0.19 meq/g) were obtained from *Novabiochem* (Nottingham, U.K.). Dimethylformamide (DMF) was purchased from *Scharlau* (Barcelona, Spain). Dichloromethane (DCM) and piperidine were purchased from *Fluka* (Neu-Ulm, Germany). Acetic acid, diethyl ether, and trifluoroacetic acid (TFA) were obtained from *Merck* (Poole, Dorset, UK). N-hydroxybenzotriazole (HOBt) and *N,N'*-diisopropylcarbodiimide (DIPCDI) coupling reagents were obtained from *Fluka* and *Novabiochem*, respectively. Other coupling reagents as O-(7-Azabenzotriazole-1-yl)-N, N,N'N'-tetramethyluronium hexafluorophosphate (HATU) and *N,N'*-diisopropylethylenamine (DEIA) were obtained from *GenScript Corporation* and *Fluka*, respectively. Scavengers such as ethanedithiol (EDT) or triisopropylsilane (TIS) were from Sigma-Aldrich.

1-Palmitoyl-2-Oleoyl-sn-Glycero-3-Phosphocholine (POPG) was purchased from Avanti Polar Lipids. Its purity was higher than 99% and it was used without further purification.

Dimethyl sulfoxide was purchased from Sigma-Aldrich and chloroform and methanol were purchased from Merck. Water was double distilled and deionized (MilliQ system, Millipore) (18.2 MΩ cm, pH 5.8). Buffer in all experiments was HEPES (from Sigma-Aldrich) 5mM and NaCl (from Merck) 20 mM, pH 7.4.

Dulbecco's modified Eagle's medium (DMEM) and penicillin/streptomycin were purchased from Biological Industries, Israel. Fetal bovine serum (FBS) was obtained from PAA Laboratories, Germany. Glutamine was purchased from Invitrogen and Glutamine from Sigma (St. Louis, MO, USA). 96- well plates were obtained from Thermo Fisher Scientific Inc and 4-[3-(4-iodophenyl)-2-(4-nitrophenyl)-2H-5-tetrazolio]-1,3-benzene disulfonate labeling reagent (WST-1) from Roche Diagnostics GmbH.

Human blood group B, collected in citrate-phosphate-dextrose (CPD) buffer, was provided by the Banc de Sang i Teixits at the Hospital Vall d'Hebron in Barcelona (www.bancsang.net/ca). PBS and Triton X-100 were purchased from Sigma (St. Louis, MO, USA).

3.2. Methods

3.2.1. Peptides Synthesis

The synthesis of the peptides: NCCAPEDIGFCLEGGCLV (P7), APEDIGFCLEGGCLVALG (P8), FCLEGGCLVALGCTICTD (P10), QAGLAVRPGKSAAQLVGE (P18) and AQLVGELGSLYGPLSVSA (P22) were obtained by solid-phase methodologies and purified by preparative high performance liquid chromatography, as previously described.[9] The fusion peptide of the HIV-1 glycoprotein gp41, HIV-1 FP/AVGIGALFLGFLGAAGSTMGAAS, was also synthesized manually.

3.2.2. Peptides Bioinformatic analysis tools for peptide characterization

Sequences with aggregation propensity were predicted using the Aggrescan server.[10] Secondary structure was predicted using Chou and Fasman Secondary Structure Prediction Server (http://www.biogem.org/tool/chou-fasman/).[11, 12]

3.2.3. Preparation of Large Unilamellar Vesicles

Phospholipids were dissolved in a chloroform:methanol (2:1, v/v) mixture and the solutions were evaporated to dryness in vacuum with a rotary evaporator. The dried lipid film was subjected to a high vacuum overnight to remove trace amounts of solvent. Then, the lipid films were hydrated with Hepes buffer (5mmol/L, pH 7.4) containing NaCl (20mM) to obtain multilamellar vesicles (MLVs). MLVs were further transformed to large unilamellar vesicles (LUVs) by extrusion under moderate pressure through a polycarbonate filter of 0.1µm pore size.[13]

3.2.4. Aggregation measurements

Liposome aggregation was estimated as an increase in light scattering after peptide addition, with both monochromators set at 450nm.[14] Fluorescence was measured in a QM4 spectrofluorimeter from PTI (Photon Technology Internacional) under stirring (1cm path-length quartz cuvettes). The widths of excitation and emission slits were 1 nm. The aggregation experiments were carried out by the addition of 10 µl aliquots of E1 peptides (1mg ml^{-1}) on a 0.1 mM POPG LUVs solution.

The hydrodynamic diameter of the POPG liposomes was determined by dynamic light scattering at 90º with a Zetasizer Nano (Malvern, EU) at 25ºC. The particle size distribution was designated by the polydispersity index (PI), which ranged from 0.0 for an entirely monodisperse sample to 1.0 for a polydisperse sample.

3.2.5. Fusion measurements

Lipid mixing of LUVs of POPG was measured using the resonance energy transfer assay of Struck et al.[15] Lipid vesicles containing 0.6 mol% each of NBD-PE (energy donor) and Rho-PE (energy acceptor) and unlabelled vesicles were prepared at a 1:5 mixture of labelled and unlabelled vesicles (100 μM total phospholipid concentration) and were suspended in HEPES buffer, pH 7.4, and a small volume of peptide was added. The increase at 535 nm was monitored (λ_{ex}= 466 nm). The fluorescence intensity of the lipid vesicles without peptide was the zero percent of lipid mixing and the fluorescence upon the addition of Triton X-100 (0.1% v/v) was referred to a 100% of lipid mixing.

$$\% \text{ fusion} = \left[\left(F - F_0\right)/\left(F_{100} - F_0\right)\right] \times 100 \qquad (1)$$

where F_0 is the initial fluorescence of LUVs, F is the fluorescence intensity after adding the peptide, and F_{100} is fluorescence intensity after addition of 10 μL of a 10% (v/v) Triton-100 solution (complete lysis of LUVs).

3.2.6. Surface Plasmon Resonance Studies

A Biacore T100 instrument (GE, Helthcare) equipped with an L1 chip was used for surface plasmon resonance (SPR) measurements at 25 ºC using vesicle buffer (HBSN+5%DMSO). The buffer solution was always filtered through a 0.22 μm filter and degassed thoroughly. POPG liposomes were attached to the surface of the L1 chip to study the interactions of the HIV-1 FP and E1 peptides in a membrane-like environment.

Firstly, the capture of the liposomes was carried out during 600 s at a flow rate of 5μl/min. A second capture step was done adding 0.1 mg/ml bovine serum albumin (BSA) during 60s at a flow rate of 10μl/min to block the L1 chip was used.[16]

Peptides were dissolved in HBSN+5% DMSO to 130μM and injected at a flow rate of 30μl/min during 60s. After the peptide injection the dissociation stage was 120s. Regeneration of the sensor chip was achieved with 20mM of CHAPS (60s, 30μl/min). All analyses were performed using BIAevaluation software (Biacore).

3.2.7. SEM

SEM analyses were performed by the Electronic Microscopy Unit, from the Technical Scientific Services of the University of Barcelona, at room temperature on a Hitachi S-4100 Field-Emission apparatus. Sample was previously fixed with 3.2% of *p*-formaldehyde, dehydrated with ethanol and finally dried using a critical point dryer (E-3100 Jumbo, Polaron). Afterwards, sample was mounted on a microscope holder with a conductor adhesive (Agar Scientific) and covered with a thin carbon layer.

3.2.8. Atomic Force Microscopy imaging

AFM experiments were performed with a Multimode microscope (Veeco, Santa Barbara, CA) controlled by Nanoscope V electronics (Veeco, Santa Barbara, CA). Images were acquired in tapping mode (TM-AFM) at minimum vertical force, maximizing the amplitude set point value and maintaining the vibration amplitude as low as possible.

3.2.9. Circular dichroism

CD spectra were recorded on a Jasco J-810 spectropolarimeter (Japan Spectroscopic Company, Tokyo). All measurements were done in water and trifluoroethanol (TFE) and peptide concentration in the cell was 0.037mg/ml. Cells 1 cm in diameter were used and the spectra were measured between 190 and 260 nm using a spectral bandwidth of 1 nm and a scan speed of 10 nm/min.

All measurements were performed at 25 °C and the data were expressed in terms of mean residue ellipticities [θ] ($deg \cdot cm^2 \cdot dmol^{-1}$). Three scans were accumulated to improve the signal to noise ratio. Before reading the peptide spectra, a spectrum of the blank solution was subtracted and the data converted to mean residue ellipticity units.[17] Moreover, Contin by the Dichroweb server at http://dichroweb.cryst.bbk.ac.uk/html/home.shtml program was used to treat experimental CD results.[18, 19]

The percentage of α-helix conformation in the peptides was estimated using the formalism of Chen et al.[20] This approach assumes that the maximum theoretical ellipticity for a given peptide or protein at 222 nm may be derived from the number of amino acid residues *n*, and the ellipticity at 222 nm of a helix of infinite length described by Eq. (3).

$$\%\ \alpha\text{-helix} = \frac{[\theta]_{222}}{\left[-39500\left(1-\frac{2.75}{n}\right)\right]} \qquad (3)$$

3.2.10. WST Cytotoxicity assays

3T3 fibroblasts were cultured in Dulbecco's modified Eagle's medium (DMEM) supplemented with 10% heat-inactivated fetal bovine serum (FBS), 1% each penicillin/streptomycin, and 1% glutamine plus 1% sodium pyruvate.

5,000 cells/well were plated in 96-well plates and after 24 h at 37 °C in 5% CO_2 atmosphere the medium was substituted by each peptide dilution in culture medium without FBS, and incubation was resumed for 48 h. 4-[3-(4-iodophenyl)-2-(4-nitrophenyl)-2H-5-tetrazolio]-1,3-benzene disulphonate labeling reagent (WST-1) was added to each well, and the plate was incubated in the same conditions for 3 h. After thoroughly mixing on a shaker, the absorbance of the samples was measured at 440 nm using a Benchmark Plus microplate reader (Bio-Rad Laboratories Inc.). Samples were prepared in triplicate for each experiment.

3.2.11. Hemolysis assay

Human blood group B, collected in citrate-phosphate-dextrose (CPD) buffer in 50-ml centrifuge tubes, was spun for 5 min at 1,200 g, and plasma and buffy coat were removed. The resulting RBC pellet was resuspended in PBS. After two other washing steps, the RBC pellet was diluted in PBS to yield a solution of 6% hematrocrit.

RBCs suspension and each sample were added to a 96-well plate (3% final hematocrit). Each sample was performed by triplicate and positive (1% Triton X-100) and negative (PBS) controls were included. After incubating for 90 minutes at 37ºC samples were collected, spun at 16000 g for 5 minutes and the supernatant absorbance was measured at 541nm using a Benchmark Plus microplate reader (Bio-Rad Laboratories Inc.)

4. CONCLUSIONS

The use of synthetic peptides offers an effective approach for designing chemically well-defined molecules of specific activity. The aim of this work is to evaluate the possibility of using synthetic peptides corresponding to the envelop protein E1 of GBV-C in future anti-HIV research. Five E1 regions have been analyzed in depth in order to demonstrate if there are capable or not of inhibiting the interaction between HIV-1 fusion peptide and model membranes.

Results show that one of the peptides behaves totally different to the others. P10 is capable of aggregating liposomes and fusing membranes but it does not inhibit the membrane fusion caused by HIV-1 FP nor its interaction with bilayers as showed

surface Plasmon resonance experiments. After the conformational study we observed that P10 is the only one that presents a low percentage of α-helix and a high percentage of β-structure. The envelope proteins (E) of flaviviruses have been described as class II fusion proteins [28], characterized by putative fusion sequences known as fusion peptides that do not present an α-helix structure but usually adopt a β-sheet conformation.[29] Therefore, the fact that P10 could be an internal fusion peptide of GBV-C is supported by means of the results obtained in this work. On the other hand, its capability of fusing membranes and the fact that it does not inhibit the membrane fusion caused by HIV-1 FP, allow us to discard P10 as a possible candidate for inhibiting HIV-1 FP activity.

Regarding P18 and P22, they didn't inhibit membrane fusion caused by HIV-1 FP either but they don't fuse membranes and they are capable of inhibit the ability of HIV-1 FP to form pores as seen in previous studies based on leakage of vesicular contents assays. Thus, probably these two peptides are not the best candidates as possible HIV inhibitors but their behavior in some aspects against HIV-1 FP suggests us not to discard them yet.

Finally, results highlight P7 and P8 as the best candidates as HIV-1 FP inhibitors. Bothare capable of inhibiting membrane fusion and the interaction of HIV-1 FP with bilayers. Moreover, previous results showed their ability to inhibit the leakage of vesicular contents caused by HIV-1 FP.

Citotoxicity experiments performed on 3T3 fibroblasts showed no significant toxicity for tested peptides. All concentrations used lead to viability greater than 90%, determined using the WST-1 colorimetric assay. These results were confirmed by hemolysis assays on human RBCs, were none of the peptides at the concentrations tested presented hemolytic activity.

Finally, our findings allow us to propose P7 and P8 for further studies *in vitro*, in order to test their activity against HIV-1 FP once incubated with cells and to explore a possible inhibition of HIV-1 invasion. Therefore, these peptides could be potentially used in future anti-HIV-1 therapies.

5. ACKNOWLEDGEMENTS

This work is supported by project CTQ2006-15396-C02-02/01-BQU from *Secretaría de Estado de Investigación, Ministerio de Ciencia e Innovación, Dirección General de Programas y transferencia de conocimiento, Subdirección General de Proyectos de Investigación* (Spain). M.J. Sánchez-Martín is a recipient of a FPI program pre-doctoral grant. The authors are members of the consolidated research group by the Generalitat de

Catalunya: *Peptides and Proteins: physicochemical studies* (2005SGR00278). The authors thank the inestimable help of Dr. Marta Taulés Marín of the Cellular Micromanipulation Unit from the Barcelona Science Park regarding Surface Plasmon Resonance studies.

6. REFERENCES

[1] J. Linnen, J. Wages, Jr., Z. Y. Zhang-Keck, K. E. Fry, K. Z. Krawczynski, H. Alter, E. Koonin, M. Gallagher, M. Alter, S. Hadziyannis, P. Karayiannis, K. Fung, Y. Nakatsuji, J. W. Shih, L. Young, M. Piatak, Jr., C. Hoover, J. Fernandez, S. Chen, J. C. Zou, T. Morris, K. C. Hyams, S. Ismay, J. D. Lifson, G. Hess, S. K. Foung, H. Thomas, D. Bradley, H. Margolis, J. P. Kim *Science (New York, N.Y.* **1996**, 271, 505-508.

[2] H. Toyoda, Y. Fukuda, T. Hayakawa, J. Takamatsu, H. Saito *J Acquir Immune Defic Syndr Hum Retrovirol*. **1998**, 17, 209-213.

[3] C. A. Sabin, H. Devereux, Z. Kinson, A. Griffioen, D. Brown, G. Dusheiko, C. A. Lee *J Acquir Immune Defic Syndr Hum Retrovirol*. **1998**, 19, 546-548.

[4] J.-J. Lefrère, F. o. Roudot-Thoraval, L. Morand-Joubert, J.-C. Petit, J. Lerable, M. Thauvin, M. Mariotti *Journal of Infectious Diseases*. **1999**, 179, 783-789.

[5] J. Xiang, S. L. George, S. Wunschmann, Q. Chang, D. Klinzman, J. T. Stapleton *Lancet*. **2004**, 363, 2040-2046.

[6] J. Xiang, S. Wunschmann, D. J. Diekema, D. Klinzman, K. D. Patrick, S. L. George, J. T. Stapleton *The New England journal of medicine*. **2001**, 345, 707-714.

[7] S. Jung, O. Knauer, N. Donhauser, M. Eichenmüller, M. Helm, B. Fleckenstein, H. Reil *AIDS*. **2005**, 19, 1267-1272.

[8] E. Herrera, S. Tenckhoff, M. J. Gomara, R. Galatola, M. J. Bleda, C. Gil, G. Ercilla, J. M. Gatell, H. L. Tillmann, I. Haro *Journal of medicinal chemistry*. **2010**, 53, 6054-6063.

[9] M. J. Sánchez-Martín, K. Hristova, M. Pujol, M. J. Gómara, I. Haro, M. Asunción Alsina, M. Antònia Busquets *Journal of Colloid and Interface Science*, In Press, Accepted Manuscript.

[10] O. Conchillo-Sole, N. de Groot, F. Aviles, J. Vendrell, X. Daura, S. Ventura *BMC Bioinformatics*. **2007**, 8, 65.

[11] P. Y. Chou, G. D. Fasman *Biochemistry*. **1974**, 13, 222-245.

[12] P. Y. Chou, G. D. Fasman *Biochemistry*. **1974**, 13, 211-222.

[13] M. J. Hope, M. B. Bally, L. D. Mayer, A. S. Janoff, P. R. Cullis *Chemistry and physics of lipids*, 40, 89-107.

[14] C. L. Avila, B. F. de Arcuri, F. Gonzalez-Nilo, J. De Las Rivas, R. Chehín, R. Morero *Biophysical Chemistry*. **2008**, 137, 126-132.

[15] D. K. Struck, D. Hoekstra, R. E. Pagano *Biochemistry*. **1981**, 20, 4093-4099.

[16] G. Anderluh, M. Besenicar, A. Kladnik, J. H. Lakey, P. Macek *Analytical biochemistry*. **2005**, 344, 43-52.

[17] N. J. Greenfield *Nature protocols*. **2006**, 1, 2876-2890.

[18] A. Lobley, L. Whitmore, B. A. Wallace *Bioinformatics (Oxford, England)*. **2002**, 18, 211-212.

[19] L. Whitmore, B. A. Wallace *Nucleic acids research*. **2004**, 32, 668-673.

[20] Y. H. Chen, J. T. Yang, K. H. Chau *Biochemistry*. **1974**, 13, 3350-3359.

[21] B. Kurganov, M. Doh, N. Arispe *Peptides*. **2004**, 25, 217-232.

[22] M. Torrent, B. G. de la Torre, V. M. Nogués, D. Andreu, E. Boix *Biochemical Journal*. **2009**, 421, 425-434.

[23] Y. Kliger, A. Aharoni, D. Rapaport, P. Jones, R. Blumenthal, Y. Shai *Journal of Biological Chemistry*. **1997**, 272, 13496-13505.

[24] S. Nir, J. Bentz, J. Wilschut *Biochemistry*. **1980**, 19, 6030-6036.

[25] R. Blumenthal *Cell Biochemistry and Biophysics*. **1988**, 12, 1-12.

[26] C. M. Carr, P. S. Kim *Science (New York, N.Y.* **1994**, 266, 234-236.

[27] J. A. Pérez, J. Cantó, F. Reig, J. J. Pérez, I. Haro *Biopolymers*. **1998**, 45, 479-492.

[28] C. Voisset, J. Dubuisson *Biology of the Cell*. **2004**, 96, 413-420.

[29] F. X. Heinz, S. L. Allison, F. A. M. A. J. S. T. J. C. a. T. P. M. Karl Maramorosch in *Flavivirus Structure and Membrane Fusion, Vol. Volume 59*, Academic Press, **2003**, pp.63-97.

3.5. Artículo 5. Effect of E1(64-81) hepatitis G peptide on the in vitro interaction of HIV-1 Fusion Peptide with membrane models

Una forma de obtener información sobre el potencial fusogénico de los péptidos sintéticos derivados de un virus es examinar sus propiedades interfaciales y estudiarlas en monocapas y bicapas. En este trabajo se estudian las propiedades superficiales del péptido E1(64-81), al que hasta ahora hemos llamado P22, y cuya secuencia es AQLVGELGSLYGPLSVSA. Este péptido se deriva de la proteína estructural E1 del virus de la hepatitis G y se observó previamente que era capaz de inhibir la liberación de contenidos vesiculares causada por el péptido de fusión del VIH-1 (PF del VIH-1). Las isotermas mixtas del P22 y el PF del VIH-1 se obtuvieron así como sus imágenes mediante microscopía de ángulo de Brewster (BAM) y microscopía de fuerza atómica (AFM). Las imágenes mostraron que el péptido P22 y el PF del VIH-1 cuando están juntos forman una estructura que no se puede observar en las imágenes de los péptidos por separado. Los estudios con las monocapas fosfolipídicas de dimiristoilfosfatidilglicerol (DMPG) y difosfatidilglicerol (DPPG) mostraron que ambos péptidos interaccionan con los dos lípidos ensayados pero que el efecto que el PF del VIH-1 tiene sobre las monocapas se reduce en presencia del P22. Además, los experimentos de calorimetría diferencial de barrido (DSC) muestran como el PF del VIH-1 es capaz de modificar las propiedades de la estructura de la bicapa y la capacidad del P22 de inhibir estas modificaciones. Los resultados indican que el P22 interacciona con el PF del VIH-1 formando una nueva estructura y ésta puede ser la vía por la que inhibe la actividad del PF del VIH-1.

Effect of E1(64-81) hepatitis G peptide on the *in vitro* interaction of HIV-1 Fusion Peptide with membrane models

Maria Jesús Sánchez-Martín[a*], *M. Antònia Busquets*[a], *Victoria Girona*[a] *Isabel Haro*[b], *M. Asunción Alsina*[a], *Montserrat Pujol*[a]

[a]Physical Chemistry Department, Faculty of Pharmacy, University of Barcelona, CSIC-Associated Unit: Peptides and proteins: Physicochemical studies. IN2UB Av. Joan XXIII s/n, 08028 Barcelona, Spain.

[b]Unit of Synthesis and Biomedical Application of Peptides. Department of Biomedical Chemistry, IQAC-CSIC, Jordi Girona 18, 08034, Barcelona, Spain.

*__Corresponding author:__ e-mail: mjsanchez@ub.edu; phone: (+34) 93 402 45 58; fax: (+34) 93 403 59 87

ABSTRACT

One way to gain information about the fusogenic potential of virus-derived synthetic peptides is to examine their interfacial properties and subsequently to study them in monolayers and bilayers. Here, we characterize the physicochemical surface properties of the peptide E1(64-81), whose sequence is AQLVGELGSLYGPLSVSA. This peptide is derived from the E1 structural protein of GBV-C/HGV which was previously shown to inhibit leakage of vesicular contents caused by the HIV-1 fusion peptide (HIV-1 FP). Mixed isotherms of E1(64-81) and HIV-1 FP were obtained and their BAM and AFM images showed that the peptide mixture forms a different structure that is not present in the pure peptides images. Studies with lipid monolayers (DMPG and DPPG) show that both peptides interact with all the lipids assayed but the effect that HIV-1 FP has on the monolayers is reduced in the presence of E1(64-81). Moreover, DSC experiments show the capacity of HIV-1 FP to modify the properties of the bilayer structure and the capacity of E1(64-81) to inhibit these modifications. Our results indicate that E1(64-81) interacts with HIV-1 FP to form a new structure, and that this may be the cause of the previously observed inhibition of the activity of HIV-1 FP by E1(64-81).

Keywords: Hepatitis GB virus C; synthetic peptide; lipid monolayer, compression isotherms, HIV-1 FP, bilayer

1. INTRODUCTION

The independently discovered human viruses GB virus C (GBV-C) [1] and hepatitis G virus (HGV) [2] are two isolates of the same single-stranded RNA virus. GBV-C/HGV shows characteristics of a *flavivirus*-like genome, closely related to the hepatitis C virus (HCV).

GBV-C/HGV is widely spread as a result of blood transfusions and sexual transmission. The virus infects lymphocytes, but not hepatocytes and there is no conclusive evidence of a causal link between GBV-C/HGV and either acute or chronic liver disease. Recently, GBV-C/HGV has been studied in the context of human immunodeficiency virus (HIV) infection and there are reports that co-infection prolonged survival of patients and therefore is potentially an effective treatment. [3-5]

Based on a co-infection model, GBV-C/HGV may influence HIV disease via inhibition of HIV by inducing chemokines, down-regulating the HIV co-receptor(s), influencing cytokine profiles, or having other –as yet undefined– effects on the host lymphocytes [4, 5]. However, the mechanism responsible for the beneficial effect that the GBV-C/HGV virus has on the course of disease caused by HIV infection has not yet been identified.

The envelope proteins (E) of flaviviruses have been described as class II fusion proteins [6], characterized by putative fusion sequences known as fusion peptides. The capacity of these fragments for vesicle fusion and cell lysis seems to correlate with the strong interaction these peptides have with membranes.

Bearing in mind the potential use of synthetic peptides as antiviral therapies, our group is currently examining the capacity of GBV-C/HGV synthetic peptides to interact with and induce fusion in model membranes. [7, 8] The capacity, observed *in vitro*, to inhibit the leakage of vesicular contents caused by the HIV-1 fusion peptide (HIV-1 FP) [9] is the property that allows us to select the sequences of the envelop protein E1 of GBV-C/HGV in order to study their interaction with model membranes and with HIV-1 FP.

In this work, an epitope of GBV-C/HGV located in the (64-81) region of the E1 structural protein is selected as a possible inhibitor of the activity of HIV-1 FP. This epitope has also been demonstrated not to be cytotoxic *in vivo* and is therefore an interesting sequence to study. The aim of this work is to study the effect of the E1(64-81) peptide on the activity of the peptide sequence that represents the 23 N-terminal residues of the surface protein gp41 of HIV which corresponds to HIV-1 FP. Both

peptide sequences are physicochemically characterized by studying their interaction with model membranes; lipopeptide interactions with lipid monolayers of 1,2-dimyiristoyl-*sn*-glycero-3-[phospho-*rac*-(1-glycerol)] (DMPG) and 1,2-dipalmitoyl-*sn*-glycero-3-phospho-*rac*-(1-glycerol) (DPPG) are studied. In addition, Langmuir monolayers are examined by Brewster angle microscopy (BAM) and atomic force microscopy (AFM). We also study the capacity of the E1(64-81) peptide sequence to inhibit the interaction with and destabilization of membranes induced by the HIV-1 FP glycoprotein. Moreover, peptide–peptide interactions are characterized by means of Langmuir monolayers and the thermotropic behaviour of DMPG and DPPG multilamellar vesicles (MLV) is studied by differential scanning calorimetry (DSC), in the absence and in the presence of E1(64-81) and HIV-1 FP, in view of the fact that lipid membranes are characterized by one main phase transition between an ordered gel state and a disordered liquid-crystalline phase, and that they could be affected by the interaction of the peptides with the bilayer.

2. EXPERIMENTAL

2.1. Materials

Amino acids and Rink amide resin (Tentagel R RAM, 0.19 meq g^{-1}) were obtained from *Novabiochem* (Nottingham, UK). Dimethylformamide (DMF) was purchased from *Scharlau* (Barcelona, Spain). Dichloromethane (DCM) and piperidine were purchased from *Fluka* (Neu-Ulm, Germany). The washing solvents acetic acid, diethyl ether, and trifluoroacetic acid (TFA) were obtained from *Merck* (Poole, UK). N-hydroxybenzotriazole (HOBt) and *N,N'*-diisopropylcarbodiimide (DIPCDI) coupling reagents were obtained from *Fluka* and *Novabiochem*, respectively. The other coupling reagents, O-(7-Azabenzotriazole-1-yl)-N, N,N'N'-tetramethyluronium hexafluorophosphate (HATU) and *N,N'*-diisopropylethylenamine (DEIA), were obtained from *GenScript Corporation* and *Fluka*, respectively. The scavengers ethanedithiol (EDT) and triisopropylsilane (TIS) were from Sigma-Aldrich.

1,2-dimyristoyl-sn-glycero-3-[phospho-rac-(1-glycerol)] (DMPG) and 1,2-dipalmitoyl-*sn*-glycero-3-phospho-*rac*-(1-glycerol) (DPPG) were purchased from Avanti Polar Lipids. Their purity was more than 99% and they were used without further purification.

Chloroform and methanol were purchased from Merck. Water was double distilled and deionised (MilliQ system, Millipore) (18.2 MΩ cm, pH 5.8). The buffer in all

experiments was HEPES (from Sigma-Aldrich) 5 mM and NaCl (from Merck) 20 mM, pH 7.4.

2.2. Methods

2.2.1. Peptide synthesis

Synthesis of the peptide E1(64-81), whose primary amino acid sequence is: AQLVGELGSLYGPLSVSA, was carried out on a Tentagel R RAM resin (0.19 meq g^{-1}), by a solid phase methodology following an Fmoc/tBu strategy by means of DIPCD/HOBt activation [10]. For difficult couplings, HATU and DEIA agents were used. Side protection was effected by: 2,2,5,7,8-pentamethyl-chroman-6-sulfonyl (Pmc) for Arg; tert-Butyl (tBu) for Tyr, Ser, Thr and Asp; and t-butyloxycarbonyl (Boc) for Lys and Trp.

A threefold molar excess of Fmoc-amino acids was used throughout the synthesis. The stepwise addition of each residue was assessed by Kaiser's (ninhydrin) test [11] and couplings were repeated when the test result was positive.

The synthesized peptide was deprotected from the side-chain groups and cleaved from the resin with a treatment of trifluoroacetic acid (TFA) containing appropriate proportions of the scavengers [12] H_2O, triisopropylsilane (TIS), and ethanedithiol (EDT): 94.0% TFA; 2.5% H_2O; 2.5% EDT; 1% TIS.

The peptide was characterized by Perkin Elmer analytical HPLC with an LC-235 Diode Array Detector and a Binary LC Pump 250; the column used was a 25×0.46-cm KROMASIL 100 C18 5 μm. The analysis was carried out using a linear gradient of 95% H_2O (0.05% TFA)/5% acetonitrile (0.05% TFA) to 5% H_2O (0.05% TFA)/95% acetonitrile (0.05% TFA). Characterization by electrospray mass spectrometry was carried out by UPLC-MS (Waters ACQUITY Ultra Performance LC™, using a 2.1×100-mm BEH C18 1.7 μm column,).

HIV-1 FP/AVGIGALFLGFLGAAGSTMGAAS was synthesized in the same way but using a ChemMatrix 100% polyethylenglycol-based resin.

2.2.2. Surface activity of E1(64-81)

Experimental measurements were recorded with a NIMA Langmuir Film Balance equipped with a Wilhelmy platinum plate (NIMA Technology, Coventry, UK) and a Teflon trough that was rinsed with ethanol and distilled water before use. All experiments were performed at room temperature.

The surface activity of the peptide was first studied to determine the equilibrium spreading pressure. Using a cylindrical PTFE trough (19.6 cm^2, 27.2 cm^3), increasing

volumes of 0.28 mM peptide solution in acetonitrile/H_2O (1:1, v/v) were injected below the HEPES subphase (pH 7.4) through a lateral hole and the adsorption of the peptide at the air/water interface was monitored by observing the increase in surface pressure as a function of time under continuous stirring of the subphase.

2.2.3. Insertion of peptide into monolayers

The kinetics of insertion of E1(64-81) into monolayers of DMPG and DPPG were measured using the same trough as for the surface activity, which was cleaned in the same way with ethanol and distilled water before use. For these experiments, a lipid stock solution in chloroform/methanol (2:1, v/v) was prepared and added dropwise onto the subphase until the desired lipid pressure was achieved. After 10-20 min, the lipid monolayer reached equilibrium. Then, 0.28 mM E1(64-81) solution in acetonitrile/H_2O (1:1, v/v) was injected into the subphase through the side hole of the trough. The subphase was magnetically stirred during the measurements and surface pressure changes were monitored as a function of time until the pressure remained constant.

2.2.4. Compression isotherms

Compression isotherms were established in a NIMA Langmuir Teflon trough (surface area 595 cm^2, volume 297.5 cm^3) with two moving Teflon barriers, which was also rinsed with ethanol and distilled water before use. By depositing appropriate volumes of chloroform/methanol (2:1, v/v) stock solutions of phospholipids (0.28 mM) and of peptides (0.28 mM), lipid–peptide spreading solutions were obtained. Monolayers were formed by applying small drops of the spreading solutions onto the HEPES subphase (pH 7.4) with a micro syringe (Hamilton Co., Reno, NV, USA). After 15 min, monolayers of the desired composition were continuously compressed with a rate of area reduction of 15 $cm^2\ min^{-1}$; the area reduction rate ranges from 4.45 to 8.89 $Å^2 \cdot molecule^{-1} \cdot min^{-1}$ depending on the volume injected for each sample necessary to achieve the collapse. The films were compressed to their collapse pressure when possible. Each run was repeated three times and the reproducibility was ±1 $Å^2\ molecule^{-1}$.

2.2.5. Brewster Angle Microscopy

BAM images were obtained on a MicroBAM3 instrument (NIMA Technology) mounted on a NIMA Langmuir balance trough. The instrument was equipped with a 30-mW laser emitting p-polarized light at 659 nm, which incises the air–water interface at 53.1º (Brewster angle). All the images were taken at room temperature.

2.2.6. DSC Experiments

Multilamellar lipid vesicles of DMPG and DPPG were prepared for DSC measurements in a VP-DSC Microcalorimeter (MicroCal LLC, Northampton, MA, USA). The lipids and the peptides were dissolved in a chloroform/methanol mixture (2:1, v/v). Mixtures of different lipid and peptide compositions were prepared and they were evaporated to dryness in vacuum. Then, the films were hydrated with HEPES buffer (5 mM, pH 7.4) to obtain MLVs [13].

2.2.7. AFM imaging

AFM experiments were performed with a multimode microscope controlled by Nanoscope IIIa electronics (Digital Instruments, Santa Barbara, CA, USA). Images were acquired in tapping mode (TM-AFM) at minimum vertical force, maximizing the amplitude set point value and maintaining the vibration amplitude as low as possible.

A KSV5000 Langmuir film balance with a Wilhelmy platinum plate and a Teflon® trough with a surface of 185 cm^2 (maximum opened barriers) and two moving Teflon® barriers were used. Deposition of monolayers was onto a fresh mica substrate (Green Muscovite Mica discs: Metafix, Montdidier, France) at constant surface pressure for the AFM study. During the film transfer to mica, the surface pressure was kept constant by the use of a feedback system. Before taking the measurements, the mica discs were glued onto a steel disc using a water-insoluble epoxy, and they were then set on the piezoelectric scanner.

2.2.8. Circular dichroism

Circular dichroism (CD) spectra were recorded on a Jasco J-810 spectropolarimeter (Japan Spectroscopic Company, Tokyo, Japan). All measurements were taken in water and trifluoroethanol (TFE). Cells 1 cm in diameter were used and the spectra were measured between 190 and 260 nm using a spectral bandwidth of 1 nm and a scan speed of 10 nm/min.

All measurements were performed at 25°C and the data were expressed in terms of mean residue ellipticities [θ] (deg cm^2 $dmol^{-1}$). Three scans were performed to improve the signal to noise ratio. E1(64-81) was incubated with POPG liposomes before the peptide spectrum was observed. Finally, a spectrum of the blank solution (POPG liposomes) was subtracted from the peptide spectrum and the data converted to mean residue ellipticity units. [14] The Contin program from the Dichroweb server at http://dichroweb.cryst.bbk.ac.uk/html/home.shtml was used to treat experimental CD results. [15, 16]

3. ***RESULTS AND DISCUSSION***

3.1. Peptide–Peptide interaction

3.1.1. Adsorption kinetic of E1(64-81)

A small gradual adsorption of E1(64-81) was observed at low peptide concentrations. The higher the peptide concentration in the subphase, the faster the incorporation process and the higher the surface pressure attained. Experiments were carried out for more than an hour in all cases but after 30 minutes the pressure remained constant and we considered that at this time equilibrium had been reached. Figure 1 shows the adsorption isotherm profile for E1(64-81). The shape of the surface activity curve approximates a rectangular hyperbola and it was fitted to equation (1) via non-linear least squares regression analysis.

$$\pi = \frac{C\,\pi_{\max}}{K + C} \qquad (1)$$

Where C is the concentration, $\pi_{\max}$ is the maximum pressure achieved and K is a characteristic constant equal to the peptide concentration that yields $\frac{1}{2}\pi_{\max}$. Fitting the data, the values obtained for E1(64-81) were 17.05 mN m^{-1} for $\pi_{\max}$ and 0.20 μM for K (R^2 = 0.982). Peptide concentrations corresponding to this K value were chosen for further penetration studies, as it corresponds to the concentration of the peptide that should be used in the bulk subphase for penetration kinetics experiments, lower than the equilibrium spreading pressure of the peptide [17].

By applying the Gibbs adsorption equation in its simple form (equation (2)) it is possible to calculate the peptide surface excess concentration (Γ):

$$\Gamma = \frac{\Delta\pi}{RT\,\Delta \ln C} \qquad (2)$$

Where R is the gas constant (8.31 J K^{-1} mol^{-1}), T is the temperature (298 K), $\Delta\pi$ is the pressure increase achieved 30 min after injection and C is the peptide concentration.

The surface excess concentration of E1(64-81) at saturation ($\Gamma_{\max}$) deduced from the slope of the Δπ – ln C curve (equation (2)) was 1.34×10^{-6} mol m^{-2}. This value allows us to calculate the surface molecular area by means of equation (3), where N is Avogadro's constant.

$$A = \frac{1}{\Gamma_{\max}\,N} \qquad (3)$$

The molecular area obtained was 1.24 nm^2 $molecule^{-1}$. This value is compatible with an α-helical conformation of the peptide and with vertical orientation at the air–water

interface [8, 18, 19], which was corroborated by means of CD experiments (section 3.1.2).

3.1.2. Circular dichroism of E1(64-81)

CD experiments and the corresponding quantitative analysis of the experimental data using a deconvolution computer program were performed. In general, short synthetic peptides do not have a preferential conformation in solution, but they can sometimes adopt moderately stable secondary structures [20]. The CD experiments were carried out in the presence of POPG liposomes and the resulting spectrum is shown in Figure 2. The negative bands located at 205 and 222 nm and the positive band around 195 nm are characteristic of an α-helix structure.

3.1.3. Miscibility studies of E1(64-81) and HIV-1 FP

To study the miscibility of the peptides E1(64-81) and HIV-1 FP, the compression isotherms of each of them and those of their mixtures were recorded (Fig. 3).

Firstly, studying the E1(64-81) isotherm, we can observe that at 17 mN m^{-1}, when lateral compression takes place [21], the molecular area was 1.25 nm^2 $molecule^{-1}$ (Fig. 3). This value, obtained from a dynamic system, is the same as that obtained from equation (3). The value is of the same order as those obtained by other authors for peptides of similar amino acid chain length and similar hydrophobic profiles based on their primary sequence; Ambroggio et al. [18] found a molecular area of 1.80 nm^2 $molecule^{-1}$ for citropin, a 16-amino-acid antibiotic peptide. Moreover, it is similar to the molecular area of an α-helix perpendicular to the interface, as reported by Conn et al., which was 1.30 nm^2 [22]. Furthermore, the limiting area (A_o) calculated by extrapolation of the steep part of the isotherm with the area axis [21], agrees with the published theoretical values and a plateau can be seen where the collapse of the monolayer takes place. Ambroggio et al. [18] obtained 1.75 nm^2 as the theoretical A_o value for an α-helix peptide oriented perpendicular to the interface; 1.80 nm^2 has been published for an ideal HIV-1 FP α-helix secondary structure, as calculated by molecular modelling [23]. In our case, the extrapolated value (1.75 nm^2 $molecule^{-1}$) is greater than the value of 1.25 nm^2 found at 17 mN m^{-1}, very close to the pressure that we postulated as the monolayer collapse (17.6 mN m^{-1}) based on BAM images recorded at this point. However, collapse does not disrupt the monolayer but the compressibility does change at the plateau (see below). This fact allows higher values of pressure to be achieved in

the steep part of the isotherm where the partial immersion of polar groups of the peptide or folding of the hydrophobic part are also possible.

From π-*A*, at low surface pressures (0~10 mN m^{-1}), it can be observed that the addition of HIV-1 FP to the E1(64-81) monolayer produces higher values of the mean molecular area as the proportion increases, indicating interactions between the two peptides. Large positive deviations observed at E1(64-81) mole fraction values in the range $0.4 \geq X_{E1(64-81)} \geq 0.2$, suggest that the E1(64-81)/HIV-1 FP complex forms clusters in the monolayer.

As can be seen, at a surface pressure of 17 mN m^{-1}, the isotherms of both peptides present a transition represented by a plateau. This has been explained in different ways. It is possible that it was the result of the formation of a bilayer [24] or of the molecular segments being lifted from the water surface [25], or of a change in orientation of the molecules upon compression [26], or it could correspond to a rearrangement of the molecules as described in the literature for other peptides with similar characteristics (area per molecule, A_o, and the absence of clear collapse pressure in compression isotherm register) [27, 28]. The inset in Figure 3 shows the values of the surface compressibility modulus (C_s^{-1}) corresponding to each isotherm. These values were calculated by applying equation (4).

$$C_s^{-1} = - A \left[\frac{\partial \pi}{\partial A} \right]_T \quad (4)$$

Where *A* is the area per molecule at the indicated surface pressure and π is the corresponding surface pressure.

The surface compressibility modulus can be used to characterize the phase state of the monolayer [29] (for liquid expanded films it ranges from 12.5 to 50 mN m^{-1}, while for the liquid condensed phase it ranges from 100 to 250 mN m^{-1}) [30].

In our case, the values of C_s^{-1} indicate that the monolayers are in the liquid expanded state before and after the transition plateau. The extension of this plateau decreases as the HIV-1 FP mole fraction increases, as can be seen in the inset in Figure 3.

To study what happens, the phase behaviour of the E1(64-81)/HIV-1 FP system was morphologically examined using BAM and AFM. Figures 4 and 5 show the BAM and AFM images respectively, corresponding to both peptides separately and to the mixture, where $X_{E1(64-81)} = 0.6$, at a pressure of 10 mN m^{-1} when the monolayers are in the liquid expanded state.

As can be seen in the BAM images, each peptide individually presents the coexistence of two phases: gas and liquid. However, in the mixture, we observe a new liquid phase, indicating an interaction between the peptides. This interaction can also be observed in the AFM images where the pure peptide LB films are quite different from the LB film of the mixture, corroborating that the structure of the peptides separately is different from that of the mixture at the same pressure. Firstly, E1(64-81) and HIV-1 FP (Fig. 5a and 5b) both present round particles that are ordered differently depending on the peptide.

The E1(64-81) LB film (Fig. 5a and 5d) shows a non-uniform extension of the peptide on the mica surface. The LB film presents large uncovered regions while the monolayer surface had a granular roughness with small round holes. The monolayer thickness was determined as the step height from the uncovered mica surface (the darkest regions in Figures 5a and 5d) and the layer, to give a main height of 1.8±0.2 nm. Meanwhile, for HIV-1 FP, and its mixture with E1(64-81), (Fig. 5b/e and 5c/f, respectively), the peptide monolayers are more uniform and the mica surface can not be observed. Furthermore, in the LB mixed film, we can observe curly filaments of a similar shape and size covering the surface that were not present in the LB films of the pure peptides. This suggests similar peptide behaviour to that observed in the BAM images.

To gain insight into the interactions established between E1(64-81) and HIV-1 FP, a thermodynamic point of view was considered and the excess Gibbs energy of mixing ($\Delta G_{\mathrm{M}}^{\mathrm{EX}}$) was calculated. The $\Delta G_{\mathrm{M}}^{\mathrm{EX}}$ values provide us with further information on the energy of the mixing process and the specific interactions of the two components. Positive values indicate that the process of mixing is not thermodynamically favourable, so the mutual interactions between the two components are weaker than the interactions between the pure component molecules themselves. Negative values indicate that the process is thermodynamically favourable. It must also be noted that when $\left|\Delta G_{\mathrm{M}}^{\mathrm{EX}}\right|$<RT, the differences from ideality are not considered statistically significant and the mixture can be considered ideal [31].

$\Delta G_{\mathrm{M}}^{\mathrm{EX}}$ was calculated using equation (5) [32] where N_A is Avogadro's number, A_{12} is the mean area per molecule in the mixed film, A_1 and A_2 are the areas per molecule in the pure films, X_1 and X_2 are the molar fractions, and π is the surface pressure (mN m^{-1}).

$$\Delta G_{\mathrm{M}}^{\mathrm{EX}} = N_A \int_{\pi\to 0}^{\pi} A_{12}\, d\pi - X_1 \int_{\pi\to 0}^{\pi} A_1\, d\pi - X_2 \int_{\pi\to 0}^{\pi} A_2\, d\pi \qquad (5)$$

Table 1 shows the ΔG_M^{EX} values calculated for the peptide–peptide mixtures assayed at different surface pressures. In all cases, it can be seen that $\left|\Delta G_M^{EX}\right|$ values increase with the HIV-1 FP mole fraction. At surface pressures of 10 mN m^{-1} or lower and $X_{E1(64-81)} \geq$ 0.6, the mixtures have $\left|\Delta G_M^{EX}\right| < RT$ so they can be considered ideal and the interactions between the two components and between each component itself are the same. In contrast, for pressures higher than 10 mN m^{-1} and when the concentration of HIV-1 FP is higher than the E1(64-81) concentration, $\left|\Delta G_M^{EX}\right|$ values are greater than *RT* and positive in all cases.

3.2. Peptide–lipid interactions

The characterization of membrane interactions with peptides or proteins is important for a better understanding of their mode of action. In order to determine some peptide–lipid binding properties, a monolayer approach is used where the peptides are inserted into the lipid monolayer.

3.2.1. Penetration kinetics

The capacity of the peptide E1(64-81) to penetrate into phospholipid monolayers was studied using a 0.200 μM peptide solution in the HEPES-buffered subphase, which corresponds to the *K* calculated from equation (1). Figure 6 shows surface pressure increases ($\Delta\pi$) due to the introduction of E1(64-81) in monolayers of different phospholipids, over the initial lipid pressure (π_i). For both lipids, the general trend observed is that the greater π_i, the lower the degree of incorporation of the peptide into the monolayer because of the closer packing of the lipids at higher initial pressures.

The monolayer exclusion pressure (that is, the surface pressure above which the peptide does not penetrate into the monolayer) was obtained by extrapolating the plot to $\Delta\pi$ = 0 mN m^{-1} (Fig. 6) [33]. It can be seen that the peptide interacts with the two lipids tested; however, a stronger interaction was observed when the monolayer was composed of DMPG. In this case, the exclusion pressure was 20.06 mN m^{-1}, clearly higher than that obtained when the monolayer was of DPPG (11.18 mN m^{-1}). DPPG and DMPG differ in their hydrocarbonated chains. For DPPG, which presents a higher C_s^{-1} value, the exclusion pressure is lower than that obtained for DMPG in a liquid expanded state, which with its lower C_s^{-1} value is a less rigid monolayer and, therefore, easier to

penetrate than a liquid condensed monolayer (see at section 2.2.2 the miscibility study). This corroborates observations in other studies. [28]

3.2.2. Lipid–peptide miscibility

To determine the effect of the peptide E1(64-81) on the state of phospholipid monolayers and better understand the lipid–peptide interaction that takes place, mixed monolayers of E1(64-81) and the two phospholipids were obtained and the compressibility modulus for all these systems was calculated according to equation (4).

Figure 7 shows the shape of the π-A isotherms obtained and, in the insets, the variation of the compressibility modulus compared to the surface pressure.

For both phospholipids, the presence of E1(64-81) results in higher mean molecular areas of the monolayer than for the pure phospholipid monolayer at all the molar fractions assayed. For the DPPG monolayer (Fig. 7a) the π-A isotherm shows a phase transition at a pressure of around 10 mN m^{-1} for pure DPPG, which is significantly modified when E1(64-81) is further incorporated into the monolayers. This phase transition shows as a minimum in the compressibility modulus. The same behaviour can be observed for DMPG monolayers, where the phase transition of pure DMPG that occurs around 30 mN m^{-1} disappears when E1(64-81) is incorporated into the monolayer, and a minimum started to appear around 15 mN m^{-1}.

To further examine the miscibility of the film components, analysis of the collapse pressures can be helpful; the variation of π_c with the molar ratio of the components indicates two-dimensional miscibility. In our case, the collapse pressure of DPPG at 63 mN m^{-1} barely change when 20% E1(64-81) is added. However, for DMPG, adding the same percentage of peptide causes the collapse pressure to decrease to 55 mN m^{-1}. When the concentration of peptide is increased, for both phospholipids the collapse pressure decreases. The variation in the collapse pressure is indicative of miscibility: thus, in both cases we could see that the peptide and the phospholipids are miscible, but for DMPG, the earlier variation of the collapse pressure corroborates the results obtained in the exclusion pressure calculation where we observed that penetration into DMPG monolayers is easier than into DPPG monolayers.

To verify the effect of E1(64-81) on the state of phospholipid monolayers, the maximum compressibility modulus were calculated. Figure 8 shows the values in function of peptide concentration. As indicated above, the incorporation of E1(64-81) into phospholipid monolayers causes a decrease in the C_{smax}^{-1} in all cases, hence, they

are less condensed. This decrease is especially marked for DPPG monolayers of $X_{E1(64-81)}$ = 0.4. Further additions of the peptide do not affect the value of C_{smax}^{-1}.

Evaluating the extent of intermolecular interactions in monolayers comprised of two components is aided by the application of the additivity rule. The additivity rule predicts that, in the case of an ideal mixture, the mean molecular area (A_{12}) at a given surface pressure will be equal to the weighted average:

$$A_{12} = X_1 A_1 + X_2 A_2 \qquad (7)$$

where A_1 and A_2 are the molecular areas of the single components at the same surface pressure and X_1 and X_2 are the mole fractions of components 1 and 2 in the mixed film. Comparison of the experimental mean molecular area with the expected values from the additivity rule, provides us with an important clue regarding the extent of miscibility and interactions in the binary monolayer. The linear dependence in the area–composition plots (Fig. 9) indicates ideal mixing or complete immiscibility of the components [34].

Analysis of the plots reveals small negative deviations from ideality at all $X_{E1(64-81)}$ molar fractions assayed and at different pressures (5, 10, 15 and 20 mN m^{-1}), suggesting that the peptide interacts with both phospholipids through attractive interactions [34, 35].

The excess free energy of mixing for the E1(64-81) and DMPG or DPPG systems was calculated (Table 2).

A positive ΔG_M^{EX} reveals that peptide–lipid interactions are less favourable, while negative values show a more favourable interaction than between the pure components themselves. In general, the mixtures have $\left|\Delta G_M^{EX}\right| < RT$, so they can be considered ideal systems.

Figure 10 shows miniBAM images of monolayers of pure DMPG (Fig. 10a), pure peptide (Fig. 10c) and a mixed monolayer of DMPG and the peptide at $X_{E1(64-81)}$=0.2 (Fig. 10b). The pictures reveal that at pressures near 15 mN m^{-1}, the monolayer is homogeneous for pure DMPG and E1(64-81), whereas for the mixture, we can observe two different phases. This pressure corresponds to the beginning of the plateau where a change in the compressibility was observed; therefore we could say that two different phases co-exist in a liquid expanded state. At a pressure of 17.6 mN m^{-1}, peptide collapse could be observed (fig. 10c); while this does not appear in the mixture (not shown). This demonstrates the lipid–peptide miscibility. On the other hand, the phase

transition observed for DMPG (fig 10a, at π = 25.5mN m^{-1}) is clearly modified when DMPG is mixed with the peptide (fig 10b, at π = 24.6 mN m^{-1}). Moreover, the collapse observed for the mixture is very different from that of the pure components, showing a clear phase separation. In previous work, where the interaction of E1(145-162) hepatitis G virus peptide and DMPC, DMPG and POPG was studied, we reported similar behaviour compatible with the formation of a peptide–lipid complex through hydrophobic interactions, which was corroborated when the interaction of the same peptide was studied in a bilayer system. [8] Hence, the higher mean molecular areas observed in monolayers due to E1(64-81) can be explained by the formation of the lipid–peptide complexes compatible with the BAM images and the phase separation observed when collapse is reached. This fact could be explained by the arrangement of a peptide–lipid complex and its separation from the lipid matrix.

3.2.3. E1(64-81)-HIV-1 FP–lipid miscibility

Figure 11a shows the *π-A* compression isotherms for the HIV-1 FP and DPPG mixed system. HIV-1 FP addition shifts the isotherm to higher mean molecular areas at all the molar fractions assayed. Although the amino acid length is similar to that of E1(64-81), and both peptides present surface activity with π_{max} ranging from 17 to 20 mN m^{-1}, their miscibility pattern is quite different (Fig. 7a and 11a).

To examine the effect of E1(64-81) on the interaction of HIV-1 FP and phospholipids, mixed monolayers of both peptides and DPPG were studied. The proportion of E1(64-81):HIV-1 FP was 10:1 as in this proportion E1(64-81) was found to inhibit the percentage of leakage caused by HIV-1 FP. [9] Figure 11b reveals the inhibition effect of E1(64-81) on the interaction of HIV-1 FP with a DPPG monolayer. The shape of the *π-A* compression isotherms in Figure 11b is very similar to that showed in Figure 7a, corresponding to the E1(64-81)/DPPG mixed monolayers. Therefore, in the presence of E1(64-81) *in vitro*, HIV-1 FP cannot interact with DPPG.

The most significant difference can be seen by studying the compressibility modulus. We observe that the presence of HIV-1 FP makes the monolayer drastically change from a liquid condensed state to a liquid expanded state, while with E1(64-81) (Fig. 7a) or with the mixture of both peptides (Fig. 11b) we observe a transition between the phases when the peptide concentration is increased. Thus, the presence of E1(64-81) inhibits the capacity of HIV-1 FP to alter the compressibility of the monolayer.

This inhibition capacity was also studied with DSC experiments and can be attributed to the new species formed when both peptides are together, as can be seen in the BAM and AFM images (Fig. 4 and 5).

On the other hand, Figure 12 shows the plots of the mean molecular area calculated from equation (7) against the composition. Analysis of Figure 12a reveals small negative deviations from ideality at $X_{\text{HIV-1 FP}}$=0.2 and at different pressures (5, 10, 15 and 20 mN m^{-1}), suggesting that the peptide interacts with the phospholipid through attractive interactions [34, 35]. However, these deviations become positive at HIV-1 FP molar ratios higher than 0.2, although they are very small. The deviations become more positive for X=0.2 and X =0.6 when HIV-1 FP is mixed with E1(64-81), and more negative for $X_{\text{E1(64-81)+HIV-1 FP}}$ =0.4 showing a change in the behaviour, but the deviations from ideality are too small to be considered significant.

an increase of the repulsion interactions between HIV-1 FP and DPPG when E1(64-81) is present.hi ha un canvi de comportament, unes cap a positives i alters cap a negatives, Les desviacions de la iealitat són molt petites i són menyspreables.

The excess free energy of mixing for HIV-1 FP and HIV-1 FP+E1(64-81) with DPPG was calculated (Table 3). All the mixtures have $\left|\Delta G_{\text{M}}^{\text{EX}}\right|$ < RT, so they can be considered ideal systems.

3.2.4. DSC Experiments

To study the modifications in the phase diagram produced by the insertion of the peptides into the bilayers, the binary DMPG/DPPG system was considered. The DMPG/DPPG phase diagram was constructed from DSC heating thermographs (scans were recorded between 10ºC and 60ºC) of the liposomes incubated with and without the peptide. In the heating thermographs (not shown) we could see how HIV-1 FP modifies the transition temperature (T_{m}) of the DPPG and DMPG liposomes, and how this temperature is again close to the T_{m} of pure phospholipids when HIV-1 FP is incubated with E1(64-81); this is clearly reflected in the phase diagrams.

The heat capacity curve of pure DMPG shows two phase transitions. The so-called pre-transition (T_{p}~20.7ºC for DMPG at pH=7.4 in 5 mM HEPES + 20 mM NaCl) stands for a transition between two gel phases ($L_{\beta'} \rightarrow P_{\beta'}$). The main phase transition (T_{m}~23.8ºC) represents the transition from $P_{\beta'}$ gel to the liquid crystalline L_{α} phase. The phase diagram is constructed considering only the main phase transition [36].

The phase diagram is constructed by the following procedure: The *onset* and e*ndset* temperatures for the gel to liquid crystalline phase transition are determined as the temperatures corresponding to the intersection between the tangent of the leading edge and the baseline of the DSC curves [36-38]. For their contribution to the total transition widths, these temperatures need to be as follows: [39]

$$T_1 = T_{onset} + (X_A \Delta T_{1A} + X_B \Delta T_{1B}) \quad (8)$$

$$T_2 = T_{endset} - (X_A \Delta T_{2A} + X_B \Delta T_{2B}) \quad (9)$$

Where,

$$\Delta T_{1A} = T_m - T_{onset} \text{ for } X_{DPPG} = 1$$

$$\Delta T_{1B} = T_m - T_{onset} \text{ for } X_{DPPG} = 0$$

$$\Delta T_{2A} = T_{endset} - T_m \text{ for } X_{DPPG} = 1$$

$$\Delta T_{2B} = T_{endset} - T_m \text{ for } X_{DPPG} = 0$$

X_A and X_B correspond to the molar fractions of lipids A (DPPG) and B (DMPG).

The temperatures calculated by equations (8) and (9) are those represented in the phase diagram for each DPPG molar fraction (Fig. 13).

The shape of a phase diagram depends mainly on the mixing behaviour of the lipids in both phases. For ideal miscibility of two lipids A and B, the *solidus* and *liquidus* curves enclose a cigar-shaped coexistence region of the gel and liquid crystalline phases. Below the *solidus* curve, only the gel phase exists; and above the *liquidus* line, only a liquid crystalline phase appears [38]. The phase diagram confirms ideal mixing of DMPG and DPPG in both phases.

Heat capacity curves were obtained for pure lipids and their mixtures, as well as for the same phospholipid mixtures with HIV-1 FP and with HIV-1 FP incubated with E1(64-81), and their phase diagrams were also constructed.

We observed the capacity of HIV-1 FP to modify the properties of the bilayer structure, changing the transition temperature, and the capacity of E1(64-81) to inhibit these modifications. The resulting lipid phase diagram is modified when HIV-1 FP is inserted into the bilayer. However, no difference is observed in the *solidus* curve when HIV-1 FP and E1(64-81) are incubated together. In the *liquidus* curve, small differences could be observed but its shape is more similar to the pure phospholipid curves than to the curve of the phospholipids incubated HIV-1 FP. The higher X_{DPPG}, the more dramatic the effect is.

4. CONCLUSIONS

E1(64-81), a synthetic peptide of the E1 structural protein of GBV-C/HGV, shows similar behaviour to that observed for other peptide sequences from Hepatitis G structural proteins. E1(64-81) has moderate surface activity that allows it to adopt an α-helix structure at the air–water interface. Its interaction with HIV-1 FP was also studied together with how the presence of E1(64-81) influences the interaction of HIV-1 FP with monolayers and bilayers.

In a dynamic system, HIV-1 FP shows an interaction pattern that is different from that observed for E1(64-81) on phospholipid monolayers and bilayers. The interaction of both peptide mixtures with the same phospholipid systems demonstrated that the presence of E1(64-81) reduces or inhibits the action of HIV-1 FP. This is observed in the lipid–peptide miscibility studies as well as in DSC measurements. Moreover, this *in vitro* inhibition of the activity of HIV-1 FP could be explained by the AFM and BAM images which allow us to conclude that the peptide E1(64-81) interacts with HIV-1 FP to form a new structure. These findings could be one more piece of evidence of the inhibition capacity of the E1(64-81) peptide, as observed in other assays (fluorescence spectroscopy), corroborating the hypothesis that synthetic peptides of GBV-C/HGV could inhibit HIV infection. Thus, our results lead us to propose further study of E1(64-81) to explore the correlation between its inhibition capacity *in vitro* and its biological activity *in vivo*. We have therefore started the pertinent studies to establish whether the main trend observed *in vitro* can be related with the biological activity *in vivo*. Furthermore, a more comprehensive analysis of the specific peptide–peptide interaction is in progress.

5. ACKNOWLEDGEMENTS

This work was supported by project CTQ2006-15396-C02-02/01-BQU from the *Secretaría de Estado de Investigación, Ministerio de Ciencia e Innovación, Dirección General de Programas y transferencia de conocimiento, Subdirección General de Proyectos de Investigación* (Spain). M.J. Sánchez-Martín is a recipient of an FPI programme pre-doctoral grant. The authors are members of the consolidated research group recognised by the *Generalitat de Catalunya* "Peptides and Proteins: physicochemical studies" (2005SGR00278).

6. ***REFERENCES***

[1] J.N. Simons, T.J. Pilot-Matias, T.P. Leary, G.J. Dawson, S.M. Desai, G.G. Schlauder, A.S. Muerhoff, J.C. Erker, S.L. Buijk, M.L. Chalmers, et al., Identification of two flavivirus-like genomes in the GB hepatitis agent, Proceedings of the National Academy of Sciences of the United States of America 92 (1995) 3401-3405.

[2] J. Linnen, J. Wages, Jr., Z.Y. Zhang-Keck, K.E. Fry, K.Z. Krawczynski, H. Alter, E. Koonin, M. Gallagher, M. Alter, S. Hadziyannis, P. Karayiannis, K. Fung, Y. Nakatsuji, J.W. Shih, L. Young, M. Piatak, Jr., C. Hoover, J. Fernandez, S. Chen, J.C. Zou, T. Morris, K.C. Hyams, S. Ismay, J.D. Lifson, G. Hess, S.K. Foung, H. Thomas, D. Bradley, H. Margolis, J.P. Kim, Molecular cloning and disease association of hepatitis G virus: a transfusion-transmissible agent, Science (New York, N.Y 271 (1996) 505-508.

[3] H.L. Tillmann, M.P. Manns, GB virus-C infection in patients infected with the human immunodeficiency virus, Antiviral research 52 (2001) 83-90.

[4] J. Xiang, S. Wunschmann, D.J. Diekema, D. Klinzman, K.D. Patrick, S.L. George, J.T. Stapleton, Effect of coinfection with GB virus C on survival among patients with HIV infection, The New England journal of medicine 345 (2001) 707-714.

[5] J. Xiang, S.L. George, S. Wunschmann, Q. Chang, D. Klinzman, J.T. Stapleton, Inhibition of HIV-1 replication by GB virus C infection through increases in RANTES, MIP-1alpha, MIP-1beta, and SDF-1, Lancet 363 (2004) 2040-2046.

[6] C. Voisset, J. Dubuisson, Functional hepatitis C virus envelope glycoproteins, Biology of the Cell 96 (2004) 413-420.

[7] M. Sánchez-Martín, J. Amigo, M. Pujol, I. Haro, M. Alsina, M. Busquets, Fluorescence study of the dynamic interaction between E1(145–162) sequence of hepatitis GB virus C and liposomes, Analytical and bioanalytical chemistry 394 (2009) 1003-1010.

[8] M.J. Sánchez-Martín, I. Haro, M.A. Alsina, M.A. Busquets, M. Pujol, A Langmuir Monolayer Study of the Interaction of E1(145-162) Hepatitis G Virus Peptide with Phospholipid Membranes, The Journal of Physical Chemistry B 114 (2010) 448-456.

[9] M.J. Sánchez-Martín, K. Hristova, M. Pujol, M.J. Gómara, I. Haro, M. Asunción Alsina, M. Antònia Busquets, Analysis of HIV-1 fusion peptide inhibition by synthetic peptides from E1 protein of GB virus C, Journal of Colloid and Interface Science 360 (2011) 124-131.

[10] W.C. Chan, P.D. White, Fmoc Solid Phase Peptide Synthesis, Oxford University Press, New Cork, 2000.

[11] E. Kaiser, Colescot.Rl, Bossinge.Cd, P.I. Cook, Color Test for Detection of Free Terminal Amino Groups in Solid-Phase Synthesis of Peptides, Analytical Biochemistry 34 (1970) 595-&.

[12] N. Rojo, M.J. Gomara, M.A. Alsina, I. Haro, Lipophilic derivatization of synthetic peptides belonging to NS3 and E-2 proteins of GB virus-C (hepatitis G virus) and its effect on the interaction with model lipid membranes, Journal of Peptide Research 61 (2003) 318-330.

[13] P. Butko, F. Huang, M. Pusztai-Carey, W.K. Surewicz, Membrane permeabilization induced by cytolytic delta-endotoxin CytA from Bacillus thuringiensis var. israelensis, Biochemistry 35 (1996) 11355-11360.

[14] N.J. Greenfield, Using circular dichroism spectra to estimate protein secondary structure, Nature protocols 1 (2006) 2876-2890.

[15] A. Lobley, L. Whitmore, B.A. Wallace, DICHROWEB: an interactive website for the analysis of protein secondary structure from circular dichroism spectra, Bioinformatics (Oxford, England) 18 (2002) 211-212.

[16] L. Whitmore, B.A. Wallace, DICHROWEB, an online server for protein secondary structure analyses from circular dichroism spectroscopic data, Nucleic acids research 32 (2004) 668-673.

[17] M. Rafalski, J.D. Lear, W.F. DeGrado, Phospholipid interactions of synthetic peptides representing the N-terminus of HIV gp41, Biochemistry 29 (1990) 7917-7922.

[18] E.E. Ambroggio, F. Separovic, J. Bowie, G.D. Fidelio, Surface behaviour and peptide-lipid interactions of the antibiotic peptides, Maculatin and Citropin, Biochimica et biophysica acta 1664 (2004) 31-37.

[19] R. Maget-Dana, D. Lelièvre, A. Brack, Surface active properties of amphiphilic sequential isopeptides: Comparison between α-helical and β-sheet conformations, Biopolymers 49 (1999) 415-423.

[20] J.A. Pérez, J. Cantó, F. Reig, J.J. Pérez, I. Haro, Conformational behavior of the HAV-VP3(110–121) peptidic sequence and synthetic analogs in membrane environments studied by CD and computational methods, Biopolymers 45 (1998) 479-492.

[21] R. Maget-Dana, The monolayer technique: a potent tool for studying the interfacial properties of antimicrobial and membrane-lytic peptides and their interactions with lipid membranes, Biochimica et Biophysica Acta (BBA) - Biomembranes 1462 (1999) 109-140.

[22] E.E. Conn, P.K. Stumpf, Outlines of biochemistry / Eric E. Conn and P. K. Stumpf, Wiley, New York :, 1976.

[23] S.E. Taylor, G. Schwarz, The molecular area characteristics of the HIV-1 gp41-fusion peptide at the air/water interface. Effect of pH, Biochimica et biophysica acta 1326 (1997) 257-264.

[24] F. Takeda, M. Matsumoto, T. Takenaka, Y. Fujiyoshi, N. Uyeda, Surface pressure dependence of monolayer structure of poly-[epsilon]-benzyloxycarbonyl--lysine, Journal of Colloid and Interface Science 91 (1983) 267-271.

[25] M. Kaku, H. Hsiung, D.Y. Sogah, M. Levy, J.M. Rodriguez-Parada, Monolayers and Langmuir-Blodgett films of poly(N-acylethylenimines), Langmuir 8 (1992) 1239-1242.

[26] K. Hac-Wydro, J. Kapusta, A. Jagoda, P. Wydro, P. Dynarowicz-Latka, The influence of phospholipid structure on the interactions with nystatin, a polyene antifungal antibiotic A Langmuir monolayer study, Chemistry and physics of lipids 150 (2007) 125-135.

[27] N. Vila Romeu, J. Miñones Trillo, O. Conde, M. Casas, E. Iribarnegaray, Mixed Calcitonin-Poly[(d,l-lactic acid)-co-(glycolic acid)] Monolayers, Langmuir 13 (1997) 76-79.

[28] C. Larios, J. Miñones, I. Haro, M.A. Alsina, M.A. Busquets, J. Miñones Trillo, Study of Adsorption and Penetration of E2(279-298) Peptide into Langmuir Phospholipid Monolayers, The Journal of Physical Chemistry B 110 (2006) 23292-23299.

[29] M.A. Alsina, A. Ortiz, D. Polo, F. Comelles, F. Reig, Synthesis and study of molecular interactions between phosphatidyl choline and two laminin derived peptides hydrophobically modified, Journal of Colloid and Interface Science 294 (2006) 385-390.

[30] J.T. Davies, E.K. Rideal, Interfacial Phenomena, Academic Press, New York, 1961.

[31] G.L. Gaines, In Insoluble Monolayers at Liquid-Gas Interfaces, Wiley-Interscience, New York, 1966, p. 286.

[32] R.E. Pagano, N.L. Gershfeld, A millidyne film balance for measuring intermolecular energies in lipid films J Colloid Interface Sci 41 (1972) 311-317.

[33] P. Bougis, H. Rochat, G. Pieroni, R. Verger, Penetration of phospholipid monolayers by cardiotoxins, Biochemistry 20 (1981) 4915-4920.

[34] D.K. Chattoraj, K.S. Birdi, Absorption and the Gibbs Surface Excess, Plenum Press, New York, 1984, pp. 219,222-223.

[35] M.J. Galvez, M.A. Cabrerizo, A study of the miscibility of bile components in mixed monolayers at the air-liquid interface I. Cholesterol, lecithin, and lithocholic acid, Colloid Polym Sci 269 (1) (1991) 77-84.

[36] P. Garidel, C. Johann, A. Blume, The calculation of heat capacity curves and phase diagrams based on regular solution theory, Journal of Thermal Analysis and Calorimetry 82 (2005) 447-455.

[37] A.W. Eliasz, D. Chapman, D.F. Ewing, Phospholipid phase transitions. Effects of n-alcohols, n-monocarboxylic acids, phenylalkyl alcohols and quaternary ammonium compounds, Biochimica et biophysica acta 448 (1976) 220-230.

[38] P. Garidel, C. Johann, A. Blume, Thermodynamics of Lipid Organization and Domain Formation in Phospholipid Bilayers, J. Liposome Res 10 (2000) 131-158.

[39] S. Mabrey, J.M. Sturtevant, Investigation of phase transitions of lipids and lipid mixtures by sensitivity differential scanning calorimetry, Proceedings of the National Academy of Sciences of the United States of America 73 (1976) 3862-3866.

FIGURES

FIGURE 1

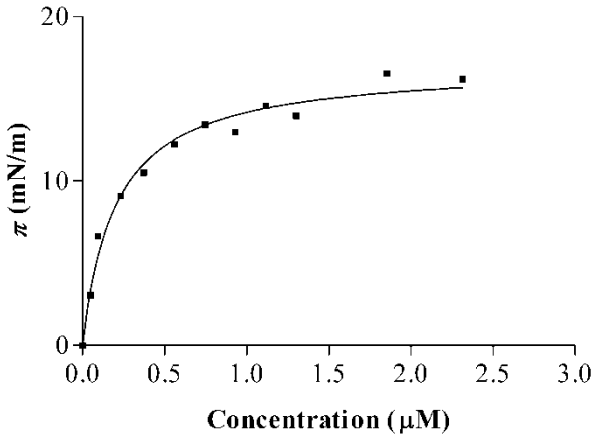

Figure 1. Surface activity curve of E1(64-81).

FIGURE 2

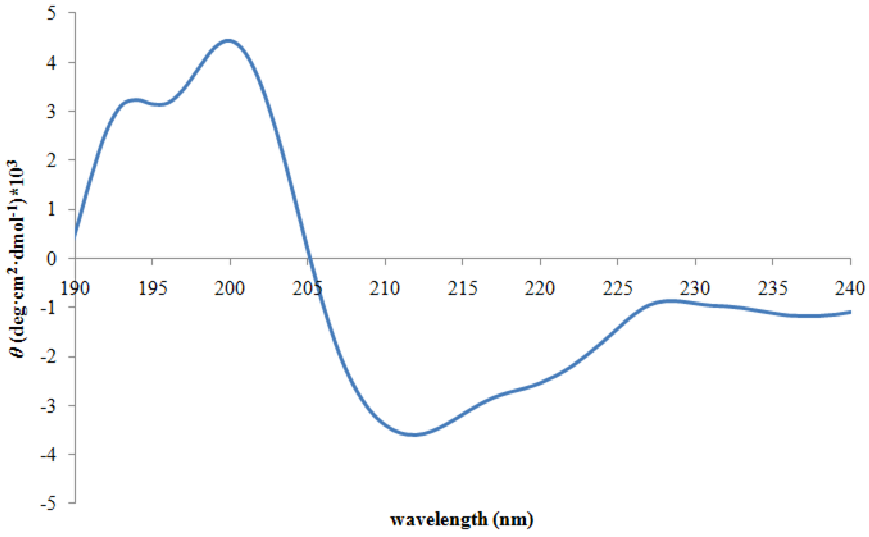

Figure 2. CD spectra of E1(64-81) in the presence of POPG liposomes.

FIGURE 3

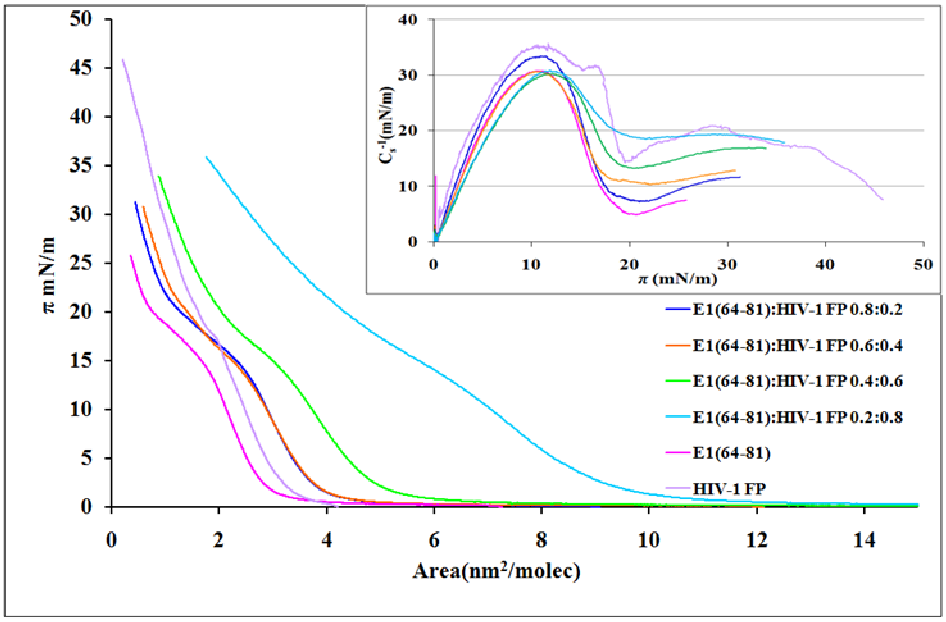

Figure 3. Surface pressure–mean area per molecule (π-A) compression isotherms of E1(64-81), HIV-1 FP and their mixtures spread on a HEPES subphase. Inset: Plot of compressibility modulus (C_s^{-1}) as a function of the surface pressure.

FIGURE 4

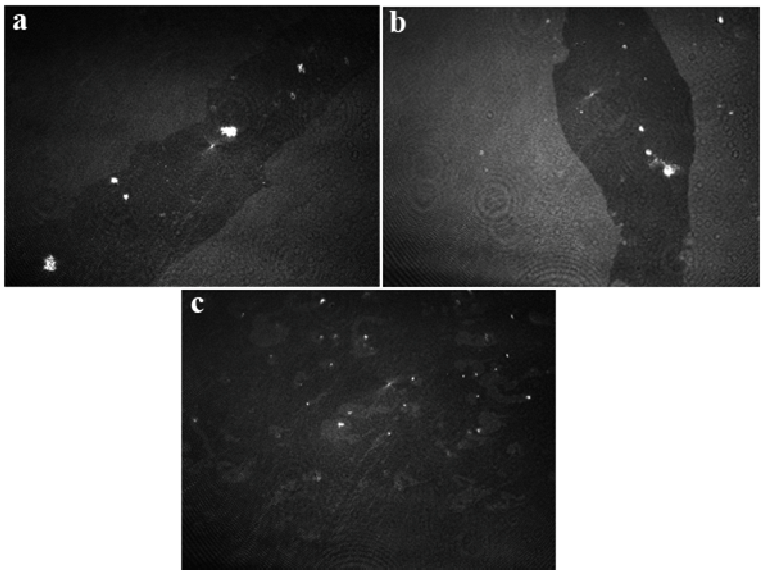

Figure 4. 4.1×3.6 mm^2 BAM images corresponding to the monolayers of: a) E1(64-81); b)HIV-1 FP; and c) E1(64-81):HIV-1 FP at a molar ratio of 0.6:0.4, spread on HEPES at a surface pressure of 10 mN m^{-1}.

FIGURE 5

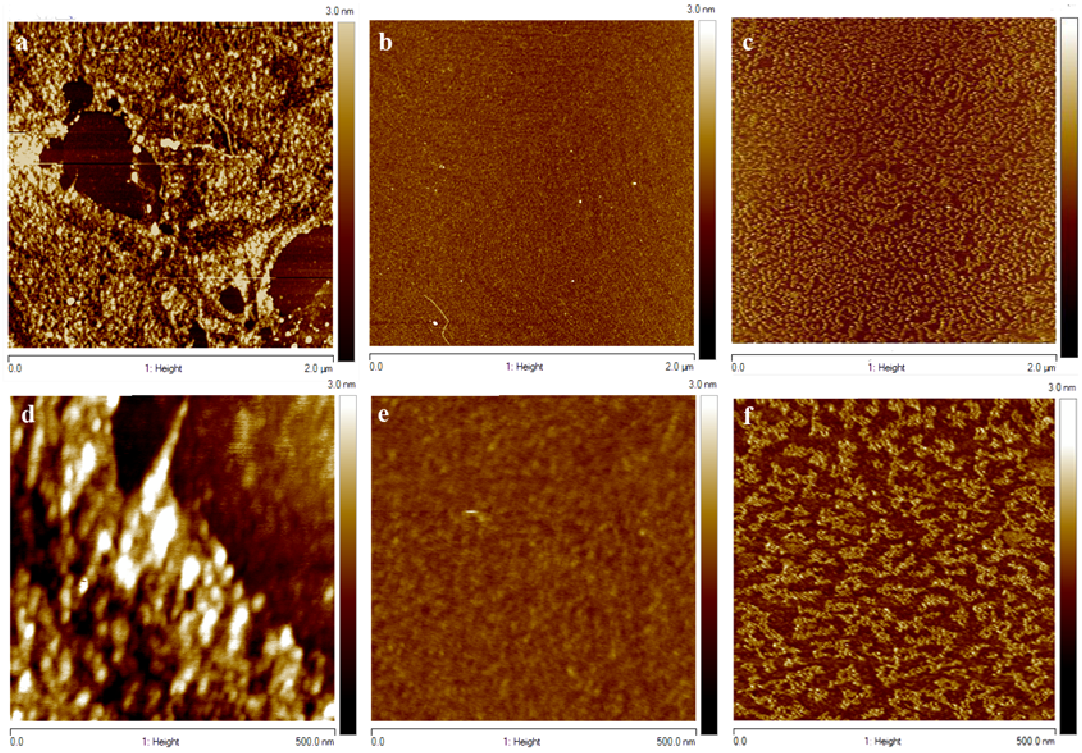

Figure 5. LB films of 2×2 µm (top) and 500×500 nm (bottom) at an extraction surface pressure of 10 mN m^{-1}: a) and d) E1(64-81); b) and e) HIV-1 FP; and c) and f) E1(64-81):HIV-1 FP at a molar ratio of 0.6:0.4.

FIGURE 6

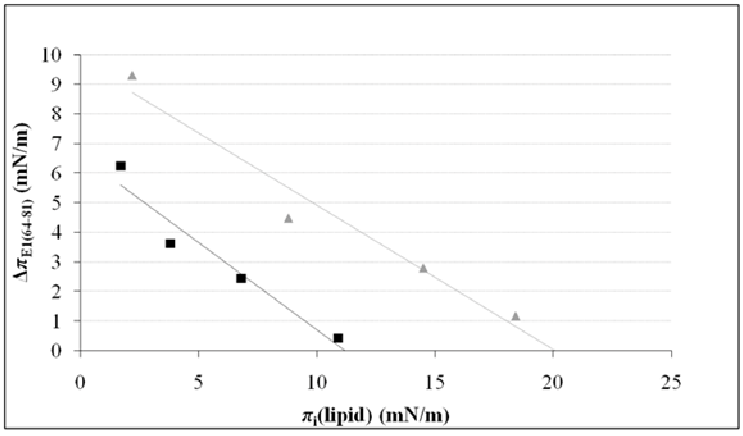

Figure 6. Surface pressure increase ($\Delta\pi$) caused by E1(64-81) in monolayers of different phospholipids in front of the initial lipid pressure (π_i). Black squares correspond to DPPG and grey triangles to DMPG.

FIGURE 7

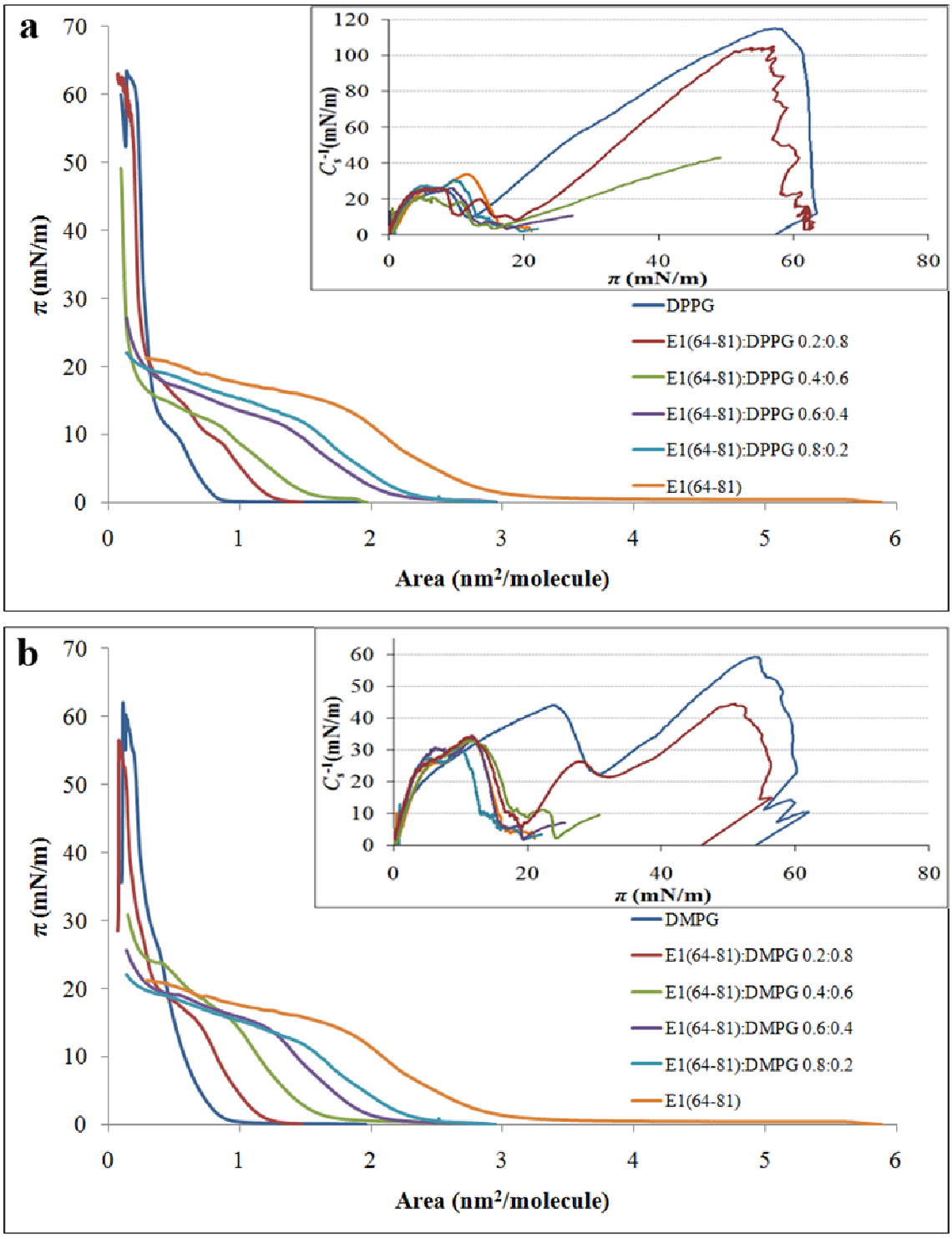

Figure 7. Surface pressure–mean area per molecule (π-*A*) compression isotherms for E1(64-81) and the lipids: (a) DPPG and (b) DMPG spread on HEPES subphase (pH=7.4) at different $X_{E1(64-81)}$. Insets: Plots of compressibility modulus (C_s^{-1}) as a function of the surface pressure.

FIGURE 8

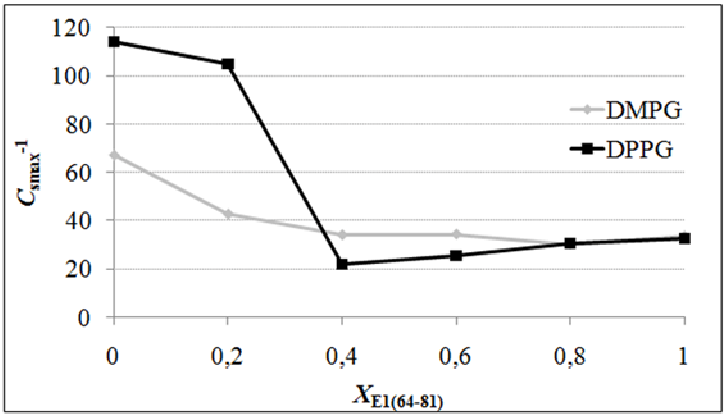

Figure 8. Maximum compressibility modulus values in function of peptide concentration for mixtures with DMPG and DPPG.

FIGURE 9

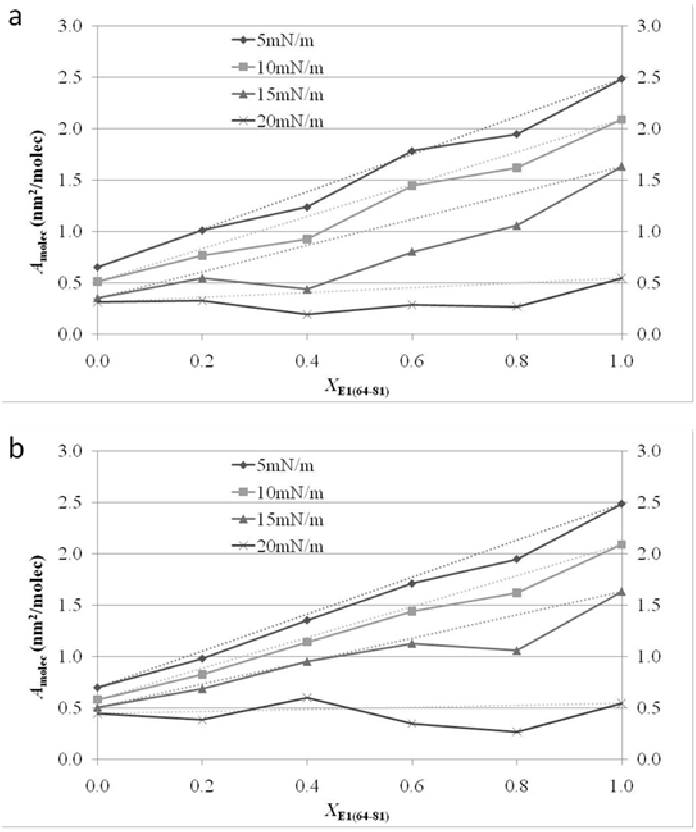

Figure 9. Plots of A_{molec} for E1(64-81) as a function of the peptide molar fractions at different surface pressures for pure and mixed monolayers of: a) DPPG and b) DMPG. Dotted lines indicate ideality

FIGURE 10

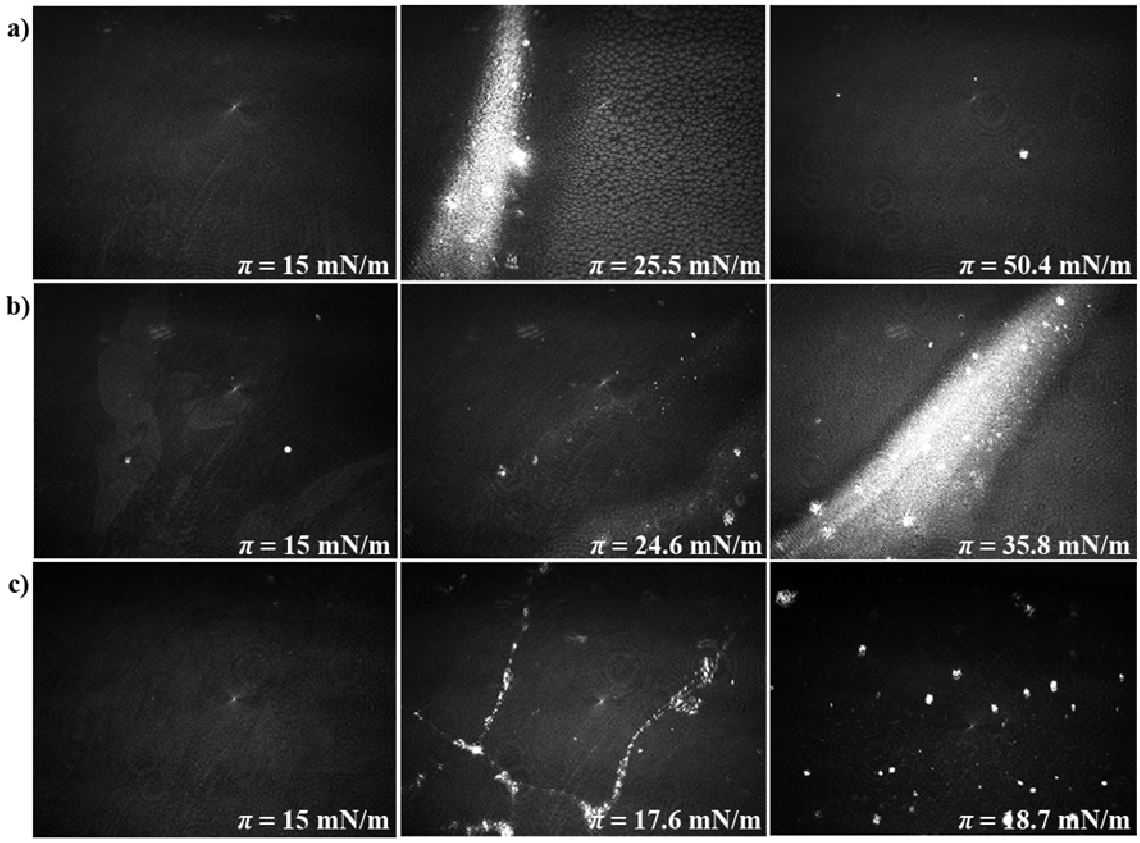

Figure 10. 4.1×3.6 mm^2 MiniBAM Images of DMPG and E1(64-81) monolayers at three different pressures, and of their mixture: a) DMPG, b) DMPG:E1(64-81) at $X_{E1(64-81)}$=0.2 and c) E1(64-81).

FIGURE 11

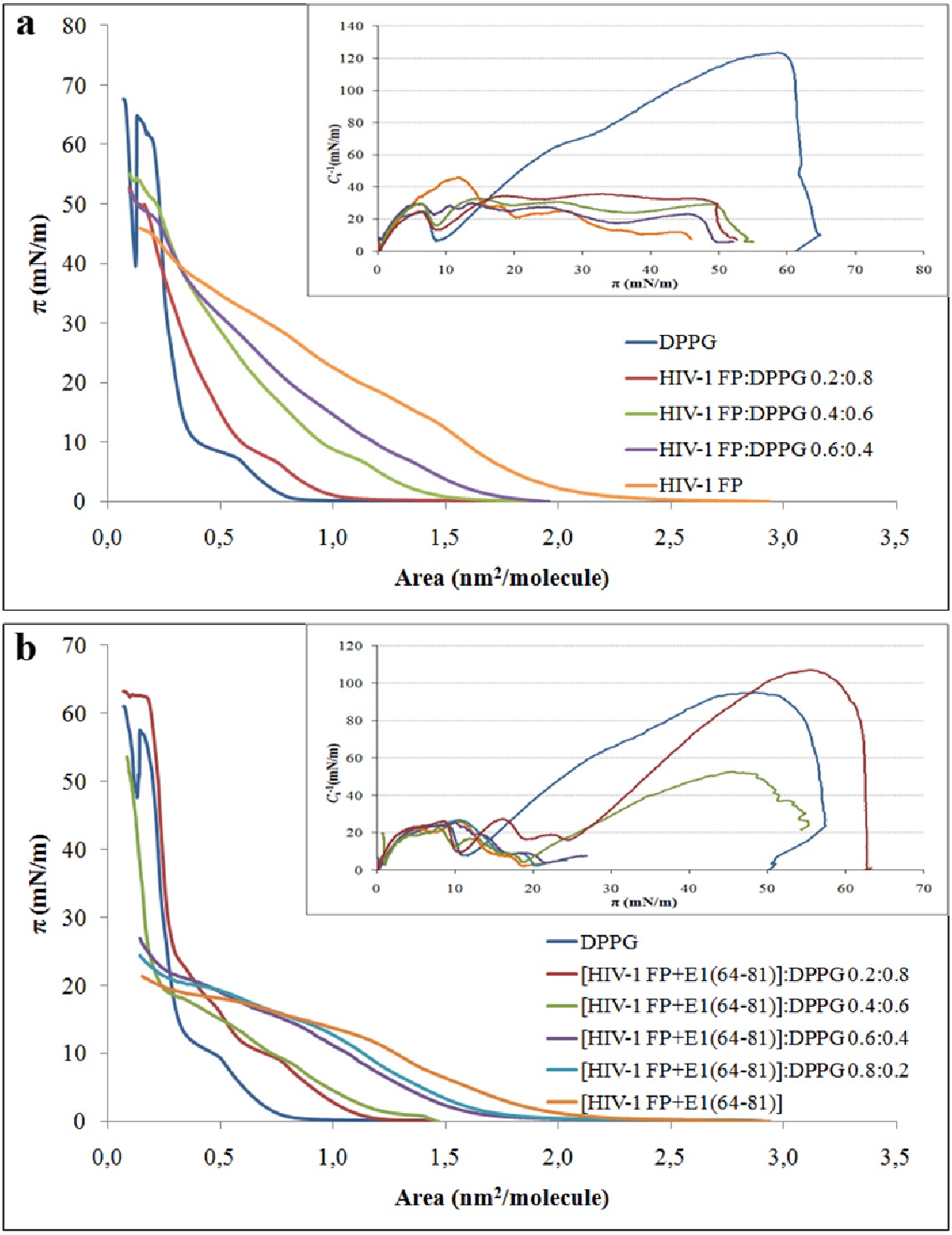

Figure 11. Surface pressure–mean area per molecule (π-A) compression isotherms for: (a) HIV-1 FP and DPPG at different $X_{\text{HIV-1 FP}}$ and (b) E1(64-81), HIV-1 FP and DPPG at different $X_{\text{E1(64-81)-HIV-1 FP}}$, spread on HEPES subphase (pH=7.4). Insets: Plots of compressibility modulus (C_s^{-1}) as a function of the surface pressure.

FIGURE 12

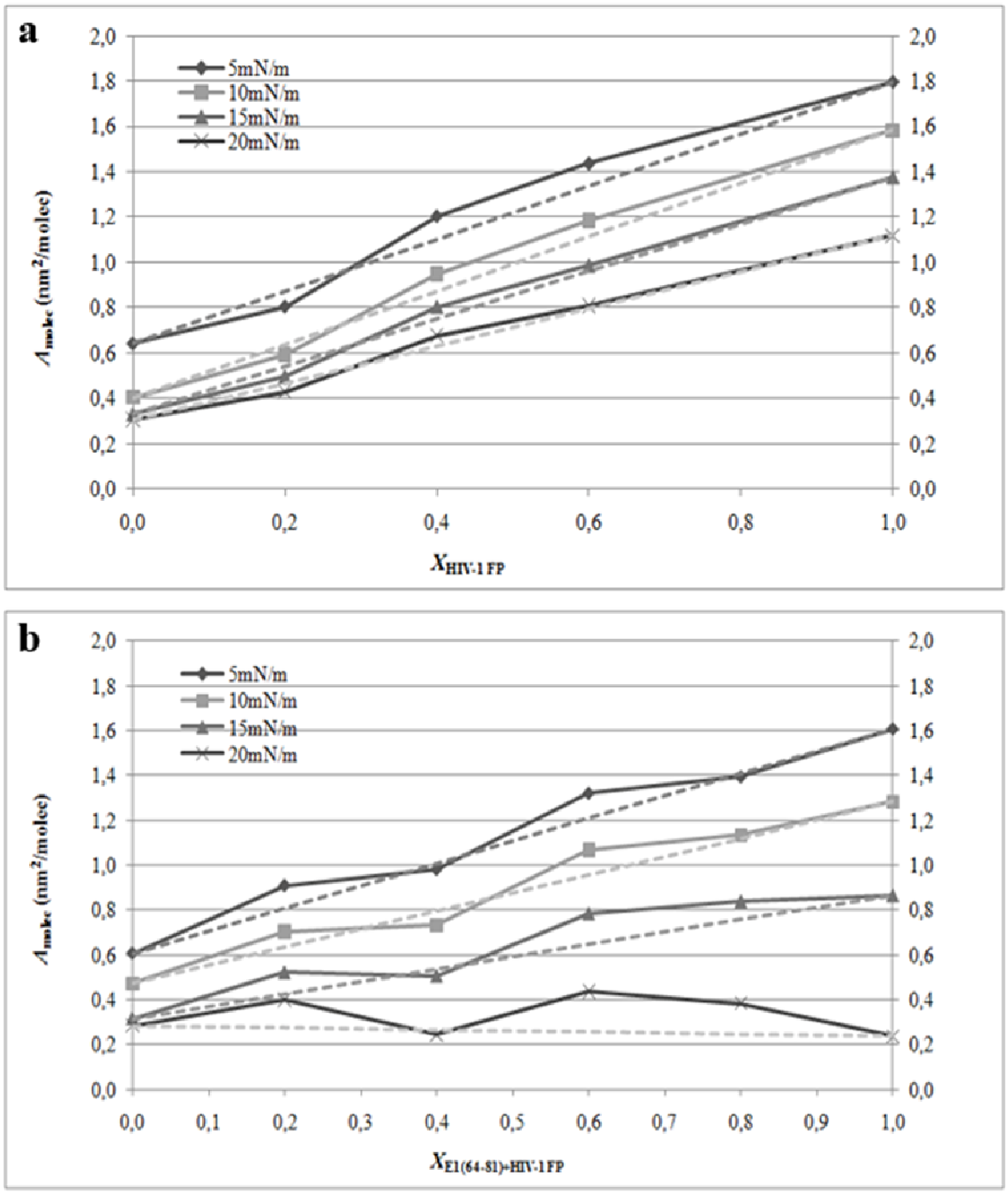

Figure 12. Plots of A_{molec} for HIV-1 FP and E1(64-81) as a function of the peptide molar fractions at different surface pressures for pure and mixed monolayers of: a) HIV-1 FP and DPPG; and b) HIV-1 FP+E1(64-81) and DPPG. Dotted lines indicate ideality

FIGURE 13

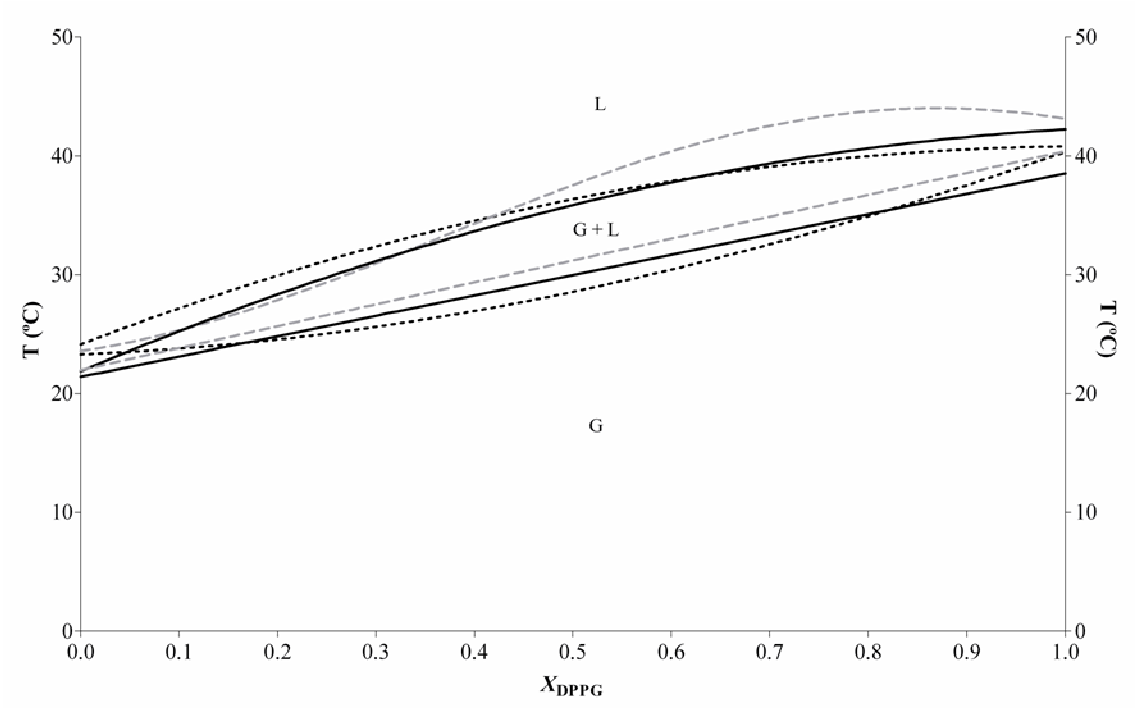

Figure 13. Phase diagram of DPPG:DMPG liposomes (solid lines) in the presence of HIV-1 FP (dashed grey lines) and in the presence of HIV-1 FP with E1(64-81) (dotted lines). G: Gel phase, L: Liquid crystalline phase.

TABLES

Table 1. ΔG_M^{EX} (J mol^{-1}) for different HIV-1 FP-E1(64-81) mixtures at various pressures.

$X_{E1(64-81)}$	π (mN·m^{-1})	ΔG^{ex} (J·mol^{-1})
0.2	5	4494
	10	8073
	20	23766
	25	31990
0.4	5	2146
	10	3352
	20	8727
	25	10980
0.6	5	814
	10	1360
	20	3861
	25	5515
0.8	5	294
	10	701
	20	3894
	25	5909

Table 2. ΔG_M^{EX} (J mol^{-1}) for different Lipid–E1(64-81) mixtures at various pressures.

		ΔG^{ex} (J·mol^{-1})	
$X_{E1(64-81)}$	π (mN·m^{-1})	DMPG	DPPG
0.2	5	-753	-737
	10	-780	-791
	15	618	486
	20	-238	-326
0.4	5	-504	-334
	10	-533	-111
	15	-470	2188
	20	721	590
0.6	5	-133	-257
	10	-196	55
	15	-523	1687
	20	-1694	-630
0.8	5	-317	-248
	10	-391	56
	15	-491	51
	20	-29	-235

Table 3. ΔG_{M}^{EX} (J mol^{-1}) for different DPPG–HIV-1 FP mixtures and DPPG–HIV-1 FP+E1(64-81) mixtures at various pressures

		ΔG^{ex} (J·mol^{-1})	
$X_{PEPTIDE(S)}$	π (mN·m^{-1})	HIV-1 FP:DPPG	HIV-1 FP+E1(64-81):DPPG
0.2	5	77	-65
	10	-42	121
	15	-71	-121
	20	-98	-418
0.4	5	11	-2
	10	122	196
	15	246	-54
	20	347	-150
0.6	5	-89	113
	10	28	134
	15	335	-107
	20	475	-601

3.6. Artículo 6. Physicochemical characterization of GBV-C E1 peptides as potential inhibitors of HIV-1 Fusion Peptide: Interaction with model membranes

Cuatro secuencias peptídicas correspondientes a la proteína E1 del virus de la hepatitis G: NCCAPEDIGFCLEGGCLV (P7), APEDIGFCLEGGCLVALG (P8), FCLEGGCLVALGCTICTD (P10) and QAGLAVRPGKSAAQLVGE (P18) se han estudiado, ya que son capaces de interaccionar con el péptido de fusión del VIH-1 (PF del VIH-1). En este trabajo se estudian las propiedades superficiales de estas secuencias correspondientes a la proteína E1 y se caracterizan fisicoquímicamente estudiando su interacción con modelos de membrana; además, se estudian las mezclas de estos péptidos con el PF del VIH-1 con el fin de observar si son capaces de modificar la interacción del PF del VIH-1 con modelos de membrana como liposomas o monocapas. Algunas propiedades fisicoquímicas de los péptidos como el punto isoeléctrico (pI) o la carga neta se predijeron utilizando algoritmos informáticos y observamos que existen similitudes entre los péptidos P7 y P8, y entre P10 y el PF del VIH-1; mientras que el P18 parece ser bastante diferente al resto. Lo mismos pudimos observar en los gráficos obtenidos según la escala de hidrofobicidad de Hopp-Woods, los cuales muestran que P10 y el PF del VIH-1 tienen un perfil altamente hidrofóbicos, mientras que P18 es el menos hidrófobo, y P7 y P8 tienen un perfil de hidrofobicidad parecido. Los estudios conformacionales mediante dicroísmo circular mostraron un incremento del porcentaje del hélice-α de P7 y P8 al mezclarlos con el PF del VIH-1 mostrando un cambio conformacional que puede ser la causa de su capacidad de inhibición. Los experimentos de penetración mostraron que todos los péptidos se insertan espontáneamente en las membranas fosfolipídicas. Mediante el análisis de las isotermas de compresión podemos ver que los péptidos interaccionan con los fosfolípidos y que los péptidos correspondientes a la proteína E1 son capaces de modificar las isotermas de compresión del PF del VIH-1; sin embargo, hay uno de los péptidos, el P7, que destaca como el mejor candidato para inhibir la actividad

del PF del VIH-1, y por lo tanto, que puede ser un candidato potencial para ser utilizado en futuras investigaciones anti-VIH-1.

Physicochemical characterization of GBV-C E1 peptides as potential inhibitors of HIV-1 Fusion Peptide: Interaction with model membranes

Maria Jesús Sánchez-Martín[a*], *M. Antònia Busquets*[a], *Isabel Haro*[b], *M. Asunción Alsina*[a], *Montserrat Pujol*[a]

[a]Physical Chemistry Department, Faculty of Pharmacy, University of Barcelona, CSIC-Associated Unit: Peptides and proteins: Physicochemical studies. IN2UB Av. Joan XXIII s/n, 08028 Barcelona, Spain.

[b]Unit of Synthesis and Biomedical Application of Peptides. Department of Biomedical Chemistry, IQAC-CSIC, Jordi Girona 18, 08034, Barcelona, Spain.

*__Corresponding author:__ e-mail: mjsanchez@ub.edu; phone: (+34) 93 402 45 58; fax: (+34) 93 403 59 87

ABSTRACT

Four peptide sequences corresponding to the E1 protein of GBV-C: NCCAPEDIGFCLEGGCLV (P7), APEDIGFCLEGGCLVALG (P8), FCLEGGCLVALGCTICTD (P10) and QAGLAVRPGKSAAQLVGE (P18) were studied as they were capable of interfering with the HIV-1 fusion peptide (HIV-1 FP). In this work, the surface properties of the E1 peptide sequences are investigated and their physicochemical characterization is done by studying their interaction with model membranes; moreover, their mixtures with HIV-1 FP were also studied in order to observe whether they are capable to modify the HIV-1 FP interaction with model membranes as liposomes or monolayers. Physicochemical properties of peptides (pI and net charge) were predicted showing similarities for P7 and P8, and P10 and HIV-1 FP, whereas P18 appears to be very different from the rest. Circular dichroism experiments showed an increase of the percentage of α-helix of P7 and P8 when mixed with HIV-1 FP indicating a conformational change that could be the cause of their inhibition ability. Penetration experiments show that all the peptides can spontaneously insert into phospholipid membranes. Analysis of compression isotherms indicates that the peptides interact with phospholipids and the E1 peptides modify the compression isotherms of HIV-1 FP, but there is one of the peptides that excelled as the best candidate for inhibiting the activity of HIV-1 FP, P7, and therefore, that could be potentially used in future anti-HIV-1 research.

Keywords: Hepatitis GB virus C; synthetic peptide; lipid monolayer, compression isotherms, HIV-1 FP, bilayer, circular dichroism.

1. INTRODUCTION

The independently discovered human viruses GB virus C (GBV-C) [1] and hepatitis G virus (HGV)[2] are two isolates of the same single-stranded RNA virus. GBV-C shows characteristics of a *flavivirus*-like genome, closely related to the hepatitis C virus (HCV). The virus infects lymphocytes, but not hepatocytes and there is no conclusive evidence of a causal link between GBV-C and either acute or chronic liver disease. GBV-C has been investigated in the context of human immunodeficiency virus (HIV) infection and there are some reports finding that co-infection prolonged survival of patients and served as a potentially effective treatment.[3-5] Based on a co-infection model, GBV-C may influence HIV disease via inhibition of HIV by inducing chemokines, down-regulating the HIV co-receptor(s), influencing cytokine profiles, or having other –as yet undefined– effects on the host lymphocytes.[4, 5] However, the mechanism responsible for the beneficial effect that the GBV-C virus has on the course of disease caused by HIV has not yet been identified.

We are currently examining the capacity of GBV-C synthetic peptides to interact and to induce fusion in model membranes. [6, 7] The capacity, observed *in vitro*, to inhibit the leakage of vesicular contents caused by the HIV-1 fusion peptide (HIV-1 FP) is the property that allows us to select the sequences of the envelop protein E1 of GBV-C/HGV in order to study their interaction with model membranes and with HIV-1 FP.

In this work, four peptides corresponding to the E1 protein of GBV-C are selected as possible inhibitors of the activity of HIV-1 FP. [8]

The aim of this work is to study the effect of the E1 peptides on the activity of the peptide sequence that represents the 23 N-terminal residues of the surface protein gp41 of HIV which corresponds to HIV-1 FP.

Surface properties are among the most important features of biomaterials. Surface functional groups and their arrangement in the nanoscale topology of the material surface have dramatic effects on amount, orientation, and conformation of adsorbed proteins. For these reasons, adsorption and conformational change of proteins on biomaterial surfaces are widely considered to be one of the most important mechanisms controlling interactions between biomaterials and the surrounding biological system.

Small variations in primary structure strongly affect the local predisposition toward secondary structure in smaller peptides. α-helix[9], β-sheet[10], and a variety of

turns[11] have been reported for short peptides. These are consistently found to depend strongly on the primary structure. For example, in model α-helical peptides, favorable intramolecular electrostatic interactions arising from charged side chains are frequently used to stabilize α-helicity[12]. In contrast, polypeptides lacking such specific interactions follow the entropic bias toward a "random coil" conformation, in which the average dihedral angles follow local torsional energetic, independent of surrounding residues[13].

As a continuation of a previous work carried out in our group[8], the surface properties of the E1 peptide sequences are investigated and their physicochemical characterization is done by studying their interaction with model membranes; lipopeptide interactions with lipid monolayers of 1,2-dimyiristoyl-*sn*-Glycero-3-[Phospho-*rac*-(1-glycerol)] (DMPG) and 1,2-Dipalmitoyl-*sn*-glycero-3-phospho-*ra*c-(1-glycerol) (DPPG) are studied, in order to observe the influence of acyl chain lengths differing by two methylene units.

In addition, conformational analysis by circular dichroism was carried out in presence of liposomes as model membranes. Moreover, we are interested in study the conformational changes when HIV-1 FP is in presence of E1 peptides in order to know if it is one of the reason for inhibiting its activity.

2. *EXPERIMENTAL*

2.1. Materials

1,2-dimyiristoyl-sn-glycero-3-[phospho-rac-(1-glycerol)] (DMPG) and 1,2-dipalmitoyl-*sn*-glycero-3-phospho-*ra*c-(1-glycerol) (DPPG) and 1-palmitoyl-2-oleoyl-sn-glycero-3-phosphocholine (POPG) were purchased from Avanti Polar Lipids. Their purity was higher than 99% and they were used without further purification.

Chloroform and methanol were purchased from Merck. Water was double distilled and deionised (MilliQ system, Millipore) (18.2 MΩ cm, pH 5.8). Buffer in all experiments was HEPES (from Sigma-Aldrich) 5mM and NaCl (from Merck) 20 mM, pH 7.4.

2.2. Methods

2.2.1. Peptides Synthesis

The peptides corresponding to E1 protein of GBV-C: NCCAPEDIGFCLEGGCLV (P7), APEDIGFCLEGGCLVALG (P8), FCLEGGCLVALGCTICTD (P10) and

QAGLAVRPGKSAAQLVGE (P18), and the HIV-1 FP, AVGIGALFLGFLGAAGSTMGAAS, were obtained by solid-phase methodologies and purified by preparative high performance liquid chromatography, as previously described.[8]

2.2.2. Preparation of Multilamellar Vesicles

1-Palmitoyl-2-Oleoyl-sn-Glycero-3-Phosphocholine (POPG) and peptides were dissolved in a chloroform:methanol (2:1, v/v) mixture. Different mixtures of POPG and E1 peptides with or without HIV-1 FP were done and the solutions were evaporated to dryness in vacuum with a rotary evaporator. The dried lipid film was subjected to a high vacuum overnight to remove trace amounts of solvent. Then, the lipid films were hydrated with double distilled and deionised water to obtain multilamellar vesicles (MLVs).

2.2.3. Bioinformatic analysis tools for peptide characterization

Physicochemical properties of peptides (pI and net charge) were predicted using the Isoelectric Plot calculation program at http://www.bioinformatics.org/JaMBW//3/1/6/index.html. Hydrophobicity profiles were obtained by means of a calculation program at http://www.vivo.colostate.edu/molkit/hydropathy/index.html, using the Hopps and Woods scale with a window size of 6.

2.2.4. Circular dichroism

CD spectra were recorded on a Jasco J-810 spectropolarimeter (Japan Spectroscopic Company, Tokyo). All measurements were done in water. Cells 1 cm in diameter were used and the spectra were measured between 170 and 250 nm using a spectral bandwidth of 1 nm and a scan speed of 10 nm/min.

All measurements were performed at 25 °C and the data were expressed in terms of mean residue ellipticities [θ] ($deg \cdot cm^2 \cdot dmol^{-1}$). Three scans were accumulated to improve the signal to noise ratio. Before reading the peptide spectra, a spectrum of the blank solution was subtracted and the data converted to mean residue ellipticity units.[14] Moreover, Contin by the Dichroweb server at http://dichroweb.cryst.bbk.ac.uk/html/home.shtml program was used to treat experimental CD results. [15, 16]

The percentage of α-helix conformation in the peptides was estimated using the formalism of Chen et al. [17] This approach assumes that the maximum theoretical ellipticity for a given peptide or protein at 222 nm may be derived from the number of amino acid residues *n*, and the ellipticity at 222 nm of a helix of infinite length described by Eq. (3).

$$\%\ \alpha\text{-helix} = \frac{[\theta]_{222}}{\left[-39500\left(1-\frac{2.75}{n}\right)\right]} \qquad (3)$$

2.2.5. Adsorption at the air-water interface

Adsorption studies at the air-water interface were carried out using a NIMA Langmuir Film Balance equipped with a Wilhelmy platinum plate (Nima Technology, Coventry) and a Teflon trough that was rinsed with ethanol and distilled water before use. All experiments were performed at room temperature.

The surface activity of peptides was first studied to determine the equilibrium spreading pressure. Using a cylindrical PTFE trough (19.6 cm^2, 27.2 cm^3), increasing volumes of a 0.28mM peptide solution were injected below HEPES subphase (pH 7.4) through a lateral hole and the adsorption of the peptide at the air/water interface was therefore monitored by following the increase in surface pressure as a function of time under continuous stirring of the subphase.

2.2.6. Insertion of peptides into monolayers

The kinetics of insertion of the peptides into monolayers of DMPG and DPPG were measured using the same trough as for the surface activity. For these experiments, a lipid stock solution was prepared and added drop wise on the subphase until the desired lipid pressure was achieved. After 10-20 min the equilibrium of the lipid monolayer was reached. Then, a 0.28 mM peptide solution was injected into the subphase through the side hole of the trough. The subphase was magnetic stirred during the measurements and surface pressure changes were monitored as function of time until it remained constant.

2.2.7. Compression isotherms

Compression isotherms were carried out on a Nima (UK) Langmuir Teflon trough (surface area 595 cm^2, volume 280 cm^3). By depositing appropriate volumes of chloroform stock solutions of phospholipids (0.28mM) and of peptides (0.28 mM), the

lipid–peptide spreading solutions were obtained. Monolayers were formed by applying small drops of the spreading solutions on the HEPES subphase (pH 7.4) with a micro syringe (Hamilton Co., Reno, NV). After 15 min, monolayers of the desired composition were continuously compressed with an area reduction rate of 15 cm^2 min^{-1}. The films were compressed to their collapse pressure when possible. Each run was repeated three times and the reproducibility was ±1$Å^2$ $molecule^{-1}$.

3. *RESULTS AND DISCUSSION*

3.1. Bioinformatic analysis tools for peptide characterization

Physical properties such as the isoelectric point (pI) or the net charge at pH 7.4 (pH of the study) of the peptides were predicted in order to know whether the behavior of the different sequences is related to these properties. Results are shown in Table 1.

Table 1. Prediction of the Isoelectric point and the net charge at pH = 7.4 for HIV-1 FP and E1 synthetic peptides

	Isoelectric point	**Net charge at pH = 7.4**
HIV-1 FP	6	-0.1
P7	2.88	-3.5
P8	2.88	-3.2
P10	3.18	-1.5
P18	11.38	+2

P7 and P8 present similar values of both properties, whereas the pI and the charge of P10 are the most close to those of HIV-1 FP. In the contrary, P18 differs much from the rest.

3.2. Circular dichroism

In order to gain insights into the differences between peptides and their interaction with HIV-1 FP, a conformational study was carried out. Circular dichroism experiments and the corresponding quantitative analysis of the experimental data using a deconvolution computer program were done. In general, short synthetic peptides do not have a preferential conformation in solution, but can sometimes adopt moderately stabilized

secondary structures.[18] CD experiments were carried out in presence of POPG vesicles as it was found that HIV-1 bound to negative phospholipids stronger than to lipids devoid of a net charge [19]. Firstly, CD spectra of the peptides separately were recorded. Afterwards, E1 peptides were incubated with HIV-1 FP and added to the liposomes solution.

We used CD to analyze if the ability of the E1 peptides to bind HIV-1 FP induces a conformational change in its secondary structure. In this sense, CD spectra of the HIV-1 FP in presence of POPG liposomes showed a negative band with a peak around 215nm which could be attributed to a β-structure contribution probably due to peptide aggregation (figure 1). In this medium, the peptide spectrum also showed a negative band near 195 nm that is typical of random coil conformation.

On the other hand, in P7, P8 and P18 spectra, the characteristic positive band around 195 nm appeared showing the spectra like those of an α-helix structure, and they also show a negative band with a peak between 215 and 220 nm which could be attributed to a β-structure contribution. CD spectra of P10 also showed a negative band near 195 nm, typical of random coil conformation.

The experimental CD spectrum of the mixture of E1 peptides and HIV-1 FP in aqueous solution is different from the theoretical spectrum obtained by summing experimental spectra of equivalent amounts of the peptides alone (dotted spectra in figure 1); thus, the results suggest that the E1 peptides interact with HIV-1 FP. The mixture demonstrated that the addition of E1 peptides to the HIV-1 FP increased significantly the mean residue ellipticity at 195 nm, thus increasing the percentage of α-helix.

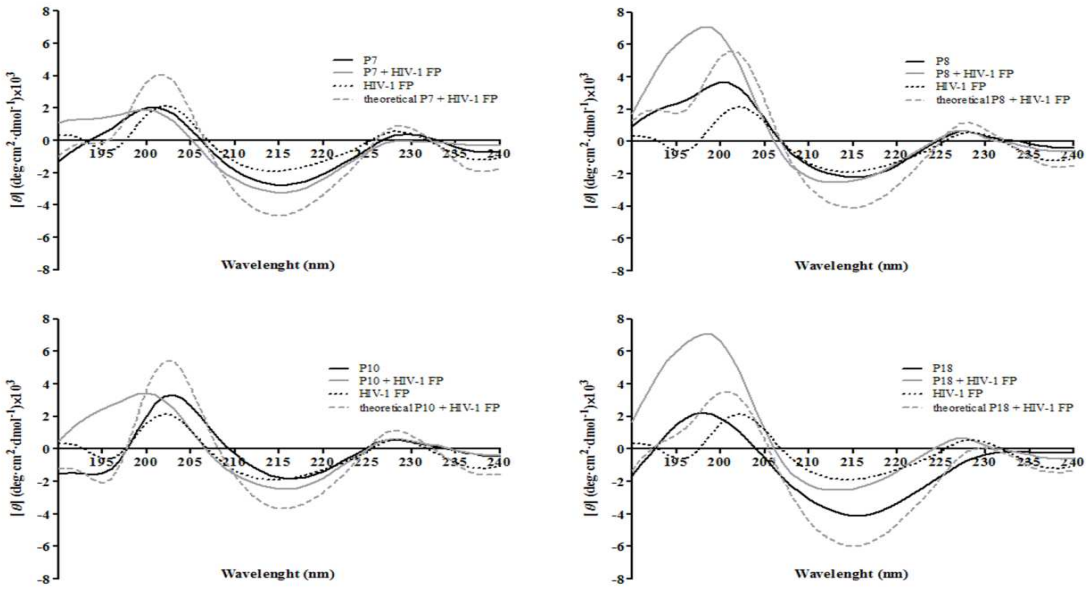

Figure 1. CD spectra of E1 synthetic peptides and HIV-1 FP in presence of POPG liposomes recorded at 298 K.

Table 2 shows the estimation, from the CD spectra, of the content of α-helical conformation of the peptides according to molar ellipticity at 222 nm (calculated from equation 3).

Table 2. Estimation, from the CD spectra, of the content of α-helical conformation of the HIV-1 FP and E1 peptides according to molar ellipticity at 222 nm.

% α-helix in presence of POPG liposomes	
	$[\theta]_{222}$
HIV-1 FP	5.2
P7	7.7
P7 + HIV-1 FP	9.3
P8	6.1
P8 + HIV-1 FP	6.4
P10	5.2
P10 + HIV-1 FP	7.2
P18	11.6
P18 + HIV-1 FP	6.4

First, results show that P18 has a high percentage of α-helix compared to the rest and the percentage obtained for P10 is equal to that obtained for HIV-1 FP; these results are coherent with those obtained in table 1, showing that P10 and P18 behave different from

P7 and P8, and that P10 has some similarities with HIV-1 FP. This similarity obtained here are coherent with the results obtained in a previous work where P10 was found that could be an internal fusion peptide of GBV-C, as HIV-1 FP, and it was discarded as a possible inhibitor of HIV-1 FP. P18 is the peptide that presents the highest change in the conformation when mixed with the HIV-1 FP, showing a clear interaction between both peptides.

3.3. Adsorption at the air-water interface

Figure 2 shows the adsorption isotherm profile for the E1 synthetic peptides. A small gradual adsorption of peptide was observed at low peptide concentration. The higher the peptide concentration in the subphase the faster the incorporation process and, therefore, the higher the surface pressure attained. The shape of the surface activity curves approximates a rectangular hyperbola and it was fitted to equation (1) via non-linear least squares regression analysis.

$$\pi = \frac{C\,\pi_{\max}}{K + C} \qquad (1)$$

Where C is the concentration, $\pi_{\max}$ is the maximum pressure achieved and K is a characteristic constant equal to the peptide concentration that yields $\frac{1}{2}\pi_{\max}$. Fitting the data, the values obtained are shown in Table 3. These K values were chosen to further penetration studies, as K corresponds to the suitable concentration of the peptide that should be used in the bulk subphase for experiments of penetration kinetics, lower than the equilibrium spreading pressure of the peptide[20].

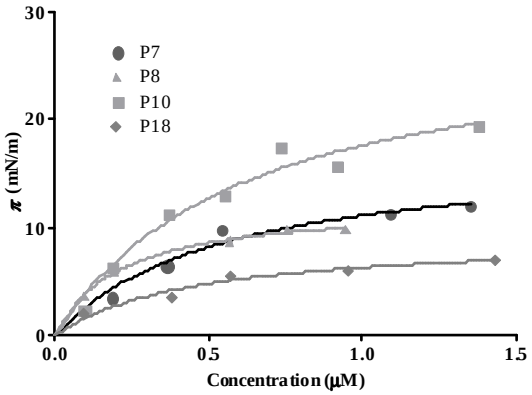

Figure 2. Surface activity curve of E1 synthetic peptides

By applying the Gibbs adsorption equation in its simpler form (equation 2) it is possible to calculate the peptide surface excess concentration (Γ)

$$\Gamma = \frac{\Delta\pi}{RT\,\Delta \ln c} \qquad (2)$$

Where R is the gas constant (8.31 J K^{-1} mol), T is the temperature (298 K), $\Delta\pi$ is the maximum pressure increase achieved for each peptide concentration and C is the peptide concentration.

The surface excess concentration of the E1 synthetic peptides at saturation (Γ_{max}) deduced from the slope of the $\Delta\pi$ – ln C curve (equation (2)) allows us to calculate the surface molecular area by means of equation (3), where N is Avogadro's constant. Results are shown in Table 3.

$$A = \frac{1}{\Gamma_{max}\, N} \qquad (3)$$

Table 3. Analysis of the adsorption isotherms of the E1 synthetic peptides. π_{max} is the maximum pressure achieved and K is a characteristic constant equal to the peptide concentration that yields $\frac{1}{2}\pi_{max}$. Γ_{max} is the surface excess concentration at saturation and A is the molecular area.

	π_{max} (mN m^{-1})	K (μM)	r^2	Γ_{max}(10^{22} res m^{-2})	A (Å^2 res^{-1})
P7	17.22	0.55	0.953	1.85	5.40
P8	12.14	0.21	0.993	1.20	8.34
P10	28.49	0.62	0.966	2.79	3.59
P18	9.20	0.46	0.947	0.83	12.05

Clearly, the four peptides decrease the surface tension of the air-water interface. However, their hydrophobic profiles based on their primary sequence are very different and this fact induces different behaviours; the main difference is the grater decrease in tension induced by P10, this suggests that P10 develops stronger hydrophobic interactions than the others when engaged in an air-water interface most likely because they adopt different structural states. This fact is corroborated with the hydrophobicity plot of P10 obtained using Hopp-Woods scale that was designed for predicting potentially antigenic regions of polypeptides. In this type of plots, values greater than 0

are hydrophilic and thus likely to be exposed on the surface of a folded protein. For P10 all the values in the plot are negative, showing a high hydrophobicity profile, as HIV-1 FP also presenting negative values in the plot. P7 and P8 have negative values from the residues 8 to 15 and 4 to 15, respectively, and P18 shows negative values for the residues 3 to 5 and 14 to 15, being the less hydrophobic peptide and corroborating the low π_{max} value obtained at the adsorption isotherm.

3.4. E1 synthetic peptides insertion into phospholipid monolayers

The ability of the E1 peptides to insert into phospholipid monolayers spread at the air-water interface was monitored by measuring variations in surface tension using different initial pressures, and by injecting a given peptide concentration in the subphase. The selected concentration corresponds to the *K* values calculated in section 3.3. Various penetration experiments were carried out using two different phospholipids, DMPC and DMPG, where the nature of the headgroups (zwitterionic and negatively charged) is different. For both lipids, the general trend observed is that the greater $\pi_{i,}$ the lower the degree of incorporation of the peptide into the monolayer because of the closer packing of the lipids at higher initial pressures (Figure 3).

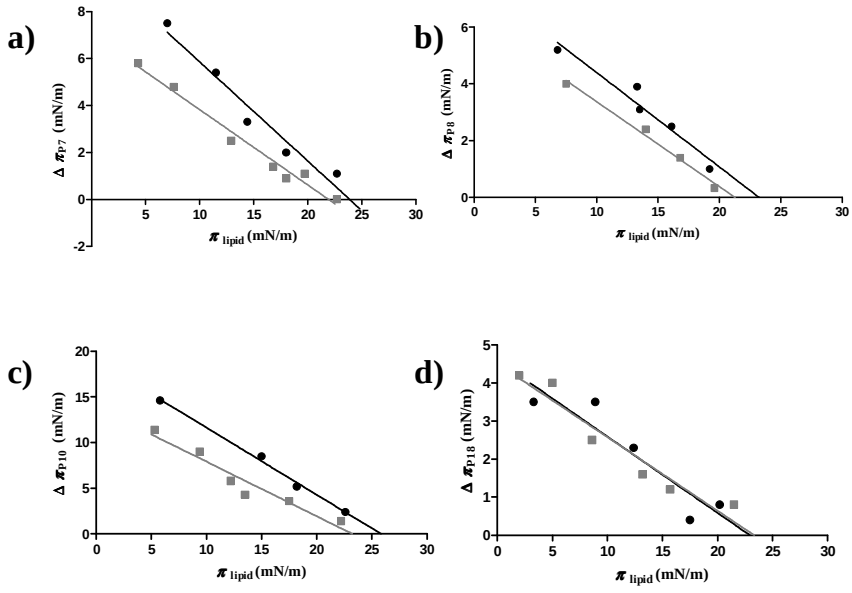

Figure 3. Surface pressure increase ($\Delta\pi$) caused by E1 synthetic peptides in monolayers of different phospholipids in front of the lipid initial pressure (π_i). Grey squares correspond to DMPG and black circles to DMPC.a) P7, b) P8, c) P10 and d) P18

The monolayer exclusion pressure π_e (that is, the surface pressure above which the peptide does not penetrate into the monolayer) was obtained by extrapolating the plot to $\Delta\pi = 0$ mN m^{-1} [21]. It can be seen that the peptide interacts with the two lipids tested; the nature of the headgroups has influence on penetration for all peptides except for P18. DMPG form anionic monolayers while monolayers of DMPC are zwitterionic. The insertion of the peptides in the anionic monolayers is lower than in the zwitterionic, probably due to the negative charge of the peptides; however, P18, that is positively charged, interacts in the same way with both phospholipids. The π_e is similar for all the peptides except for P10 that has a π_e for DMPC higher than the others peptides, indicating a better uptake by this zwitterionic phospholipid.

3.5. Spreading at the Air-Water Interface: Compression isotherms

Figure 4 shows the compression isotherms obtained for the E1 peptides and their mixtures with HIV-1 FP when mixed with DMPC (column a) and DMPG (column b). We could observe how the shape of the isotherms of HIV-1 FP and phospholipids changes drastically when HIV-1 FP is mixed with any of the other E1 peptides. The isotherms were analyzed by examining the variation of the mean molecular area (that of the contributions of both the peptide and the lipid) as a function of the peptide/lipid ratio at a given and constant surface pressure. These variations are reported on figure 5 and correspond to a pressure of 10 mN/m, although for 5, 20 and 30 mN/m the same trends are observed for all the peptides. Analysis of the plots reveals several similar situations in both lipid-peptide combinations. First, they show a nonlinear behavior for all the peptides and their mixtures, indicating that all the peptides are miscible and interact with the phospholipids assayed[22]. The mixtures present positive deviations of ideality, at any peptide molar fraction assayed, except when HIV-1 FP is mixed with P7, suggesting that the peptides interact with phospholipids through repulsive interactions[23]. Although all the E1 peptides decrease the deviations caused by HIV-1 FP, P7 is the only one that make these deviations become negative and, at lower $X_{\text{HIV-1 FP+P7}}$, they show an ideal behavior. The contraction observed in the case of P7 indicates that peptide-lipid interactions are attractive and may reflect the formation of peptide-lipid complexes through hydrophobic interactions[24]. The deviations from ideality of the mixed monolayers of P18 with DMPG are smaller than for the other peptides, this

behavior is related with the positive charge of P18 and, therefore, the electrostatic attraction towards DMPG.

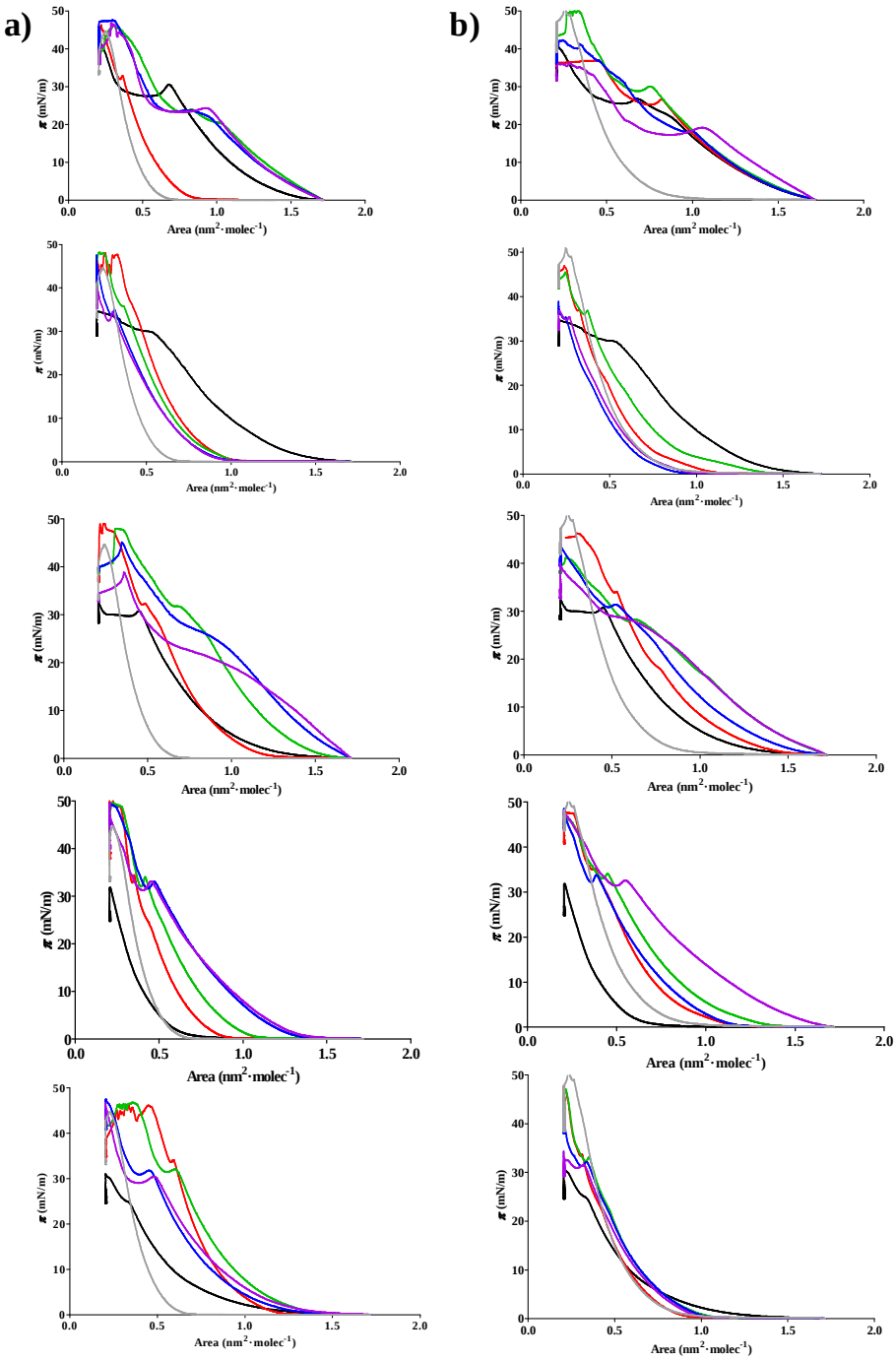

Figure 4. Surface pressure-mean molecular area (π-*A*) compression isotherms for: from top to bottom HIV-FP, P7+HIV-1 FP, P8+HIV-1 FP, P10+HIV-1 FP and P18+HIV-1 FP and the lipids: (a) DMPC, (b) DMPG spread on HEPES subphase (pH=7.4). Black

line for $X_{peptide(s)}$=1, red line for $X_{peptide(s)}$=0.2, green line for $X_{E1(145-162)}$=0.4, blue line for $X_{E1(145-162)}$=0.6, violet line for $X_{E1(145-162)}$=0.8 and grey line for the lipid isotherm.

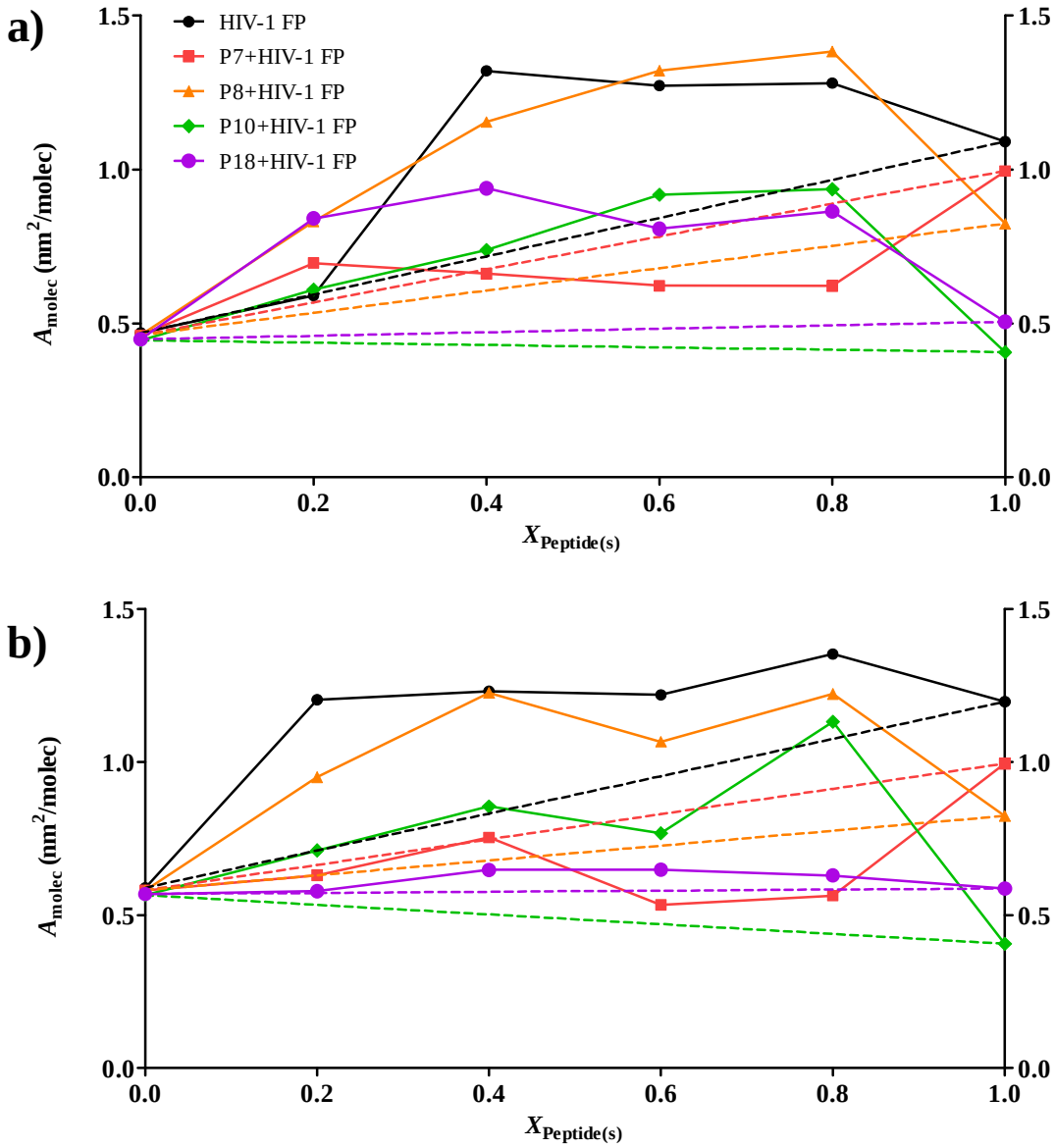

Figure 5. Plots of *A* for the mixtures of E1 peptides and HIV-1 FP as a function of the peptides molar fractions for mixed monolayers of: (a) DMPC and (b) DMPG

4. *CONCLUSIONS*

The present investigations try to offer some light on the interaction of four sequences corresponding to E1 protein of GBV-C with the HIV-1 FP in order to expand the study carried out in a past work[8]. Previously, P10 was discarded as a possible inhibitor of the HIV-1 FP activity and suggested as a possible fusion peptide of GBV-C; these results are coherent with those obtained in this study. We have found that pI and the charge of P10 are the most close to those of HIV-1 FP as well as the estimation of the content of α-helical conformation according to molar ellipticity at 222nm is equal for both peptides. Moreover, P10 shows stronger hydrophobic interactions when engaged in an air-water interface than the others, corroborated by Hopp and Woods hydrophobicity profile that is also very similar to HIV-1 FP profile.

P18 was found not to inhibit the interaction with bilayers or the membrane fusion caused by HIV-1 FP. The present results show that P18 is the least hydrophobic of all and it is the only one that, in presence of HIV-1 FP, reduces its percentage of α-helix instead of increasing it as the others. Compression isotherms show its high miscibility with the negatively charged phospholipid and how it is capable of reducing the expansion of the mean molecular area caused by HIV-1 FP; thus, we have another evidence of its ability to inhibit the activity of HIV-1 FP in the same way that it was capable of inhibiting the leakage of vesicular contents caused by HIV-1 FP. [8]

P7 and P8 behave very similar. They were capable of inhibiting the leakage of vesicular contents, the membrane fusion and the interaction with bilayers of HIV-1 FP. These results reflect again the similarities between both peptides as the pI and the net charge, the surface activity curves or the increase of the percentage of α-helix when mixed with HIV-1 FP showing a conformational change that could be the cause of the inhibition effect. Moreover, the contraction of the mean molecular area observed in the case of HIV-1 FP in presence of P7 indicates that peptide-lipid interactions are attractive and may reflect the formation of peptide-lipid complexes through hydrophobic interactions. The interaction between P7 and HIV-1 FP was also observed by isothermal titration calorimetry were the binding of P7 to HIV-1 FP was found to be endothermic[8]. On the contrary, P8 doesn't seem to change the deviations in the mean molecular area

caused by HIV-1 FP nor its interaction with HIV-1 FP in solution was observed by isothermal titration calorimetry.

In conclusion, after several studies to evaluate the possibility of using synthetic peptides corresponding to the envelop protein E1 of GBV-C in future anti-HIV research, there is one of the peptides studied that excels in all the experiments, P7, that corresponds to the region E1(19-36); therefore, this peptide could be potentially used in future anti-HIV-1 therapies. P8 and P18 are capable of inhibiting some actions that HIV-1 FP has on membrane models, therefore, we could not discard them and we need to investigate deeply these peptides to understand the reason for this ability and why they don't act in same way in all the experiments assayed.

5. *ACKNOWLEDGEMENTS*

This work was supported by project CTQ2006-15396-C02-02/01-BQU from the *Secretaría de Estado de Investigación, Ministerio de Ciencia e Innovación, Dirección General de Programas y transferencia de conocimiento, Subdirección General de Proyectos de Investigación* (Spain). M.J. Sánchez-Martín is a recipient of an FPI programme pre-doctoral grant. The authors are members of the consolidated research group recognised by the *Generalitat de Catalunya* "Peptides and Proteins: physicochemical studies" (2005SGR00278).

6. *REFERENCES*

[1] J.N. Simons, T.J. Pilot-Matias, T.P. Leary, G.J. Dawson, S.M. Desai, G.G. Schlauder, A.S. Muerhoff, J.C. Erker, S.L. Buijk, M.L. Chalmers and et al., Identification of two flavivirus-like genomes in the GB hepatitis agent, Proceedings of the National Academy of Sciences of the United States of America, 92 (1995) 3401-3405.

[2] J. Linnen, J. Wages, Jr., Z.Y. Zhang-Keck, K.E. Fry, K.Z. Krawczynski, H. Alter, E. Koonin, M. Gallagher, M. Alter, S. Hadziyannis, P. Karayiannis, K. Fung, Y. Nakatsuji, J.W. Shih, L. Young, M. Piatak, Jr., C. Hoover, J. Fernandez, S. Chen, J.C. Zou, T. Morris, K.C. Hyams, S. Ismay, J.D. Lifson, G. Hess, S.K. Foung, H. Thomas, D. Bradley, H. Margolis and J.P. Kim, Molecular cloning and disease association of hepatitis G virus: a transfusion-transmissible agent, Science (New York, N.Y, 271 (1996) 505-508.

[3] H.L. Tillmann and M.P. Manns, GB virus-C infection in patients infected with the human immunodeficiency virus, Antiviral research, 52 (2001) 83-90.

[4] J. Xiang, S. Wunschmann, D.J. Diekema, D. Klinzman, K.D. Patrick, S.L. George and J.T. Stapleton, Effect of coinfection with GB virus C on survival among patients with HIV infection, The New England journal of medicine, 345 (2001) 707-714.

[5] J. Xiang, S.L. George, S. Wunschmann, Q. Chang, D. Klinzman and J.T. Stapleton, Inhibition of HIV-1 replication by GB virus C infection through increases in RANTES, MIP-1alpha, MIP-1beta, and SDF-1, Lancet, 363 (2004) 2040-2046.

[6] M. Sánchez-Martín, J. Amigo, M. Pujol, I. Haro, M. Alsina and M. Busquets, Fluorescence study of the dynamic interaction between E1(145–162) sequence of hepatitis GB virus C and liposomes, Analytical and bioanalytical chemistry, 394 (2009) 1003-1010.

[7] M.J. Sánchez-Martín, I. Haro, M.A. Alsina, M.A. Busquets and M. Pujol, A Langmuir Monolayer Study of the Interaction of E1(145-162) Hepatitis G Virus Peptide with Phospholipid Membranes, The Journal of Physical Chemistry B, 114 (2010) 448-456.

[8] M.J. Sánchez-Martín, K. Hristova, M. Pujol, M.J. Gómara, I. Haro, M. Asunción Alsina and M. Antònia Busquets, Analysis of HIV-1 fusion peptide inhibition by synthetic peptides from E1 protein of GB virus C, Journal of Colloid and Interface Science, 360 (2011) 124-131.

[9] R. Parthasarathy, S. Chaturvedi and K. Go, Design of alpha-helical peptides: their role in protein folding and molecular biology, Progress in biophysics and molecular biology, 64 (1995) 1-54.

[10] M. Ramirez-Alvarado, F.J. Blanco, H. Niemann and L. Serrano, Role of beta-turn residues in beta-hairpin formation and stability in designed peptides, J Mol Biol, 273 (1997) 898-912.

[11] A. Perczel and M. Hollosi, Turns, in: G.D. Fasman (Ed.) Circular Dichroism and the Conformational Analysis of Biokolecules, Plenum Press, New York, 1996.

[12] M.J.I. Andrews and A.B. Tabor, Forming stable helical peptides using natural and artificial amino acids, Tetrahedron, 55 (1999) 11711-11743.

[13] D.A. Brant and P.J. Flory, The Configuration of Random Polypeptide Chains. II. Theory, Journal of the American Chemical Society, 87 (1965) 2791-2800.

[14] N.J. Greenfield, Using circular dichroism spectra to estimate protein secondary structure, Nature protocols, 1 (2006) 2876-2890.

[15] A. Lobley, L. Whitmore and B.A. Wallace, DICHROWEB: an interactive website for the analysis of protein secondary structure from circular dichroism spectra, Bioinformatics (Oxford, England), 18 (2002) 211-212.

[16] L. Whitmore and B.A. Wallace, DICHROWEB, an online server for protein secondary structure analyses from circular dichroism spectroscopic data, Nucleic acids research, 32 (2004) 668-673.

[17] Y.H. Chen, J.T. Yang and K.H. Chau, Determination of the helix and beta form of proteins in aqueous solution by circular dichroism, Biochemistry, 13 (1974) 3350-3359.

[18] J.A. Pérez, J. Cantó, F. Reig, J.J. Pérez and I. Haro, Conformational behavior of the HAV-VP3(110–121) peptidic sequence and synthetic analogs in membrane environments studied by CD and computational methods, Biopolymers, 45 (1998) 479-492.

[19] M. Wu, S.-Q. Nie, Y. Qiu, K.-C. Lin, S.-X. Wang and S.-F. Sui, Study of the relationship between structure and function of HIV-1 gp 41 N terminus fusion peptide, in: Peptides Biology and Chemistry, 2002, pp. 104-107.

[20] M. Rafalski, J.D. Lear and W.F. DeGrado, Phospholipid interactions of synthetic peptides representing the N-terminus of HIV gp41, Biochemistry, 29 (1990) 7917-7922.

[21] P. Bougis, H. Rochat, G. Pieroni and R. Verger, Penetration of phospholipid monolayers by cardiotoxins, Biochemistry, 20 (1981) 4915-4920.

[22] G.L. Gaines, In Insoluble Monolayers at Liquid-Gas Interfaces, in, Wiley-Interscience, New York, 1966, pp. 286.

[23] M.J. Galvez and M.A. Cabrerizo, A study of the miscibility of bile components in mixed monolayers at the air-liquid interface I. Cholesterol, lecithin, and lithocholic acid, Colloid Polym Sci, 269 (1) (1991) 77-84.

[24] S. Deshayes, T. Plenat, G. Aldrian-Herrada, G. Divita, C. Le Grimellec and F. Heitz, Primary amphipathic cell-penetrating peptides: structural requirements and interactions with model membranes, Biochemistry, 43 (2004) 7698-7706.

4. Discusión

El trabajo presentado en esta tesis puede dividirse en dos fases. En la primera, se seleccionó un epítopo de la proteína estructural E1 del virus de la hepatitis G mediante algoritmos teóricos de predicción y se estudiaron las propiedades de dicho péptido. En la segunda fase se sintetizaron 58 secuencias peptídicas de 18 aminoácidos cada una (incluida la primera secuencia seleccionada) que cubrían toda la proteína E1 y estaban solapadas en 15 residuos. De todas estas secuencias, tras realizar un ensayo de *screening,* se seleccionaron las cinco secuencias que parecían poder inhibir la actividad del péptido de fusión de la glicoproteína gp41 del VIH-1. Todas estas secuencias se enumeraron desde P1 a P58.

4.1. Síntesis y caracterización del péptido E1(145-162) del GBV-C/HGV seleccionado mediante algoritmos teóricos de predicción.

La selección de la secuencia peptídica E1(145-162) se basó en dos requisitos: por un lado, la posible actividad antigénica y, por otro, la presencia de algún aminoácido que confiriera fluorescencia intrínseca al péptido.

Los perfiles de hidrofilicidad y de accesibilidad de las proteínas, de acuerdo con Janin [136] y Hopp y Woods [137], se han considerado buenos indicadores para predecir sitios antigénicos en las proteínas. La secuencia E1(145-162) estudiada en los dos primeros artículos corresponde al péptido P49. Esta secuencia mostró unos perfiles de antigenicidad y accesibilidad que la señalaban como posible sitio antigénico de la proteína. Además, dentro de las 58 secuencias que estaba previsto sintetizar, en ella encontramos triptófano y, por lo tanto, permitía realizar estudios de fluorescencia.

En el artículo 1 se estudian las propiedades superficiales del péptido E1(145-162) y sus interacciones con monocapas fosfolipídicas como modelos de membrana. Por otro lado, en el artículo 2 se estudian dichas interacciones pero utilizando bicapas (liposomas) como modelos de membrana.

Las propiedades superficiales del E1(145-162) concuerdan con una estructura de hélice α adoptada en la interfase aire-agua, principalmente orientada perpendicularmente a la interfase cuando el empaquetamiento es elevado.

Esta estructura se obtiene también en la predicción computacional, aunque la estructura del péptido se predice como una mezcla entre hélice α y una parte desordenada.

En los estudios de interacción con monocapas de DMPC, DMPG y POPG se ha observado que el péptido es capaz de interaccionar con todos estos fosfolípidos, aunque la interacción es mayor cuando la monocapa se compone de DMPG. El péptido penetra mejor en monocapas en las que el lípido se encuentra en estado de líquido expandido, como es el caso de las monocapas de DMPG y DMPC, para todas las presiones estudiadas; en cambio, para POPG esto sólo sucede a presiones por debajo de 10mN/m, ya que por encima de esta presión se encuentra en estado de líquido condensado. Por otro lado, la inserción del péptido en monocapas aniónicas es mayor que en las zwitteriónicas, probablemente debido a la carga positiva del péptido que interacciona mejor con una monocapa cargada negativamente.

Para los tres fosfolípidos, por debajo de 10mN/m de presión inicial, la incorporación del péptido en la monocapa fosfolipídica es mayor que en el ensayo de actividad superficial. Este hecho demuestra que el proceso que tiene lugar es el resultado de una interacción péptido-lípido real y no se trata únicamente de un proceso de adsorción. [138]

Estudiando las isotermas de compresión se puede observar que la presencia del péptido, en el caso de los tres fosfolípidos, produce una expansión de la monocapa del fosfolípido puro en todas las fracciones molares estudiadas. Además, modifica la compresibilidad de las monocapas pasando a estar en estado de líquido expandido. Es posible que esta expansión se deba a la formación de complejos péptido-lípido a través de interacciones hidrofóbicas o a un cambio en la orientación del péptido respecto a la interfase aire-agua de una posición paralela a una más vertical. [139]

El estudio termodinámico corrobora la miscibilidad péptido-lípido a una fracción molar de péptido de 0.2 y a presiones entre 20 y 25 mN/m, cuando las monocapas presentan una zona de transición sobre 20mN/m compatible con la formación de un complejo péptido-lípido que se separa cuando se alcanza el colapso. Estos resultados concuerdan con los obtenidos en el artículo 2. En este trabajo se realizan experimentos de fluorescencia aprovechando la

presencia de triptófano en la secuencia peptídica, el cual es sensible a cambios causados por alteraciones en la conformación del péptido y por la asociación a la membrana. La longitud de onda de emisión (λ_{max}) máxima del E1(145-162) fue 353nm en tampón, indicando que el Trp se encuentra expuesto al medio [140]. Al añadir los liposomas de DMPC o DMPG la λ_{max} se desvía a longitudes de onda más cortas a la vez que disminuye la intensidad de fluorescencia (artículo 2, figura 4). Ambos efectos sugieren que el residuo de Trp se encuentra en un entorno menos polar, mostrando interacción y penetración parcial del péptido en la parte hidrofóbica de la bicapa pero sin insertarse completamente. [141]

Los espectros de fluorescencia se modelaron mediante resolución multivariable de curvas con el algoritmo de mínimos cuadrados alternos (MCR-ALS, del inglés *Multivariate Curve Resolution – Alternating Least Squares*), la cual nos permitió describir la evolución de los perfiles espectrales a través de las contribuciones de los componentes puros individualmente. Los resultados de MCR-ALS (artículo 2, figura 6) muestran como a medida que se van añadiendo los liposomas, el perfil de concentración del péptido va disminuyendo, mientras que una nueva especie aparece a una fracción molar alrededor de 0.2, la cual se puede atribuir a la unión y penetración parcial del péptido en el núcleo hidrofóbico de la monocapa.

En los experimentos de anisotropía (*r*) se observa de nuevo que la interacción del péptido con liposomas cargados negativamente es mayor que con liposomas zwitteriónicos. El efecto más claro se observa cuando adicionamos el péptido a liposomas de DMPG marcados con la sonda TMA-DPH, la cual se encuentra anclada en la interfase aire-lípido. El aumento de los valores de *r* en presencia del péptido muestra que la sonda se encuentra en un entorno más rígido, indicando así la unión del péptido a la membrana. En presencia de liposomas de DMPC también se observa interacción pero la elevada dispersión de los valores puede ser indicativa de agregación de los liposomas o ruptura de las bicapas cuando los valores de *r* pasan a ser muy bajos.

4.2. Síntesis y caracterización de dominios peptídicos de la proteína E1 del GBV-C/HGV y selección, mediante métodos biofísicos, de péptidos capaces de inhibir la entrada del VIH-1

El *screening* de la proteína E1 del GBV-C/HGV se describe en el artículo 3 y se lleva a cabo mediante la síntesis de 58 secuencias peptídicas de 18 aminoácidos solapados en 15 residuos. Esta síntesis nos permite hacer un *screening* de toda la proteína para evaluar los péptidos en cuanto a su capacidad de inhibir el proceso de desestabilización de vesículas lipídicas inducido por el péptido de fusión del VIH-1 (PF del VIH-1).

El PF del VIH-1 tiene la capacidad de formar poros en las membranas lipídicas y aprovechamos esta propiedad para realizar los ensayos de liberación de contenidos vesiculares. Para este ensayo se preparan liposomas de POPG por su gran estabilidad y porque se ha observado que el PF del VIH-1 se une más fuertemente a fosfolípidos cargados negativamente que a aquellos lípidos que no tienen carga [142]. Estos liposomas que contienen dos sondas fluorescentes (ANTS y DPX), una de las cuales actúa como apantallador (*quencher*) de la otra, presentan una cierta fluorescencia que aumenta considerablemente al ponerlos en contacto con el PF del VIH-1, ya que éste desestabiliza la membrana y permite la liberación de las sondas, reduciéndose así el efecto apantallador (*quenching*) y dando como resultado un aumento de fluorescencia. Después de seleccionar la concentración de PF del VIH-1 que provoca el 50% de liberación de contenidos vesiculares, se incuba esta cantidad con cada uno de los 58 péptidos sintetizados a una relación PF-VIH-1:péptido E1 de 1:20 y se mide el porcentaje de liberación. Como resultado se obtiene que únicamente 5 péptidos son capaces de reducir el porcentaje de liberación por debajo del 50%. Las secuencias seleccionadas corresponden a los péptidos denominados P7, P8, P10, P18 y P22, cuyas regiones y secuencias peptídicas dentro de la proteína E1 se muestran en la tabla 1. Entre estos péptidos vemos que no se encuentra el péptido que se seleccionó mediante algoritmos de predicción, el P49; en este caso, obtuvimos un porcentaje de liberación de contenidos vesiculares en torno al 80%, por lo tanto, este péptido también provoca un cierto porcentaje de liberación que se suma al que causa el PF del VIH-1, lo que

concuerda con los datos obtenidos en los ensayos de anisotropía en los que observábamos cierta dispersión de los datos que podía ser debida a la ruptura de la bicapa. Por este motivo, este péptido fue descartado como objeto de estudio de esta tesis y nos centramos en los 5 péptidos que dieron inhibición en el ensayo de liberación de contenidos vesiculares.

Tabla 1. Secuencia peptídica y región de la proteína E1 a la que corresponden los péptidos seleccionados y denominados como P7, P8, P10, P18 y P22.

	Región	**Secuencia peptídica**
P7	E1(19-36)	NCCAPEDIGFCLEGGCLV
P8	E1(22-39)	APEDIGFCLEGGCLVALG
P10	E1(28-45)	FCLEGGCLVALGCTICTD
P18	E1(52-69)	QAGLAVRPGKSAAQLVGE
P22	E1(64-81)	AQLVGELGSLYGPLSVSA

Mediante análisis bioinformático se predijeron el punto isoeléctrico (pI) y la carga neta de estos péptidos a pH 7.4 (pH de trabajo), los resultados se muestran en la tabla 2.

Tabla 2. Predicción del punto isoeléctrico y la carga neta a pH = 7.4 para los péptidos sintéticos de la proteína E1 del GBV-C/HGV.

	punto iseléctrico (pI)	**Carga neta a pH = 7.4**
P7	2.88	-3.5
P8	2.88	-3.2
P10	3.18	-1.5
P18	11.38	+2
P22	3.18	-1

Se puede ver que el P7 y el P8 tienen valores similares para ambas propiedades, mientras que el pI y la carga del P10 y del P22 son más próximos entre ellos. El P18 difiere mucho del resto.

4.2.1. Caracterización de la interacción entre el PF del VIH-1 y los péptidos seleccionados. Estudios de toxicidad.

Con el fin de evaluar la interacción entre los péptidos de la proteína E1 y el péptido de fusión del VIH-1 se realizaron ensayos de calorimetría isotérmica de titulación (ITC) en los que se estudiaron los parámetros termodinámicos asociados a la interacción de los péptidos E1 al PF del VIH-1. Para los péptidos P8 y P10 el sistema no alcanzó la saturación, mientras que para P7, P18 y P22, a medida que avanzaba la valoración, la señal disminuía hasta que al final sólo se observó la señal correspondiente al calor de dilución. Las curvas de unión se muestran en la figura 3 del artículo 3. Los picos positivos muestran que la unión de P7, P18 y P22 al PF del VIH-1 es endotérmica, así como los valores positivos de entalpía. Por otro lado, obtenemos una energía de Gibbs (ΔG) negativa que nos indica que la unión entre estos péptidos y el PF es espontánea. La estequiometria para la unión de los péptidos de la proteína E1 al PF del VIH-1 es de 1:1 para el P18 y el P22, mientras que resultó ser de 2:1 para el P7. Con este ensayo podemos deducir que estos tres péptidos son capaces de interaccionar con el PF del VIH-1 en disolución, mientras que no podemos afirmar lo mismo para P8 y P10, los cuales, sin embargo, podrían interaccionar a nivel de membrana.

Con el fin de intentar profundizar en estas interacciones se seleccionó el péptido P22 por su menor hidrofobicidad y se estudiaron las isotermas de compresión del péptido por separado y sus mezclas con el PF del VIH-1 (artículo 5, figura 3). Podemos observar que a bajas presiones (0-10 mN m^{-1}), la adición del PF del VIH-1 en las monocapas de P22, produce valores mayores del área molecular media a medida que la proporción es mayor, indicando interacciones entre los dos péptidos. Las desviaciones son mayores cuando la fracción molar de P22 se encuentra entre 0.2 y 0.4. Con el fin de estudiar el

comportamiento de fase del sistema P22/PF del VIH-1 se examinó morfológicamente utilizando las técnicas de microscopía de ángulo de Brewster y de fuerza atómica (BAM y AFM, respectivamente). Las figuras 4 y 5 del artículo 3 muestran las imágenes obtenidas por ambas técnicas para una fracción molar de P22 de 0.6 y a una presión de 10 mN m^{-1}, cuando la monocapa se encuentra en estado de líquido expandido. En las imágenes de BAM, se puede observar que cada péptido individualmente presenta la coexistencia de dos fases, y en la mezcla también, pero la fase más condensada es muy diferente a la que se ve en las imágenes de los péptidos por separado. Estas diferencias también se observan en las imágenes de AFM, donde las películas de Langmuir-Blodgett (LB) de los péptidos puros son bastante diferentes a la película LB de la mezcla, mostrando una estructura de los péptidos diferente cuando están solos y cuando están mezclados. El P22 y el PF del VIH-1 en las figuras 5a y 5b presentan partículas redondeadas y ordenadas de forma diferente según el péptido. La película obtenida con el P22 muestra una extensión no uniforme sobre la mica, con grandes regiones sin cubrir y algunos pequeños agujeros; en cambio, las monocapas del PF del VIH-1 y la de la mezcla de ambos péptidos son más uniformes y no se observa la superficie de la mica. La película de LB de la mezcla muestra filamentos curvados de tamaño y forma similares cubriendo toda la superficie, los cuales no están presentes en las monocapas de los péptidos puros, sugiriendo un comportamiento similar al observado en las imágenes BAM.

Finalmente, con el fin de comprobar si todos los péptidos seleccionados podrían ser utilizados en futuras terapias anti-VIH o poder descartar alguno, se realizaron ensayos de toxicidad. Se estudió la citotoxidad de los péptidos utilizando fibroblastos 3T3 de ratones y también se realizaron ensayos de hemólisis en sangre humana (artículo 4). Ninguno de los péptidos mostró actividad hemolítica y todos dieron un porcentaje de viabilidad mayor del 90% en los ensayos con fibroblastos (tablas 4 y 5 del artículo 4), de manera que no se descartó ninguno de ellos.

4.2.2. Estudio de la capacidad de los péptidos seleccionados de inhibir la actividad del PF del VIH-1 mediante la utilización de monocapas de extensión como modelos de membrana

En los artículos 5 y 6 se estudian las interacciones de los 5 péptidos de la proteína E1 y de sus mezclas con el PF del VIH-1, utilizando monocapas de extensión.

Primeramente se estudiaron los perfiles de adsorción en la interfase aire-agua de los péptidos observando que en todos los casos había una adsorción gradual de los péptidos a medida que la concentración aumentaba. Por otro lado, se estudiaron las cinéticas de penetración en monocapas de fosfolípidos y se observó que todos los péptidos interaccionaban con los fosfolípidos ensayados de manera muy parecida, excepto el P18 que interaccionaba de igual forma con DMPG y con DMPC, posiblemente debido a su carga neta positiva.

Cuando se mezclan los péptidos con el PF del VIH-1 se observan varios cambios en las isotermas de compresión de las mezclas con los diferentes lípidos. Los estudios realizados con el P22 en presencia de DPPG (artículo 5, figura 11) muestran que cuando este péptido está mezclado con el PF del VIH-1, las isotermas del lípido son muy similares a cuando el péptido de fusión no está presente. En este caso, el PF del VIH-1 sólo, influye significativamente en las isotermas de DPPG, lo que indica una interacción entre ambos péptidos que parece reducir el efecto que el PF del VIH-1 tiene sobre las isotermas de DPPG. Este efecto se confirma por el cambio en la compresibilidad de las monocapas.

Para los otros 4 péptidos podemos observar un comportamiento similar. En todos los casos, al añadir los péptidos de la proteína E1 a las monocapas del PF del VIH-1 y los fosfolípidos, las isotermas que se obtienen son más parecidas a las que se obtienen cuando el péptido de fusión no está presente. Las isotermas se analizaron examinando la variación del área molecular media en función la relación molar péptido/lípido (artículo 6, figura 5). Observamos comportamientos similares, no lineal para todos los péptidos y sus mezclas, lo que indica que todos ellos son miscibles e interaccionan con los fosfolípidos estudiados [86]. Las mezclas presentan desviaciones positivas respecto a la

idealidad a todas las fracciones molares, excepto para el P7; todos los péptidos disminuyen las desviaciones que provoca el PF del VIH-1. El P7 es el único que hace que estas desviaciones pasen a ser negativas, e incluso, a bajas fracciones molares de la mezcla de péptidos, muestran un comportamiento ideal. La contracción observada en el caso del P7 indica que las interacciones péptido-lípido son atractivas y pueden reflejar la formación de complejos péptido-lípido a través de interacciones hidrofóbicas. [143]

4.2.3. Estudio de la capacidad de los péptidos seleccionados de inhibir la actividad del PF del VIH-1 mediante la utilización de liposomas

En el artículo 3 se estudia la unión de los péptidos a vesículas lipídicas utilizando dos métodos de separación diferentes. Por un lado, se estudia la unión de los péptidos a liposomas que contienen fosfatidilcolina bromada, los cuales se centrifugan y se separan del sobrenadante para poder determinar la cantidad de péptido que se ha unido a la membrana fosfolipídica. En este ensayo se incuban los péptidos de la proteína E1 con el PF del VIH-1 con el fin de observar si en presencia de estos péptidos, la cantidad del PF del VIH-1 que se une a las membranas disminuye. . Algunos como el P7 y el P18 aumentaron su unión a los liposomas en presencia del PF del VIH-1, pero este se unía en menor proporción en presencia de los péptidos de la E1 que cuando se encontraba solo. Por otro lado, El P10 y el P22 disminuyeron su unión a los liposomas reduciendo a la vez el porcentaje de PF unido a los liposomas. El P8 en cambio, parece no interaccionar con el PF del VIH-1 y no disminuye su unión a los liposomas. El coeficiente de partición del PF del VIH-1 disminuye cuando se mezcla con los otros 4 péptidos.

Por otro lado, se estudia la unión de los péptidos a liposomas mediante diálisis de equilibrio. Por un lado, si los liposomas y el PF del VIH-1 se encuentran en la misma celda, el PF del VIH-1 no se equilibra con la otra celda ni en presencia ni en ausencia de los péptidos de la proteína E1, lo cual puede ser indicativo de una unión entre el péptido de fusión y los liposomas, formando un complejo

que no puede atravesar la membrana. En cambio, cuando los liposomas se ponen en la celda en la que no tenemos los péptidos, se observa que la cantidad de PF del VIH-1 que permanece con los péptidos de la proteína E1 es mucho mayor que la que pasa a la otra celda a través de la membrana de diálisis. Este resultado evidencia una posible interacción entre los péptidos y el PF del VIH-1 en disolución. Mediante microscopía confocal se observó el efecto que el PF del VIH-1 produce sobre vesículas unilamelares gigantes (ruptura y fusión de membranas) y cómo este efecto desaparece en presencia de los péptidos de la proteína E1 del GBV-C/HGV (artículo 3, figuras 4 y 5).

Los estudios de agregación de liposomas (artículo 4) muestran que el P10 es el único de los péptidos que, al igual que el PF del VIH-1, es capaz de inducir agregación de vesículas. Esto se debe a la presencia de algún dominio capaz de promover dicha agregación en el extremo N-terminal [144]. Estudiando los péptidos mediante el software de predicción Aggrescan (artículo 4, tabla 1), se observa que el P10 presenta unos valores de THSAr (Total Hot Spot Area per residue) muy similares al PF del VIH-1, que también promueve la agregación de las vesículas y la desestabilización de las membranas [145]. Los experimentos de fusión mostraron que los péptidos de la proteína E1 no causaban fusión de membranas excepto para el P10 que presenta un porcentaje de fusión bajo; este resultado es coherente con los obtenidos en los ensayos de agregación ya que la fusión de membranas fosfolipídicas se basa en tres pasos, siendo el primero de ellos la agregación de vesículas, seguida de la desestabilización de las membranas para su posterior fusión [146-148], y el P10 es el único que tiene la capacidad de fusionar membranas. Estos resultados apoyan la idea de que el P10 puede ser un péptido de fusión del GBV-C/HGV y, por otro lado, su capacidad de fusionar membranas y que no es capaz de inhibir la fusión causada por el PF, nos llevan a descartarlo como posible inhibidor de la actividad del PF del VIH-1.

El porcentaje de fusión producido por el PF del VIH-1 se reduce cuando previamente se ha incubado con P7 o con P8, lo que indica que estos péptidos son capaces de reducir la fusión causada por el péptido de fusión en un 21.7 y un 29.7%, respectivamente (artículo 4, tabla 2). En cuanto a P18 y P22,

tampoco inhiben la fusión causada por el PF del VIH-1 pero, por otro lado, ellos no causan fusión de membranas.

Los liposomas también se utilizaron como modelos de membrana en los ensayos de resonancia de plasmón de superficie, en los que se fijaron sobre un chip sensor L1. Estos chips están recubiertos con dextrano y están modificados con substancias lipofílicas que permiten la unión de los liposomas sin necesidad de incorporarles moléculas para anclarlos. Se pudo observar que los péptidos por separado interaccionan con las membranas, uniéndose a los liposomas e incrementando la respuesta. El PF del VIH-1 presenta una unión mayor. Seguidamente, se estudiaron las mezclas de los péptidos de la proteína E1 con el PF del VIH-1, y se obtuvieron respuestas más bajas que con los péptidos por separado. Además, en las mezclas de P7 y P8 con el péptido de fusión, se obtuvo una respuesta inferior que para el PF del VIH-1, mostrando una vez más una inhibición parcial de la interacción del péptido de fusión con las membranas. P10, P18 y P22 incubados con el péptido de fusión dieron mayor respuesta que el péptido de fusión por separado (artículo 4, figura 3).

El péptido P22 se utilizó en los ensayos de calorimetría diferencial de barrido, con el fin de estudiar su capacidad y la del péptido de fusión del VIH de modificar la temperatura de transición de los fosfolípidos y, por lo tanto, de alterar el diagrama de fases que se obtiene para una mezcla de DMPG/DPPG. El diagrama de la mezcla se construyó a partir de los termogramas obtenidos por calorimetría diferencial de barrido de los liposomas. El PF del VIH-1 modifica la temperatura de transición (T_m) de los liposomas de DPPG y DMPG; cuando se incuban el péptido de fusión y el P22, la T_m vuelve a modificarse, siendo más parecida a la de los fosfolípidos puros (en ausencia del péptido de fusión). Esto se puede observar en los diagramas de fases (artículo 5, figura 13).

Por último, también se utilizaron liposomas en los ensayos de dicroísmo circular (CD) con el fin de analizar si la habilidad de los péptidos del GBV-C/HGV de unirse al péptido de fusión inducía algún cambio conformacional en su estructura secundaria. Inicialmente, antes de obtener los espectros de dicroísmo circular de los péptidos en presencia de liposomas, se registraron los espectros de los péptidos solos y en presencia de trifluoroetanol (TFE) como

agente estructurante. En general, los péptidos de secuencia corta no tienen una conformación preferente en disolución, aunque a veces pueden adoptar alguna estructura secundaria estable.[149] Los espectros de CD en agua mostraban una banda negativa cercana a 195 nm típica de una conformación al azar (*random coil*). Sin embargo, cuando los experimentos se llevan a cabo en presencia de TFE, el cual se ha demostrado que es helicogénico, se inducen estructuras secundarias. Aparecen las bandas negativas localizadas a 205 y 222 nm y la positiva a 195 nm características de la estructura de hélice α. El espectro del P10 muestra una banda negativa con un pico entre 215 y 220 nm que puede atribuirse a la contribución de estructura β (artículo 4, figura 4); es el único que presenta un bajo porcentaje de hélice α y un elevado porcentaje de estructura β, corroborando la idea de que se trata de un posible péptido de fusión.

En presencia de liposomas de POPG, el espectro de dicroísmo circular del PF del VIH-1 mostró una banda negativa con un pico alrededor de 215nm que se puede atribuir a la contribución de una estructura tipo β, probablemente debida a la agregación del péptido. También aparece una banda negativa cerca de 195nm, típica de un plegamiento al azar (*random coil*); esta banda también está presente en el espectro del P10. Los espectros de P7, P8 y P18 muestran una banda positiva alrededor de 195nm típica de la estructura de hélice α, y también una banda negativa entre 215 y 220nm debida a una contribución de estructura β (artículo 6, figura 1). El P22 muestra dos bandas negativas alrededor de 205 y 222nm y una positiva sobre 195nm, todas ellas características de una estructura de hélice α (artículo 5, figura 2).

Al incubar los péptidos de la proteína E1 junto con el péptido de fusión antes de añadirlos a los liposomas, los espectros que se obtienen son diferentes del espectro teórico obtenido sumando los espectros experimentales de los péptidos por separado, lo cual es indicativo de una cierta interacción entre los péptidos. También se observa un incremento de la elipticidad media por residuo a 195 nm y, por lo tanto, un incremento del porcentaje de hélice α. En la figura 12 se pueden observar los espectros de dicroísmo circular del péptido P22 y el PF del VIH-1 en presencia de liposomas de POPG.

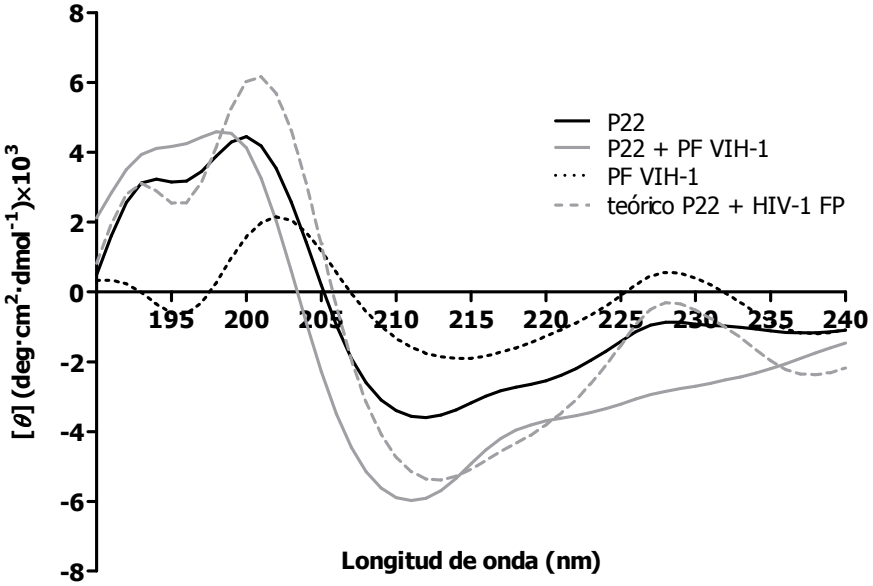

Figura 12. Espectros de dicroísmo circular del péptido P22 perteneciente a la proteína E1 del GBV-C/HGV y del péptido de fusión del VIH-1 en presencia de liposomas de POPG, registrados a 298 K.

En la tabla 3 se muestra la estimación, a partir de los espectros, del contenido de hélice α de los péptidos, de acuerdo con la elipticidad molar a 222 nm calculado a partir de la ecuación 3 del artículo 6, según Chen et al. [150]

Tabla 3. Estimación, a partir del espectro de dicroísmo circular, del porcentaje de hélice α del PF del VIH-1 y los péptidos de la proteína E1 del GBV-C/HGV, de acuerdo con la elipticidad molar a 222 nm.

	$[\theta]_{222}$
PF VIH-1	5.2
P7	7.7
P7 + PF VIH-1	9.3
P8	6.1
P8 + PF VIH-1	6.4
P10	5.2
P10 + PF VIH-1	7.2
P18	11.6
P18 + PF VIH-1	6.4
P22	8.2
P22 + PF VIH-1	12.5

Los resultados muestran que el P18 tiene un mayor porcentaje de hélice α que el resto y que el porcentaje obtenido para el P10 es idéntico al del PF del VIH-1; estos resultados concuerdan con los obtenidos en la tabla 2, mostrando que P10 tiene similitudes con el PF del VIH-1, tanto aquí como en su capacidad de fusionar membranas, y que P18 y P22 también son diferentes de P7 y P8. Los cambios de conformación al mezclarlos con el PF del VIH-1 más significativos se pueden observar para P18 y P22, hecho que muestra una clara interacción entre ambos péptidos.

5. Conclusiones

❖ Se ha llevado a cabo de forma satisfactoria y con buen rendimiento, la síntesis de 58 péptidos que cubren en su totalidad la estructura primaria de la proteína de envoltura E1 del GBV-C/HGV, mediante procedimientos semiautomatizados de síntesis de péptidos en fase sólida.

❖ Inicialmente se seleccionó una de las secuencias mediante algoritmos de predicción: P49. Los estudios realizados indican que este podría corresponderse con un posible péptido de fusión del GBV-C/HGV pero no muestra capacidad de inhibición de la actividad del péptido de fusión del VIH-1.

❖ Empleando técnicas fluorimétricas, se han seleccionado cinco regiones peptídicas (P7, P8, P10, P18 y p22), que inhiben la capacidad del PF del VIH-1 de liberar el contenido vesicular en modelos de membrana.

❖ Se ha caracterizado la interacción entre las secuencias seleccionadas y el PF del VIH-1 en presencia y ausencia de modelos de membrana:

- P7 es capaz de inhibir la fusión de membranas y la interacción del PF con bicapas. También se observó su interacción con el PF mediante ITC. En presencia de P7, se observó una contracción del área molecular media en las isotermas de compresión, indicando una interacción atractiva. Por otro lado, se obtuvo un incremento del porcentaje de hélice α cuando este péptido se incubó con el PF, lo cual corrobora un cambio conformacional que podría ser la causa de su efecto inhibidor.

- P8 se comporta de manera muy similar a P7 en cuanto a la fusión, agregación e interacción del PF con bicapas. En cambio, no influyó en las desviaciones del área molecular media causada por el PF y no se observó una clara interacción en disolución mediante ITC. En los experimentos de unión a liposomas tampoco actuó como un inhibidor.

- P10 destaca como el único péptido capaz de agregar liposomas y fusionar membranas. Por otro lado, no fue capaz de inhibir la fusión de membranas causada por el PF del VIH-1 ni su interacción con bicapas, tal y como se observó en los experimentos de resonancia de plasmón de superficie. Los estudios conformacionales en presencia de liposomas, así como el pI y la carga neta corroboran que el P10 se comporta diferente al

resto de los péptidos estudiados apoyando el hecho de que no es un buen inhibidor de la actividad del PF. Además se han observado muchas similitudes entre P10 y el PF que sugieren que podría tratarse de un péptido de fusión del GBV-C/HGV.

- P18 es el menos hidrofóbico de todos los péptidos seleccionados y es el único que, en presencia del PF, reduce su porcentaje de hélice α en lugar de aumentarlo como sucede con el resto de las secuencias ensayadas. Las isotermas de compresión muestran tanto su elevada miscibilidad con los fosfolípidos cargados negativamente como su capacidad de reducir la expansión del área molecular media causada por el PF. Estos resultados aportan otra evidencia de su capacidad de inhibir o reducir la actividad del PF. Aunque por otro lado no es capaz de inhibir la fusión de membranas ni la interacción del PF con bicapas.

- P22 tampoco inhibe la fusión de membranas ni la interacción del PF con bicapas pero, tanto en los estudios de miscibilidad péptido-lípido como en los experimentos de DSC se ha observado que la presencia de P22 reduce o inhibe la acción del PF. La causa de esta inhibición podría ser la interacción observada entre ambos péptidos cuando están en contacto, tal y como se observó en las imágenes de AFM y de BAM.

❖ P10 queda descartado como posible inhibidor de la actividad del PF del VIH-1 y podría tratarse de un péptido de fusión del GBV-C/HGV.

❖ P8, P18 y P22 muestran un comportamiento ambivalente. Los resultados negativos en algunos experimentos harían descartarlos para estudios posteriores. Pero en otros ensayos realizados en presencia del PF hace que se puedan considerar para futuros estudios.

❖ P7, que se corresponde con la región E1(19-36), parece estar claramente involucrado en la inhibición de la actividad del PF en modelos de membrana. Este péptido podría ser un candidato potencial para ser utilizado en futuras terapias anti-VIH, aunque son necesarios más estudios por tal de elucidar el mecanismo exacto de la interacción P7-PF.

6. Bibliografía

[1] F.B. Hollinger, W.S. Robinson, R.H. Purcell, J.L. Gerin, J. Ticehurst, Hepatitis B virus, Viral hepatitis, Raven Press, New York, 1990, pp. 73-138.

[2] D.W. Bradley, Introduction: The diversity of human hepatitis viruses, Seminars in Virology 4 (1993) 269-271.

[3] N. Boyce, Virologists rece to develop hepatitis G assay, Labmed Int 13 (1996).

[4] J.N. Simons, T.J. Pilot-Matias, T.P. Leary, G.J. Dawson, S.M. Desai, G.G. Schlauder, A.S. Muerhoff, J.C. Erker, S.L. Buijk, M.L. Chalmers, et al., Identification of two flavivirus-like genomes in the GB hepatitis agent, Proceedings of the National Academy of Sciences of the United States of America 92 (1995) 3401-3405.

[5] J. Linnen, J. Wages, Jr., Z.Y. Zhang-Keck, K.E. Fry, K.Z. Krawczynski, H. Alter, E. Koonin, M. Gallagher, M. Alter, S. Hadziyannis, P. Karayiannis, K. Fung, Y. Nakatsuji, J.W. Shih, L. Young, M. Piatak, Jr., C. Hoover, J. Fernandez, S. Chen, J.C. Zou, T. Morris, K.C. Hyams, S. Ismay, J.D. Lifson, G. Hess, S.K. Foung, H. Thomas, D. Bradley, H. Margolis, J.P. Kim, Molecular cloning and disease association of hepatitis G virus: a transfusion-transmissible agent, Science (New York, N.Y 271 (1996) 505-508.

[6] J. Bukh, J.P. Kim, S. Govindarajan, C.L. Apgar, S.K. Foung, J. Wages, Jr., A.J. Yun, M. Shapiro, S.U. Emerson, R.H. Purcell, Experimental infection of chimpanzees with hepatitis G virus and genetic analysis of the virus, The Journal of infectious diseases 177 (1998) 855-862.

[7] T.P. Leary, A.S. Muerhoff, J.N. Simons, T.J. Pilot-Matias, J.C. Erker, M.L. Chalmers, G.G. Schlauder, G.J. Dawson, S.M. Desai, I.K. Mushahwar, Sequence and genomic organization of GBV-C: a novel member of the flaviviridae associated with human non-A-E hepatitis, Journal of medical virology 48 (1996) 60-67.

[8] G.J. Dawson, G.G. Schlauder, T.J. Pilot-Matias, D. Thiele, T.P. Leary, P. Murphy, J.E. Rosenblatt, J.N. Simons, F.E. Martinson, R.A. Gutierrez, J.R. Lentino, C. Pachucki, A.S. Muerhoff, A. Widell, G. Tegtmeier, S. Desai, I.K. Mushahwar, Prevalence studies of GB virus-C infection using reverse transcriptase-polymerase chain reaction, Journal of medical virology 50 (1996) 97-103.

[9] J.J. Lefrere, C. Ferec, F. Roudot-Thoraval, P. Loiseau, J.F. Cantaloube, P. Biagini, M. Mariotti, G. LeGac, B. Mercier, GBV-C/hepatitis G virus (HGV) RNA load in immunodeficient individuals and in immunocompetent individuals, Journal of medical virology 59 (1999) 32-37.

[10] J.J. Huang, W.C. Lee, M.K. Ruaan, M.C. Wang, T.T. Chang, K.C. Young, Incidence, transmission, and clinical significance of hepatitis G virus infection in hemodialysis patients, Eur J Clin Microbiol Infect Dis 20 (2001) 374-379.

[11] T. Berg, U. Naumann, T. Fukumoto, W.O. Bechstein, P. Neuhaus, H. Lobeck, M. Hohne, E. Schreier, U. Hopf, GB virus C infection in patients with chronic hepatitis B and C before and after liver transplantation, Transplantation 62 (1996) 711-714.

[12] D. Rey, J. Vidinic-Moularde, P. Meyer, C. Schmitt, S. Fritsch, J.M. Lang, F. Stoll-Keller, High prevalence of GB virus C/hepatitis G virus RNA and antibodies in patients infected with human immunodeficiency virus type 1, Eur J Clin Microbiol Infect Dis 19 (2000) 721-724.

[13] L.M. Jarvis, F. Davidson, J.P. Hanley, P.L. Yap, C.A. Ludlam, P. Simmonds, Infection with hepatitis G virus among recipients of plasma products, Lancet 348 (1996) 1352-1355.

[14] J.N. Simons, S.M. Desai, I.K. Mushahwar, The GB viruses, Current topics in microbiology and immunology 242 (2000) 341-375.

[15] M.F. Scallan, D. Clutterbuck, L.M. Jarvis, G.R. Scott, P. Simmonds, Sexual transmission of GB virus C/hepatitis G virus, Journal of medical virology 55 (1998) 203-208.

[16] J.J. Lefrere, A. Sender, B. Mercier, M. Mariotti, F. Pernot, J.C. Soulie, A. Malvoisin, M. Berry, A. Gabai, F. Lattes, J.C. Galiay, C. Pawlak, V. de Lachaux, V. Chauveau, G. Hreiche, M. Larsen, C. Ferec, F. Parnet-Mathieu, F. Roudot-Thoraval, Y. Brossard, High rate of GB virus type C/HGV transmission from mother to infant: possible implications for the prevalence of infection in blood donors, Transfusion 40 (2000) 602-607.

[17] H.H. Feucht, B. Zollner, S. Polywka, B. Knodler, M. Schroter, H. Nolte, R. Laufs, Prevalence of hepatitis G viremia among healthy subjects, individuals with liver disease, and persons at risk for parenteral transmission, Journal of clinical microbiology 35 (1997) 767-768.

[18] K.E. Brown, S. Wong, M. Buu, T.V. Binh, T.V. Be, N.S. Young, High prevalence of GB virus C/hepatitis G virus in healthy persons in Ho Chi Minh City, Vietnam, The Journal of infectious diseases 175 (1997) 450-453.

[19] R.A. Gutierrez, G.J. Dawson, M.F. Knigge, S.L. Melvin, C.A. Heynen, C.R. Kyrk, C.E. Young, R.J. Carrick, G.G. Schlauder, T.K. Surowy, B.J. Dille, P.F. Coleman, D.L. Thiele, J.R. Lentino, C. Pachucki, I.K. Mushahwar, Seroprevalence of GB virus C and persistence of RNA and antibody, Journal of medical virology 53 (1997) 167-173.

[20] D.L. Thomas, D. Vlahov, H.J. Alter, J.C. Hunt, R. Marshall, J. Astemborski, K.E. Nelson, Association of antibody to GB virus C (hepatitis G virus) with viral clearance and protection from reinfection, The Journal of infectious diseases 177 (1998) 539-542.

[21] M. Tacke, S. Schmolke, V. Schlueter, S. Sauleda, J.I. Esteban, E. Tanaka, K. Kiyosawa, H.J. Alter, U. Schmitt, G. Hess, B. Ofenloch-Haehnle, A.M. Engel, Humoral immune response to the E2 protein of hepatitis G virus is associated with long-term recovery from infection and

reveals a high frequency of hepatitis G virus exposure among healthy blood donors, Hepatology (Baltimore, Md) 26 (1997) 1626-1633.

[22] T. Kanda, O. Yokosuka, T. Ehata, Y. Maru, F. Imazeki, H. Saisho, Y. Shiratori, M. Omata, Detection of GBV-C RNA in patients with non-A-E fulminant hepatitis by reverse-transcription polymerase chain reaction, Hepatology (Baltimore, Md 25 (1997) 1261-1265.

[23] R. Sallie, J. Shaw, D. Mutimer, GBV-C virus and fulminant hepatic failure, Lancet 347 (1996) 1552.

[24] H.J. Alter, G-pers creepers, where'd you get those papers? A reassessment of the literature on the hepatitis G virus, Transfusion 37 (1997) 569-572.

[25] A.J. Nahmias, J. Weiss, X. Yao, F. Lee, R. Kodsi, M. Schanfield, T. Matthews, D. Bolognesi, D. Durack, A. Motulsky, et al., Evidence for human infection with an HTLV III/LAV-like virus in Central Africa, 1959, Lancet 1 (1986) 1279-1280.

[26] J. Coffin, A. Haase, J.A. Levy, L. Montagnier, S. Oroszlan, N. Teich, H. Temin, K. Toyoshima, H. Varmus, P. Vogt, et al., Human immunodeficiency viruses, Science (New York, N.Y 232 (1986) 697.

[27] F. Clavel, K. Mansinho, S. Chamaret, D. Guetard, V. Favier, J. Nina, M.O. Santos-Ferreira, J.L. Champalimaud, L. Montagnier, Human immunodeficiency virus type 2 infection associated with AIDS in West Africa, The New England journal of medicine 316 (1987) 1180-1185.

[28] M. Guyader, M. Emerman, P. Sonigo, F. Clavel, L. Montagnier, M. Alizon, Genome organization and transactivation of the human immunodeficiency virus type 2, Nature 326 (1987) 662-669.

[29] Casos de SIDA notificados en España a 30 de Junio de 1999, Plan Nacional sobre el sida, Ministerio de Sanidad Política Social e Igualdad, 1999.

[30] D. Baltimore, RNA-dependent DNA polymerase in virions of RNA tumour viruses, Nature 226 (1970) 1209-1211.

[31] H.M. Temin, S. Mizutani, RNA-dependent DNA polymerase in virions of Rous sarcoma virus, Nature 226 (1970) 1211-1213.

[32] M.B. Oldstone, HIV versus cytotoxic T lymphocytes--the war being lost, The New England journal of medicine 337 (1997) 1306-1308.

[33] F. García, N. Climent, L. Assoumou, C. Gil, N. González, J. Alcamí, A. León, J. Romeu, J. Dalmau, J. Martínez-Picado, J. Lifson, B. Autran, D. Costagliola, B. Clotet, J.M. Gatell, M. Plana, T. Gallart, A Therapeutic Dendritic Cell-Based Vaccine for HIV-1 Infection, Journal of Infectious Diseases 203 473-478.

[34] C.T. Wild, D.C. Shugars, T.K. Greenwell, C.B. McDanal, T.J. Matthews, Peptides corresponding to a predictive alpha-helical domain of human immunodeficiency virus type 1 gp41 are potent inhibitors of virus infection, Proceedings of the National Academy of Sciences of the United States of America 91 (1994) 9770-9774.

[35] J.M. Kilby, S. Hopkins, T.M. Venetta, B. DiMassimo, G.A. Cloud, J.Y. Lee, L. Alldredge, E. Hunter, D. Lambert, D. Bolognesi, T. Matthews, M.R. Johnson, M.A. Nowak, G.M. Shaw, M.S. Saag, Potent suppression of HIV-1 replication in humans by T-20, a peptide inhibitor of gp41-mediated virus entry, Nature medicine 4 (1998) 1302-1307.

[36] E. Poveda, V. Briz, V. Soriano, Enfuvirtide, the first fusion inhibitor to treat HIV infection, AIDS reviews 7 (2005) 139-147.

[37] M.L. Heil, J.M. Decker, J.N. Sfakianos, G.M. Shaw, E. Hunter, C.A. Derdeyn, Determinants of human immunodeficiency virus type 1 baseline susceptibility to the fusion inhibitors enfuvirtide and T-649 reside outside the peptide interaction site, Journal of virology 78 (2004) 7582-7589.

[38] C.A. Derdeyn, J.M. Decker, J.N. Sfakianos, Z. Zhang, W.A. O'Brien, L. Ratner, G.M. Shaw, E. Hunter, Sensitivity of human immunodeficiency

virus type 1 to fusion inhibitors targeted to the gp41 first heptad repeat involves distinct regions of gp41 and is consistently modulated by gp120 interactions with the coreceptor, Journal of virology 75 (2001) 8605-8614.

[39] F.G. Hermann, L. Egerer, F. Brauer, C. Gerum, H. Schwalbe, U. Dietrich, D. von Laer, Mutations in gp120 contribute to the resistance of human immunodeficiency virus type 1 to membrane-anchored C-peptide maC46, Journal of virology 83 (2009) 4844-4853.

[40] J. Munch, L. Standker, K. Adermann, A. Schulz, M. Schindler, R. Chinnadurai, S. Pohlmann, C. Chaipan, T. Biet, T. Peters, B. Meyer, D. Wilhelm, H. Lu, W. Jing, S. Jiang, W.G. Forssmann, F. Kirchhoff, Discovery and optimization of a natural HIV-1 entry inhibitor targeting the gp41 fusion peptide, Cell 129 (2007) 263-275.

[41] J.T. Stapleton, GB virus type C/Hepatitis G virus, Seminars in liver disease 23 (2003) 137-148.

[42] P.M. Polgreen, J. Xiang, Q. Chang, J.T. Stapleton, GB virus type C/hepatitis G virus: a non-pathogenic flavivirus associated with prolonged survival in HIV-infected individuals, Microbes and infection / Institut Pasteur 5 (2003) 1255-1261.

[43] H.L. Tillmann, M.P. Manns, GB virus-C infection in patients infected with the human immunodeficiency virus, Antiviral research 52 (2001) 83-90.

[44] J. Xiang, S. Wunschmann, D.J. Diekema, D. Klinzman, K.D. Patrick, S.L. George, J.T. Stapleton, Effect of coinfection with GB virus C on survival among patients with HIV infection, The New England journal of medicine 345 (2001) 707-714.

[45] A.K. Van der Bij, N. Kloosterboer, M. Prins, B. Boeser-Nunnink, R.B. Geskus, J.M. Lange, R.A. Coutinho, H. Schuitemaker, GB virus C coinfection and HIV-1 disease progression: The Amsterdam Cohort Study, The Journal of infectious diseases 191 (2005) 678-685.

[46] P. Bjorkman, L. Flamholc, A. Naucler, V. Molnegren, E. Wallmark, A. Widell, GB virus C during the natural course of HIV-1 infection: viremia at diagnosis does not predict mortality, Aids 18 (2004) 877-886.

[47] H. Toyoda, Y. Fukuda, T. Hayakawa, J. Takamatsu, H. Saito, Effect of GB virus C/hepatitis G virus coinfection on the course of HIV infection in hemophilia patients in Japan, J Acquir Immune Defic Syndr Hum Retrovirol 17 (1998) 209-213.

[48] S. Heringlake, J. Ockenga, H.L. Tillmann, C. Trautwein, D. Meissner, M. Stoll, J. Hunt, C. Jou, N. Solomon, R.E. Schmidt, M.P. Manns, GB virus C/hepatitis G virus infection: a favorable prognostic factor in human immunodeficiency virus-infected patients?, The Journal of infectious diseases 177 (1998) 1723-1726.

[49] A.E. Yeo, A. Matsumoto, M. Hisada, J.W. Shih, H.J. Alter, J.J. Goedert, Effect of hepatitis G virus infection on progression of HIV infection in patients with hemophilia. Multicenter Hemophilia Cohort Study, Annals of internal medicine 132 (2000) 959-963.

[50] H.L. Tillmann, M.P. Manns, C. Claes, H. Heiken, R.E. Schmidt, M. Stoll, GB virus C infection and quality of life in HIV-positive patients, AIDS care 16 (2004) 736-743.

[51] H.L. Tillmann, H. Heiken, A. Knapik-Botor, S. Heringlake, J. Ockenga, J.C. Wilber, B. Goergen, J. Detmer, M. McMorrow, M. Stoll, R.E. Schmidt, M.P. Manns, Infection with GB virus C and reduced mortality among HIV-infected patients, The New England journal of medicine 345 (2001) 715-724.

[52] P. Bjorkman, L. Flamholc, V. Molnegren, A. Marshall, N. Guner, A. Widell, Enhanced and resumed GB virus C replication in HIV-1-infected individuals receiving HAART, Aids 21 (2007) 1641-1643.

[53] J. Xiang, S.L. George, S. Wunschmann, Q. Chang, D. Klinzman, J.T. Stapleton, Inhibition of HIV-1 replication by GB virus C infection through

increases in RANTES, MIP-1alpha, MIP-1beta, and SDF-1, Lancet 363 (2004) 2040-2046.

[54] S. Jung, O. Knauer, N. Donhauser, M. Eichenmüller, M. Helm, B. Fleckenstein, H. Reil, Inhibition of HIV strains by GB virus C in cell culture can be mediated by CD4 and CD8 T-lymphocyte derived soluble factors, vol. 19, 2005, pp. 1267-1272.

[55] R. Jahn, T.C. Sudhof, Membrane fusion and exocytosis, Annu Rev Biochem 68 (1999) 863-911.

[56] J.M. White, Viral and cellular membrane fusion proteins, Annual review of physiology 52 (1990) 675-697.

[57] T.S. Jardetzky, R.A. Lamb, Virology: a class act, Nature 427 (2004) 307-308.

[58] Y.G. Yu, D.S. King, Y.K. Shin, Insertion of a coiled-coil peptide from influenza virus hemagglutinin into membranes, Science (New York, N.Y 266 (1994) 274-276.

[59] J.K. Ghosh, Y. Shai, Direct evidence that the N-terminal heptad repeat of Sendai virus fusion protein participates in membrane fusion, J Mol Biol 292 (1999) 531-546.

[60] N.C. Santos, M. Prieto, M.A. Castanho, Interaction of the major epitope region of HIV protein gp41 with membrane model systems. A fluorescence spectroscopy study, Biochemistry 37 (1998) 8674-8682.

[61] T. Suarez, W.R. Gallaher, A. Agirre, F.M. Goni, J.L. Nieva, Membrane interface-interacting sequences within the ectodomain of the human immunodeficiency virus type 1 envelope glycoprotein: putative role during viral fusion, Journal of virology 74 (2000) 8038-8047.

[62] J.J. Skehel, D.C. Wiley, Receptor binding and membrane fusion in virus entry: the influenza hemagglutinin, Annu Rev Biochem 69 (2000) 531-569.

[63] D.C. Chan, D. Fass, J.M. Berger, P.S. Kim, Core structure of gp41 from the HIV envelope glycoprotein, Cell 89 (1997) 263-273.

[64] W. Weissenhorn, A. Dessen, L.J. Calder, S.C. Harrison, J.J. Skehel, D.C. Wiley, Structural basis for membrane fusion by enveloped viruses, Molecular membrane biology 16 (1999) 3-9.

[65] K.A. Baker, R.E. Dutch, R.A. Lamb, T.S. Jardetzky, Structural basis for paramyxovirus-mediated membrane fusion, Molecular cell 3 (1999) 309-319.

[66] W. Weissenhorn, A. Carfi, K.H. Lee, J.J. Skehel, D.C. Wiley, Crystal structure of the Ebola virus membrane fusion subunit, GP2, from the envelope glycoprotein ectodomain, Molecular cell 2 (1998) 605-616.

[67] F.X. Heinz, S.L. Allison, F.A.M.A.J.S.T.J.C.a.T.P.M. Karl Maramorosch, Flavivirus Structure and Membrane Fusion, Advances in Virus Research, vol. Volume 59, Academic Press, 2003, pp. 63-97.

[68] S.E. Delos, J.M. Gilbert, J.M. White, The central proline of an internal viral fusion peptide serves two important roles, Journal of virology 74 (2000) 1686-1693.

[69] Y. Gaudin, C. Tuffereau, P. Durrer, J. Brunner, A. Flamand, R. Ruigrok, Rabies virus-induced membrane fusion, Molecular membrane biology 16 (1999) 21-31.

[70] S.L. Allison, J. Schalich, K. Stiasny, C.W. Mandl, F.X. Heinz, Mutational evidence for an internal fusion peptide in flavivirus envelope protein E, Journal of virology 75 (2001) 4268-4275.

[71] J. Lescar, A. Roussel, M.W. Wien, J. Navaza, S.D. Fuller, G. Wengler, G. Wengler, F.A. Rey, The Fusion glycoprotein shell of Semliki Forest virus: an icosahedral assembly primed for fusogenic activation at endosomal pH, Cell 105 (2001) 137-148.

[72] C.D. Laxton, D. McMillan, V. Sullivan, A.M. Ackrill, Expression and characterization of the hepatitis G virus helicase, Journal of viral hepatitis 5 (1998) 21-26.

[73] V.D. Del Angel, F. Dupuis, J.P. Mornon, I. Callebaut, Viral fusion peptides and identification of membrane-interacting segments, Biochem Biophys Res Commun 293 (2002) 1153-1160.

[74] J.M. White, Membrane fusion, Science (New York, N.Y 258 (1992) 917-924.

[75] N.M. Qureshi, D.H. Coy, R.F. Garry, L.A. Henderson, Characterization of a putative cellular receptor for HIV-1 transmembrane glycoprotein using synthetic peptides, Aids 4 (1990) 553-558.

[76] J.L. Nieva, A. Agirre, Are fusion peptides a good model to study viral cell fusion?, Biochimica et biophysica acta 1614 (2003) 104-115.

[77] A.G. Buckland, D.C. Wilton, Anionic phospholipids, interfacial binding and the regulation of cell functions, Biochimica et biophysica acta 1483 (2000) 199-216.

[78] M. Rappolt, A.L. Liu, Chapter 9 The Biologically Relevant Lipid Mesophases as "Seen" by X-Rays, Advances in Planar Lipid Bilayers and Liposomes, vol. Volume 5, Academic Press, 2006, pp. 253-283.

[79] A.G. Lee, Lipid phase transitions and phase diagrams. I. Lipid phase transitions, Biochimica et biophysica acta 472 (1977) 237-281.

[80] D. Lichtenberg, R.J. Robson, E.A. Dennis, Solubilization of phospholipids by detergents. Structural and kinetic aspects, Biochimica et biophysica acta 737 (1983) 285-304.

[81] N.A. Williams, N.D. Weiner, Interactions of small polypeptides with dimyristoylphosphatidylcholine monolayers: effect of size and hydrophobicity, International Journal of Pharmaceutics 50 (1989) 261-266.

[82] R. Verger, F. Pattus, Lipid-protein interactions in monolayers, Chemistry and physics of lipids 30 (1982) 189-227.

[83] I. Langmuir, THE CONSTITUTION AND FUNDAMENTAL PROPERTIES OF SOLIDS AND LIQUIDS. II. LIQUIDS.1, Journal of the American Chemical Society 39 (1917) 1848-1906.

[84] C.M. Knobler, Recent Developments in the Study of Monolayers at the Air-Water Interface, John Wiley & Sons, Inc. 2007.

[85] M.M. Lipp, K.Y. Lee, J.A. Zasadzinski, A.J. Waring, Phase and morphology changes in lipid monolayers induced by SP-B protein and its amino-terminal peptide, Science (New York, N.Y 273 (1996) 1196-1199.

[86] G.L. Gaines, In Insoluble Monolayers at Liquid-Gas Interfaces, Wiley-Interscience, New York, 1966, p. 286.

[87] C. McFate, D. Ward, J. Olmsted, Organized collapse of fatty acid monolayers, Langmuir 9 (1993) 1036-1039.

[88] P. Cea, C. Lafuente, J.S. Urieta, M.C. López, F.M. Royo, Langmuir and Langmuir-Blodgett Films of a Phosphorus Derivative, Langmuir 12 (1996) 5881-5887.

[89] L. Dei, A. Casnati, P.L. Nostro, P. Baglioni, Selective Complexation by p-tert-Butylcalix[6]arene in Monolayers at the Water-Air Interface, Langmuir 11 (1995) 1268-1272.

[90] R.B. Merrifield, Solid Phase Peptide Synthesis. I. The Synthesis of a Tetrapeptide, Journal of the American Chemical Society 85 (1963) 2149-2154.

[91] E. Kaiser, R.L. Colescott, C.D. Bossinger, P.I. Cook, Color test for detection of free terminal amino groups in the solid-phase synthesis of peptides, Analytical biochemistry 34 (1970) 595-598.

[92] W.C. Wimley, S.H. White, Designing transmembrane alpha-helices that insert spontaneously, Biochemistry 39 (2000) 4432-4442.

[93] B. Christiaens, S. Symoens, S. Verheyden, Y. Engelborghs, A. Joliot, A. Prochiantz, J. Vandekerckhove, M. Rosseneu, B. Vanloo, Tryptophan fluorescence study of the interaction of penetratin peptides with model membranes, European journal of biochemistry / FEBS 269 (2002) 2918-2926.

[94] M. Smolarsky, D. Teitelbaum, M. Sela, C. Gitler, A simple fluorescent method to determine complement-mediated liposome immune lysis, Journal of Immunological Methods 15 (1977) 255-265.

[95] D.K. Struck, D. Hoekstra, R.E. Pagano, Use of resonance energy transfer to monitor membrane fusion, Biochemistry 20 (1981) 4093-4099.

[96] C.L. Avila, B.F. de Arcuri, F. Gonzalez-Nilo, J. De Las Rivas, R. Chehín, R. Morero, Role of electrostatics on membrane binding, aggregation and destabilization induced by NAD(P)H dehydrogenases. Implication in membrane fusion, Biophysical Chemistry 137 (2008) 126-132.

[97] J. Slavik, Anilinonaphthalene sulfonate as a probe of membrane composition and function, Biochimica et biophysica acta 694 (1982) 1-25.

[98] W. Stillwell, W. Ehringer, S.R. Wassall, Interaction of alpha-tocopherol with fatty acids in membranes and ethanol, Biochimica et biophysica acta 1105 (1992) 237-244.

[99] G. van Ginkel, H. van Langen, Y.K. Levine, The membrane fluidity concept revisited by polarized fluorescence spectroscopy on different model membranes containing unsaturated lipids and sterols, Biochimie 71 (1989) 23-32.

[100] B.W. Williams, A.W. Scotto, C.D. Stubbs, Effect of proteins on fluorophore lifetime heterogeneity in lipid bilayers, Biochemistry 29 (1990) 3248-3255.

[101] R.D. Kaiser, E. London, Location of diphenylhexatriene (DPH) and its derivatives within membranes: comparison of different fluorescence

quenching analyses of membrane depth, Biochemistry 37 (1998) 8180-8190.

[102] F.J. Aranda, J. Villalain, The interaction of abietic acid with phospholipid membranes, Biochimica et biophysica acta 1327 (1997) 171-180.

[103] N. Poklar, J. Fritz, P. Macek, G. Vesnaver, T.V. Chalikian, Interaction of the pore-forming protein equinatoxin II with model lipid membranes: A calorimetric and spectroscopic study, Biochemistry 38 (1999) 14999-15008.

[104] R. Koynova, M. Caffrey, Phases and phase transitions of the phosphatidylcholines, Biochimica et biophysica acta 1376 (1998) 91-145.

[105] C. Lheveder, Hénon, J. Meunier, in: M.D. Inc. (Ed.), Physical chemistry of biological interfaces, New York, 2000.

[106] J.E. Ladbury, B.Z. Chowdhry, Sensing the heat: the application of isothermal titration calorimetry to thermodynamic studies of biomolecular interactions, Chemistry & biology 3 (1996) 791-801.

[107] M. Marvin, Microscopy apparatus, Minsky, Marvin, United States, 1961.

[108] M. Petrán, M. HadravskÝ, M.D. Egger, R. Galambos, Tandem-Scanning Reflected-Light Microscope, J. Opt. Soc. Am. 58 (1968) 661-664.

[109] A. Boyde, Confocal optical microscopy, Microscopy and analysis 2 (1988) 7-13.

[110] M. Fivash, E.M. Towler, R.J. Fisher, BIAcore for macromolecular interaction, Current opinion in biotechnology 9 (1998) 97-101.

[111] P. Pattnaik, Surface plasmon resonance: applications in understanding receptor-ligand interaction, Applied biochemistry and biotechnology 126 (2005) 79-92.

[112] A. Szabo, L. Stolz, R. Granzow, Surface plasmon resonance and its use in biomolecular interaction analysis (BIA), Current opinion in structural biology 5 (1995) 699-705.

[113] U. Jonsson, L. Fagerstam, S. Lofas, E. Stenberg, R. Karlsson, A. Frostell, F. Markey, F. Schindler, Introducing a biosensor based technology for real-time biospecific interaction analysis, Annales de biologie clinique 51 (1993) 19-26.

[114] D.J. O'Shannessy, M. Brigham-Burke, K. Peck, Immobilization chemistries suitable for use in the BIAcore surface plasmon resonance detector, Analytical biochemistry 205 (1992) 132-136.

[115] J. Homola, Present and future of surface plasmon resonance biosensors, Analytical and bioanalytical chemistry 377 (2003) 528-539.

[116] R.L. Rich, D.G. Myszka, Survey of the year 2004 commercial optical biosensor literature, J Mol Recognit 18 (2005) 431-478.

[117] R.L. Rich, D.G. Myszka, Survey of the year 2003 commercial optical biosensor literature, J Mol Recognit 18 (2005) 1-39.

[118] M.O. Roy, M. Pugniere, M. Jullien, J. Chopineau, J.C. Mani, Study of hydrophobic interactions between acylated proteins and phospholipid bilayers using BIACORE, J Mol Recognit 14 (2001) 72-78.

[119] W. Huber, F. Mueller, Biomolecular interaction analysis in drug discovery using surface plasmon resonance technology, Current pharmaceutical design 12 (2006) 3999-4021.

[120] H. Sota, Y. Hasegawa, M. Iwakura, Detection of conformational changes in an immobilized protein using surface plasmon resonance, Analytical chemistry 70 (1998) 2019-2024.

[121] L.M. May, D.A. Russell, The characterization of biomolecular secondary structures by surface plasmon resonance, The Analyst 127 (2002) 1589-1595.

[122] T.H. Lee, H. Mozsolits, M.I. Aguilar, Measurement of the affinity of melittin for zwitterionic and anionic membranes using immobilized lipid biosensors, J Pept Res 58 (2001) 464-476.

[123] H. Mozsolits, M.I. Aguilar, Surface plasmon resonance spectroscopy: an emerging tool for the study of peptide-membrane interactions, Biopolymers 66 (2002) 3-18.

[124] M. Radmacher, R.W. Tillamnn, M. Fritz, H.E. Gaub, From molecules to cells: imaging soft samples with the atomic force microscope, Science (New York, N.Y 257 (1992) 1900-1905.

[125] A. Ulman, Introduction to Ultrathin Organic Films from Langmuir-Blodgett to Self-Assembly, Academic Press, San Diego, CA, 1991.

[126] J. Garnaes, D.K. Schwartz, R. Viswanathan, J.A.N. Zasadzinski, Domain boundaries and buckling superstructures in Langmuir-Blodgett films, Nature 357 (1992) 54-57.

[127] J.M. Solletti, M. Botreau, F. Sommer, W.L. Brunat, S. Kasas, T.M. Duc, M.R. Celio, Elaboration and Characterization of Phospholipid Langmuirâ˜Blodgett Films, Langmuir 12 (1996) 5379-5386.

[128] Q. Zhong, D. Inniss, K. Kjoller, V.B. Elings, Fractured polymer/silica fiber surface studied by tapping mode atomic force microscopy, Surface Science Letters 290 (1993) L688-L692.

[129] Z. Shao, J. Mou, D.M. Czajkowsky, J. Yang, J.-Y. Yuan, Biological atomic force microscopy: what is achieved and what is needed, Advances in Physics 45 (1996) 1 - 86.

[130] Z. Oren, Y. Shai, Selective lysis of bacteria but not mammalian cells by diastereomers of melittin: structure-function study, Biochemistry 36 (1997) 1826-1835.

[131] M. Tejuca, G. Anderluh, P. Macek, R. Marcet, D. Torres, J. Sarracent, C. Alvarez, M.E. Lanio, M. Dalla Serra, G. Menestrina, Antiparasite activity

of sea-anemone cytolysins on Giardia duodenalis and specific targeting with anti-Giardia antibodies, International journal for parasitology 29 (1999) 489-498.

[132] M.L. Mangoni, A.C. Rinaldi, A. Di Giulio, G. Mignogna, A. Bozzi, D. Barra, M. Simmaco, Structure-function relationships of temporins, small antimicrobial peptides from amphibian skin, European journal of biochemistry / FEBS 267 (2000) 1447-1454.

[133] F.A. Barile, P.J. Dierickx, U. Kristen, In vitro cytotoxicity testing for prediction of acute human toxicity, Cell biology and toxicology 10 (1994) 155-162.

[134] J.C. Davila, C.G. Reddy, P.J. Davis, D. Acosta, Toxicity assessment of papaverine hydrochloride and papaverine-derived metabolites in primary cultures of rat hepatocytes, In Vitro Cell Dev Biol 26 (1990) 515-524.

[135] M.D. Todd, X. Lin, L.F. Stankowski, Jr., M. Desai, G.H. Wolfgang, Toxicity Screening of a Combinatorial Library: Correlation of Cytotoxicity and Gene Induction to Compound Structure, J Biomol Screen 4 (1999) 259-268.

[136] J. Janin, Surface and inside volumes in globular proteins, Nature 277 (1979) 491-492.

[137] T.P. Hopp, K.R. Woods, Prediction of protein antigenic determinants from amino acid sequences, Proceedings of the National Academy of Sciences of the United States of America 78 (1981) 3824-3828.

[138] H. Brockman, Lipid monolayers: why use half a membrane to characterize protein-membrane interactions?, Current opinion in structural biology 9 (1999) 438-443.

[139] K. Hac-Wydro, J. Kapusta, A. Jagoda, P. Wydro, P. Dynarowicz-Latka, The influence of phospholipid structure on the interactions with nystatin, a polyene antifungal antibiotic A Langmuir monolayer study, Chemistry and physics of lipids 150 (2007) 125-135.

[140] W.C. Wimley, S.H. White, Designing transmembrane alpha-helices that insert spontaneously, Biochemistry 39 (2000) 4432-4442.

[141] A.S. Ladokhin, S. Jayasinghe, S.H. White, How to measure and analyze tryptophan fluorescence in membranes properly, and why bother?, Analytical Biochemistry 285 (2000) 235-245.

[142] M. Wu, S.-Q. Nie, Y. Qiu, K.-C. Lin, S.-X. Wang, S.-F. Sui, Study of the relationship between structure and function of HIV-1 gp 41 N terminus fusion peptide, Peptides Biology and Chemistry, 2002, pp. 104-107.

[143] S. Deshayes, T. Plenat, G. Aldrian-Herrada, G. Divita, C. Le Grimellec, F. Heitz, Primary amphipathic cell-penetrating peptides: structural requirements and interactions with model membranes, Biochemistry 43 (2004) 7698-7706.

[144] M. Torrent, B.G. de la Torre, V.M. Nogués, D. Andreu, E. Boix, Bactericidal and membrane disruption activities of the eosinophil cationic protein are largely retained in an N-terminal fragment, Biochemical Journal 421 (2009) 425-434.

[145] Y. Kliger, A. Aharoni, D. Rapaport, P. Jones, R. Blumenthal, Y. Shai, Fusion Peptides Derived from the HIV Type 1 Glycoprotein 41 Associate within Phospholipid Membranes and Inhibit Cell-Cell Fusion, Journal of Biological Chemistry 272 (1997) 13496-13505.

[146] S. Nir, J. Bentz, J. Wilschut, Mass action kinetics of phosphatidylserine vesicle fusion monitored by coalescence of internal vesicle volumes, Biochemistry 19 (1980) 6030-6036.

[147] R. Blumenthal, Cooperativity in viral fusion, Cell Biochemistry and Biophysics 12 (1988) 1-12.

[148] C.M. Carr, P.S. Kim, Flu virus invasion: halfway there, Science (New York, N.Y 266 (1994) 234-236.

[149] J.A. Pérez, J. Cantó, F. Reig, J.J. Pérez, I. Haro, Conformational behavior of the HAV-VP3(110–121) peptidic sequence and synthetic analogs in membrane environments studied by CD and computational methods, Biopolymers 45 (1998) 479-492.

[150] Y.H. Chen, J.T. Yang, K.H. Chau, Determination of the helix and beta form of proteins in aqueous solution by circular dichroism, Biochemistry 13 (1974) 3350-3359.